





Parameterized Modeling and Model Order Reduction  
for Large Electrical Systems

Geparametriseerde modellering en modelordereductie  
voor grote elektrische systemen

Elizabeth Rita Samuel

Promotoren: prof. dr. ir. L. Knockaert, prof. dr. ir. T. Dhaene  
Proefschrift ingediend tot het behalen van de graad van  
Doctor in de Ingenieurswetenschappen: Elektrotechniek

Vakgroep Informatietechnologie  
Voorzitter: prof. dr. ir. D. De Zutter  
Faculteit Ingenieurswetenschappen en Architectuur  
Academiejaar 2014 - 2015



ISBN 978-90-8578-774-7  
NUR 959  
Wettelijk depot: D/2015/10.500/18



Universiteit Gent  
Faculteit Ingenieurswetenschappen en Architectuur  
Vakgroep Informatietechnologie

Promotoren: prof. dr. ir. Luc Knockaert  
prof. dr. ir. Tom Dhaene

Universiteit Gent  
Faculteit Ingenieurswetenschappen en Architectuur  
Vakgroep Informatietechnologie  
Gaston Crommenlaan 8 bus 201, B-9050 Gent, België  
Tel.: +32-9-331.49.00  
Fax.: +32-9-331.48.99



Dit werk kwam tot stand in het kader van een  
mandaat als Aspirant bij het Fonds voor  
Wetenschappelijk Onderzoek Vlaanderen.



Proefschrift tot het behalen van de graad van  
Doctor in de Ingenieurswetenschappen:  
Elektrotechniek  
Academiejaar 2014-2015



# Acknowledgments

*“You can’t fail if you don’t climb, but there’s no joy in living your whole life on the ground.”*

–Anonymous (Inspiring quotes)

Inspiration made me climb further and take up the challenge of relocating to Gent with my family to do a doctoral program. It was with lots of mixed feelings I started off. All was calmed with my first meeting with my promoters, would like to rather refer to as my research guardians, Prof. Tom Dhaene and Prof. Luc Knockaert. I have enjoyed the opportunity to watch and learn from both of your knowledge and experience. Thanks for being more than a teacher-mentor, guide and philosopher. Thank you for blessing me.

I take this opportunity to also thank the IBCN research group and the INTEC Electromagnetic group, headed by Prof. Piet Demeester and Prof. Daniel De Zutter, respectively and all the technical and administrative staffs for helping me during my program. Would like to specially thank Mike Van Puyenbroeck, for his guidance during the initial admission phase. Also grateful to, Martine Buysse and Davinia Stevens with their constant support. I would also like to thank the Research Foundation Flanders (FWO) and the interuniversity Attraction Poles Programme BESTCOM initiated by the Belgian Science Policy Office for funding my PhD research.

Prof. Yves Rolain, Prof. Davy Pissoort, Prof. Joris Degroote and Dr. Dirk Deschrijver, I thank you all for being a part of my jury and helping me to improve the quality of my PhD thesis. A special thank you to Prof. Yves for teaching me ‘how to read a graph’.

I am grateful to Dr. Francesco Ferranti who helped me immensely to carry out a good research work and for providing a good foundation for me to build on my research. I also thank Dr. Dirk Deschrijver for introducing to me, many new modeling techniques and projects. Both of them were really helpful in achieving my PhD thesis. They always were open to research discussions and taught me how to write a research contribution.

I thank my colleagues Dr. Krishnan, Dr. Domenico, Dr. Ivo, Selvakumar and Joachim for their valuable time to discuss on though provoking research ideas.

I am thankful to my techno-economics colleagues: Marlies, do really appreciate the efforts you have put into bringing the office 3.19 together, though majority of times I was the missing link. Bram, thanks for visiting our country and hope to see you again in India. Frederic, thanks for appreciating our cuisine and your

mentality to help in any situation. Also would like to thank Jan, Gregory, Jonathan, Joeri and former colleagues Erik, Mathieu, Minh and Simon.

The stay in Gent would not have been pleasant without the friends I gained in my past four years: Krishnan, who helped us from the first day we came here and to Sreedha who made us feel we were back in Kerala, with her talks and hospitality. Selva and Prashant were like my small brothers and they did show that respect (which I never asked for) by calling me 'Chechii' (meaning big sister), wishing you both all the success. To have an Italian flavor, there was Domenico, who always cracked jokes and introduced me to lot of tasty Italian recipes. Also for the important Italian words that you have taught us and introducing us to Sonia. Sonia, thank you for joining the in between get together. Special thanks to my friends from Greece, Ioanna, Marina and Ioannis, for finding the time to gather for lunch and short coffee chit chats. I also would like to thank Arun, Amrita, Srinath, Mitra, Dinesh, Farhan, Neelum, Abhishek, Sachin and Hajar.

I would like to thank Jijo, Shalet and their boys who were always willing to help and for making us feel at home. Then also to all the little friends of my daughter, who tried their best to make me speak Netherlands and later settled for sign languages. Also would like to specially thank all my friends through Daikin: Baris, Öykü, Luoana, Stef and Seetha. I would like to thank Richard Hanze and Sonja Van de Walle for their support during our stay in Gent and for the help when we shifted our home.

In 2007, for the first time I came to Brussels for an assignment with 3M Belgium, never then thinking that in future I will be back for a doctoral program. I take this opportunity to thank my 3M manager Bruno Tuyls and his wonderful wife Marina, who took great care during my stay then, and also continue till now.

This opportunity would never have been fulfilled without my loving family and I dedicate my work to them. As said, to every girl her father is the hero and for me it is true. My late father, Chachen, taught me how important family is and this helped me to balance my professional and family life. No words can thank my Mummy for her constant support, through her prayers and love. Also would like to thank Appa and Amma, my in-laws, who is always there to help and to guide us in the challenges we take. Then to Skype and whatsapp, which connected me to my siblings to the parts of the world they are. I thank my elder sister and family: Chechii, Jeevanchettan, Sarah, Fiona; my brother and family: Manjit, Dane, Max, Ira; my youngest sister and family: Manju, Bobby, Ruthu; my brother-in-law and family: Sunu, Shwetha, Rachel, Jessa, Michelle and my sister-in-law and family: Betsy and Ciju, for being there for me. This acknowledgment would not be complete without a special mention to my motivator and family guide Manu (John Mathew), my husband and our sweet daughter Achu (Joanne), who helped me achieve this degree through all the ups and downs we had as a family.

*Gent, March 2015*  
*Elizabeth Rita Samuel*



# Table of Contents

<b>Acknowledgments</b>	<b>i</b>
<b>Samenvatting</b>	<b>xix</b>
<b>Summary</b>	<b>xxiii</b>
<b>1 Introduction</b>	<b>1</b>
1.1 Overview . . . . .	1
1.2 Research contributions . . . . .	3
1.3 Outline of the Thesis . . . . .	6
1.4 Publications . . . . .	9
1.4.1 Publications in international journals (listed in the Science Citation Index) . . . . .	9
1.4.2 Publications in book chapters . . . . .	10
1.4.3 Publications in international conferences (listed in the Science Citation Index) . . . . .	10
1.4.4 Publications in national conferences . . . . .	11
References . . . . .	12
<b>2 Introduction to Model Order Reduction and Parameterized Model Order Reduction</b>	<b>15</b>
2.1 Linear Time-Invariant Systems (LTI) . . . . .	15
2.1.1 State-space systems . . . . .	15
2.1.1.1 Descriptor Systems . . . . .	17
2.1.2 Moments . . . . .	17
2.1.3 Poles and Residues . . . . .	17
2.1.4 Stability . . . . .	18
2.1.5 Passivity . . . . .	18
2.2 Model Order Reduction . . . . .	18
2.2.1 Asymptotic Waveform Evaluation (AWE) . . . . .	21
2.2.2 Padé-via-Lanczos (PVL) . . . . .	21
2.2.3 Arnoldi and PRIMA . . . . .	22
2.2.4 Laguerre-SVD . . . . .	22
2.2.5 Balanced Truncation . . . . .	23
2.2.6 Proper Orthogonal Decomposition (POD) . . . . .	24

---

2.2.7	Multipoint MOR . . . . .	24
2.3	Parameterized Model Order Reduction (PMOR) . . . . .	25
2.3.1	Multiparameter moment matching . . . . .	25
2.3.2	Interpolation based PMOR . . . . .	26
2.3.2.1	PMOR based on input-output interpolation . . . . .	26
2.3.2.2	PMOR based on state-space interpolation . . . . .	27
	References . . . . .	28
<b>3</b>	<b>Model Order Reduction of Time-Delay Systems using a Laguerre Expansion Technique</b>	<b>31</b>
3.1	Introduction . . . . .	32
3.2	Overview of Laguerre-based Model Order Reduction . . . . .	34
3.3	Proposed algorithm . . . . .	36
3.3.1	Delay Approximation . . . . .	36
3.3.2	Reduced Order Estimation . . . . .	37
3.3.2.1	Zero-order Approximation Technique (ZAT) . . . . .	37
3.3.3	Higher-Order Laguerre Approximation Technique (HLAT) . . . . .	38
3.4	Numerical Results . . . . .	40
3.4.1	BPV: Backplane Vias . . . . .	42
3.4.2	RLC: RLC Network With Delay Elements . . . . .	46
3.5	Conclusion . . . . .	48
	References . . . . .	50
<b>4</b>	<b>A Hybrid Adaptive Sampling Algorithm for Multipoint Model order reduction</b>	<b>53</b>
4.1	Introduction . . . . .	54
4.2	Multipoint MOR for frequency independent state-space matrices using reflective exploration . . . . .	57
4.2.1	PRIMA . . . . .	57
4.2.2	Multipoint projection matrix . . . . .	58
4.2.3	Reflective Exploration . . . . .	58
4.2.4	Model compacting . . . . .	60
4.2.5	Passivity Preservation . . . . .	61
4.2.6	Numerical Results for frequency independent state-space matrices . . . . .	63
4.2.6.1	LTL: Lossless Transmission Line Example . . . . .	63
4.2.6.2	TL: Lossy Transmission Line . . . . .	67
4.2.6.3	MNA: Modified Nodal Analysis . . . . .	71
4.3	Multipoint MOR for frequency dependent state-space matrices using hybrid adaptive sampling algorithm . . . . .	74
4.3.1	Common projection matrix . . . . .	74
4.3.2	Hybrid Adaptive Sampling Algorithm . . . . .	74
4.3.2.1	Reflective exploration (RE) . . . . .	75
4.3.2.2	Binary search (BS) . . . . .	77
4.3.2.3	Model compacting (MC) . . . . .	77

4.3.3	Numerical Results for frequency dependent state-space matrices . . . . .	79
4.3.3.1	2TL: Two coupled transmission lines . . . . .	79
4.3.3.2	IEM: Inverted Embedded microstrip line . . . . .	85
4.4	Conclusion . . . . .	89
	References . . . . .	90
<b>5</b>	<b>Guaranteed Passive Parameterized Macromodeling by Using Sylvester State-Space Realizations</b>	<b>93</b>
5.1	Introduction . . . . .	94
5.2	Parameterized Macromodeling . . . . .	95
5.3	State-Space Realization For Parameterized Macromodeling . . . . .	96
5.3.1	Gilbert Realization . . . . .	96
5.3.2	Balanced Realization . . . . .	96
5.3.3	Barycentric Realization . . . . .	97
5.3.3.1	Passive Parameterized Interpolation . . . . .	99
5.3.4	Sylvester Realization . . . . .	102
5.4	Numerical Examples . . . . .	105
5.4.1	CM: Two Coupled Microstrip with Variable Spacing . . . . .	105
5.4.2	NF: Folded Stub Notch Filter with Variable Length and Variable Spacing . . . . .	112
5.5	Conclusion . . . . .	118
	References . . . . .	119
<b>6</b>	<b>Passivity-Preserving Parameterized Model Order Reduction using Singular Values and Matrix Interpolation</b>	<b>123</b>
6.1	Introduction . . . . .	124
6.2	Passivity-Preserving Parameterized Model Order Reduction using Singular Values and Matrix Interpolation . . . . .	126
6.2.1	Estimation of the reduced order based on Grammians . . . . .	126
6.2.2	Common projection matrix computation . . . . .	128
6.2.3	Multivariate Interpolation . . . . .	131
6.2.4	Systems with a special state-space form . . . . .	132
6.2.4.1	System with a general state-space form . . . . .	133
6.2.5	Numerical Results . . . . .	133
6.2.5.1	EM: EM model . . . . .	133
6.2.5.2	3MTL: Three coupled microstrip lines . . . . .	139
6.3	Model Order Reduction of Parameterized State-Space Systems with Sequential Sampling . . . . .	144
6.3.1	PMOR with Sequential Sampling . . . . .	144
6.3.1.1	Sequential Sampling . . . . .	144
6.3.2	5CM: Five Coupled Microstrip Lines . . . . .	145
6.4	Conclusion . . . . .	150
	References . . . . .	152

<b>7</b>	<b>Matrix Interpolation based Parametric Model Order Reduction for Multiconductor Transmission Lines with Delays</b>	<b>157</b>
7.1	Introduction . . . . .	158
7.2	Overview of Model Order Reduction for TDSs . . . . .	159
7.3	Parameterized Model Order Reduction . . . . .	160
7.3.1	Common projection matrix computation . . . . .	161
7.3.2	Multivariate Interpolation . . . . .	162
7.3.3	Complexity . . . . .	164
7.4	Numerical Examples . . . . .	164
7.4.1	CASE I: Variation in Length of the lossless TLs . . . . .	165
7.4.2	CASE II: Variation in Length of the TLs and P.U.L. parameters . . . . .	165
7.4.3	Computational complexity . . . . .	167
7.5	Conclusion . . . . .	168
	References . . . . .	170
<b>8</b>	<b>Conclusion</b>	<b>173</b>
8.1	Contribution . . . . .	173
8.1.1	Model order reduction . . . . .	173
8.1.2	Parameterized modeling . . . . .	174
8.2	Future scope . . . . .	175
	References . . . . .	178

# List of Figures

1.1	Idea of Model Order Reduction [11]	3
1.2	Idea of Parameterized Model Order Reduction	4
1.3	Schematic position of the different chapters in this dissertation	7
2.1	Not passive ROMs can produce unstable systems when connected to other stable, even passive, loads	18
2.2	Low dimensional subspace	19
2.3	Projecting a system of ODEs onto a low dimensional space.	20
2.4	The single point expansion based MOR.	24
2.5	The multiple point expansion based MOR.	25
2.6	Parameterized Model Order Reduction approaches (Orange arrows correspond to interpolation based PMOR and the blue arrows correspond to multiparameter moment matching).	26
3.1	Flowchart of the proposed algorithm.	41
3.2	BPV: Block Diagram of backplane vias.	42
3.3	BPV: Hankel Singular Values (state contributions) of the approximated model using ZAT.	43
3.4	BPV: Magnitude of $S_{14}$ .	44
3.5	BPV: Phase of $S_{14}$ .	45
3.6	BPV: Approximation of the delay term.	45
3.7	Schematic of RLC network including delay elements.	46
3.8	RLC: Magnitude of $Y_{14}$ .	47
3.9	RLC: Phase of $Y_{14}$ .	48
4.1	Reflective Exploration.	59
4.2	Truncation of the projection matrix.	62
4.3	LTL: Error per frequency used to select the new expansion point for the adaptive sampling loop.	64
4.4	LTL: RMS error between the iterated models during the addition of new expansion points.	65
4.5	LTL: Magnitude of lossless line $Y_{11}$ for each iterative step with the adaptively chosen expansion points.	65
4.6	LTL: Magnitude of lossless line $Y_{11}$ with the original response after model compacting.	66

4.7	TL: Error per frequency for the adaptive sampling loop. . . . .	68
4.8	TL: RMS error between the iterated models with new expansion points. . . . .	69
4.9	TL: Magnitude of lossy line $\mathbf{Y}_{11}$ for each iteration with the adaptively chosen expansion points. . . . .	69
4.10	TL: Magnitude of lossy line $\mathbf{Y}_{11}$ after model compacting. . . . .	70
4.11	MNA: Error per frequency used to select the new expansion point for the adaptive sampling loop. . . . .	71
4.12	MNA: Magnitude of $Y_{11}$ for each iterative step with the adaptively chosen expansion points. . . . .	72
4.13	MNA: Magnitude of $Y_{11}$ with the original response after model compacting. . . . .	73
4.14	Flowchart for Reflective Exploration. . . . .	76
4.15	Flowchart for Binary Search. . . . .	78
4.16	2TL: Magnitude of $Y_{11}$ for the different iteration steps of RE. . . .	81
4.17	2TL: Magnitude of $Y_{11}$ obtained with BS. . . . .	82
4.18	2TL: Singular value of the common projection matrix. . . . .	83
4.19	2TL: Variation of matrix element with frequency. . . . .	83
4.20	2TL: Magnitude of $Y_{11}$ obtained using the HAS algorithm. . . . .	84
4.21	2TL: Relative error of the original model with the reduced order models obtained from RE and BS. . . . .	84
4.22	IEM: Cross section of IEM line. . . . .	85
4.23	IEM: Variation of matrix element with frequency. . . . .	86
4.24	IEM: Magnitude of $Y_{11}$ obtained using the HAS algorithm. . . . .	87
4.25	IEM: Relative error of the original model with the reduced order models obtained from RE and BS. . . . .	87
4.26	IEM: Magnitude of $Y_{13}$ obtained using the HAS algorithm. . . . .	88
4.27	IEM: Phase of $Y_{13}$ obtained using the HAS algorithm. . . . .	88
5.1	CM: Two coupled microstrips. . . . .	105
5.2	CM: Eigenvalues of the pivot matrix and the <i>root macromodels</i> obtained from Gilbert realization. . . . .	106
5.3	CM: Magnitude of the bivariate macromodel $S_{11}(s, S)$ (Sylvester realization). . . . .	107
5.4	CM: Magnitude of the bivariate macromodel of $S_{11}(s, S)$ ( $S = \{1.08, 2.08, 2.91\}$ mm using the Sylvester realization. . . . .	108
5.5	CM: Error comparison for the different realizations. . . . .	109
5.6	CM: Model poles as a function of spacing for the <i>root macromodels</i> . . . . .	109
5.7	CM: Magnitude of the bivariate macromodel $S_{11}(s, S)$ using the Gilbert realization. . . . .	110
5.8	CM: Poles of the bivariate macromodel $S(s, S)$ using the Sylvester realization. . . . .	111
5.9	CM: $H_\infty$ norm for the bivariate macromodel $S(s, S)$ using the Sylvester realization. . . . .	111
5.10	NF: Layout of the folded stub notch filter. . . . .	112

5.11	NF: Eigenvalues of the pivot matrix and the <i>root macromodels</i> obtained from Gilbert realization. . . . .	113
5.12	NF: Magnitude of the trivariate macromodel $S_{12}(s, L, S)$ for $S = 0.5\text{mm}$ using Sylvester realization. . . . .	114
5.13	NF: Magnitude of the trivariate macromodel for $S = 0.6\text{ mm}$ of $S_{12}(s, L, S)$ ( $L = \{5.5, 6.5, 7.5, 8.5\}\text{ mm}$ ) using Sylvester realization. . . . .	115
5.14	NF: Error comparison for the different state-space realizations. . .	115
5.15	NF: Magnitude of the trivariate macromodel $S_{12}(s, L, S)$ using balanced realization for each <i>root macromodel</i> ). . . . .	116
5.16	NF: An entry of the $A_{\bar{p}}$ . . . . .	116
5.17	NF: Poles of the trivariate macromodel $S(s, L, S)$ using Sylvester realization. . . . .	117
5.18	NF: $H_\infty$ norm of the trivariate macromodel $S(s, L, S)$ (Sylvester realization). . . . .	117
6.1	Example of an uniformly sampled estimation and validation design space grids. . . . .	126
6.2	Flowchart of the proposed technique. . . . .	130
6.3	EM: Cross section of multiconductor system. . . . .	134
6.4	EM: Singular values of the projection matrix (best-case <i>local</i> approach). . . . .	135
6.5	EM: Magnitude of $\mathbf{Y}_{16}(s, S_x, S_y)$ for $S_x = 1.2\text{ mm}$ . . . . .	136
6.6	EM: Magnitude of $\mathbf{Y}_{16}(s, S_x, S_y)$ for $S_x = 1.2\text{ mm}$ and $S_y = 2.1\text{ mm}$ using a best-case <i>local</i> projection. . . . .	137
6.7	EM: RMS error using the <i>local</i> approach for the design space. . .	137
6.8	EM: Singular values of the projection matrix (best-case <i>global</i> approach). . . . .	138
6.9	EM: Magnitude of $\mathbf{Y}_{16}(s, S_x, S_y)$ for $S_x = 1.3\text{ mm}$ and $S_y = \{2.2, 2.5, 2.9\}\text{ mm}$ using a best-case <i>global</i> common projection matrix. . . . .	138
6.10	3MTL: Cross section of three coupled microstrip line. . . . .	139
6.11	3MTL: Singular values of the projection matrix (best-case <i>global</i> approach). . . . .	140
6.12	3MTL: Magnitude of $\mathbf{Y}_{11}(s, S, L)$ for $S = 200\text{ }\mu\text{m}$ . . . . .	141
6.13	3MTL: Magnitude of $\mathbf{Y}_{11}(s, S, L)$ for $S = 200\text{ }\mu\text{m}$ and $L = \{3, 5\}\text{ cm}$ using a best-case <i>global</i> common projection matrix. . .	142
6.14	3MTL: Singular values of the projection matrix (best-case <i>local</i> approach). . . . .	142
6.15	3MTL: Magnitude of $\mathbf{Y}_{11}(s, S, L)$ for $S = 246.15\text{ }\mu\text{m}$ and $L = 3\text{ cm}$ using a best-case <i>local</i> projection. . . . .	143
6.16	Division of the design space. . . . .	145
6.17	Flowchart of sequential sampling algorithm. . . . .	146
6.18	5CM: Layout of five coupled microstrip. . . . .	147
6.19	Hankel singular values of a node. . . . .	148

6.20	Sequentially sampled design space (validation points marked as *)	149
6.21	5CM: Magnitude bivariate PMOR $S_{1\ 8}(L, S)$ for $S = 0.045$ mm.	149
6.22	5CM: Magnitude bivariate PROM $S_{1\ 10}(L, S)$ for $L = 12.8$ mm. .	150
6.23	5CM: Magnitude of $S_{11}$ at validation points (uniform and sequential sampling). . . . .	151
7.1	Schematic of RLC network including delay elements [8]. . . . .	164
7.2	Magnitude of input admittance parameter $Y_{11}(s, d)$ for $d = \{1.083, 1.25, 1.42\}$ cm. . . . .	166
7.3	Phase of input admittance parameter $Y_{11}(s, d)$ for $d = \{1.083, 1.25, 1.42\}$ cm. . . . .	167
7.4	PMOR of transfer admittance parameter $Y_{13}(s, d, T)$ for $T = 30^\circ\text{C}$ .	168
7.5	Comparison of the computational efficiency. . . . .	169
8.1	Contribution (orange solid line boxes) and future scope (purple dotted line boxes). . . . .	176



## List of Tables

3.1	BPV: Efficiency comparison for achieving a weighted RMS error of 0.001 . . . . .	43
3.2	BPV: Computational Information . . . . .	44
3.3	RLC: Efficiency comparison for achieving a weighted RMS error of 0.001 . . . . .	47
3.4	RLC: Computational Information . . . . .	48
4.1	LTL: Adaptive truncation for model compacting. . . . .	64
4.2	TL: Adaptive truncation for model compacting. . . . .	68
4.3	MNA: Adaptive truncation for model compacting. . . . .	72
4.4	Threshold values set for the HAS algorithm. . . . .	79
4.5	2TL: Sampling and Modeling in Reflective Exploration with RMS error. . . . .	80
4.6	2TL: Sampling using Binary Search. . . . .	81
4.7	2TL: Adaptive truncation for model compacting. . . . .	82
4.8	IEM: Sampling and Modeling in Reflective Exploration with RMS error. . . . .	85
4.9	IEM: Samples, Size of ROM and Computation time for each step of the HAS algorithm. . . . .	86
5.1	CM: Parameters of the coupled microstrip . . . . .	105
5.2	CM: Comparison of the different techniques . . . . .	107
5.3	NF: Parameters of the folded stub filter . . . . .	112
5.4	NF: Comparison of the different techniques . . . . .	113
6.1	Column size ( $w$ ) of the Projection matrix ( $\mathbf{P}_{union}$ ) . . . . .	130
6.2	EM:Parameters of the model . . . . .	134
6.3	EM:Column size of the projection matrix with computation time . . . . .	136
6.4	3MTL:Parameters of the model . . . . .	139
6.5	3MTL: Column of projection matrix with computation time . . . . .	143
6.6	Parameters of coupled microstrips . . . . .	147
6.7	5CM: Comparison of Mean Absolute Error . . . . .	148



# List of Acronyms

## A

ADI	Alternating Direction Implicit
ADS	Advanced Design System
ARE	Algebraic Riccati Equation
AWE	Asymptotic Waveform Evaluation

## B

BESTCOM	BELgian network on STochastic modeling, analysis, design and optimization of COMMunication systems
BIBO	Bounded-Input Bounded-Output
BS	Binary Search

## C

CM	Coupled Microstrip
----	--------------------

## E

EDA	Electronic Design Automation
EM	Electromagnetic

## F

FD	Frequency Domain
FDEs	Functional Differential Equations

FE	Finite Element
FWO	Research Foundation Flanders

## H

HAS	Hybrid Adaptive Sampling
HLAT	Higher-order Laguerre Approximation Technique
HSV	Hankel Singular Value

## I

ICs	Integrated Circuits
IEEE	Institute of Electrical and Electronics Engineers
IEM	Inverted Embedded Microstrip

## L

LMI	Linear Matrix Inequality
LTI	Linear Time-Invariant

## M

MC	Model Compacting
MIMO	Multi-Input Multi-Output
MMTs	Moment Matching Techniques
MNA	Modified Nodal Analysis
MOR	Model Order Reduction
MoC	Method of Characteristics
MTL	Multiconductor Transmission Line

## N

NF	Notch Filter
----	--------------

**O**

ODEs                      Ordinary Differential Equations

**P**

PCB                      Printed Circuit Board  
PIMTAP                  Parameterized Interconnect Macromodeling via a Two-  
                                directional Arnoldi Process  
PMOR                    Parameterized Model Order Reduction  
POD                      Proper Orthogonal Decomposition  
PRIMA                   Passive Reduced-order Interconnect Macromodeling  
                                Algorithm  
PROM                    Parameterized Reduced Order Model  
P.U.L.                    Per-Unit-Length  
PVL                      Padé-via-Lanczos

**R**

RE                       Reflective Exploration  
RMS                      Root Mean Square  
ROMs                    Reduced Order Models

**S**

SI                        Signal Integrity  
SISO                    Single-Input Single-Output  
SVD                      Singular Value Decomposition

**T**

TD                       Time Domain  
TDSs                    Time Delay Systems  
TLs                      Transmission Lines

## **Z**

ZAT                      Zero-order Approximation Technique







# Samenvatting

## – Summary in Dutch –

Naargelang de grootte afneemt en complexiteit toeneemt van de huidige geïntegreerde schakelingen is er een nood aan innovatieve ontwerptechnieken. Omwille van de trend naar hogere kloksnelheden is het belangrijk om rekening te houden met de interacties tussen schakelingen en hun omliggende componenten. Hierdoor winnen nauwkeurige circuitsimulatie methodes aan belang. Een manier om dit probleem aan te pakken is door gebruik te maken van snellere computer hardware. Soms is het probleem niet enkel gerelateerd aan de omvang van het circuit, maar ook aan de tijd die simulaties innemen of de complexiteit van het model. Derhalve de efficiëntie van het simulatieproces te verbeteren is het belangrijk om bijzondere kenmerken van het probleem te benutten met behulp van een algoritme of techniek.

Een mogelijke aanpak maakt gebruik te maken van Model Orde Reductie (MOR) technieken. MOR capteert de belangrijkste kenmerken van de schakeling en berekent hiervoor een vereenvoudigd dynamisch model. Dit leidt tot meer efficiënte berekeningen, een lagere opslagcapaciteit en hogere accurate. Basistechnieken voor MOR werden reeds in de jaren tachtig en jaren negentig voorgesteld. Technieken zoals de afgeknotte evenwichtige realisatie (TBR), Hankel norm reductie en een orthogonale decompositie (POD) zijn speciaal ontwikkeld geweest voor systeem- en controle theorie. Technieken die gebaseerd zijn op Krylov deelruimten zoals Padé via Lanczos, PRIMA en Laguerre-SVD werden later ontwikkeld. Het compact modelleren van passieve RLC interconnecties is een intensief onderzoeksgebied omwille van dominante vertragingseffecten in het huidige systeem-op-een-chip ontwerp en het belang van signaalintegriteit. De Krylov MOR technieken zijn ook uitgebreid naar systemen met vertraging en niet-lineair gedrag. Om accurate gereduceerde modellen te genereren over het gehele frequentiebereik kan een meerpunts MOR gebruikt worden.

MOR technieken voeren enkel reductie uit met betrekking tot de tijd of frequentie. Tijdens het ontwerp van grootschalige systemen is het ook essentieel om het gedrag van een schakeling als functie van ontwerpveranderlijken te bestuderen, zoals omgevingsveranderlijken, thermische effecten, productvariaties en schommelingen in de kritische afmetingen van geometrische veranderlijken. Een typische ontwerpprocedure die optimalisatie en ontwerpverkenning van de ruimte omvat, vereist herhaalde simulaties voor verschillende waarden van de ontwerpveranderlijken. Het is vaak niet mogelijk om een groot aantal simulaties van grote

circuits uit te voeren vanwege de grote rekenkost per simulatie. Deze ontwerpactiviteiten vragen om de ontwikkeling van parametrisatietechnieken.

Geparametriseerde model orde reductie (PMOR) werkwijzen kunnen grote stelsels vergelijkingen reduceren met betrekking tot tijd en frequentie en ook andere ontwerpveranderlijken van de schakeling. Ze zijn daarom goed geschikt om ontwerpactiviteiten efficiënter uit te voeren. De twee belangrijkste klassen van PMOR technieken zijn multiparameter moment matching en multivariate interpolatie. De eerste methode bepaalt een gemeenschappelijke projector die de informatie over het systeem en parameters bewaart; de laatste reduceert elk systeem met meerdere veranderlijken met behulp van hun individuele projectoren en verkrijgt een globaal PMOR model via multivariate interpolatie. De interpolatie kan worden uitgevoerd op de ingang-uitgang representatie (overdrachtsfunctie) en de toestandsruimte matrices.

Dit proefschrift richt zich voornamelijk op interpolatie gebaseerde PMOR technieken en bespreekt er verschillende aspecten van, zoals het schatten van de gereduceerde orde, lokale versus globale aanpak, het behoud van systeemeigenschappen en het compacteren van de gemeenschappelijke projectiematrix voor de ontwerprijimte op basis van singuliere waarde ontbinding. Ook de voordelen van het combineren van een sequentiële sampling techniek samen met een PMOR techniek worden geïllustreerd.

Een geparametriseerd model kan ook worden verkregen via het identificatieproces uitgaande van een set van multivariate datapunten. Zoals eerder vermeld, kan het geparametriseerde model worden verkregen door multivariate interpolatie van de frequentie respons of toestandsruimte matrices. De passieve interpolatie van de toestandsruimte matrices van een aantal univariate modellen geeft een verhoogd modelleringsvermogen ten opzicht van input-output interpolatie, maar is meer gevoelig voor problemen met de gladheid van de toestandsruimte matrices als een functie van de veranderlijken.

Het proefschrift is als volgt opgebouwd: Hoofdstuk 1 geeft een algemene inleiding van het werk en de grote onderzoeksbijdragen. In Hoofdstuk 2 wordt een literatuuroverzicht gegeven over de verschillende MOR en PMOR technieken. Een korte introductie over lineaire tijd-invariante (LTI) systemen worden gegeven, alsook de algemene notaties die worden gebruikt in de volgende hoofdstukken. In hoofdstuk 3 wordt de hogere orde Krylov deelruimte MOR techniek voor tijdsvertraagde systemen (TDSs) gepresenteerd die gebaseerd is op Laguerre expansies. Hoofdstuk 3 presenteert een gereduceerde orde schattingstechniek voor TDSs. In Hoofdstuk 4, het wordt het belang van meerpuntsexpansie MOR technieken geïntroduceerd en een hybride adaptieve frequentiebemonsteringstechniek wordt gepresenteerd. In het eerste deel van hoofdstuk 4 wordt de reflectieve exploratie techniek geïntroduceerd voor quasi-statische systemen, d.w.z. systemen die beschreven zijn door frequentieonafhankelijke toestandsruimte matrices. Vervolgens wordt de techniek toegepast op systemen met frequentieafhankelijke toestandsruimte matrices. Om het systeem te valideren wordt het model zoals verkregen na reflecterende exploratie verder verfijnd middel van een binaire zoektocht. Het afknotten van de gemeenschappelijke projectie matrix op basis van de

singuliere waarden wordt geïntroduceerd in hoofdstuk 4. Vervolgens wordt een unieke realisatie voor de interpolatie van toestandsruimte matrices van ontwerp veranderlijken besproken in hoofdstuk 5. De Sylvester realisatie wordt geïntroduceerd in hoofdstuk 5 en vergeleken met de Gilbert realisatie, de gebalanceerde realisatie en barycentrische realisatie wat de nauwkeurigheid van de voorgestelde techniek illustreert. In hoofdstuk 6 wordt passiviteitsbewarende PMOR met behulp van singuliere waarden en matrix interpolatie voorgesteld. In hoofdstuk 6 worden twee strategieën voorgesteld voor de schatting van de gereduceerde orde voor een ontwerpruimte in PMOR. De techniek kan als lokaal of globaal worden geïnterpreteerd en afhankelijk van het scenario varieert de computationele complexiteit en nauwkeurigheid zoals aangetoond in hoofdstuk 6. In het tweede deel van hoofdstuk 6 wordt aangetoond dat de totale simulatiekosten gereduceerd kunnen worden door het implementeren van een sequentiële bemonsteringstechniek om veranderlijken te modelleren. In Hoofdstuk 7 wordt de in hoofdstuk 6 voorgestelde PMOR techniek uitgebreid tot TDSs die gemodelleerd worden met behulp van de methode der karakteristieken (MOC). In Hoofdstuk 7 wordt een adaptief algoritme ingevoerd voor het afknotten van de gemeenschappelijke projectiematrix. Tot slot wordt het proefschrift afgerond met conclusies en een uitzicht op toekomstige werkzaamheden in hoofdstuk 8.



# Summary

Design techniques are increasingly elaborate and innovative with the decreasing size and increasing complexity of today's integrated circuits. Also with the ongoing trend of increasing the speed of operations, it is important to take into account the interaction between the circuits and its surrounding, thereby necessitating accurate circuit simulation methods. One way to address this issue is through the use of faster computer hardware. However, at times the difficulty may not only be related to the size of the circuit but also on the time needed for the simulations, or on the model complexity involved. Thus to improve the efficiency of the simulation process it is important to exploit the characteristic features of the particular problem using some algorithm or technique. One way to do this is by using model order reduction (MOR) techniques.

MOR captures the essential feature of a circuit and provides a simplified dynamical model for it. This yields efficient computation and storage capacity with reliable accuracy. Basic techniques for MOR were proposed in the 80's and 90's of the last century. Techniques like truncated balanced realization, Hankel-norm reduction and proper orthogonal decomposition were developed especially for system and control theory. Later techniques based on Krylov subspaces are mainly Padé via Lanczos, PRIMA and Laguerre-SVD. Compact modeling of passive RLC interconnects has been an intensive research area owing to the increasing signal integrity and dominant delay effects in current system-on-a-chip design. The Krylov MOR techniques have also been extended to systems with delays and nonlinearities. To generate accurate reduced models over the whole frequency range of interest, multipoint MOR has recently been proposed.

MOR techniques perform model order reduction only with respect to time or frequency. However, during the circuit design synthesis of large-scale systems, it is also essential to analyze the response of a circuit as a function of design parameters, such as environmental effects, thermal effects, manufacturing variations and fluctuations in the critical dimensions of geometrical layout features. A typical design procedure includes optimization and design space exploration, and thus requires repeated simulations for different design parameter values. It is often not feasible to perform multiple simulations of large circuits, due to the high computational cost per simulation. These design activities call for the development of parameterization techniques.

Parameterized model order reduction (PMOR) methods can reduce large systems of equations with respect to time or frequency and also other design parameters of the circuit and are therefore well suited to efficiently perform design

activities. The two main classes of PMOR techniques are multiparameter moment matching and multivariate interpolation. The former finds a common projector which preserves the information about system and parameters; the latter reduces each system with different parameters using their individual projectors and obtains a global PMOR model by multivariate interpolation. The interpolation can be performed using input-output representation (transfer function) and state-space matrices.

This PhD thesis focuses mainly on interpolation based PMOR techniques and discusses different aspects, such as the estimation of the reduced order, *local* versus *global* approaches based on the design space, preservation of system properties and compacting the common projection matrix for the design space based on singular values. Also the advantages of combining a sequential sampling technique along with a PMOR technique is illustrated.

A parameterized model can also be obtained via the identification process starting from a set of multivariate data samples. As mentioned before, the parameterized model can be obtained by the multivariate interpolation of input-output or state-space matrices. The passive interpolation of the state-space matrices of a set of root models provides an increased modeling capability over input-output interpolation, but is sensitive to issues related to the interpolation of state-space matrices, such as the smoothness of the state-space matrices as a function of the parameters.

The PhD thesis is organized as follows: Chapter 1 gives a general introduction of the work and the major research contributions. In Chapter 2 a literature survey is provided about the different MOR and PMOR techniques. Also a brief introduction to linear time-invariant (LTI) systems is provided with the general notations that will be used in the following chapters. In Chapter 3, the higher order Krylov subspace MOR technique for time-delay systems (TDSs) based on Laguerre expansions is presented. Chapter 3 also presents a reduced order estimation technique for TDSs. In Chapter 4, the importance of multi point expansion MOR techniques are introduced and an hybrid adaptive frequency sampling technique is presented. In the first part of Chapter 4, the reflective exploration technique is introduced for quasi-static systems i.e., systems described by frequency independent state-space matrices. Then the technique is applied to systems with frequency dependent state-space matrices. In order to validate the system the model obtained after reflective exploration is further refined using a binary search. The truncation of the common projection matrix based on the singular values is introduced in Chapter 4. Next the significance of a unique realization for the interpolation of state-space matrices for parameterized modeling is discussed in Chapter 5. The Sylvester realization is introduced in Chapter 5 and is compared with Gilbert realization, Balanced realization and Barycentric realization to illustrate the accuracy of the proposed technique. In Chapter 6, passivity-preserving PMOR using singular values and matrix interpolation is proposed. In Chapter 6 two strategies are proposed for the estimation of the reduced order for a design space in PMOR. Also the technique can be interpreted in two ways as *local* or *global* and depending on the scenario the computational complexity and the accuracy varies as demon-

strated in Chapter 6. In the second part of Chapter 6 it is shown that the overall simulation cost can be reduced by implementing a sequential sampling approach for parameterized modeling. In Chapter 7 the PMOR technique proposed in Chapter 6 is extended to TDSs that are modeled using method of characteristics (MoC). In Chapter 7 an adaptive algorithm is introduced for the truncation of the common projection matrix. Finally, the dissertation is finalized with conclusions and future work in Chapter 8.





# 1

## Introduction

*“We have no idea about the 'real' nature of things ... The function of modeling is to arrive at descriptions which are useful.”*

–Richard Bandler and John Grinder (1979)

Computational science has become an important part of today's technological world and can be considered as a discipline on its own, besides the discipline of theory and experiments. Computer simulations are now performed routinely for a wide variety of processes, and virtual design environments have been set up for a variety of problem classes in order to ease the work of designers and engineers. In this way new products can be made faster and more reliable. The ever increasing demand for realistic simulations of complex products represents a great challenge for researchers working in the area of computational science and engineering. Realistic simulations imply that the errors of the virtual models should be small and a variety of the different features of the product must be taken into account [1].

### 1.1 Overview

The rapid advances of high frequency circuit technology have significantly affected the construction of different types of microwave, millimeter-wave, optical and VLSI devices commonly used in mobile communications, radio links, optical communications, and various other automotive electronics systems. Electrically

large electromagnetic (EM) structures are involved in the current wireless systems such as waveguides, antennas, microwave circuits, and optical components, which are very complex in both geometry and material properties [2]. The advances in circuit technology have significantly reduced the feature size of high-speed electronic circuits and increased the density of chips. Therefore it is important to meet the need for efficient analysis and design tools for simulating and modeling the behavior of such structures. Moreover, circuit designers also demand that the simulation techniques be fast and run on relatively small computing platforms, such as standard personal computers [2]. Hence at higher frequencies, integrated and microwave circuits require fast and accurate modeling and simulation techniques for the optimization and design space exploration problems. All together, this implies that in order to describe an EM structure properly, it is necessary to construct mathematical models which may contain many variables. In order to perform simulations, it becomes necessary to approximate those models by models of lower complexity, while approximately maintaining the same behavior. This is known as model order reduction (MOR) [1, 3–7]. MOR has a long history in the systems and control literature. The main idea is that a high-dimensional state vector might belong to a low-dimensional subspace. When the low-dimensional subspace is known, the dynamical system can be projected on it. This projection yields the required low-dimensional approximation. Model reduction aims to substantially increase the applicability of the traditional methods to structures such as vias, high-speed packages, interconnects, and on-chip passive components [8–10].

The concept of MOR is founded mathematically in eigenvalue or singular value (SVD) problems, and as this requires a considerable amount of computation, it would be helpful if one could reduce the size of the model while keeping the accuracy of the eigenvalue or SVD decomposition. Fundamental ideas and theories which are used in MOR are developed from solving eigenvalue or SVD problems. The application of MOR is especially important in the control engineering field because reduced order models (ROMs) are very convenient to design a controller. The demands for MOR also arises from structural analysis, especially as the finite element (FE) analysis is nowadays widely used. The principle of the FE method is approximating a continuous physical structure by discretized elements. As the structure is divided into finer elements, the approximated model is closer to the real structure. To increase the accuracy of structural analysis, a complex large structure needs to be divided into small elements. Consequently the model has a very large size, that increases proportionally to the number of elements in the structure. Several hundred thousand degrees of freedom can result to large, complex structures. This increases the computational time and effort, which is undesirable. Here MOR comes into the picture, since it enables a formal approximation of the physical model and hence, the generation of a compact model suitable for system level simulation as shown in Fig. 1.1.

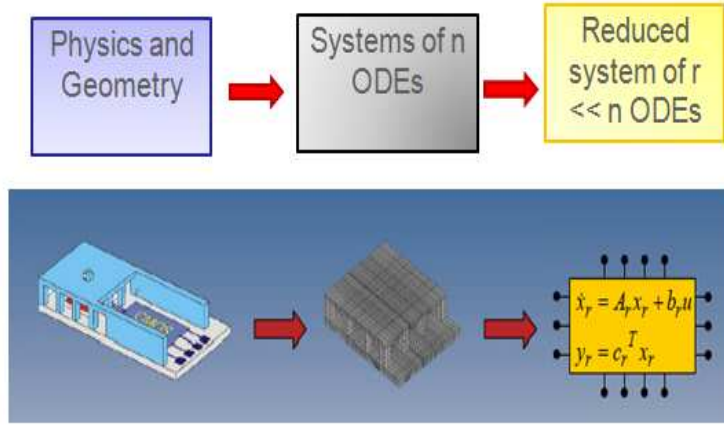


Figure 1.1: Idea of Model Order Reduction [11]

Traditional MOR techniques perform model order reduction only with respect to time or frequency. However, during the circuit design synthesis of large-scale applications, it is also essential to analyze the response of a circuit as a function of design parameters, such as geometrical and other features. A typical design procedure includes optimization and design space exploration. It requires repeated simulations for different design parameter values. Parameterized model order reduction (PMOR) methods can reduce large systems of equations with respect to time or frequency and also other design parameters and therefore are well suited to efficiently perform design activities. Fig. 1.2 (a) and Fig. 1.2 (b) plots the system response with respect to frequency for a value of length (parameter) and with respect to length for a frequency point respectively. In Fig. 1.2 (c) a parameterized model is plotted with respect to frequency and length which helps in better analysis of the system.

PMOR not only makes the model smaller. It also reduces model manageable with respect to the effects of the parameters, so that once the model reduction phase is over, the reduced model with general parameter values can be obtained from the reduced space only, regardless of the original large model; this ability is of course very useful in optimization problems.

## 1.2 Research contributions

This PhD thesis focuses on efficient MOR and PMOR techniques for linear systems and time-delay systems (TDSs) using state-space matrices. The challenging need for building a computationally efficient parameterized model and a reduced order model over the design space of interest is addressed by novel techniques.

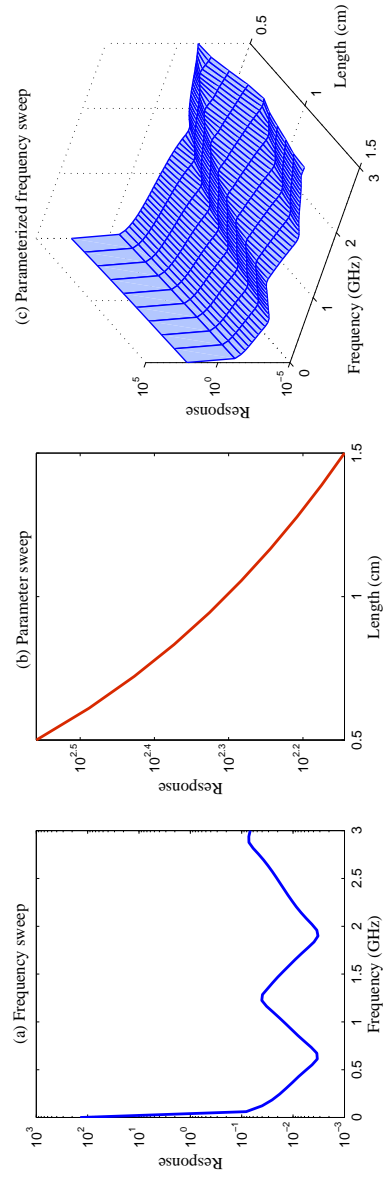


Figure 1.2: Idea of Parameterized Model Order Reduction

When the signal waveform rise time decreases and the corresponding spectral content increases, the geometric dimensions become electrically large. Time delays must be taken into account and included in the modeling [12, 13]. This PhD thesis proposes a higher order Krylov subspace algorithm for MOR of TDSs based on a Laguerre expansion technique to incorporate this delay. A zero-order approximation technique is also proposed to estimate the reduced order for the MOR. This tackles an important and practical common problem in prominently used order-reduction techniques, is namely the estimation of the reduced order for the reduced model. The proper choice of order is important to achieve the pre-defined accuracy.

The model obtained after MOR must not only be accurate in the vicinity of a single point in the frequency range but also over the whole frequency range of interest. To implement this, multipoint reduction algorithms have been developed over the years [5, 14, 15]. These allow to generate accurate reduced models over the whole frequency range of interest. This PhD thesis proposes an hybrid adaptive sampling algorithm for the selection of the expansion points for systems described with frequency independent and frequency dependent state-space matrices. In order to have an optimum number of frequency samples, the proposed algorithm uses a reflective exploration (RE) technique for the adaptive selection of the samples. The sampling is further refined using a binary search (BS). RE is a selective sampling technique. The model is improved incrementally using the best possible data at every step. It uses the reflective functions to propose candidate exploration points [16]. RE is an effective technique to be used when it is expensive to obtain the actual model response from the EM simulator.

MOR is known to be an efficient tool for replacing very large dynamical systems in numerical simulations by systems of much smaller dimension while keeping a desired accuracy in the approximation of the original system response. However, significant modifications to the underlying physical model such as geometric variations, changes in material properties, or alterations in boundary conditions are usually not dealt with in the ROMs. This motivates the development of new model reduction methods which preserve the parameterized dependence of the original system in the ROM. For such cases PMOR has proved to be an efficient and accurate technique [17–21]. The PMOR technique reduces large systems of equations with respect to time or frequency and also other design parameters and is therefore well suited to efficiently perform design activities. In this PhD thesis, an efficient state-space interpolation technique is proposed for obtaining accurate PMOR's. The technique introduces two strategies for the estimation of the reduced order for the design space as it is important for repeated simulation tasks to avoid unnecessary computational cost. A common projection matrix is found locally or globally as per the designer requirement. This PhD thesis also demonstrates the importance of sequential sampling for selecting the interpolation root models and building the

parameterized models. It is shown that sequential sampling algorithms can significantly reduce the model generation cost.

The parameterized models can also be obtained by the interpolation of the transfer function [17–19, 21] or by the interpolation of the state-space matrices [20] of multivariate data obtained through an identification process. In comparison to the transfer function interpolation, in state-space matrices based interpolation the matrices of the same order are interpolated and hence the model order is kept the same throughout the design space considered. Thus in general state-space interpolation gives a more compact model. In the literature an interpolation based on amplitude and frequency scaling coefficients has been proposed which overcomes the problem of model oversize with transfer function interpolation [22]. Also, state-space interpolation helps to parameterize the poles and residues of the system and hence has a higher modeling capability in comparison with transfer function interpolation.

Unfortunately, it is known that state-space matrices do not have a unique realization, which could affect the assumed smoothness of the state-space matrices with respect to the design parameters. To address this the PhD thesis proposes a novel state-space realization using a Sylvester technique. The Sylvester technique is used in combination with suitable interpolation schemes to interpolate a set of state-space matrices, and hence the poles and residues indirectly, in order to build accurate parameterized macromodels. The key points of the technique are the choice of a proper pivot matrix and a well-conditioned solution of a Sylvester equation. Stability and passivity are guaranteed by construction over the design space of interest.

### 1.3 Outline of the Thesis

An overview of the different chapters is provided in the following paragraphs and is indicated schematically in Fig. 1.3.

#### Chapter 2

Chapter 2 first gives a basic introduction to LTI systems and basic notations that are necessary for understanding the main chapters of this PhD thesis. Then an overview of the different MOR techniques is briefly discussed in Section 2.2. In this PhD thesis the PRIMA and Laguerre-SVD based MOR techniques are in general used for the algorithms. In the next section the PMOR techniques are described based on two main streams, i.e., the multiparameter moment matching method and the interpolation based method.

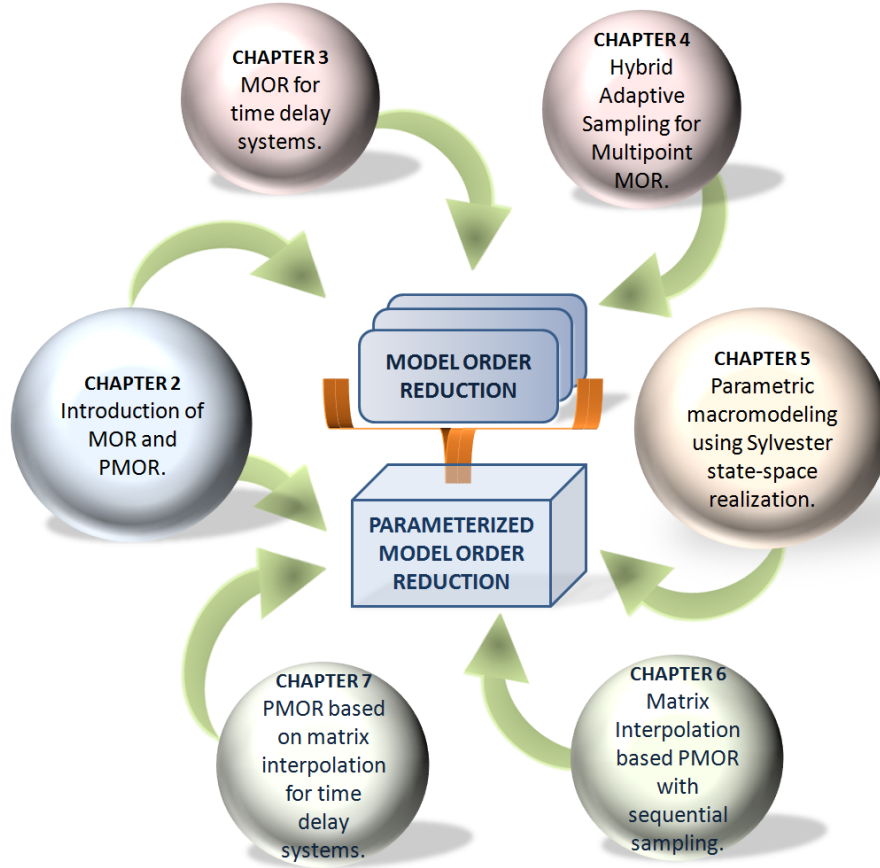


Figure 1.3: Schematic position of the different chapters in this dissertation

### Chapter 3

Chapter 3 provides a MOR technique for large scale systems that is described by delayed differential equations. The technique is a generalization and extension of the well-known Laguerre-SVD method to TDSs. The algorithm proposes a Laguerre expansion for the delays together with a higher-order Krylov subspace technique for obtaining the ROMs for the TDSs.

### Chapter 4

Chapter 4 deals with the importance of adaptive frequency sampling for multipoint MOR techniques using reflective exploration. In the first part of Chapter 4 the reflective exploration technique is discussed using frequency independent

state-space matrices and in the second part a hybrid adaptive sampling technique is proposed. The hybrid adaptive sampling technique is a combination of a reflective exploration and a binary search technique, which illustrates the generation of ROMs for systems described by large scale frequency dependent state-space models. The importance of optimizing the sampling over the frequency range of interest in order to avoid oversampling or undersampling is demonstrated.

## **Chapter 5**

In Chapter 5 a novel state-space realization is proposed to build accurate parameterized macromodels. An intelligent choice of the state-space realizations is required for the state-space interpolation. This is needed in order to guarantee the assumed smoothness of state-space matrices with respect to the design parameters. The technique also guarantees stability and passivity of the model by construction over the design space of interest.

## **Chapter 6**

Chapter 6 presents a PMOR method based on singular values and matrix interpolation. The design space is divided into cells and a Krylov subspace is computed for each cell. Next the merged Krylov subspace is truncated with respect to its singular values to obtain a common projection matrix for the design space. Finally, the reduced system matrices are interpolated using positive interpolation schemes to obtain a guaranteed passive parameterized reduced order model. Chapter 6 also demonstrates the importance of sequential sampling for selecting the interpolation nodes and building the PMOR. It is shown that sequential sampling algorithms can significantly reduce the model evaluation cost.

## **Chapter 7**

Chapter 7 is an application of Chapter 6 to time-delay systems. As introduced in Chapter 3, the delays are approximated using an expansion series and uses higher-order Krylov subspace based MOR. An adaptive truncation of the singular values of the common projection matrix for the design space considered is introduced in this Chapter.

## **Conclusions**

A summary of the research contributions of this PhD thesis is provided in this chapter. The possibilities for future directions are also discussed.



## 1.4 Publications

The research results obtained during this PhD research have been published in scientific journals and presented at a series of international conferences. The following list provides an overview of the publications during my PhD research.

### 1.4.1 Publications in international journals (listed in the Science Citation Index<sup>1</sup>)

1. **Elizabeth Rita Samuel**, Luc Knockaert, Francesco Ferranti, Tom Dhaene. *Guaranteed Passive Parameterized Macromodeling by Using Sylvester State-Space Realizations*. Published in IEEE Transactions on Microwave Theory and Techniques, 61(4):1444–1454, April 2013.
2. **Elizabeth Rita Samuel**, Francesco Ferranti, Luc Knockaert, Tom Dhaene. *Passivity-Preserving Parameterized Model Order Reduction Using Singular Values and Matrix Interpolation*. Published in IEEE Transactions on Components Packaging and Manufacturing Technology, 3(6):1028–1037, June 2013.
3. **Elizabeth Rita Samuel**, Luc Knockaert, Tom Dhaene. *Model Order Reduction of Time-Delay Systems Using a Laguerre Expansion Technique*. Published in IEEE Transactions on Circuits and Systems I: Regular Papers, 61(6):1815–1823, June 2014.
4. **Elizabeth Rita Samuel**, Luc Knockaert, Tom Dhaene. *Matrix Interpolation based Parameterized Model Order Reduction for Multiconductor Transmission Lines with Delays*. Accepted in IEEE Transactions on Circuits and Systems II, September 2014.
5. **Elizabeth Rita Samuel**, Francesco Ferranti, Luc Knockaert, Tom Dhaene. *A Hybrid Adaptive Sampling Algorithm for Obtaining Reduced Order Models for Frequency Dependent State-Space Matrices*. Submitted to SIAM Journal on Scientific Computing, January 2015.
6. **Elizabeth Rita Samuel**, Dirk Deschrijver, Luc Knockaert, Tom Dhaene. *Rational Modeling Of Multivariate Multifidelity Data*. Submitted to Simulation Modeling Practice and Theory, December 2014.

---

<sup>1</sup>The publications listed are recognized as ‘A1 publications’, according to the following definition used by Ghent University: A1 publications are articles listed in the Science Citation Index, the Social Science Citation Index or the Arts and Humanities Citation Index of the ISI Web of Science, restricted to contributions listed as article, review, letter, note or proceedings paper.

### 1.4.2 Publications in book chapters

1. **Elizabeth Rita Samuel**, Luc Knockaert, Tom Dhaene, “*Passive Parametric Macromodeling by Using Sylvester State-Space Realizations*”. Chapter in the book *Informatics in Control, Automation and Robotics, Lecture Notes Electrical Engineering*, ISBN: 978-3-319-10890-2, Springer International Publishing Switzerland, pages 311-327, 2014.

### 1.4.3 Publications in international conferences (listed in the Science Citation Index<sup>2</sup>)

1. **Elizabeth Rita Samuel**, Francesco Ferranti, Luc Knockaert, Tom Dhaene. *Parameterized reduced order models with guaranteed passivity using matrix interpolation*. Published in proceedings of the IEEE 16th Workshop on Signal and Power Integrity, pages 65–68, Sorrento, Italy, 2012.
2. **Elizabeth Rita Samuel**, Francesco Ferranti, Luc Knockaert, Tom Dhaene. *Robust passivity preserving parametric model order reduction using matrix interpolation*. Published in proceedings of the 7th IFAC Symposium on Robust Control Design, pages 705–710, Aalborg, Denmark, 2012.
3. **Elizabeth Rita Samuel**, Luc Knockaert, Tom Dhaene. *Parametric macromodeling using interpolation of Sylvester based state-space realizations*. Published in proceedings of 10th International Conference on Informatics in Control, Automation and Robotics, pages 319–325, Reykjavik, Iceland, 2013.
4. **Elizabeth Rita Samuel**, Krishnan Chemmangat, Dirk Deschrijver, Luc Knockaert, Tom Dhaene. *Model order reduction of parameterized state-space systems with sequential sampling*. Published in proceedings of the International Symposium on Electromagnetic Compatibility, pages 342–347, Brugge, Belgium, 2013.
5. **Elizabeth Rita Samuel**, Francesco Ferranti, Luc Knockaert, Tom Dhaene. *Reduced order delayed systems by means of Laguerre functions and Krylov subspaces*. Published in proceedings of the 18th IEEE Workshop on Signal and Power Integrity, pages 1–4, Ghent, Belgium, 2014.
6. **Elizabeth Rita Samuel**, Francesco Ferranti, Luc Knockaert, Tom Dhaene. *Multipoint Model Order Reduction using Reflective Exploration*. Published

<sup>2</sup>The publications listed are recognized as ‘P1 publications’, according to the following definition used by Ghent University: P1 publications are proceedings listed in the Conference Proceedings Citation Index - Science or Conference Proceedings Citation Index - Social Science and Humanities of the ISI Web of Science, restricted to contributions listed as article, review, letter, note or proceedings paper, except for publications that are classified as A1.

in the 10th International Conference on Scientific Computing in Electrical Engineering , pages 109-110, Wuppertal, Germany, 2014.

7. **Elizabeth Rita Samuel**, Luc Knockaert, Tom Dhaene. *Passivity preserving Multipoint Model Order Reduction using Reflective Exploration*. Published in proceedings of 10th International Conference on Informatics in Control, Automation and Robotics, pages 483–491, Vienna, Austria, 2014.
8. **Elizabeth Rita Samuel**, Luc Knockaert, Tom Dhaene. *Multipoint Model Order Reduction using Reflective Exploration*. Submitted to Springer Series Mathematics in Industry, October 2014.

#### 1.4.4 Publications in national conferences

1. **Elizabeth Rita Samuel**, Luc Knockaert, Tom Dhaene. *Parametric model order reduction: obtaining concise mathematical models that work*. Published in the 13th UGent - FEA PhD symposium, Ghent, Belgium, Dec. 2013.

## References

- [1] J. R. W. H. A. Schilders, H. A. van der Vorst. *Model Order Reduction: Theory, Research Aspects and Applications*. Springer, 2008.
- [2] B. Notaros, M. Djordjevic, and M. Ilic. *Higher order electromagnetic modeling for wireless technology applications*. In IEEE Topical Conference on Wireless Communication Technology, 2003, pages 229–232, Oct 2003.
- [3] K. Gallivan, E. Grimme, and V. P. Dooren. *Asymptotic waveform evaluation via a Lanczos method*. Applied Mathematics Letter, 7(5):75–80, Sept. 1994.
- [4] P. Feldmann and W. R. Freund. *Efficient linear circuit analysis by Padè approximation via the Lanczos process*. IEEE Transactions on Computer-Aided Design of Integrated Circuits and Systems, 14(5):639–649, May 1995.
- [5] K. Gallivan, E. Grimme, and P. V. Dooren. *A rational Lanczos algorithm for model reduction*. Numerical Algorithms, 12(1):33–63, Mar. 1996.
- [6] A. Odabasioglu, M. Celik, and L. Pileggi. *PRIMA: passive reduced-order interconnect macromodeling algorithm*. IEEE Transactions on Computer-Aided Design of Integrated Circuits and Systems, 17(8):645 –654, Aug. 1998.
- [7] L. Knockaert and D. De Zutter. *Laguerre-SVD reduced-order modeling*. IEEE Transactions on Microwave Theory and Techniques, 48(9):1469 – 1475, Sept. 2000.
- [8] A. Ruehli. *Progress in circuit oriented techniques for electrical interconnect and package (EIP) modeling*. In Electrical Performance of Electronic packaging, 1994., IEEE 3rd Topical Meeting on, pages 59–61, Nov 1994.
- [9] R. Achar and M. Nakhla. *Simulation of high-speed interconnects*. Proceedings of the IEEE, 89(5):693–728, May 2001.
- [10] B. Denecker, F. Olyslager, L. Knockaert, and D. De Zutter. *Generation of FDTD subcell equations by means of reduced order modeling*. IEEE Transactions on Antennas and Propagation, 51(8):1806–1817, Aug 2003.
- [11] T. Becthold, T. Hauck, L. Voss, and E. B. Rudnyi. *Efficient Electro-Thermal Simulation of Power Semiconductor Devices via Model Order Reduction*. Electronics cooling, Dec. 2011.
- [12] C. Paul. *Analysis of Multiconductor Transmission Lines*. Wiley, New York, 1994.

- [13] A. Maffucci and G. Miano. *An accurate time-domain model of transmission lines with frequency-dependent parameters*. International Journal of Circuit Theory and Applications, 28(3):263–280, 2000.
- [14] L. Silveira and J. Phillips. *Resampling Plans for Sample Point Selection in Multipoint Model-Order Reduction*. Computer-Aided Design of Integrated Circuits and Systems, IEEE Transactions on, 25(12):2775–2783, Dec. 2006.
- [15] F. Ferranti, M. Nakhla, G. Antonini, T. Dhaene, L. Knockaert, and A. Ruehli. *Multipoint Full-Wave Model Order Reduction for Delayed PEEC Models With Large Delays*. IEEE Transactions on Electromagnetic Compatibility, 53(4):959–967, Nov. 2011.
- [16] U. Beyer and F. Śmieja. *Data exploration with reflective adaptive models*. Computational Statistics & Data Analysis, 22(2):193 – 211, 1996.
- [17] P. K. Gunupudi, R. Khazaka, M. Nakhla, T. Smy, and D. Celo. *Passive parameterized time-domain macromodels for high-speed transmission-line networks*. IEEE Transactions on Microwave Theory and Techniques, 51(12):2347 – 2354, Dec. 2003.
- [18] L. Daniel, O. C. Siong, L. Chay, K. H. Lee, and J. White. *A multiparameter moment-matching model-reduction approach for generating geometrically parameterized interconnect performance models*. IEEE Transactions on Computer-Aided Design of Integrated Circuits and Systems, 23(5):678 – 693, May 2004.
- [19] X. Li, P. Li, and L. Pileggi. *Parameterized interconnect order reduction with explicit-and-implicit multi-parameter moment matching for inter/intra-die variations*. pages 806 – 812, Nov. 2005.
- [20] H. Panzer, J. Mohring, R. Eid, and B. Lohmann. *Parametric Model Order Reduction by Matrix Interpolation*. Automatisierungstechnik, pages 475–484, Aug. 2010.
- [21] F. Ferranti, G. Antonini, T. Dhaene, and L. Knockaert. *Guaranteed Passive Parameterized Model Order Reduction of the Partial Element Equivalent Circuit (PEEC) Method*. IEEE Transactions on Electromagnetic Compatibility, 52(4):974–984, Nov. 2010.
- [22] F. Ferranti, T. Dhaene, and L. Knockaert. *Compact and Passive Parametric Macromodeling using Reference Macromodels and Positive Interpolation Operators*. IEEE Transactions on Components, Packaging and Manufacturing Technology, 2(12):2080–2088, Dec. 2012.



# 2

## Introduction to Model Order Reduction and Parameterized Model Order Reduction

*Most physical real-world systems are described by partial differential or distributed equations. An accurate representation requires millions of degrees of freedom and hence the solution of the system will require a considerable amount of data storage and computation time. The aim of model order reduction (MOR) and parametrized model order reduction (PMOR) is to significantly reduce the degrees of freedom needed to describe the physical system. Henceforth in this chapter, we focus on the state-of-the-art techniques for MOR and PMOR. MOR replaces a given mathematical model of a system or process by another model that is much smaller than the original model and this involves a number of important issues.*

### **2.1 Linear Time-Invariant Systems (LTI)**

This section gives an introduction to LTI from the viewpoint of MOR and numerical linear algebra. The stability and passivity of LTI systems is also addressed.

#### **2.1.1 State-space systems**

The state-space representation is a convenient way to model and analyze systems with multiple inputs and outputs. The most general state-space representation of a

LTI system can be mathematically described as follows:

$$\begin{aligned}\dot{\mathbf{x}}(t) &= \mathbf{A}\mathbf{x}(t) + \mathbf{B}\mathbf{u}(t) \\ \mathbf{y}(t) &= \mathbf{C}\mathbf{x}(t) + \mathbf{D}\mathbf{u}(t),\end{aligned}\tag{2.1}$$

where  $\mathbf{A} \in \mathbb{R}^{n \times n}$ ,  $\mathbf{B} \in \mathbb{R}^{n \times m}$ ,  $\mathbf{C} \in \mathbb{R}^{p \times n}$ ,  $\mathbf{x}(t) \in \mathbb{R}^n$ ,  $\mathbf{u}(t) \in \mathbb{R}^m$ ,  $\mathbf{y}(t) \in \mathbb{R}^p$  and  $\mathbf{D} \in \mathbb{R}^{p \times m}$ . The matrix  $\mathbf{A}$  is called the state-space matrix, the matrices  $\mathbf{B}$  and  $\mathbf{C}$  are called the input and output matrices respectively, and  $\mathbf{D}$  is the feed-forward matrix which allows the system input to affect the system output directly. For the systems considered in this PhD thesis the  $\mathbf{D}$  is the zero matrix. The order of the system is  $n$ . If  $m, p > 1$ , the system is called multi-input multi-output (MIMO). If  $m = p = 1$  the system is called single-input single-output (SISO).

By applying the Laplace transform to (2.1) the transfer function matrix  $\mathbf{H}$  of the system is obtained as

$$\mathbf{H}(s) = \mathbf{C}(s\mathbf{I} - \mathbf{A})^{-1}\mathbf{B} + \mathbf{D},\tag{2.2}$$

under the condition that the initial states are zero. The input-output relation in the Laplace domain is simply  $\mathbf{Y}(s) = \mathbf{H}(s)\mathbf{U}(s)$ , where  $\mathbf{Y}(s)$  and  $\mathbf{U}(s)$  are the Laplace transforms of  $\mathbf{y}(t)$  and  $\mathbf{u}(t)$ , respectively. The lower limit  $\hat{n} \leq n$  on the order of the system is called the McMillan degree of the system and a realization of order  $\hat{n}$  is called a minimal realization. In what follows, we generally assume, unless stated otherwise, that all state-space realizations are minimal.

State controllability means that it is possible, by admissible inputs to steer the states from any initial value to any final value within some finite time window [1]. A continuous time-invariant linear state-space model is controllable if and only if

$$\text{rank} [\mathbf{B} \quad \mathbf{AB} \quad \mathbf{A}^2\mathbf{B} \quad \dots \quad \mathbf{A}^{n-1}\mathbf{B}] = n.\tag{2.3}$$

Where the rank of a matrix is the number of linearly independent rows.

Observability is a measure for how well internal states of a system can be inferred by knowledge of its external outputs. A continuous time-invariant linear state-space model is observable if and only if

$$\text{rank} \begin{bmatrix} \mathbf{C} \\ \mathbf{CA} \\ \vdots \\ \mathbf{CA}^{n-1} \end{bmatrix} = n.\tag{2.4}$$

The observability and controllability of a system are mathematical duals (i.e., as controllability infers that an input is available that brings any initial state to any desired final state, observability infers that knowing an output trajectory provides enough information to predict the initial state of the system).



### 2.1.1.1 Descriptor Systems

A system in its descriptor form is represented as:

$$\begin{aligned}\mathbf{E}\dot{\mathbf{x}}(t) &= \mathbf{A}\mathbf{x}(t) + \mathbf{B}\mathbf{u}(t) \\ \mathbf{y}(t) &= \mathbf{C}\mathbf{x}(t) + \mathbf{D}\mathbf{u}(t),\end{aligned}\tag{2.5}$$

with  $\mathbf{E} \in \mathbb{R}^{n \times n}$  possibly singular but with  $\mathbf{A} - s\mathbf{E}$  a regular matrix pencil. The linear system (2.5) is called regular if  $\mathbf{E}$  is nonsingular, else it is called singular.

Such representations are common for interconnected systems and in this PhD thesis the systems are generally represented in their descriptor state-space form. The transfer function can be written as:

$$\mathbf{H}(s) = \mathbf{C}(s\mathbf{E} - \mathbf{A})^{-1}\mathbf{B} + \mathbf{D}.\tag{2.6}$$

The development of reliable numerical algorithms for analysis and synthesis of descriptor state-space systems has been an active area of research in the last decade.

### 2.1.2 Moments

The transfer function is a function in  $s$  (2.6), and can therefore be expanded into a Taylor expansion around  $s = 0$ :

$$\mathbf{H}(s) = \mathbf{M}_0 + \mathbf{M}_1 s + \mathbf{M}_2 s^2 + \dots\tag{2.7}$$

where  $\mathbf{M}_0, \mathbf{M}_1, \mathbf{M}_2, \dots$  are the moments of the transfer function. In electronics,  $\mathbf{M}_0$  corresponds with the DC operating point. The transfer function can also be expanded around some non-zero  $s_0$ . We then obtain a similar expansion in terms of the moments.

$$\mathbf{H}(s) = \mathbf{M}_0 + \mathbf{M}_1(s - s_0) + \mathbf{M}_2(s - s_0)^2 + \dots\tag{2.8}$$

### 2.1.3 Poles and Residues

The transfer function can also be represented as a rational function:

$$\mathbf{H}(s) = \sum_{j=1}^n \frac{\mathbf{R}_j}{s - z_j},\tag{2.9}$$

where the  $z_j$  are the poles, and  $\mathbf{R}_j$  are the corresponding residue matrices. The poles are the eigenvalues of the system (2.5). During the approximation of systems it is important to approximate the dominant poles.

### 2.1.4 Stability

The stability of a LTI system is simply a property of its poles. For LTI systems, stability is guaranteed if and only if the real part of every pole is non-positive, and all poles with zero real part are simple (i.e. the poles on the imaginary axis are all distinct from one another). If all poles have strictly negative real parts, the system is strictly or asymptotically stable. If one or more poles have positive real parts the system is unstable.

### 2.1.5 Passivity

Stability is a necessary, but not in general a sufficient condition for an LTI system to be passive or dissipative. Roughly speaking, a dissipative system is characterized by the property that at any time the amount of energy which the system can conceivably supply to the environment cannot exceed the amount of energy that has been supplied to the system itself. A merely stable system can become unstable when non-active nonlinear loads are connected to it. On the contrary, a passive system remains passive when non-active nonlinear loads are connected to it. While a passive system is also stable, the converse is not necessarily true. A

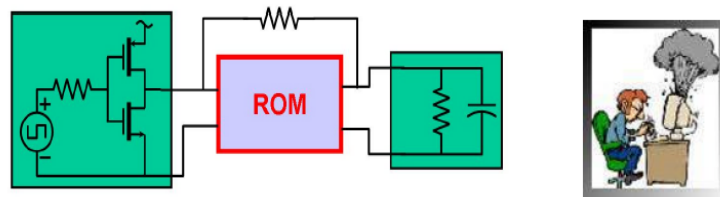


Figure 2.1: Not passive ROMs can produce unstable systems when connected to other stable, even passive, loads

passive system denotes a system that is incapable of generating energy, and hence one that can only absorb energy from the sources used to power it [2]. If a system is passive then the appropriate MOR procedure to use is of course the one that preserves passivity.

## 2.2 Model Order Reduction

MOR is a mathematical tool used to find a low-dimensional approximation for a system of ordinary differential equations (ODEs) [3]. MOR has been used extensively in the circuit analysis community over the past years. The need for MOR techniques was inspired by the desire to decrease the simulation time required for

large-scale computer-generated models in analysis and design, while retaining sufficient accuracy. The main idea is that the high-dimensional state vector belongs to a low-dimensional subspace as shown in Fig. 2.2.

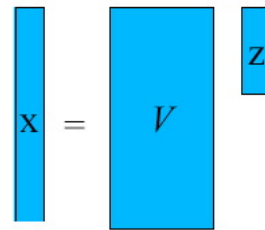
$$\mathbf{x} = V\mathbf{z} + \varepsilon$$


Figure 2.2: Low dimensional subspace

Provided that the low-dimensional subspace of  $\mathbf{z}$  is known, the ordinary differential equations can be projected on it. This is shown in Fig. 2.3 in the case of a linear system of ODEs and it is seen that the projection gives us the required low-dimensional approximation.

$$\begin{aligned}
 E \dot{x} &= Ax + Bu \\
 y &= Cx \\
 V^T E V \dot{z} &= V^T A V z + V^T B u \\
 y &= C V z
 \end{aligned}$$

Figure 2.3: Projecting a system of ODEs onto a low dimensional space.

In the following sections an overview of some typical MOR approaches are given.

### 2.2.1 Asymptotic Waveform Evaluation (AWE)

AWE was one of the initial contributions to MOR [4]. In AWE the transfer function is reduced by means of a Padé approximation with numerator  $\mathbf{P}(s)$  and denominator  $\mathbf{Q}(s)$ . AWE computes a finite degree approximation for  $\mathbf{P}(s)$  and  $\mathbf{Q}(s)$  with  $\deg(\mathbf{P}(s)) \leq \deg(\mathbf{Q}(s))$ . As indicated in formula (2.8) the transfer function can be represented in terms of its moments and can be approximated as:

$$\hat{\mathbf{H}}(s) = \sum_{j=0}^n \mathbf{M}_j (s - s_0)^j, \quad (2.10)$$

for some finite  $n$ . Then a Padé approximation  $\hat{\mathbf{H}}(s)$  of the transfer function is computed as:

$$\hat{\mathbf{H}}(s) = \frac{\mathbf{P}(s)}{\mathbf{Q}(s)},$$

$$\mathbf{P}(s) = \sum_{k=0}^p a_k (s - s_0)^k, \quad \mathbf{Q}(s) = \sum_{k=0}^{p+1} b_k (s - s_0)^k. \quad (2.11)$$

On equating the coefficients of  $(s - s_0)$  and setting  $b_0 = 1$ , the coefficients  $b_k$  and  $a_k$  can be computed. Calculating the poles and residues in AWE is inherently a computational challenge, since ill conditioning frequently occurs in the AWE scheme [5, 6].

### 2.2.2 Padé-via-Lanczos (PVL)

The motivation for the development of PVL [7] was to overcome some of the issues and limitations of AWE. In PVL the moment matching is not explicitly performed. The algorithm requires the same computational effort as AWE, but is able to extract several more poles per expansion point and is more robust. In PVL the transfer function is written as:

$$\mathbf{H}(s) = \mathbf{C}(\mathbf{I} - (s - s_0)\hat{\mathbf{A}})^{-1}\mathbf{r}, \quad (2.12)$$

where  $\hat{\mathbf{A}} = -(s_0\mathbf{I} - \mathbf{A})^{-1}$  and  $\mathbf{r} = (s_0\mathbf{I} - \mathbf{A})^{-1}\mathbf{B}$ . The Padé approximation is calculated by means of the two-sided Lanczos algorithm. This which is an iterative algorithm that is also applicable to eigenvalue problems [8].  $\hat{\mathbf{A}}$  is approximated in the form of a tridiagonal matrix  $\mathbf{T}_q$ . This results in the reduced transfer function:

$$\mathbf{H}_q(s) = \mathbf{C}\mathbf{r}\mathbf{e}_1'(\mathbf{I} - (s - s_0)\mathbf{T}_q)^{-1}\mathbf{e}_1. \quad (2.13)$$

Here,  $\mathbf{e}_1$  is the first unit vector and the other parameters can be found in [7].

### 2.2.3 Arnoldi and PRIMA

In the Arnoldi process a Krylov subspace is formed as follows [9]:

$$\mathcal{K}_q(\mathbf{r}, \hat{\mathbf{A}}) = \text{span}\{\mathbf{r}, \hat{\mathbf{A}}\mathbf{r}, \dots, \hat{\mathbf{A}}^q\mathbf{r}\}. \quad (2.14)$$

In comparison with PVL, in the Arnoldi method only one Krylov space is generated by means of the (block) Arnoldi process, and the projections are performed with orthogonal operators. The expansion point can be chosen either real or complex, leading to different approximations of the poles of the system.

The passive reduced-order interconnect macromodeling algorithm (PRIMA) [10] generates Krylov subspace similarly as in Arnoldi method and generates an orthogonal basis for the Krylov subspace. The projection of the matrices is done explicitly as:

$$\mathbf{A}_q = \mathbf{V}_q' \mathbf{A} \mathbf{V}_q, \quad (2.15)$$

where  $\mathbf{V}_q$  is the projection matrix associated with the orthonormal basis for the Krylov space. The PRIMA algorithm ensures the preservation of stability and passivity.

### 2.2.4 Laguerre-SVD

In this method the transfer function is expanded in terms of Laguerre functions [11, 12] using  $\alpha$ , a positive real scaling parameter called the Laguerre parameter or the time-scale factor [11, 13]

In the frequency domain, the Laplace transforms of the scaled Laguerre functions can be written as

$$\Phi_i^\alpha(s) = \frac{\sqrt{2\alpha}}{s + \alpha} \left( \frac{s - \alpha}{s + \alpha} \right)^i \quad i = 0, 1, \dots \quad (2.16)$$

In [11], it is shown that the transfer function of any system can be expanded into the Laguerre orthonormal basis  $\Phi_i^\alpha(s)$  as

$$\mathbf{H}(s) = \mathbf{C}(s\mathbf{E} - \mathbf{A})^{-1}\mathbf{B} = \frac{\sqrt{2\alpha}}{s + \alpha} \sum_{i=0}^{\infty} \mathbf{F}_i \left( \frac{s - \alpha}{s + \alpha} \right)^i \quad (2.17)$$

where  $\mathbf{F}_i$ 's are the matrices of the Laguerre coefficients. Then considering the bilinear transformation,

$$s = \alpha \frac{1 + u}{1 - u} \quad (2.18)$$

the Laguerre expansion is mapped from  $s$ -domain to the  $u$ -domain as:

$$\mathbf{H}(u) = \mathbf{C}(u(\alpha\mathbf{E} + \mathbf{A}) - (\mathbf{A} - \alpha\mathbf{E}))^{-1}\mathbf{B} = \frac{1}{\sqrt{2\alpha}} \sum_{i=0}^{\infty} \mathbf{F}_i u^i \quad (2.19)$$

The Krylov subspaces for the Laguerre based reduction approaches are defined as,  $\mathcal{K}_q(\mathbf{A}_u^{-1}\mathbf{E}_u, \mathbf{A}_u^{-1}\mathbf{B})$  and  $\mathcal{K}_q(\mathbf{A}_u^{-T}\mathbf{E}_u, \mathbf{A}_u^{-T}\mathbf{B})$ .

As in the PRIMA method, the Laguerre-based method makes use of explicit projection of the system matrices. Consequently, these methods preserve stability and passivity. Since  $\alpha$  is a real number, the matrices in the Laguerre algorithm remain real during projection, thereby making it suitable for circuit synthesis. For this PhD thesis, the PRIMA and Laguerre-SVD techniques of MOR were used.

### 2.2.5 Balanced Truncation

In control theory, the poles define the system stability, where the Hankel singular values (HSV) define the energy of each state of the system. Keeping the dominant energy states of a system, preserves most of its characteristics in terms of stability, frequency and time responses. This is the rationale for the use of balanced truncation based MOR. The major advantage of balanced truncation is that it gives a deterministic global bound for the approximation error and produces nearly optimal models in terms of error and model sizes [14, 15].

The controllability  $\mathbf{W}_c$  and observability Gramians  $\mathbf{W}_o$  are obtained from the solutions of two Lyapunov equations:

$$\begin{aligned} \mathbf{A}\mathbf{W}_c + \mathbf{W}_c\mathbf{A}' + \mathbf{B}\mathbf{B}' &= 0 \\ \mathbf{A}'\mathbf{W}_o + \mathbf{W}_o\mathbf{A} + \mathbf{C}'\mathbf{C} &= 0. \end{aligned} \quad (2.20)$$

After computing the Gramians, the system (2.2) is transformed in order to balance the system. A system is said to be balanced if  $\mathbf{W}_c = \mathbf{W}_o = \Sigma$ , where  $\Sigma$  is the diagonal Hankel singular value matrix. The balancing transformation  $\mathbf{T}$  is applied to the system as shown:

$$\begin{aligned} \mathbf{A}_r &= \mathbf{T}^{-1}\mathbf{A}\mathbf{T} \\ \mathbf{B}_r &= \mathbf{T}^{-1}\mathbf{B} \\ \mathbf{C}_r &= \mathbf{C}\mathbf{T} \\ \mathbf{D}_r &= \mathbf{D} \end{aligned} \quad (2.21)$$

with

$$\mathbf{T} = \mathbf{R}'\mathbf{U}'\Sigma^{\frac{1}{2}} \quad \text{and} \quad \mathbf{T}^{-1} = \Sigma^{\frac{1}{2}}\mathbf{U}\mathbf{R}^{-1}. \quad (2.22)$$

Since  $\mathbf{W}_c$  and  $\mathbf{W}_o$  are positive definite. The Cholesky factorization of  $\mathbf{W}_c$  gives  $\mathbf{W}_c = \mathbf{R}'\mathbf{R}$ . Then the HSV are computed as  $\mathbf{R}\mathbf{W}_o\mathbf{R}' = \mathbf{U}'\Sigma^2\mathbf{U}$ . Balanced MOR

is finally performed by truncating the matrices with respect to the most significant HSV.

### 2.2.6 Proper Orthogonal Decomposition (POD)

The POD method is a sampling based reduction method. From snapshots of the states, the optimal bases to describe these snapshots are found. The relation between POD and SVD makes POD applicable for model order reduction. It is used for dynamic analysis of structures [16], and Micro Electro-Mechanical Systems (MEMS) [17]. Since POD is applicable to nonlinear systems, it is often used in the field of fluid dynamics or aerodynamics. However, the accuracy of the reduced model is significantly dependent on the choice of the snapshots.

### 2.2.7 Multipoint MOR

ROMs obtained by MOR methods must be accurate over the whole frequency range of interest. To obtain this, multipoint reduction algorithms have proved to be efficient [18–20]. These algorithms allow to match a substantial number of derivatives (or moments) around many distinct Taylor series expansion points.

To illustrate this, first consider the approximation achieved by expanding around a single frequency point, as shown in Fig.2.4. It works by increasing the accuracy

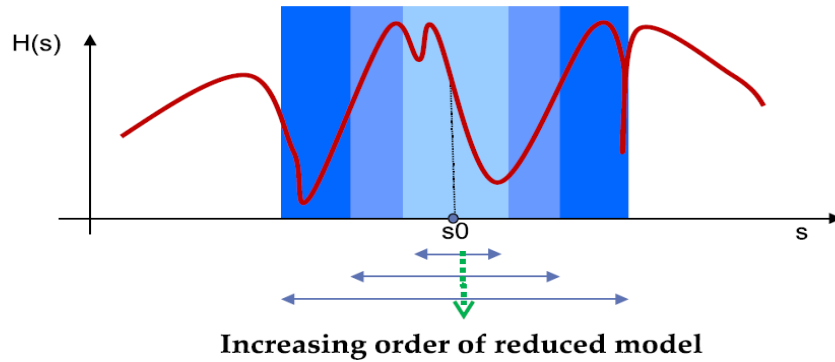


Figure 2.4: The single point expansion based MOR.

of the approximation as the order of the reduced model is increased. However, to achieve satisfactory levels of accuracy at points further away from the expansion point, a much larger increase is needed in the order of the reduced model. Instead, if multiple expansion points are used, as shown in Fig. 2.5, the same level of accuracy can be achieved over the entire bandwidth with a much smaller reduced model. One of the research contributions of this PhD thesis is to automate the



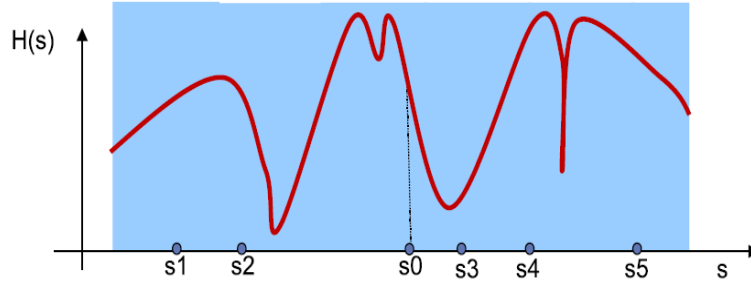


Figure 2.5: The multiple point expansion based MOR.

choice of the expansion points and the determination of the order of approximation per expansion point.

## 2.3 Parameterized Model Order Reduction (PMOR)

PMOR is an adaptive and efficient approach for constructing ROMs that are robust with respect to parameter changes in a given design space. The goal is to include parametric effects into the reduced space based on general MOR methods, such as SVD and Krylov [21]. Focusing on system parameters, the two main streams used in PMOR are multiparameter moment matching and interpolation based. The former finds a common projector which preserves the information about both the system and the parameters; the latter reduces each system with a different parameter set individually using their own projector and approximating the response via interpolation. The interpolation is performed using input-output representation (transfer function) and state-space matrices. In this PhD thesis we focus on the interpolation based PMOR technique.

### 2.3.1 Multiparameter moment matching

Moment matching algorithms have gained a well-deserved fame in nominal MOR due to their simplicity and efficiency of application. The extension of these techniques to parametric cases is usually based on the implicit and explicit moment matching of the parametric transfer function [22]. These techniques approximate the parameterized behavior using Taylor series expansions. Some of the multiparameter moment matching methods presented in the literature [23–25] are suitable only for a low-dimensional design space as in nearly all multiparameter moment-matching based PMOR techniques. If the system has very distinctive parameter sets, or if the system is nonlinearly dependent on parameters, the accuracy of reduced order model tends to be low. Consequently the required order of the pro-

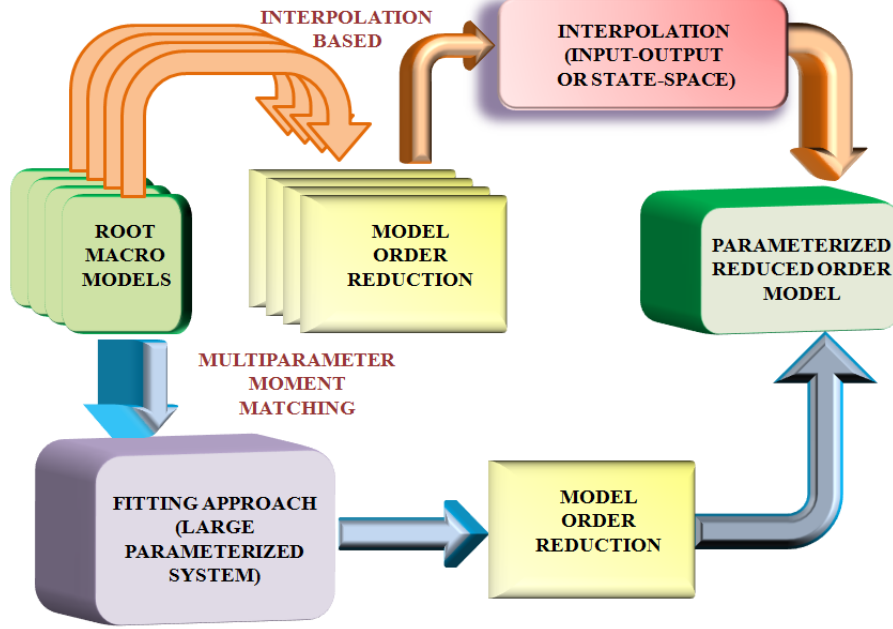


Figure 2.6: Parameterized Model Order Reduction approaches (Orange arrows correspond to interpolation based PMOR and the blue arrows correspond to multiparameter moment matching).

jector needed to maintain a certain level of accuracy will be high; that is the point where interpolation methods come in. Interpolation based methods are a combination of two different fields of study: MOR and interpolation.

### 2.3.2 Interpolation based PMOR

There are many variations to interpolation based PMOR. In this PhD thesis we focus on the input-output (transfer function) interpolation and the state-space interpolation.

#### 2.3.2.1 PMOR based on input-output interpolation

Input-output based interpolation for PMOR is a quite robust technique. In input-output interpolation the order of the PMOR increases due to the nature of the input-output system level interpolation. A weighted sum of LTI systems does indeed result in a LTI system with order equal to the sum of the orders of the individual LTI systems. An increased model order leads to a reduction of the CPU time efficiency of PMOR. The modeling capability is then much reduced in compari-

son with state-space interpolation techniques. In order to increase the modeling capability, a technique based on amplitude and frequency scaling of coefficients technique was introduced [26] and proved to be an efficient PMOR technique. The technique in [27] combines traditional passivity-preserving MOR methods and interpolation schemes based on a class of positive interpolation operators. A PMOR method based on EM matrix parameterization and projection subspaces is proposed in [28]. Overall passivity of parameterized ROMs is guaranteed over the design space of interest in [27, 28].

### 2.3.2.2 PMOR based on state-space interpolation

A parameterized dynamical system with  $N$  design parameters  $\vec{p} = (p^{(1)}, \dots, p^{(N)})$  can be represented in descriptor state-space form as:

$$\begin{aligned} \mathbf{E}(\tilde{\mathbf{p}}) \frac{d\mathbf{x}(t, \tilde{\mathbf{p}})}{dt} &= \mathbf{A}(\tilde{\mathbf{p}})\mathbf{x}(t, \tilde{\mathbf{p}}) + \mathbf{B}\mathbf{u}(t) \\ \mathbf{y}(t, \tilde{\mathbf{p}}) &= \mathbf{C}\mathbf{x}(t, \tilde{\mathbf{p}}) + \mathbf{D}\mathbf{u}(t). \end{aligned} \quad (2.23)$$

As in [27, 29] using (2.23), a set of reduced system matrices is computed in a common subspace and then interpolated to generate a PMOR. The state-space matrices have the same order when they are interpolated, thus keeping the same model order throughout the design space. It allows to parameterize the poles and the residues and thus has higher modeling capabilities. This technique avoids the oversize problem of multiparameter moment matching algorithms, but the reduced system matrices needed for interpolation must have the same reduced order and must be postprocessed for reprojection onto a common subspace. The passivity of PROM is not guaranteed with this approach. In this PhD thesis, we propose a PMOR technique which generates a common projection matrix for the design space and also preserves the properties of the system.

To obtain an accurate parameterized model by interpolation of the state-space matrices, the choice of the state-space realization is fundamental [30]. Here, we propose to use a Sylvester realization technique for the unique representation of the state-space matrices.

## References

- [1] E. de Souza and S. Bhattacharyya. *Controllability, observability and the solution of  $AX - XB = C$* . Linear Algebra and its Applications, 39:167 – 188, 1981.
- [2] B. Anderson and S. Vongpanitlerd. *Network Analysis and Synthesis*. Prentice-Hall, Englewood Cliffs, NJ., 1973.
- [3] W. Schilders. *Model Order Reduction: Theory, Research Aspects and Applications*. Mathematics in Industry, 13:3–32, 2008.
- [4] L. Pillage and R. Rohrer. *Asymptotic waveform evaluation for timing analysis*. IEEE Transactions on Computer-Aided Design of Integrated Circuits and Systems, 9(4):352–366, Apr 1990.
- [5] E. Chiprout and M. S. Nakhla. *Asymptotic Waveform Evaluation and Moment Matching for Interconnect Analysis*. Kluwer Academic Publishers, Norwell, MA, USA, 1994.
- [6] K. Gallivan, E. Grimme, and P. V. Dooren. *Asymptotic waveform evaluation via a Lanczos method*. Applied Mathematics Letters, 7(5):75 – 80, 1994.
- [7] P. Feldmann and R. Freund. *Efficient linear circuit analysis by Pade approximation via the Lanczos process*. IEEE Transactions on Computer-Aided Design of Integrated Circuits and Systems, 14(5):639–649, May 1995.
- [8] C. Lanczos. *An iterative method for the solution of the eigenvalue problem of linear differential and integral*. Journal of Research of the National Bureau of Standards, 45(4):255–282, Oct. 1950.
- [9] Y. Saad. *Iterative Methods for Sparse Linear Systems*. SIAM, Philadelphia, 2nd edition, 2003.
- [10] A. Odabasioglu, M. Celik, and L. Pileggi. *PRIMA: passive reduced-order interconnect macromodeling algorithm*. IEEE Transactions on Computer-Aided Design of Integrated Circuits and Systems, 17(8):645 –654, Aug. 1998.
- [11] L. Knockaert and D. De Zutter. *Laguerre-SVD reduced-order modeling*. IEEE Transactions on Microwave Theory and Techniques, 48(9):1469 – 1475, Sept. 2000.
- [12] L. Knockaert and D. De Zutter. *Stable Laguerre-SVD reduced-order modeling*. IEEE Transactions on Circuits and Systems I:Fundamental Theory and Applications, 50(4):576 – 579, April 2003.

- [13] G.Szegö. *Orthogonal Polynomials*. American Mathematical Society, New York, 1939.
- [14] J. Phillips and L. M. Silveira. *Poor Man's TBR: A Simple Model Reduction Scheme*. Proceedings of the conference on Design, automation and test in Europe - Volume 2, pages 20938–20943, 2004.
- [15] A. C. Antoulas. *Approximation of Large-Scale Dynamical Systems*. SIAM series on Advances in Design and Control, 2005.
- [16] M. Xianghong, V. Alexander, F., and B. Lawrence, A. *Karhunen-Loève Modes of a Truss: Transient Response Reconstruction and Experimental Verification*. AIAA Journal, 39(4):687–696, 2001.
- [17] W. Z. Lin, K. H. Lee, S. P. Lim, and Y. C. Liang. *Proper orthogonal decomposition and component mode synthesis in macromodel generation for the dynamic simulation of a complex MEMS device*. Journal of Micromechanics and Microengineering, 13(5):646, 2003.
- [18] L. Silveira and J. Phillips. *Resampling Plans for Sample Point Selection in Multipoint Model-Order Reduction*. Computer-Aided Design of Integrated Circuits and Systems, IEEE Transactions on, 25(12):2775–2783, Dec. 2006.
- [19] H. Wang, S. X.-D. Tan, and R. Rakib. *Compact Modeling of Interconnect Circuits over Wide Frequency Band by Adaptive Complex-Valued Sampling Method*. ACM Trans. Des. Autom. Electron. Syst., 17(1):5:1–5:22, 2012.
- [20] F. Ferranti, M. Nakhla, G. Antonini, T. Dhaene, L. Knockaert, and A. Ruehli. *Multipoint Full-Wave Model Order Reduction for Delayed PEEC Models With Large Delays*. IEEE Transactions on Electromagnetic Compatibility, 53(4):959–967, 2011.
- [21] D. Weile, E. Michielssen, E. Grimme, and K. Gallivan. *A method for generating rational interpolant reduced order models of two-parameter linear systems*. Applied Mathematics Letters, 12(5):93 – 102, 1999.
- [22] X. Li, P. Li, and L. Pileggi. *Parameterized interconnect order reduction with explicit-and-implicit multi-parameter moment matching for inter/intra-die variations*. pages 806 – 812, Nov. 2005.
- [23] P. K. Gunupudi, R. Khazaka, M. Nakhla, T. Smy, and D. Celo. *Passive parameterized time-domain macromodels for high-speed transmission-line networks*. IEEE Transactions on Microwave Theory and Techniques, 51(12):2347 – 2354, Dec. 2003.

- [24] L. Daniel, O. C. Siong, L. Chay, K. H. Lee, and J. White. *A multiparameter moment-matching model-reduction approach for generating geometrically parameterized interconnect performance models*. IEEE Transactions on Computer-Aided Design of Integrated Circuits and Systems, 23(5):678 – 693, May 2004.
- [25] Y.-T. Li, Z. Bai, Y. Su, and X. Zeng. *Model Order Reduction of Parameterized Interconnect Networks via a Two-Directional Arnoldi Process*. IEEE Transactions on Computer-Aided Design of Integrated Circuits and Systems, 27(9):1571 –1582, Sept. 2008.
- [26] F. Ferranti, L. Knockaert, and T. Dhaene. *Passivity-Preserving Parametric Macromodeling by Means of Scaled and Shifted State-Space Systems*. IEEE Transactions on Microwave Theory and Techniques, 59(10):2394–2403, Oct 2011.
- [27] F. Ferranti, G. Antonini, T. Dhaene, and L. Knockaert. *Guaranteed Passive Parameterized Model Order Reduction of the Partial Element Equivalent Circuit (PEEC) Method*. IEEE Transactions on Electromagnetic Compatibility, 52(4):974–984, Nov. 2010.
- [28] F. Ferranti, G. Antonini, T. Dhaene, L. Knockaert, and A. Ruehli. *Physics-Based Passivity-Preserving Parameterized Model Order Reduction for PEEC Circuit Analysis*. IEEE Transactions on Components, Packaging and Manufacturing Technology, 1(3):399 –409, Mar. 2011.
- [29] H. Panzer, J. Mohring, R. Eid, and B. Lohmann. *Parametric Model Order Reduction by Matrix Interpolation*. Automatisierungstechnik, pages 475–484, Aug. 2010.
- [30] P. Triverio, S. Grivet-Talocia, and M. Nakhla. *A Parameterized Macromodeling Strategy With Uniform Stability Test*. IEEE Transactions on Advanced Packaging, 32(1):205 –215, Feb. 2009.

# 3

## Model Order Reduction of Time-Delay Systems using a Laguerre Expansion Technique

Based on the publication:

**Elizabeth Rita Samuel, Luc Knockaert, Tom Dhaene,**  
**“Model Order Reduction of Time-Delay Systems Using a Laguerre Expansion**  
**Technique”, published in IEEE Transactions on Circuits and Systems I:**  
**Regular Papers, 61(6):1815–1823, June 2014.**

\*\*\*

*The demands for miniature sized circuits with higher operating speeds have increased the complexity of the circuit, while at high frequencies it is known that effects such as crosstalk, attenuation and delay can have adverse effects on signal integrity. To capture these high speed effects a very large number of system equations is normally required and hence MOR techniques are required to make the simulation of the circuits computationally feasible. As briefed in the previous chapter, it can be noted that MOR for LTI systems are quite well developed and these techniques have been extended to time-delay systems (TDSs) and nonlinear systems. In this chapter, a higher order Krylov subspace algorithm for model order reduction of TDSs based on a Laguerre expansion technique is proposed. The proposed technique consists of three sections i.e., first the delays are approximated*

*using the recursive relation of Laguerre polynomials, then in the second part, the reduced order is estimated for the TDSs using a delay truncation in the Laguerre domain and in the third part, a higher order Krylov technique using Laguerre expansion is computed for obtaining the reduced order TDS. The proposed technique is validated by means of real world numerical examples.*

### 3.1 Introduction

The ever increasing quest for high density and high operating speed requires more accurate models in modern electronic design, and this implies that the analysis of interconnects and high-speed circuits has become a critical aspect for studying system reliability, and speed of operation [1, 2]. The gigabit per second range for high-speed links has made signal integrity (SI) analysis and design of interconnections of great importance.

For printed circuit board (PCB) structures, long transmission lines (TLs) are often needed for accurate simulations. Lossy TLs are traditionally modeled by ladder networks with cascaded sections of RLC components [3]. The effects of different packaging components such as bond wires, traces, vias and balls can also be modeled as RLC lumped components. When geometric dimensions become electrically large and the frequency content of signal waveform increases, time delays must be taken into account and, included in the modeling process [4, 5]. A major drawback of this brute force approach is the potentially huge number of system equations leading to high CPU cost in the circuit simulation. To alleviate this, efficient model order reduction (MOR) techniques can be used.

Most MOR approaches are based on moment matching techniques (MMTs) and in general, MOR methods can be classified as explicit or implicit MMTs. The explicit MMT using a single Padé expansion [6–8] is known as asymptotic waveform evaluation (AWE). However, AWE and the underlying Padé approximation induces numerical ill-conditioning, while the approximant may produce unstable poles as briefed in Section 2.2. Also, AWE does not guarantee passivity. The implicit MMTs based on Krylov-subspace algorithms [5, 9–13] use congruence transformation to deal with ill-conditionedness, and can also guarantee the preservation of passivity in the reduced models.

TDSs are systems with aftereffect or dead-time, which belong to the class of functional differential equations (FDEs), as opposed to ordinary differential equations (ODEs) [14]. TDSs in the Laplace domain contain elements with exponential factors  $e^{-s\tau}$  where  $\tau$  corresponds to the time delays present in the circuit. In [15], the equivalent representation of the TDSs are build as an infinite-dimensional linear problem and is then reduced to a system without delay. In [16, 17], the exponential terms corresponding to the delays are expanded in a Taylor series and subsequently the moments of the system are obtained via Krylov-subspace tech-



niques. This MOR technique guarantees passivity preservation for certain specific cases of RLC networks by means of congruence transformations. But in [16, 17] the original system needs to be augmented by introducing extra state variables, and finally the resulting reduced order model does not preserve the TDS structure of the original system. In the approach of [5, 12], the moments are calculated using extra state variables, but the dimension of the row of the augmented system moments that is used for the reduction of the original model is same as the number of state variables in the original model. But still the computation effort is excessive, as the moment matrix is calculated with the extra state variables.

These shortcomings were somewhat alleviated in [13] by proposing multiorder Arnoldi. In that technique the moments of the original system are calculated implicitly using a higher order Krylov technique [18, 19] without having to introduce extra state variables and the structure of the reduced model resembles the original.

In this chapter we propose a novel technique using a higher order Krylov subspace decomposition with orthonormal Laguerre functions, which do provide good approximations for a large class of time-delay systems [20]. The link with the singular value decomposition (SVD) leads to a simple and stable implementation of the algorithm. The present technique is a generalization and extension of the well-known Laguerre-SVD method [21] to TDS.

As a first step towards improving the efficiency, the proposed technique estimates the reduced order using a smart approximation of the delay terms after approximating the delays using a recursive relation using Laguerre polynomials. As a second step higher order Laguerre approximation is used to obtain the reduced order TDS.

More precisely, the three steps of the proposed algorithm are:

1. Delay Approximation - The time delay term  $e^{-s\tau}$ , is approximated using a recursive relation of Laguerre polynomial.
2. Zero-Order Approximation Technique (ZAT) - The time delay term  $e^{-s\tau}$ , is approximated as  $e^{-2\alpha\tau}$ , where  $\alpha$  is the Laguerre parameter [20–22]. So an approximate linear time-invariant (LTI) system is obtained, whose Hankel singular values (HSVs) are computed. HSVs provides a measure of the energy of each state in a system and can be computed using the Matlab command *hsvd*. From the HSVs an initial guess of the reduced order can be estimated depending on the required (predefined) accuracy.
3. Higher-order Laguerre Approximation Technique (HLAT) - The delays are replaced by their approximations in the Laguerre domain and then the higher order Krylov subspace is computed [23] in order to reduce the original system.

Thereby, the proposed Laguerre expansion technique computes the Krylov subspace more efficiently, and generates an accurate reduced order model.

## 3.2 Overview of Laguerre-based Model Order Reduction

As described in Section 2.2.4 a MIMO descriptor system is considered of the form

$$\begin{aligned} \mathbf{E}\dot{x}(t) &= \mathbf{A}x(t) + \mathbf{B}u(t) \\ y(t) &= \mathbf{C}x(t) + \mathbf{D}u(t) \end{aligned} \quad (3.1)$$

with (McMillan) degree  $n$  and number of ports  $p$ . The transfer function of this system is

$$\mathbf{H}(s) = \mathbf{C}(s\mathbf{E} - \mathbf{A})^{-1}\mathbf{B} + \mathbf{D}. \quad (3.2)$$

Note that it is usually required that  $s\mathbf{E} - \mathbf{A}$  is a regular matrix pencil [24].

The  $i^{th}$  Laguerre polynomial is defined as

$$\mathcal{L}_i(t) = \frac{e^t}{i!} \frac{d^i}{dt^i} (e^{-t} t^i). \quad (3.3)$$

and the scaled Laguerre functions are

$$\Phi_i^\alpha(t) = \sqrt{2\alpha} e^{-\alpha t} \mathcal{L}_i(2\alpha t) \quad i = 0, 1, \dots \quad (3.4)$$

Here  $\alpha$  is a positive scaling parameter called the Laguerre parameter or time-scale factor [25]

In the Laplace domain, the transformation of the scaled Laguerre functions can be written as

$$\Phi_i^\alpha(s) = \frac{\sqrt{2\alpha}}{s + \alpha} \left( \frac{s - \alpha}{s + \alpha} \right)^i \quad i = 0, 1, \dots \quad (3.5)$$

In [21], it has been shown that the transfer function of a strictly proper ( $\mathbf{D} = 0$ ) stable system can be expanded into the Laguerre orthonormal basis  $\Phi_i^\alpha(s)$  as

$$\mathbf{H}(s) = \mathbf{C}(s\mathbf{E} - \mathbf{A})^{-1}\mathbf{B} = \frac{\sqrt{2\alpha}}{s + \alpha} \sum_{i=0}^{\infty} \mathbf{F}_i \left( \frac{s - \alpha}{s + \alpha} \right)^i \quad (3.6)$$

where the  $\mathbf{F}_i$ 's are the Laguerre coefficients, which are matrices in general. Applying the bilinear transformation (3.7) to the r.h.s of formula (3.6),

$$s = \alpha \frac{1 + u}{1 - u} \quad (3.7)$$

we obtain

$$\mathbf{C}(u(\alpha\mathbf{E} + \mathbf{A}) - (\mathbf{A} - \alpha\mathbf{E}))^{-1}\mathbf{B} = \frac{1}{\sqrt{2\alpha}} \sum_{i=0}^{\infty} \mathbf{F}_i u^i. \quad (3.8)$$

From this it can be inferred that the  $q$ th-order Padé approximation of the modified transfer matrix

$$\hat{\mathbf{H}}(u) = \mathbf{C}(u(\alpha\mathbf{E} + \mathbf{A}) - (\mathbf{A} - \alpha\mathbf{E}))^{-1}\mathbf{B} \quad (3.9)$$

in the  $u$ -domain is equivalent to the  $q$ th-order Laguerre approximation in the  $s$ -domain.

Note that the bilinear transformation (3.6) maps the Laplace  $s$ -domain onto the Laguerre  $u$ -domain. It is seen, by comparing (3.9) and (3.2) that the state-space matrices have been modified to  $\mathbf{E}_u = \alpha\mathbf{E} + \mathbf{A}$  and  $\mathbf{A}_u = \mathbf{A} - \alpha\mathbf{E}$ .

Thus, on defining  $\mathbf{G} = \mathbf{A}_u^{-1}\mathbf{E}_u$  and  $\mathbf{L} = \mathbf{A}_u^{-1}\mathbf{B}$ , for a reduced order  $q$  the  $n \times q$  modified Krylov subspace  $\mathcal{K}_q$  [26, 27] is:

$$\mathcal{K}_q(\mathbf{G}, \mathbf{L}) = \text{colspan}[\mathbf{L}, \mathbf{GL}, \mathbf{G}^2\mathbf{L}, \dots, \mathbf{G}^{q-1}\mathbf{L}] \quad (3.10)$$

This yields a reduced order system described by

$$\begin{aligned} \mathbf{A}_r &= \mathbf{Q}'\mathbf{A}\mathbf{Q}, \\ \mathbf{E}_r &= \mathbf{Q}'\mathbf{E}\mathbf{Q}, \\ \mathbf{B}_r &= \mathbf{Q}'\mathbf{B}, \\ \mathbf{C}_r &= \mathbf{C}\mathbf{Q}. \end{aligned} \quad (3.11)$$

Here the column-orthogonal matrix  $\mathbf{Q}$  is found through the singular value decomposition (SVD) approach on the Krylov subspace  $\mathcal{K}_q$  (3.10) i.e;

$$\mathbf{U}\Sigma\mathbf{V}' = \text{SVD}(\mathcal{K}_q(\mathbf{G}, \mathbf{L})) \quad (3.12)$$

where  $\mathbf{U}$  is the column-orthogonal matrix,  $\Sigma$  is a diagonal matrix containing the singular values and  $\mathbf{V}$  is orthogonal matrix of dimensions  $N \times q$ ,  $q \times q$  and  $q \times q$  respectively,  $q$  is the reduced order.

Thus  $\mathbf{Q}$  is equal to the left  $\text{SVD}$  column-orthogonal factor  $\mathbf{U}$ .

Note that the algorithm makes use of the Laguerre functions, but they do not appear in the algorithm. The main aim of using the Laguerre functions is to get rid of the  $s$  term in  $(s\mathbf{E} - \mathbf{A})^{-1}$  (3.2). Instead the algorithm makes use of the inverse of  $\mathbf{A}_u = (\mathbf{A} - \alpha\mathbf{E})$ . The parameter  $\alpha$  is chosen such that the inverse exists.

### 3.3 Proposed algorithm

Consider a time-delay system of degree  $n$  with  $p$  ports having  $k$  delays  $\tau_j$ , present in both the state and descriptor matrices, which can be represented in general delayed state space form as:

$$\begin{aligned} \mathbf{E}_0 \dot{x}(t) + \sum_{j=1}^k \mathbf{E}_j \dot{x}(t - \tau_j) &= \mathbf{A}_0 x(t) + \sum_{j=1}^k \mathbf{A}_j x(t - \tau_j) + \mathbf{B}u(t) \\ y(t) &= \mathbf{C}x(t) + \mathbf{D}u(t). \end{aligned} \quad (3.13)$$

Here,  $x(t) \in \mathcal{R}^n$  is the state vector;  $u(t) \in \mathcal{R}^p$  is the control input with  $u(t) = 0$  for  $t < 0$ ;  $y(t) \in \mathcal{R}^p$  is the output.  $\mathbf{A}_0, \mathbf{A}_j, \mathbf{E}_0, \mathbf{E}_j, \mathbf{B}, \mathbf{C}, \mathbf{D}$  are constant matrices with appropriate dimensions. From (3.13) we obtain the transfer function  $\mathbf{H}(s)$  as:

$$\mathbf{H}(s) = \mathbf{C}(s(\mathbf{E}_0 + \sum_{j=1}^k \mathbf{E}_j e^{-s\tau_j}) - (\mathbf{A}_0 + \sum_{j=1}^k \mathbf{A}_j e^{-s\tau_j}))^{-1} \mathbf{B} + \mathbf{D}. \quad (3.14)$$

#### 3.3.1 Delay Approximation

The delay terms  $e^{-s\tau_j}$  in (3.14) are mapped onto the Laguerre domain by applying the bilinear transformation (3.7). Thus obtaining:

$$e^{-s\tau_j} = e^{-a_j \left( \frac{1+u}{1-u} \right)} \quad (3.15)$$

where  $a_j = \alpha\tau_j$ . As the generating function of the Laguerre polynomial [28] [29] is given by,

$$\frac{e^{\frac{-xt}{1-t}}}{(1-t)} = \sum_{i=0}^{\infty} \mathcal{L}_i(x) t^i. \quad (3.16)$$

we can easily prove that

$$e^{-a_j \left( \frac{1+u}{1-u} \right)} = e^{-a_j} e^{-2a_j \left( \frac{u}{1-u} \right)} = e^{-a_j} (1-u) \sum_{i=0}^{\infty} \mathcal{L}_i(2a_j) u^i. \quad (3.17)$$

Using the recurrence relation of Laguerre polynomials, we obtain the approximation series in powers of  $u$  as shown,

$$e^{-a_j \left( \frac{1+u}{1-u} \right)} = e^{-a_j} + \sum_{i=1}^{\infty} e^{-a_j} (\mathcal{L}_i(2a_j) - \mathcal{L}_{i-1}(2a_j)) u^i. \quad (3.18)$$

This will help us to obtain a suitable form for the transfer function of the TDSs in  $u$  domain for deriving the higher-order Krylov.

The delay term is approximated to an order  $r$  i.e;

$$e^{-a_j \left( \frac{1+u}{1-u} \right)} \approx T_d^r = e^{-a_j} + \sum_{i=1}^r e^{-a_j} (\mathcal{L}_i(2a_j) - \mathcal{L}_{i-1}(2a_j)) u^i. \quad (3.19)$$

Such that the error is below a defined threshold as shown

$$\| e^{-a_j \left( \frac{1+u}{1-u} \right)} - T_d^r \|_2 \leq \text{threshold}. \quad (3.20)$$

The threshold is set to a desired level of accuracy required for the reduced order model.

Then (3.14) is mapped to the  $u$ -domain similar to that of (3.9), in which the approximated delay term (3.19) is substituted to obtain an accurate reduced order TDS as described in the following section.

### 3.3.2 Reduced Order Estimation

A priori reduced order estimation makes the construction of the reduced order TDS much more efficient. The reduced order can be estimated by studying the Hankel singular values (HSVs) of the system. The HSVs provides a measure of energy for each state in a system [30].

#### 3.3.2.1 Zero-order Approximation Technique (ZAT)

To obtain an initial estimation for the reduced order of the TDSs we consider a zero order approximation for the delay term i.e;

$$e^{-a_j \left( \frac{1+u}{1-u} \right)} \approx e^{-a_j} \quad (3.21)$$

Thus, approximating the system matrices of (3.13) with delay as:

$$\begin{aligned} \mathbf{E}_{ZAT}(u) &= \mathbf{E}_0 + \sum_{j=1}^k \mathbf{E}_j (e^{-a_j \left( \frac{1+u}{1-u} \right)}) \approx \mathbf{E}_0 + \sum_{j=1}^k \mathbf{E}_j (e^{-a_j}) \\ \mathbf{A}_{ZAT}(u) &= \mathbf{A}_0 + \sum_{j=1}^k \mathbf{A}_j (e^{-a_j \left( \frac{1+u}{1-u} \right)}) \approx \mathbf{A}_0 + \sum_{j=1}^k \mathbf{A}_j (e^{-a_j}) \end{aligned} \quad (3.22)$$

From the decay rate of the HSVs of the system  $(\mathbf{A}_{ZAT}, \mathbf{B}, \mathbf{C}, \mathbf{D}, \mathbf{E}_{ZAT})$ , the reduced order  $q$  can be estimated [31]. Then the reduced order is increased from  $q$  by a bottom-up approach depending on the required pre-defined accuracy.

### 3.3.3 Higher-Order Laguerre Approximation Technique (HLAT)

After estimating the reduced order, the transfer function (3.14) of the strictly proper TDS is then written in terms of Laguerre expansion similar to that of (3.9), i.e. by mapping  $s$ -domain to  $u$ -domain

$$\mathbf{H}(u) = \mathbf{C} \left( \alpha \left( \frac{1+u}{1-u} \right) \mathbf{E}_{TDS}(u) - \mathbf{A}_{TDS}(u) \right)^{-1} \mathbf{B} \quad (3.23)$$

Then, (3.19) is substituted for the delay term in (3.23) such that (3.22) becomes:

$$\begin{aligned} \mathbf{E}_{TDS}(u) &= \mathbf{E}_0 + \sum_{j=1}^k \mathbf{E}_j(e^{-a_j})(1 + \sum_{i=1}^r e^{-a_j}(\mathcal{L}_i(2a_j) - \mathcal{L}_{i-1}(2a_j))u^i) \\ \mathbf{A}_{TDS}(u) &= \mathbf{A}_0 + \sum_{j=1}^k \mathbf{A}_j(e^{-a_j})(1 + \sum_{i=1}^r e^{-a_j}(\mathcal{L}_i(2a_j) - \mathcal{L}_{i-1}(2a_j))u^i). \end{aligned} \quad (3.24)$$

On substituting (3.24) in (3.23) we can write the modified transfer function in  $u$ -domain as,

$$\hat{\mathbf{H}}(u) = \mathbf{C} (\phi_{r+1}u^{r+1} + \phi_r u^r + \dots + \phi_1 u + \phi_0)^{-1} \mathbf{B}. \quad (3.25)$$

Here  $\phi_i$  for  $i = 0, 1, \dots, r+1$  are the coefficients of  $i^{th}$  power of  $u$ , where the constant term

$$\phi_0 = \alpha(\mathbf{E}_0 + \sum_{j=1}^k \mathbf{E}_j(e^{-a_j})) - (\mathbf{A}_0 + \sum_{j=1}^k \mathbf{A}_j(e^{-a_j})), \quad (3.26)$$

the coefficient of  $u$

$$\phi_1 = \alpha(\mathbf{E}_0 + \sum_{j=1}^k \mathbf{E}_j(e^{-a_j})(1 - 2a_j)) + \mathbf{A}_0 + \sum_{j=1}^k \mathbf{A}_j(e^{-a_j})(1 + 2a_j), \quad (3.27)$$

the coefficient of  $u^i$  for  $i = 2, \dots, r$

$$\begin{aligned} \phi_i &= \alpha \sum_{j=1}^k \mathbf{E}_j(e^{-a_j}(\mathcal{L}_i(2a_j) - \mathcal{L}_{i-2}(2a_j))) \\ &\quad - \sum_{j=1}^k \mathbf{A}_j(e^{-a_j}(\mathcal{L}_i(2a_j) - 2\mathcal{L}_{i-1}(2a_j) + \mathcal{L}_{i-2}(2a_j))) \end{aligned} \quad (3.28)$$

and the coefficient of  $u^{r+1}$

$$\phi_{r+1} = \sum_{j=1}^k (\alpha \mathbf{E}_j + \mathbf{A}_j) (e^{-a_j} (\mathcal{L}_r(2a_j) - \mathcal{L}_{r-1}(2a_j))). \quad (3.29)$$

Note that different order of approximation can be chosen for each delay thereby the coefficients of  $u$  will change accordingly for (3.25). In this chapter, the order of approximation is considered equal for all the delays and is equal to that of the largest delay in the TDSs so that the accuracy is guaranteed.

In [32, 33], moment matching theorems for Krylov subspace based model reduction of higher order linear dynamical systems are presented in the context of higher order Krylov subspaces.

For a transfer function of the form,

$$\mathbf{H}(s) = \mathbf{C} (\sigma_r s^r + \sigma_{r-1} s^{r-1} + \dots + \sigma_1 s + \sigma_0)^{-1} \mathbf{B}. \quad (3.30)$$

The  $r$ th order Krylov subspace is defined as

$$\mathcal{K}_q(\mathbf{G}_1, \mathbf{G}_2, \dots, \mathbf{G}_r, \mathbf{L}) = \text{colspan} [P_0, P_1, \dots, P_{q-1}], \quad (3.31)$$

where  $\mathbf{L} = \sigma_0^{-1} \mathbf{B}$  and  $\mathbf{G}_i = \sigma_0^{-1} \sigma_i$  for  $i = 1, 2, \dots, r$  and

$$\begin{aligned} P_0 &= \mathbf{L}; & P_i &= 0 \quad \text{for } i < 0 \\ P_i &= \mathbf{G}_1 P_{i-1} + \dots + \mathbf{G}_r P_{i-r}, \end{aligned} \quad (3.32)$$

This subspace is a generalization of Krylov subspaces for higher order systems and eliminates the linearization step of rewriting the higher-order system in an equivalent first-order form to prove moment-matching properties. However, to match the moments of an  $r$ -th order model, the matrix  $\sigma_0$  should be invertible. Thus, (3.25) can be inferred as Padé approximation of the modified transfer matrix in the  $u$ -domain.

Thereby, the higher order Krylov subspace  $\mathcal{K}_q$  is defined as in (3.31), with  $\mathbf{L} = \phi_0^{-1} \mathbf{B}$  and  $\mathbf{G}_i = \phi_0^{-1} \phi_i$  for  $i = 1, 2, \dots, r + 1$ . The column-orthogonal matrix  $\mathbf{Q}$  for congruence transformation is found through the singular value decomposition (SVD) approach i.e;

$$\mathbf{U} \Sigma \mathbf{V}' = \text{SVD}(\mathcal{K}_q(\mathbf{G}_1, \mathbf{G}_2, \dots, \mathbf{G}_r, \mathbf{L})) \quad (3.33)$$

Thus  $\mathbf{Q}$  is equal to the left SVD column-orthogonal factor  $\mathbf{U}$  of dimension  $n \times q$  associated with the  $(r + 1)^{th}$  Krylov subspace.

The column-orthogonal matrix  $\mathbf{Q}$  thus yields reduced order state-space matrices through congruence transformation described by

$$\begin{aligned}
\mathbf{A}_{0r} &= \mathbf{Q}' \mathbf{A}_0 \mathbf{Q} \quad , \quad \mathbf{A}_{j_r} = \mathbf{Q}' \mathbf{A}_j \mathbf{Q}, \\
\mathbf{E}_{0r} &= \mathbf{Q}' \mathbf{E}_0 \mathbf{Q} \quad , \quad \mathbf{E}_{j_r} = \mathbf{Q}' \mathbf{E}_j \mathbf{Q}, \\
\mathbf{B}_r &= \mathbf{Q}' \mathbf{B} \quad , \quad \mathbf{C}_r = \mathbf{C} \mathbf{Q},
\end{aligned} \tag{3.34}$$

such that the reduced-order transfer matrix  $\mathbf{H}_r(s)$  is

$$\begin{aligned}
\mathbf{H}_r(s) &= \mathbf{C}_r \left( s(\mathbf{E}_{0r} + \sum_{j=1}^k \mathbf{E}_{j_r} e^{-s\tau_j}) \right. \\
&\quad \left. - (\mathbf{A}_{0r} + \sum_{j=1}^k \mathbf{A}_{j_r} e^{-s\tau_j}) \right)^{-1} \mathbf{B}_r
\end{aligned} \tag{3.35}$$

The algorithmic steps of the proposed techniques is shown as a flowchart in Fig. 3.1.

Concerning the complexity of the proposed technique, it can be noted that the most expensive step is related to ZAT for an initial guess of the reduced order and its complexity is  $O(n^3)$  with  $n$  equal to the actual order of the system. If the order of the system  $n$  is larger than 3000, then its advisable to estimate the order using the bottom-up approach. Next, the higher-order Krylov subspace is computed and the SVD has to be performed to obtain the column-orthogonal matrix  $\mathbf{Q}$  (3.33), which has a complexity of  $O(4n^2q)$  where  $q$  is the column size of the  $\mathbf{Q}$  matrix.

### 3.4 Numerical Results

The numerical simulations were performed on a Windows 7 platform on Intel<sup>(R)</sup> Core<sup>(TM)</sup>2 Duo P8700 2.53 GHz machine with 2 GB RAM and has been implemented in Matlab R2010a.

#### Error criteria

The reduced order estimation using ZAT as described in Section 3.3.2.1 depends on the pre-defined accuracy required. The weighted RMS error is used to assess the accuracy of the reduced order model with a target accuracy of 0.001.

The weighted RMS error between the original frequency response  $H_{ij}$  and the reduced order model  $H_{r,(ij)}$  is defined as:

$$\begin{aligned}
Err &= \sqrt{\frac{\sum_{k=1}^{K_s} \sum_{i=1}^{P_{in}} \sum_{j=1}^{P_{out}} \frac{|H_{r,(ij)}(s_k) - H_{(ij)}(s_k)|^2}{W_{(ij)}(s_k)}}{P_{in} P_{out} K_s}} \\
W_{(ij)}(s_k) &= |H_{(ij)}(s_k)|^2.
\end{aligned} \tag{3.36}$$

In (3.36)  $K_s$ ,  $P_{in}$  and  $P_{out}$  are the number of frequency samples, input and output ports of the system, respectively.



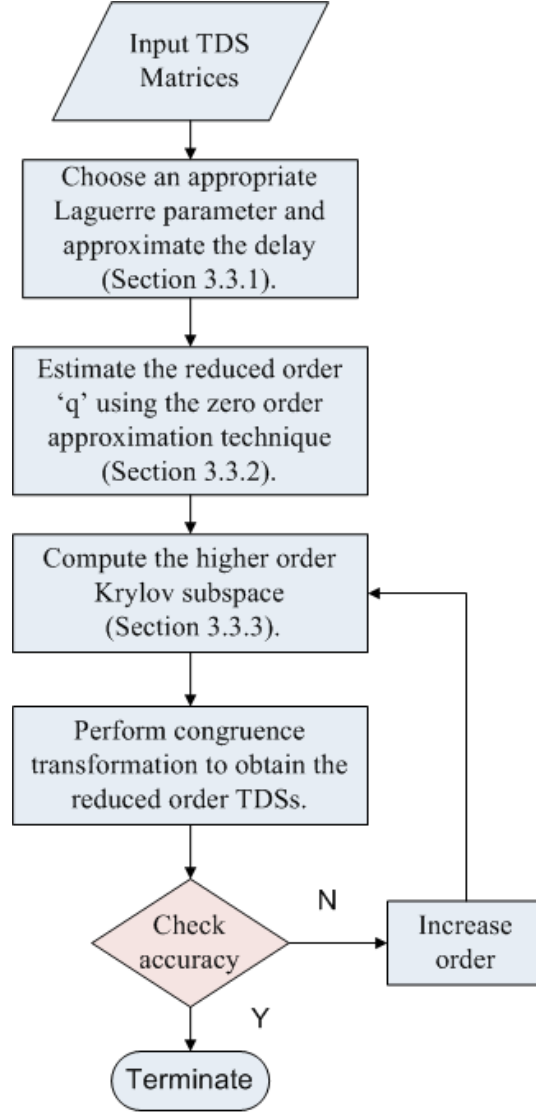


Figure 3.1: Flowchart of the proposed algorithm.

The results obtained using the proposed technique is validated by comparing with Augmented MOR [5] and multiorder Arnoldi MOR [13].

### 3.4.1 BPV: Backplane Vias

A simple backplane via is considered [34] which consists of a probe launch, the differential via, which includes the through part and the stub part, and the uniform stripline section. A simple topology that includes these features is shown in Fig. 3.2. Each probe launch is composed of four uniform transmission line elements which is modeled using the conventional lumped model as in [21]. The via model is the simplest possible model and the uniform stripline structure is modeled using the method of characteristics [5] as a simple, dual lossless stripline based on the geometry as described in [34, 35].

Then the TDSs is constructed as a linear interconnect network with a set of TJs as elaborated in [5]. For the modeling, the per-unit-length (PUL) parameter matrices of the TJs are extracted utilizing the approaches described in [1].

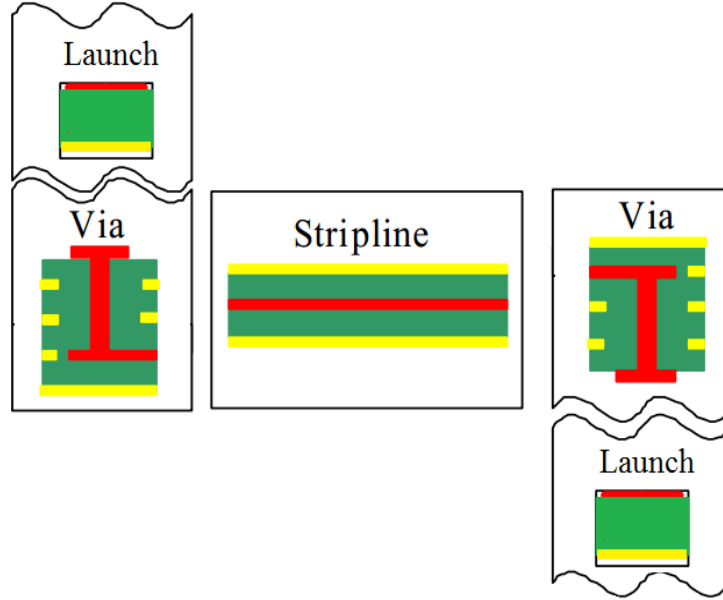


Figure 3.2: BPV: Block Diagram of backplane vias.

The order of the original model is 1448 with  $\tau_{max} = 0.057ns$ . The Laguerre parameter  $\alpha$  for the proposed technique is  $38\pi e9$  and the expansion point for the comparison technique is set to half of the maximum frequency.

Fig. 3.3 plots the HSVs of the approximated TDS, from which an initial guess for the reduced order of the TDSs is obtained.

Fig. 3.4 and Fig. 3.5 plots the magnitude and phase of  $S_{14}(s)$  of the original model with reduced order models of order 387 obtained using the proposed

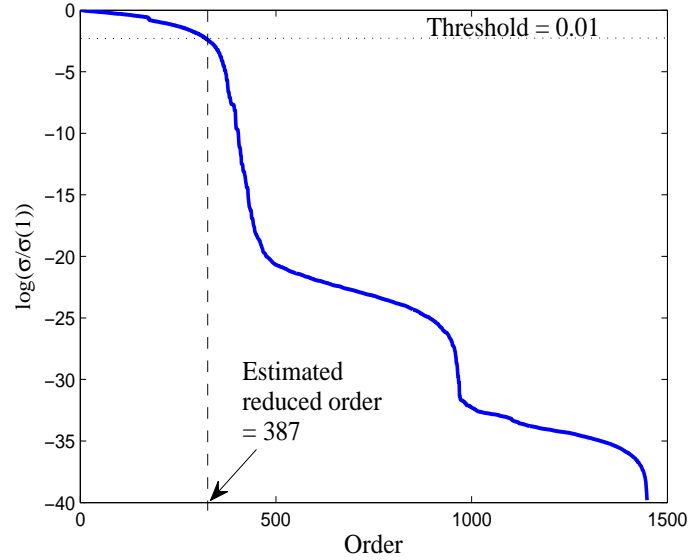


Figure 3.3: BPV: Hankel Singular Values (state contributions) of the approximated model using ZAT.

Technique	Multiorder Arnoldi [13]	Proposed
Initial Order	1448	1448
Order of delay approximation	7	7
Reduced Order	388	387
CPU time (sec)	897.7	702.2

Table 3.1: BPV: Efficiency comparison for achieving a weighted RMS error of 0.001

technique.

Table 3.1 compares the efficiency of the different techniques for achieving a weighted RMS error (3.36) smaller than 0.001 with 201 frequency samples in the range [1-10] GHz. For both the techniques the delays are approximated to an order of 7 and is obtained by setting a threshold of 0.01 for (3.20). If we consider a higher threshold then we might not be able to obtain an accuracy of 0.001 for the reduced order TDSs. Fig. 3.6 shows the approximation curve for  $\tau_{max} = 0.057ns$  considering  $r=2,5,7$ .

In Table 3.1 the CPU time for the proposed technique includes the time for

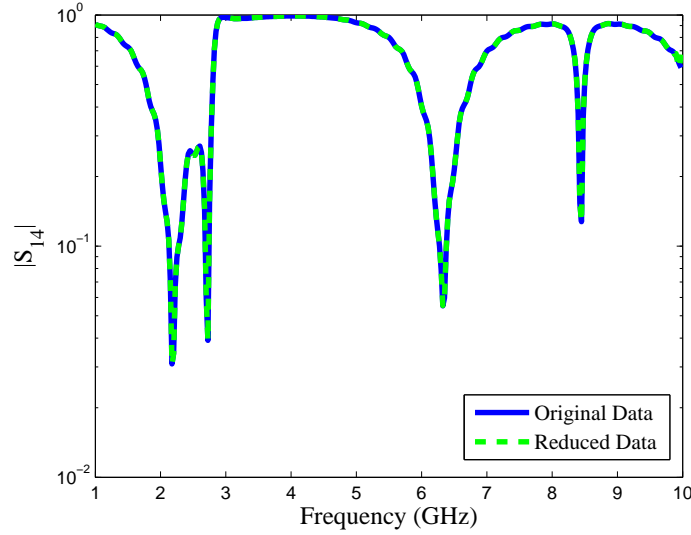


Figure 3.4: BPV: Magnitude of  $S_{14}$ .

Solution method	Size	CPU Time for generating the reduced TDSs	Simulation Time
Original System	1448		2406.82
Proposed	387	702.2	6.21

Table 3.2: BPV: Computational Information

the reduced order estimation and the time for generating the reduced TDSs, while that for the multiorder Arnoldi is with a bottom-up approach for generating the reduced order TDSs with the required accuracy. The technique presented in [5] using augmented first order systems could not be used for the comparison due to memory limitations.

Table 3.2 compares the total size and simulation times of the original and proposed algorithm. For this example, the simulation time of the reduced order TDSs is about 388 times faster when compared to the original system.

Thus in this example the proposed method is able to model the S-parameter of the system accurately. In the next example, the technique models the admittance (Y) parameter which is in general more difficult to accurately capture the model behavior due to the resonance peaks.

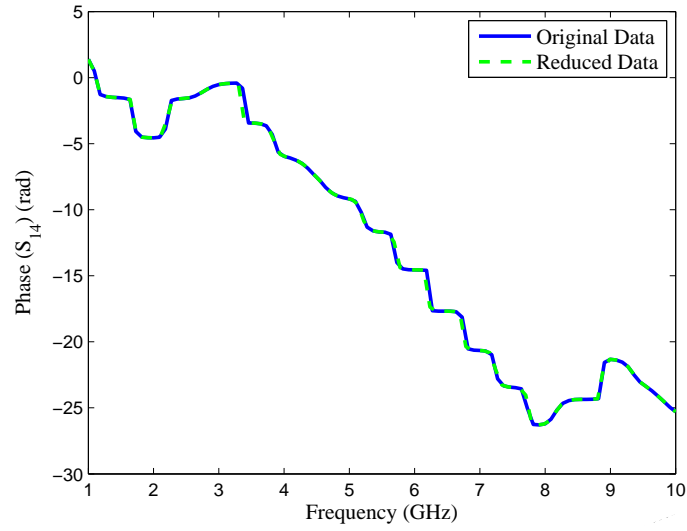


Figure 3.5: BPV: Phase of  $S_{14}$ .

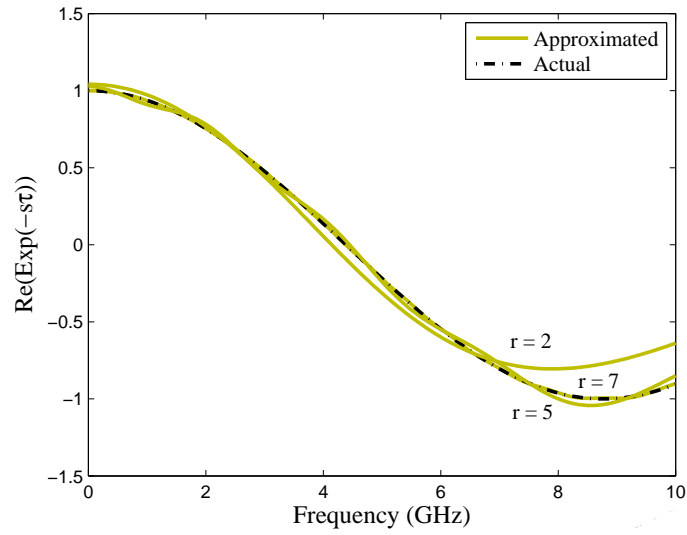


Figure 3.6: BPV: Approximation of the delay term.

### 3.4.2 RLC: RLC Network With Delay Elements

A system consisting of two lossless multiconductor transmission lines (MTLs) and three RLC networks has been modeled ( see Fig. 3.7). The detailed procedures of constructing such TDSs are elaborated in [5]. Each MTL block is composed of three conductors and it has a length equal to 2 cm in total and the RLC network has a length of 1.5 cm in total.

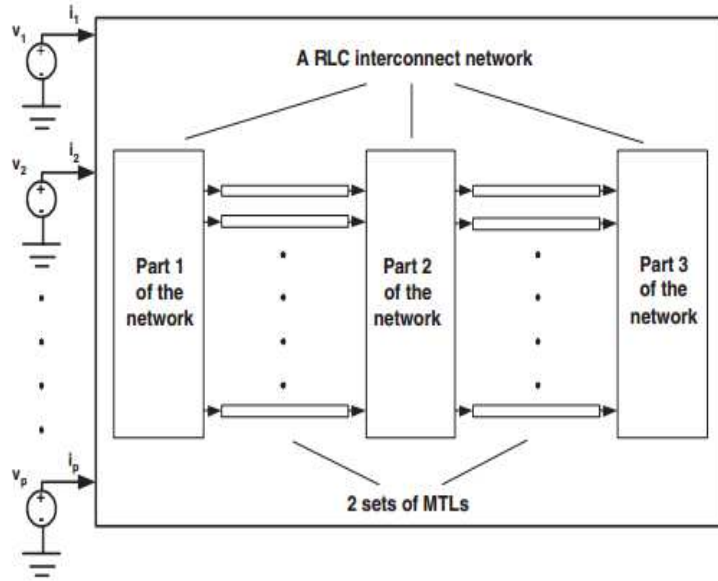


Figure 3.7: Schematic of RLC network including delay elements.

The order of the original network is 2625 with  $\tau_{max} = 0.02ns$ . The frequency range of interest for this system is [0-6] GHz. The Laguerre parameter  $\alpha$  for the proposed method is  $24\pi e9$  and the expansion point for the compared techniques is set to half of the maximum frequency.

The reduced order is estimated as described in Section 3.3.2, from the HSVs of the approximated TDSs.

Fig. 3.8 - Fig 3.9 compares the magnitude and phase of the original and Laguerre-based reduced delayed model  $Y_{14}(s)$ . A good agreement is obtained between the original and reduced model.

Table 3.3 compares the efficiency of the different techniques for achieving a weighted RMS error (3.36) smaller than 0.001 with 201 frequency samples in the range [0-6] GHz. As in the former example for a threshold of 0.01 for (3.20), the order of approximation for the delay is 5 for both the techniques. The CPU

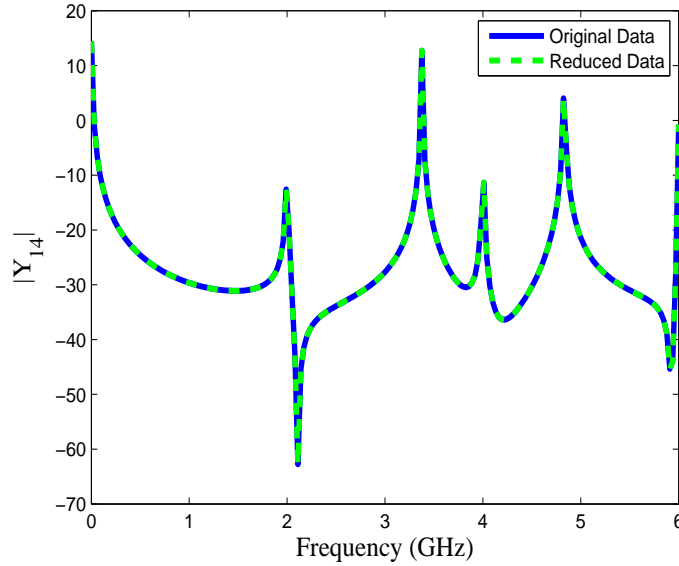


Figure 3.8: RLC: Magnitude of  $Y_{14}$ .

Technique	Multiorder Arnoldi [13]	Proposed
Initial Order	2625	2625
Order of delay approximation	5	5
Reduced Order	212	213
CPU time (sec)	934.70	896.73

Table 3.3: RLC: Efficiency comparison for achieving a weighted RMS error of 0.001

time for the proposed technique includes the time for the reduced order estimation and the time for generating the reduced TDSs, while that for the multiorder Arnoldi is with a bottom-up approach for generating the reduced order TDSs with the required accuracy. The technique presented in [5] using augmented first order systems could not be used for the comparison due to memory limitations.

Similar to the previous example Table 3.4 compares the total size and simulation times of the original and proposed algorithm and the simulation time of the reduced order TDSs is about 980 times faster when compared to the original system.

Thus, from the above results we see that the proposed technique is able to

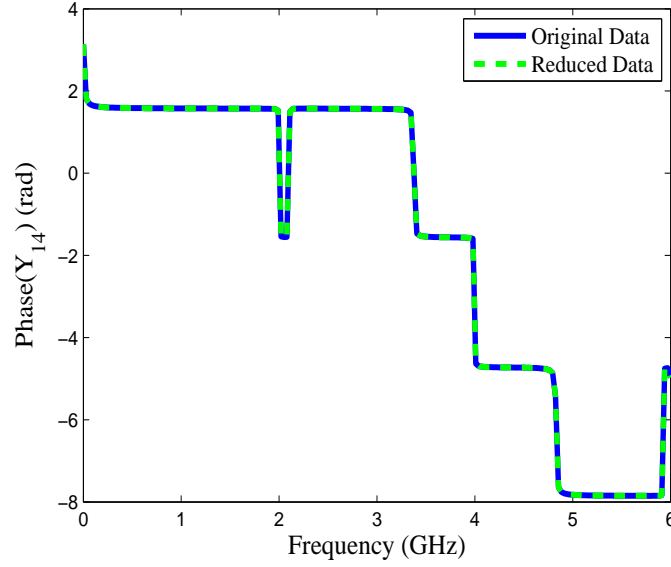


Figure 3.9: RLC: Phase of  $Y_{14}$ .

Solution method	Size	CPU Time for generating the reduced TDSs	Simulation Time
Original System	2625		3409.42
Proposed	213	896.73	3.48

Table 3.4: RLC: Computational Information

reduce TDS more efficiently to achieve the required accuracy using Laguerre expansion.

### 3.5 Conclusion

In this chapter, a novel model order reduction method for large linear networks that contain delay elements is presented. The algorithm is based on higher order Krylov subspace for model order reduction of time-delay systems based on a Laguerre expansion technique. The proposed technique consists of three parts: 1) the delays are approximated using recursive relation of Laguerre polynomial then 2) the reduced order is estimated for the time-delay system using a smart truncation of



the delay term and 3) a higher order Krylov subspace is computed using Laguerre expansion for obtaining the congruence-based reduced order time-delay system.

The approximation of the delays using a recursive relation of the Laguerre polynomial gives a better approximation with lesser terms in comparison with the Taylor series expansion. This is obtained with the proper choice of the Laguerre parameter  $\alpha$ , and for systems with large delays this can be difficult. To have an accurate reduced order model for systems with large delays, multipoint expansion technique must be considered. In Chapter 4 an adaptive multipoint expansion MOR technique is proposed.

## Acknowledgment

This work was supported by the Interuniversity Attraction Poles Programme BEST-COM initiated by the Belgian Science Policy Office and the Research Foundation Flanders (FWO).

## References

- [1] C. Paul. *Analysis of Multiconductor Transmission Lines*. Wiley, New York, 1994.
- [2] R. Achar and M. Nakhla. *Simulation of high-speed interconnects*. Proceedings of the IEEE, 89(5):693–728, May 2001.
- [3] T. Dhaene and D. de Zutter. *Selection of lumped element models for coupled lossy transmission lines*. IEEE Transactions on Computer-Aided Design of Integrated Circuits and Systems, 11(7):805–815, Jul. 1992.
- [4] J.-P. Richard. *Time-delay systems: an overview of some recent advances and open problems*. Automatica, 39(10):1667–1694, 2003.
- [5] W. Tseng, C. Chen, E. Gad, M. Nakhla, and R. Achar. *Passive Order Reduction for RLC Circuits With Delay Elements*. IEEE Transactions on Advanced Packaging, 30(4):830–840, Nov. 2007.
- [6] E. Chiprout and M. Nakhla. *Analysis of interconnect networks using complex frequency hopping (CFH)*. IEEE Transactions on Computer-Aided Design of Integrated Circuits and Systems, 14(2):186–200, Feb. 1995.
- [7] T. Tang and M. Nakhla. *Analysis of high-speed VLSI interconnects using the asymptotic waveform evaluation technique*. IEEE Transactions on Computer-Aided Design of Integrated Circuits and Systems, 11(3):341–352, Mar. 1992.
- [8] P. Feldmann and R. Freund. *Efficient linear circuit analysis by Pade approximation via the Lanczos process*. IEEE Transactions on Computer-Aided Design of Integrated Circuits and Systems, 14(5):639–649, May 1995.
- [9] P. Gunupudi, M. Nakhia, and R. Achar. *Simulation of high-speed distributed interconnects using Krylov-space techniques*. IEEE Transactions on Computer-Aided Design of Integrated Circuits and Systems, 19(7):799–808, Jul. 2000.
- [10] A. Charest, M. Nakhla, and R. Achar. *Passive model-order reduction of RLC circuits with embedded time-delay descriptor systems*. IEEE 20th Conference on Electrical Performance of Electronic Packaging and Systems, pages 223–226, Oct. 2011.
- [11] A. Charest, M. Nakhla, R. Achar, and D. Saraswat. *Passivity Verification of Delayed Rational Function Based Macromodels of Tabulated Networks Characterized by Scattering Parameters*. IEEE Transactions on Components, Packaging and Manufacturing Technology, 1(3):386–398, Mar. 2011.

- [12] F. Ferranti, M. Nakhla, G. Antonini, T. Dhaene, L. Knockaert, and A. Ruehli. *Multipoint Full-Wave Model Order Reduction for Delayed PEEC Models With Large Delays*. IEEE Transactions on Electromagnetic Compatibility, 53(4):959–967, Nov. 2011.
- [13] E. Rasekh and A. Dounavis. *Multiorde Arnoldi Approach for Model Order Reduction of PEEC Models With Retardation*. IEEE Transactions on Components, Packaging and Manufacturing Technology, 2(10):1629–1636, Oct. 2012.
- [14] G. Kequin, K. L. Vladimir, and C. Jie. *Stability of Time-Delay Systems*. Birkhauser Boston, New York, 2003.
- [15] W. Michiels, E. Jarlebring, and K. Meerbergen. *Krylov-Based Model Order Reduction of Time-delay Systems*. SIAM J. Matrix Anal. Appl., 32(4):1399–1421, 2011.
- [16] J. Phillips, E. Chiprout, and D. Ling. *Efficient full-wave electromagnetic analysis via model-order reduction of fast integral transforms*. 33rd Design Automation Conference Proceedings 1996, pages 377–382, Jun., 1996.
- [17] J. Cullum, A. Ruehli, and T. Zhang. *A method for reduced-order modeling and simulation of large interconnect circuits and its application to PEEC models with retardation*. IEEE Transactions on Circuits and Systems II: Analog and Digital Signal Processing, 47(4):261–273, Apr. 2000.
- [18] Y. Su, J. Wang, X. Zeng, Z. Bai, C. Chiang, and D. Zhou. *SAPOR: second-order Arnoldi method for passive order reduction of RCS circuits*. IEEE/ACM International Conference on Computer Aided Design, 2004. ICCAD-2004., pages 74–79, Nov. 2004.
- [19] Z. Bai and Y. Su. *Dimension Reduction of Large-Scale Second-Order Dynamical Systems via a Second-Order Arnoldi Method*. SIAM Journal on Scientific Computing, 26(5):1692–1709, 2005.
- [20] P. M. Mäkilä. *Laguerre series approximation of infinite dimensional systems*. Automatica, 26(6):985–995, 1990.
- [21] L. Knockaert and D. De Zutter. *Laguerre-SVD reduced-order modeling*. IEEE Transactions on Microwave Theory and Techniques, 48(9):1469–1475, Sept. 2000.
- [22] X.-L. Wang and Y.-L. Jiang. *Model order reduction methods for coupled systems in the time domain using Laguerre polynomials*. Computers and Mathematics with Applications, 62(8):3241–3250, October 2011.

- [23] B. Salimbahrami, R. Eid, and B. Lohmann. *Model reduction by second order Krylov subspaces: Extensions, stability and proportional damping*. 2006 IEEE International Symposium on Intelligent Control, pages 2997–3002, Oct. 2006.
- [24] L. Knockaert, T. Dhaene, F. Ferranti, and D. D. Zutter. *Model order reduction with preservation of passivity, non-expansivity and Markov moments*. Systems & Control Letters, 60(1):53–61, Jan. 2011.
- [25] G. Szegő. *Orthogonal Polynomials*. American Mathematical Society, New York, 1939.
- [26] W. E. Arnoldi. *The principle of minimized iterations in the solution of the matrix eigenvalue problem*. Quarterly of Applied Mathematics, 9, 1951.
- [27] E. J. Grimme. *Krylov Projection Methods For Model Reduction*. PhD Thesis, Electrical Engineering, University of Illinois, 1997.
- [28] A. H. Al-mohy and N. J. Higham. *Computing the action of the matrix exponential, with an application to exponential integrators*. Electronic Transactions on Numerical Analysis, 37:147–165, 2010.
- [29] N. N. Lebedev. *Special functions and their applications*. Courier Dover Publications, 308 Seiten, 1972.
- [30] K. Zhou, J. C. Doyle, and K. Glover. *Robust and Optimal Control*. Prentice-Hall, Englewood Cliffs, New Jersey, 1996.
- [31] A. C. Antoulas, D. C. Sorensen, and Y. Zhou. *On the decay rate of Hankel singular values and related issues*. CONTROL LETT, 46:323–342, 2002.
- [32] R. W. Freund. *SPRIM structure-preserving reduced-order interconnect macromodeling*. Proceedings of the 2004 IEEE/ACM International conference on Computer-aided design, pages 80–87, 2004.
- [33] K. Tsuyoshi and G. Sanjay. *Moment Matching Theorems for Dimension Reduction of Higher-Order Dynamical Systems via Higher-Order Krylov Subspaces*. Report No. UCB/SEMM-2008/04, University of California, Berkeley, 2008.
- [34] E. Bogatin, L. Simonovich, S. Gupta, and M. Resso. *Practical analysis of backplane vias*. in Proc. DesignCon, pages 1–24, Feb. 2009.
- [35] L. Simonovich, E. Bogatin, and Y. Cao. *Differential Via Modeling Methodology*. IEEE Transactions on Components, Packaging and Manufacturing Technology, 1(5):722–730, May 2011.

# 4

## A Hybrid Adaptive Sampling Algorithm for Multipoint MOR

Based on the publications:

**Elizabeth Rita Samuel, Luc Knockaert, Tom Dhaene,**  
*“Passivity preserving Multipoint Model Order Reduction using Reflective Exploration”, published in proceedings of 10th International Conference on Informatics in Control, Automation and Robotics, pages 483–491, Vienna, Austria, 2014.*

**Elizabeth Rita Samuel, Francesco Ferranti, Luc Knockaert, Tom Dhaene,**  
*“A Hybrid Adaptive Sampling Algorithm for Obtaining Reduced Order Models for Systems with Frequency Dependent State-Space Matrices”, submitted to IEEE Transactions on Components Packaging and Manufacturing Technology, August 2014*

\*\*\*

*MOR techniques are now standard for reducing the complexity of large scale models and the computational cost of the simulations, while retaining the important physical features of the original system. In order to have a sufficiently accurate reduced order model not only at a single frequency point but over a whole range of frequencies, multipoint MOR was proposed. Multipoint MOR raises many*

*practical implementation questions. In this chapter, the focus is put on three points namely;*

- *the order considered for each expansion point.*
- *the adaptive frequency sampling using reflective exploration [1].*
- *obtaining a compact projection matrix.*

*A new adaptive algorithm for selecting the expansion points is proposed using a hybrid technique of reflective exploration and binary search. In the first section of the chapter, the reflective exploration technique for adaptive frequency sampling is illustrated on quasi-static systems i.e., systems with frequency independent state-space matrices. In the next section, the hybrid technique is applied to systems with frequency dependent state-space matrices to illustrate the adaptive frequency sampling.*

## 4.1 Introduction

As the system data rates achieve multi-gigabit levels for nanometer scale integrated circuits (ICs) and printed circuit boards (PCBs), it is increasingly important for designers to consider the system interconnect in its entirety. From this vantage point, IC package design has become of great importance. High-speed IC package designers must ensure both signal and power integrity by designing IC package structures that are properly modeled, extracted, and simulated. Fortunately, integrated modeling and analysis techniques and tools are available to describe a complicated package structure with true three-dimensional representations, and simulate those representations in the context of system interconnects. These tools help designers take into account the package effect from designs and make decisions based on actual conditions. This reduces the number of design iterations, cycles, and development time [2, 3].

For the three-dimensional field solvers both full-wave and quasi-static solvers are useful in representing package behavior, depending on the application. Quasi-static field solvers are used for obtaining complex algebraic systems of equations with frequency independent state space matrices while full-wave solvers provide frequency dependent matrices in the frequency domain.

The three-dimensional field solvers are very accurate but that is at the cost of very large system of equations which are expensive to solve. Hence, obtaining a compact macromodel for the electromagnetic (EM) systems has become increasingly important over the last years. Model order reduction (MOR) is a technique that has been developed to speed up the EM simulations.

Reduced state-space models obtained by MOR techniques must be accurate over the whole frequency range of interest and must also preserve the properties

of the original system. For a quasi-static electromagnetic analysis, several robust MOR techniques have been proposed over the years [4–8]. The Krylov subspace projection methods such as PVL [6] and PRIMA [8] are the most utilized algorithms over the past decade. It can be noted that for Krylov-based MOR the projection space can be constructed from multipoint Krylov subspaces [9–11]. For a given reduced order the multipoint approximation tends to be more accurate but is usually numerically very expensive to obtain. Multipoint expansion provides a better framework for frequency dependent models and also for models with varying parameters [12]. Some techniques have been proposed for the model order reduction of full-wave systems [13–15], where a state-space representation with frequency dependent matrices is obtained. In [13], a hybrid algorithm which incorporates features of orthogonalized Krylov methods and the series-expansion-based methods to construct a multipoint rational approximant is proposed to obtain reduced order models (ROMs). The approach in [14] extracts exponential terms (primary phase factors) after which the remainders are expanded into a linear form and then projected to obtain the reduced model. Hence, the extraction of primary phase factors and the segregation of the system into multiple remainder phase matrices, each corresponding to a primary phase factor, is needed. In [15], systems described by neutral delayed differential equations are considered, which are also frequency dependent, and the reduced model is obtained by a binary search.

In Section 4.2 of the chapter, multipoint reduction technique using reflective exploration is proposed to adaptively choose the expansion points for quasi-static systems i.e., systems with frequency independent state-space matrices. The projection matrices are computed using the PRIMA technique [8], which is known to be an efficient technique for the reduction of large systems. The expansion points are selected adaptively using a reflective exploration (RE) technique. It is a sequential sampling algorithm, where the model is improved incrementally using the best possible data at every time step and also has additional properties allowing it to propose candidate exploration points [1]. An error-based exploration is implemented to find the expansion points. The corresponding projection matrices are then computed using a Krylov based MOR technique. Finally, the projection matrices are merged to obtain the overall projection matrix. When the number of expansion points increases, the merged projection matrix also grows and might fail to provide a satisfactory model dimension reduction. An adaptive truncation algorithm is proposed to truncate the merged projection matrix based on its singular values, thereby obtaining a more compact ROM which preserves the system properties. The technique is illustrated using suitable numerical examples in Section 4.2.6.

In Section 4.3, systems described with frequency dependent state-space matrices are considered. For the frequency dependent model it can be noted that the solver can have samples over a specified frequency range. These samples can be

obtained from numerical simulations, which can be very expensive. The simulations can be done in the time domain (TD) and as well as in the frequency domain (FD), but phenomena like skin effect, dielectric loss and delays require additional information for modeling and these can be more easily modeled in the FD [16]. To obtain the evaluation of the state-space matrices for each frequency sample can be computationally expensive and sometimes even lead to oversampling. If the sampling rate is reduced then there could be undersampling, which might lead to loss of important features of the frequency response. Prior knowledge of the dynamics of the EM system is always beneficial for the appropriate selection of the frequency sample distribution [17]. Uniform gridding or random selection of samples are uninformed algorithms and thus may not be ideal. This section of the chapter proposes a hybrid adaptive sampling algorithm to automate the generation of reduced order models for systems described by large scale frequency dependent state-space models. The evaluation of the frequency dependent state-space model for each frequency sample can be computationally expensive. The distribution of frequency samples must be optimized to avoid oversampling and undersampling. In order to have an optimum number of frequency samples, the proposed algorithm uses reflective exploration technique for the adaptive selection of the samples and the sampling is further refined using a binary search to validate the frequency dependent reduced order models. Projection based model order reduction techniques are used for obtaining the reduced order model. The projection matrices obtained for each frequency sample are merged to obtain a common projection matrix for all the samples. However, in certain cases when the number of sample points becomes large, the merged projection matrix also increases in dimension and might fail to provide a satisfactory model order reduction. Thus, the merged projection matrix is truncated based on its singular values to obtain a compact common projection matrix. The reduced order state-space matrices per frequency are interpolated over the frequency range of interest to obtain the complete system response.

The proposed algorithm thus has three main sections:

1. Reflective exploration (RE): As explained in Section 4.2.3. RE is a selective sampling method, where the model is improved incrementally using the best possible datum at every time step using the reflective functions. These functions allow it to propose candidate exploration points [1, 18].
2. Binary search (BS): It is a dichotomic divide and conquer search. At each step the ROM is computed at the midpoint of two samples by linear interpolation to validate the model obtained through RE. The interpolation is then compared with the actual model simulated at that point using an EM simulator. This is continued till all the sections are modeled accurately [15].
3. Model compacting: After the samples are chosen adaptively the reduced frequency dependent state-space matrices are interpolated linearly to repre-



sent the frequency behavior over a frequency range of interest. Note that for quasi-static systems there is no interpolation as the state-space matrix is frequency independent. Interpolation is only present for systems represented using frequency dependent state-space matrices. For obtaining the ROM, a common projection matrix is used and to make the model more compact the singular value of the merged projection matrices obtained from the samples are truncated [19].

Pertinent examples in Section 4.3.3 illustrate the proposed hybrid adaptive sampling algorithm.

## 4.2 Multipoint MOR for frequency independent state-space matrices using reflective exploration

### 4.2.1 PRIMA

Here, a brief overview is provided of the PRIMA algorithm for a MIMO descriptor system of the form

$$\begin{aligned} \mathbf{E}\dot{x}(t) &= \mathbf{A}x(t) + \mathbf{B}u(t) \\ y(t) &= \mathbf{C}x(t) + \mathbf{D}u(t). \end{aligned} \quad (4.1)$$

Let  $s_0$  be a suitably chosen expansion point such that the matrix  $s_0\mathbf{E} - \mathbf{A}$  is nonsingular. Then the transfer function can be rewritten as:

$$\begin{aligned} \mathbf{H}(s) &= \mathbf{C}(s_0\mathbf{E} - \mathbf{A} + (s - s_0)\mathbf{E})^{-1}\mathbf{B} + \mathbf{D} \\ &= \mathbf{C}(\mathbf{I} + (s - s_0)\mathbf{M})^{-1}\mathbf{R} + \mathbf{D} \end{aligned} \quad (4.2)$$

where  $\mathbf{M} = (s_0\mathbf{E} - \mathbf{A})^{-1}\mathbf{E}$ ,  $\mathbf{R} = (s_0\mathbf{E} - \mathbf{A})^{-1}\mathbf{B}$ .

The  $q$ -th block Krylov-subspace is given by

$$\mathcal{K}_q(M, R) = \text{colspan}[\mathbf{R} \ \mathbf{M}\mathbf{R} \ \mathbf{M}^2\mathbf{R} \ \dots \ \mathbf{M}^{(q-1)}\mathbf{R}]. \quad (4.3)$$

This yields  $P_q$  the column orthogonal matrix computed from the Krylov subspace  $\mathcal{K}_q(M, R)$ , from which using congruence transformation (4.4) the reduced state-space matrices  $(\mathbf{A}_q, \mathbf{E}_q, \mathbf{B}_q, \mathbf{C}_q, \mathbf{D}_q)$  are obtained as:

$$\begin{aligned} \mathbf{A}_q &= P_q^T \mathbf{A} P_q, \quad \mathbf{E}_q = P_q^T \mathbf{E} P_q, \\ \mathbf{B}_q &= P_q^T \mathbf{B}, \quad \mathbf{C}_q = \mathbf{C} P_q, \quad \mathbf{D}_q = \mathbf{D}. \end{aligned} \quad (4.4)$$

### 4.2.2 Multipoint projection matrix

After model order reduction, the resulting model must not only be accurate at one frequency point but over the whole range of interest and must also preserve passivity. For this the multipoint reduction algorithm is used [15].

At each expansion point, the column orthogonal matrix is computed as described in Section 4.2.1, i.e., for  $N$  expansion points the corresponding matrices  $P_{q_i}$  ( $i = 1, 2, \dots, N$ ) are merged to give;

$$\mathbf{P}_{union} = \text{colspan}[P_{q_1} \ P_{q_2} \ \dots \ P_{q_N}]. \quad (4.5)$$

The merged projection matrix is not truncated during the iterative procedure of the reflective exploration. The matrix is truncated however after all the expansion points are adaptively chosen as is described in the following section.

### 4.2.3 Reflective Exploration

The process of selecting expansion points and building the model in an adaptive way is referred to as reflective exploration [1]. RE is an effective technique when it is very expensive to obtain the model from EM simulators. For the exploration a reflective function is required to select a new expansion point. The reflective function used for the proposed multipoint MOR algorithm is the error norm between the best model and the second best model. As described in [18], the algorithm has two loops: an adaptive modeling loop and an adaptive sampling loop.

1. Adaptive Modeling Loop: The algorithm starts with two expansion points selected at  $\omega_{min}$  and  $\omega_{max}$  of the frequency range of interest. It should be noted that the initial number of sample points that is uniformly distributed along the frequency range of interest can be varied as needed, if prior knowledge of the system is available.

The reduced order  $q$  at the chosen expansion points is considered to be equal to the number of input ports of the system initially. Then the reduced model is obtained with a common projection matrix as explained in Section 4.2.2. If the RMS error (4.6) between the two best models ( $I^{th}$  and  $(I - 1)^{th}$ ) is more than a threshold  $\delta_{mod}$ , then the reduced order  $q$  is increased by the number of input ports for all the expansion points. In this chapter the threshold is chosen to be  $10^{-3}$ .

$$Err_{est}^{(I)} = \sqrt{\frac{\sum_{k=1}^{K_s} \sum_{i=1}^{P_{in}} \sum_{j=1}^{P_{out}} \frac{|H_{I,(ij)}(s_k) - H_{I-1,(ij)}(s_k)|^2}{W_{(ij)}(s_k)}}{P_{in} P_{out} K_s}} \quad (4.6)$$

$$W_{(ij)}(s_k) = |H_{I,(ij)}(s_k)|^2.$$

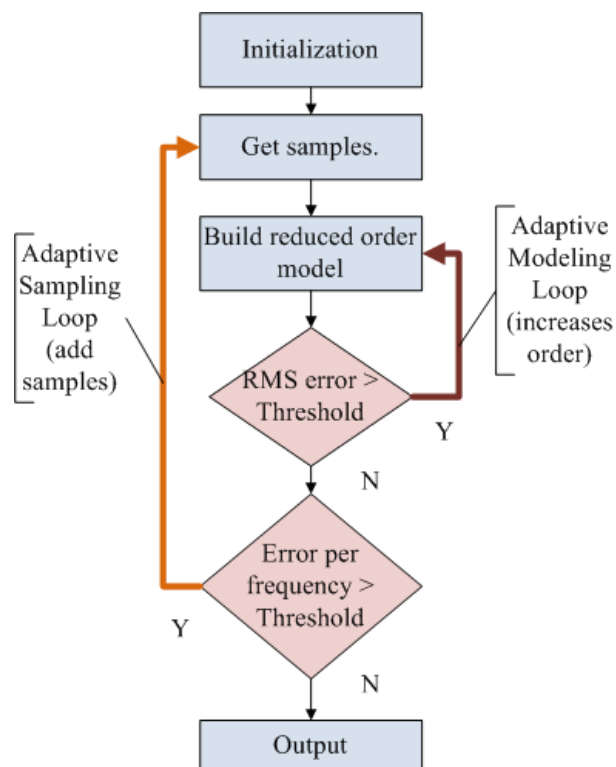


Figure 4.1: Reflective Exploration.

Here,  $K_s$ ,  $P_{in}$  and  $P_{out}$  are the number of frequency samples considered on a dense grid, input and output ports of the system, respectively.

2. Adaptive Sampling Loop: When the difference in RMS error (4.6), between the two consecutive models is very small i.e.,

$$\frac{Err_{est}^{(I)} - Err_{est}^{(I-1)}}{Err_{est}^{(I-1)}} < \delta_{samp} \quad (4.7)$$

(for the chapter the difference is considered to be less than 10%), then a new expansion point is selected. For selecting the new expansion point, the error per frequency is first computed by taking the standard 2- norm of the frequency response of the best model ( $H_I$ ) and the original model ( $H_{act}$ ), and then the frequency at which  $Err_{s_k}$  is maximum is chosen to be as the new expansion point.

$$Err_{s_k} = \|H_{act}(s_k) - H_I(s_k)\|; \quad k = 1, \dots, K_s. \quad (4.8)$$

This process is iteratively repeated until the RMS error between the original frequency response and the reduced model is  $10^{-3}$ . Figure 4.1 shows a flowchart of the RE algorithm.

#### 4.2.4 Model compacting

After obtaining the best ROM from the iterative procedure, it might be possible to further compact the model with the information obtained from the singular values  $\Sigma$  (4.9) of the  $P_{union}$  (4.5).

The economy-size  $SVD$  is computed for the common projection matrix  $V_{comm}$  (4.5), to obtain the singular values  $\Sigma$  of the merged projection matrix. In matlab the economy-sized  $SVD$  is computed as shown:

$$\mathbf{U}\Sigma\mathbf{V}' = SVD(\mathbf{P}_{union}, 0) \quad (4.9)$$

Here,  $\mathbf{U}$  and  $\mathbf{V}$  are orthogonal matrices, which are known as the left and right singular values. The diagonal of  $\Sigma$  gives the singular values of the system.

$$\sigma = diag(\Sigma). \quad (4.10)$$

The reduced order for the system is defined based on the first  $q_{comm}$  significant singular values of  $\mathbf{P}_{union}$ , which is computed by adaptively setting a threshold on the ratio of the singular values with respect to the largest singular value as shown

in Fig.4.2. The ROM obtained by the truncation of the merged projection matrix with respect to the singular value, is compared with the best model obtained from reflective exploration. If the RMS error after truncation is less than  $10^{-4}$ , then we shall truncate the singular values. If the error is large we keep the model with the number of singular values obtained before.

The compact projection matrix  $\mathbf{Q}_{comm}$  is equal to the left singular value  $\mathbf{U}$  where the column is truncated to a size  $q_{comm}$  based on the significance of the singular values.

$$\mathbf{Q}_{comm} = \mathbf{U}(:, 1 : q_{comm}). \quad (4.11)$$

After truncation it can be noted that, on average per expansion point an order of  $q_{samp}$  (4.12) is required to guarantee the desired accuracy at that expansion point.

$$q_{samp} = q_{comm}/N. \quad (4.12)$$

Here,  $n$  is the number of expansion points.

Once the compact projection matrix  $\mathbf{Q}_{comm}$  is computed, it is applied to the original system (4.1) and a reduced system (4.4) is obtained through congruence transformation.

#### 4.2.5 Passivity Preservation

For transient behavior, stability and passivity are the fundamental properties to be guaranteed by the system, as stated in Section 2.1.5. A passive system denotes a system that is incapable of generating energy, and hence one that can only absorb energy from the sources used to excite it [20]. Passivity is an important property to satisfy because stable, but not passive macromodels can produce unstable systems when connected to other stable, even passive, loads.

If the descriptor state-space model in (4.1) satisfies the following properties [8]:

$$\begin{aligned} \mathbf{E} &= \mathbf{E}' \geq 0 \\ \mathbf{A} + \mathbf{A}' &\leq 0 \\ \mathbf{B} &= \mathbf{C}', \end{aligned} \quad (4.13)$$

then it ensures the passivity of the admittance model  $\mathbf{Y}(s) = \mathbf{C}(s\mathbf{E} - \mathbf{A})^{-1}\mathbf{B}$  and with congruence transformation the passivity of the model is preserved,

$$\begin{aligned} \mathbf{E}_r(\mathbf{g}) &= \mathbf{Q}_{comm}' \mathbf{E}(\mathbf{g}) \mathbf{Q}_{comm} \geq 0 \\ \mathbf{A}_r(\mathbf{g}) &= \mathbf{Q}_{comm}' \mathbf{A}(\mathbf{g}) \mathbf{Q}_{comm} \leq 0 \\ \mathbf{B}_r(\mathbf{g}) &= \mathbf{Q}_{comm}' \mathbf{B}(\mathbf{g}) \\ \mathbf{C}_r(\mathbf{g}) &= \mathbf{Q}_{comm} \mathbf{C}(\mathbf{g}). \end{aligned} \quad (4.14)$$

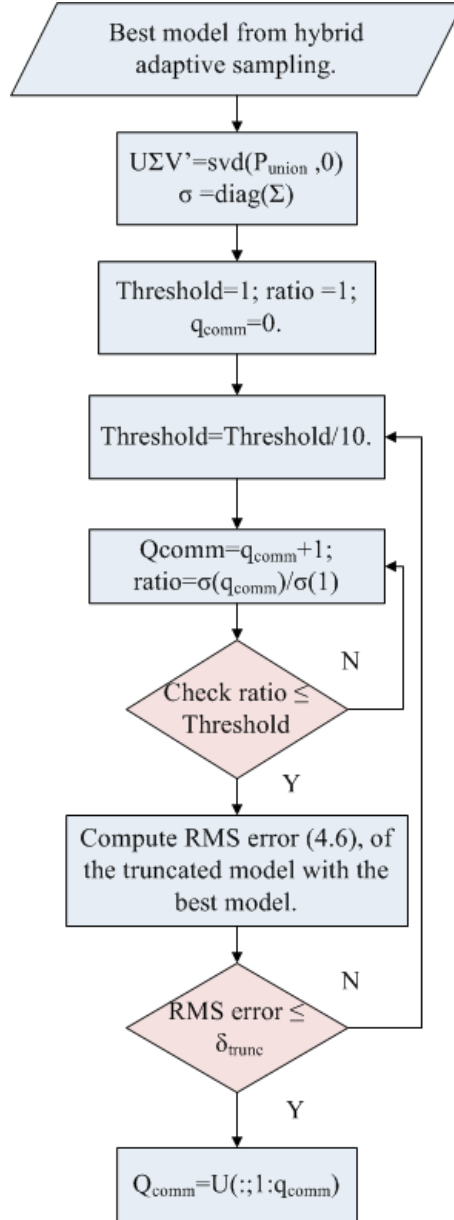


Figure 4.2: Truncation of the projection matrix.

If the system fails to have the state-space properties described in (4.13) then the technique of Linear Matrix Inequalities (LMI's) [21] has to be used. The solution obtained from the LMI's [22, 23] gives a descriptor state space format that preserves both positive-realness and the bounded realness of the system. Solving the LMI can be replaced by equivalently solving an ARE, which is known to be a more efficient approach [24, 25] as the number of operations required to solve a Riccati equation is  $O(n^3)$ , while the cost of solving an equivalent LMI is  $O(n^6)$ . Thus for high orders it is advisable to solve the ARE which is computationally cheaper in comparison with LMI.

#### 4.2.6 Numerical Results for frequency independent state-space matrices

Transmission line examples are used to illustrate the accuracy and efficiency of the adaptive frequency sampling technique using RE.

##### 4.2.6.1 LTL: Lossless Transmission Line Example

For this example, a 20 cm lossless uniform coupled microstrip structure with two strips with the following per-unit-length matrices [26],

$$\begin{aligned} l_{pul} &= \begin{bmatrix} 425.6 & 74.83 \\ 74.83 & 425.6 \end{bmatrix} \text{ nH/m} \\ c_{pul} &= \begin{bmatrix} 174.9 & 14.25 \\ 14.25 & 174.9 \end{bmatrix} \text{ pF/m.} \end{aligned} \quad (4.15)$$

for a frequency range of interest  $[1 \text{ KHz} - 1 \text{ GHz}]$ , is modeled as described in [27]. The original system has an order of 1604 with 4 ports.

Similar to the previous TL example, two expansion points at  $\omega_{min}$  and  $\omega_{max}$  are considered. The reduced order for the first iteration is equal to 4, the number of ports. Then as briefed in Section 4.2.2, the frequency responses are computed using a merged projection matrix (4.5). Then similar to the previous case the difference in response between the two models (4.6) is computed and as the error is bigger than the threshold set, the algorithm checks for the next expansion point using the adaptive sampling loop as shown in Fig.4.11.

Similarly in this manner the sampling process is iterated till the RMS error (4.6) is less than threshold value of  $10^{-3}$ .

Figure 4.4 plots the RMS error (4.6) of the best two models during each iteration of the reflective exploration algorithm.

Figure 4.12, shows the frequency responses obtained during the reflective exploration for different iterations. The best model has dimension 64 and is obtained with 4 expansion points within a CPU time of 14.8 secs.

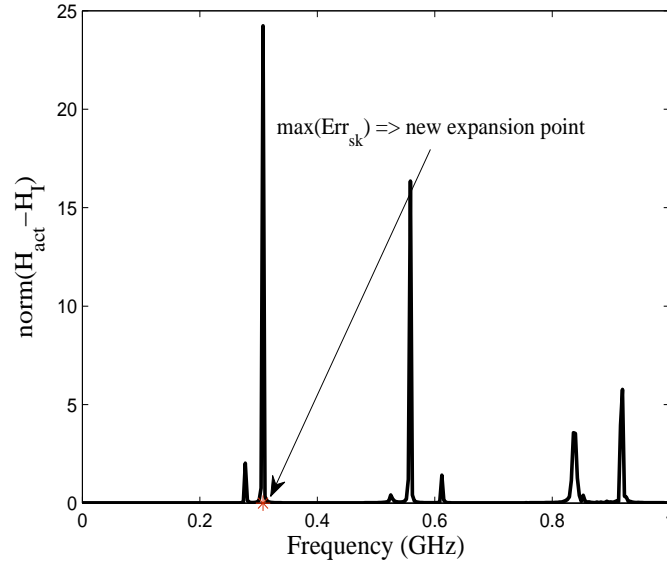


Figure 4.3: LTL: Error per frequency used to select the new expansion point for the adaptive sampling loop.

Finally, the model is compacted based on the truncation of the singular values of the common projection matrix. With the truncation algorithm described in Section 4.2.4, we obtain a model of order 35 by adaptively choosing a threshold of  $10^{-2}$  in 0.16 secs as shown in Table 4.1.

Threshold	RMS Error	Dimension of ROM
$10^{-1}$	8.04	29
$10^{-2}$	$8.645 \times 10^{-4}$	35

Table 4.1: LTL: Adaptive truncation for model compacting.

Figure 4.13 plots the magnitude of  $Y_{11}$  for the original and the reduced model using 4 expansion points with a reduced order of 9 per expansion point..



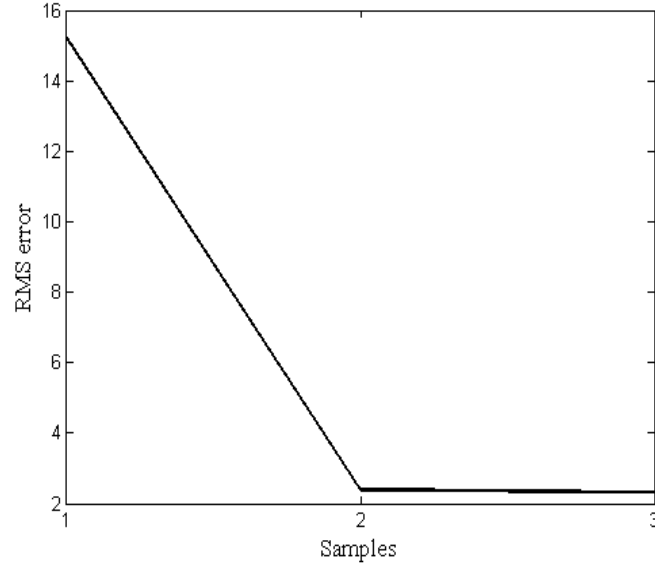


Figure 4.4: LTL: RMS error between the iterated models during the addition of new expansion points.

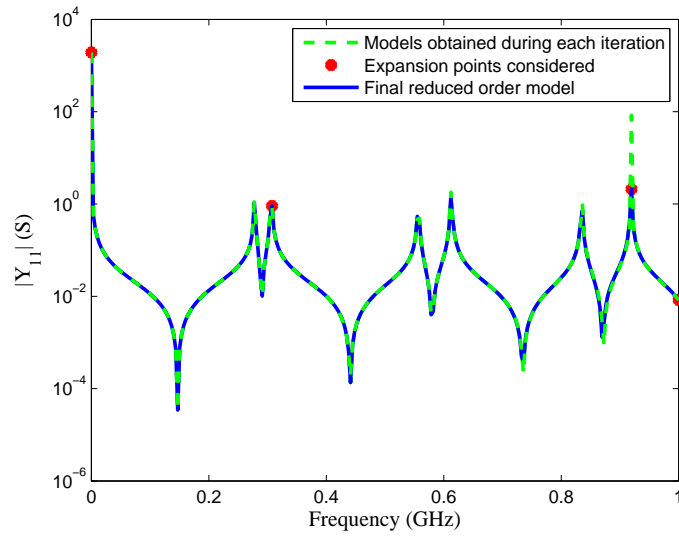


Figure 4.5: LTL: Magnitude of lossless line  $Y_{11}$  for each iterative step with the adaptively chosen expansion points.

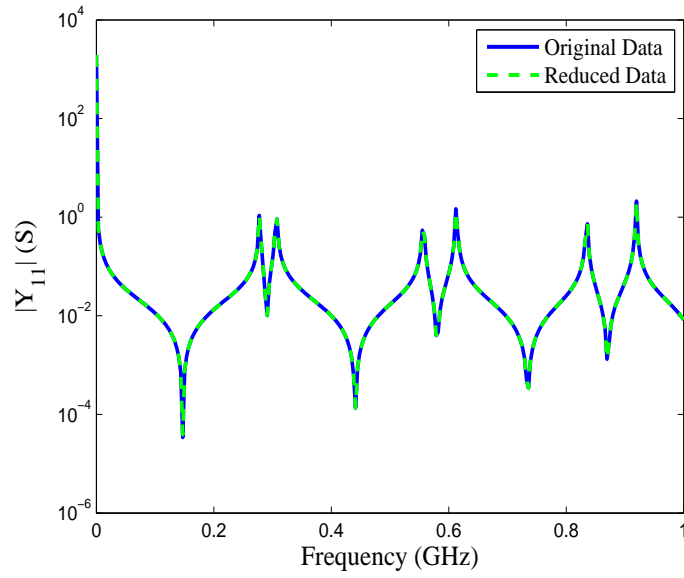


Figure 4.6: LTL: Magnitude of lossless line  $Y_{11}$  with the original response after model compacting.

#### 4.2.6.2 TL: Lossy Transmission Line

For this example, a 10 cm long two conductor lossy transmission line with the following per-unit-length matrices

$$\begin{aligned}
 r_{pul} &= \begin{bmatrix} 75 & 15 \\ 15 & 75 \end{bmatrix} \Omega/\text{m} \\
 l_{pul} &= \begin{bmatrix} 494.6 & 63.3 \\ 63.3 & 494.6 \end{bmatrix} \text{nH}/\text{m} \\
 g_{pul} &= \begin{bmatrix} 0.1 & 0 \\ 0 & 0.1 \end{bmatrix} \text{S}/\text{m} \\
 c_{pul} &= \begin{bmatrix} 62.8 & -4.9 \\ -4.9 & 62.8 \end{bmatrix} \text{pF}/\text{m}.
 \end{aligned} \tag{4.16}$$

for a frequency range of  $[1 \text{ KHz} - 1 \text{ GHz}]$ , is modeled as described in [27]. The original state-space order of the system is 1202 with 4 ports.

The sampling starts by considering two expansion points at  $\omega_{min}$  and  $\omega_{max}$ . The reduced order for the first iteration is equal to 4, the number of ports of the system. Then, as briefed in Section 4.2.2, the frequency responses is computed using a merged projection matrix (4.5) formed from the two expansion points. For the next iteration, the frequency response is computed for the same expansion points with an increased order of 8, i.e.: it is increased by the number of ports. Then the difference in response between the two models is computed using (4.6). The error obtained is 2.147, which is significantly greater than  $10^{-3}$ , the threshold set for the RMS error. Therefore, the algorithm increases the order of the expansion points and again computes the RMS error. Since the difference in the RMS error in the successive iterations is less than 10%, the algorithm checks for the new expansion point by computing the standard 2-norm of the best model and the original model. As shown in Fig.4.7, the standard 2-norm of the frequency responses of the best model and the actual response gives the error per frequency and the new expansion point is considered at the frequency at which the error is maximum.

Then, the frequency response which is the admittance parameter  $\mathbf{Y}(s)$ , is again computed with all the expansion points, with a reduced order of 12 per expansion point. Similarly in this manner the sampling process is iterated till the RMS error (4.6) is less than the  $10^{-3}$ , the accuracy threshold value set.

Figure 4.8 plots the RMS error (4.6) between the iterated models when new expansion points are added during reflective exploration.

Figure 4.9, shows the magnitude of the admittance parameter  $\mathbf{Y}_{11}$  obtained during the reflective exploration for different iterations. A best model of dimension 96 is obtained with 4 expansion points within a CPU time of 15.23 secs.

Then the model is compacted based on the truncation of the singular values of the common projection matrix. With the truncation algorithm described in Section

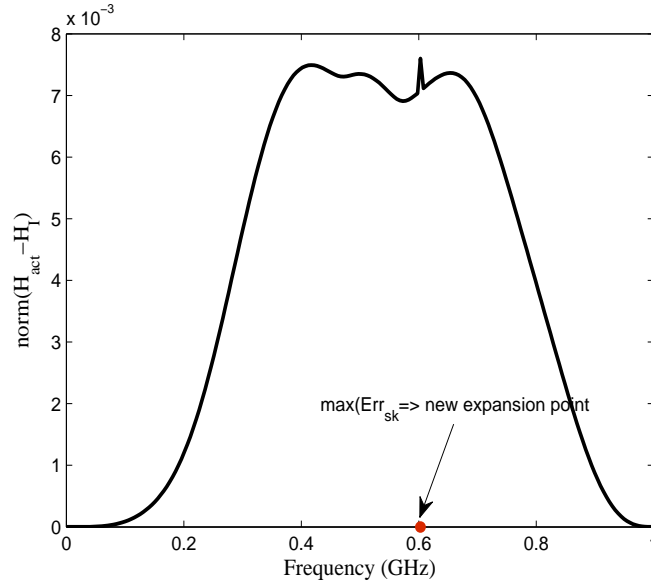


Figure 4.7: TL: Error per frequency for the adaptive sampling loop.

4.2.4, we obtain a model of order 85 by adaptively choosing a threshold of  $10^{-4}$  in 0.715 secs as shown in Table 4.7.

Threshold	RMS Error	Dimension of ROM
$10^{-1}$	$2.23 \times 10^{-1}$	61
$10^{-2}$	$1.703 \times 10^{-1}$	71
$10^{-3}$	$6.96 \times 10^{-2}$	77
$10^{-4}$	$9.72 \times 10^{-4}$	85

Table 4.2: TL: Adaptive truncation for model compacting.

Figure 4.10 plots the magnitude of  $\mathbf{Y}_{11}$  for the original and the reduced model using 4 expansion points with a reduced order of 22 per expansion point.

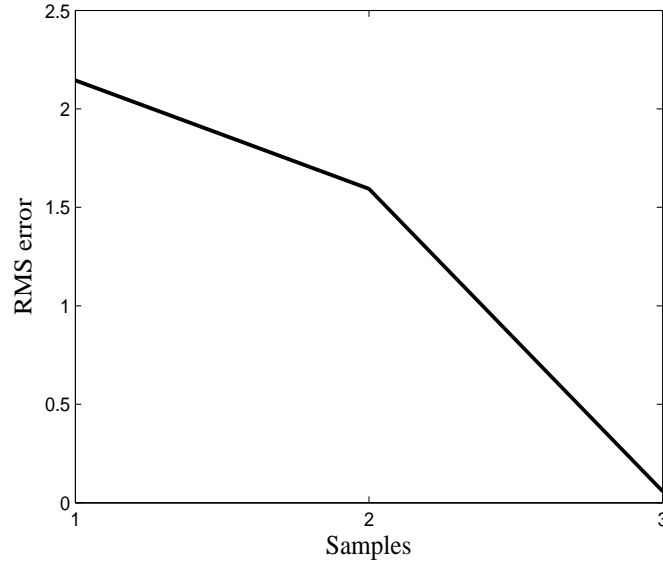


Figure 4.8: TL: RMS error between the iterated models with new expansion points.

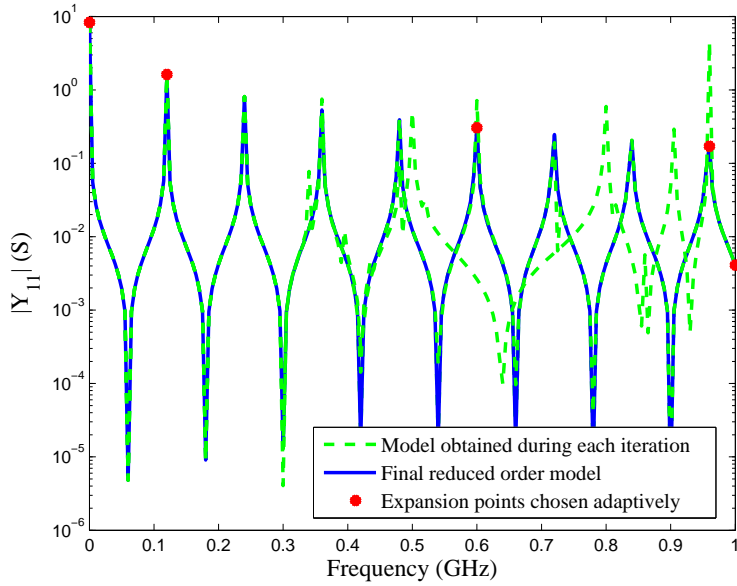


Figure 4.9: TL: Magnitude of lossy line  $\mathbf{Y}_{11}$  for each iteration with the adaptively chosen expansion points.

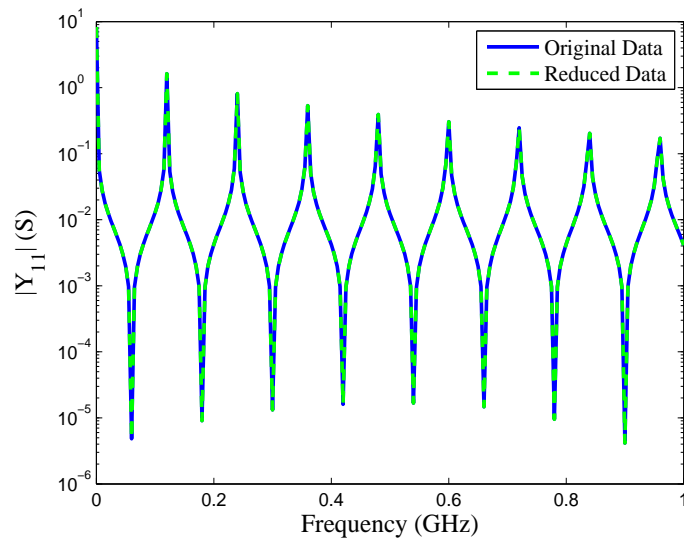


Figure 4.10: TL: Magnitude of lossy line  $\mathbf{Y}_{11}$  after model compacting.

#### 4.2.6.3 MNA: Modified Nodal Analysis

A modified nodal analysis (MNA) formulation for a 22 port circuit as given in the Niconet benchmark collections<sup>1</sup> is considered for this example. The original system has an order of 4863 with 22 ports for a frequency range of interest  $[1 \text{ KHz} - 5 \text{ GHz}]$ .

Similar to the previous examples, two expansion points at  $\omega_{min}$  and  $\omega_{max}$  are considered. The reduced order for the first iteration is equal to 22, the number of ports. Then as briefed in Section 4.2.2, the frequency responses are computed using a merged projection matrix (4.5). Then similar to the previous case the difference in response between the two models (4.6) is computed and as the error is bigger than the threshold set, the algorithm checks for the next expansion point using the adaptive sampling loop as shown in Fig.4.11.

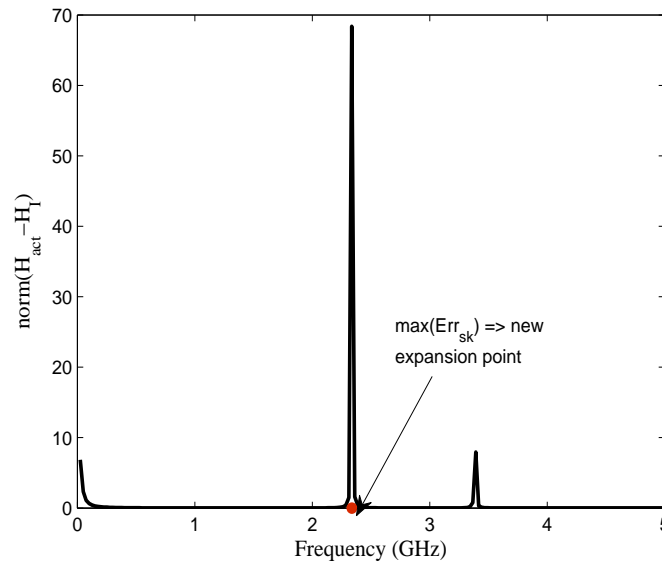


Figure 4.11: MNA: Error per frequency used to select the new expansion point for the adaptive sampling loop.

Similarly in this manner the sampling process is iterated till the RMS error (4.6) is less than threshold value of  $10^{-3}$ .

Figure 4.12, shows the frequency responses obtained during the reflective exploration for different iterations. The best model has dimension 1122 and is obtained with 9 expansion points within a CPU time of 2048.5 secs.

<sup>1</sup><http://www.win.tue.nl/niconet/niconet.html>

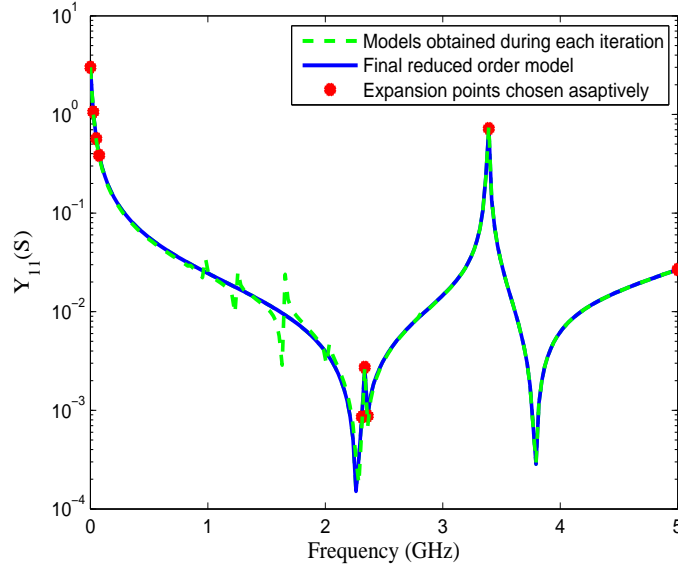


Figure 4.12: MNA: Magnitude of  $Y_{11}$  for each iterative step with the adaptively chosen expansion points.

Finally, the model is compacted based on the truncation of the singular values of the common projection matrix. As shown in Table 4.3, with the truncation algorithm described in Section 4.2.4, we obtain a model of order 202 by adaptively choosing a threshold of  $10^{-2}$  in 4.38 secs.

Threshold	RMS Error	Dimension of ROM
$10^{-1}$	15.09	88
$10^{-2}$	$2.645 \times 10^{-3}$	202

Table 4.3: MNA: Adaptive truncation for model compacting.

Figure 4.13 plots the magnitude of  $Y_{11}$  for the original and the reduced model using 9 expansion points with a reduced order of 22 per expansion point..

From the examples described it can be illustrated that the proposed technique is able to capture the behavior of the system accurately and is able to preserve passivity of the original model by construction.



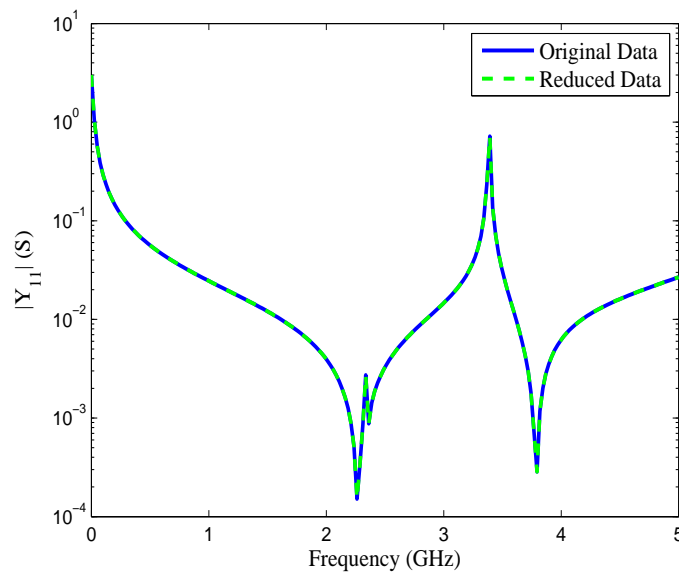


Figure 4.13: MNA: Magnitude of  $Y_{11}$  with the original response after model compacting.

### 4.3 Multipoint MOR for frequency dependent state-space matrices using hybrid adaptive sampling algorithm

#### 4.3.1 Common projection matrix

For frequency dependent state-space matrices, (4.1) will have matrices that are frequency dependent i.e.,  $\mathbf{E}(s)$ ,  $\mathbf{A}(s)$ ,  $\mathbf{B}(s)$ ,  $\mathbf{C}(s)$  and  $\mathbf{D}(s)$ . For obtaining the ROM for each frequency, the projection matrix is computed for each frequency sample by considering the expansion point as equal to the corresponding frequency sample.

After obtaining the projection matrix for each frequency sample, the frequency response of the system is obtained by interpolating the reduced state-space matrices as a function of frequency. To interpolate the reduced state-space matrices they must be in the same subspace and to obtain this a common projection matrix is required for all the samples that are selected. It is assumed that since the frequency dependent state-space matrices are obtained from a common simulator using the same meshing topology, they belong to a common space and hence projecting with a common projection matrix will generate reduced state-space matrices in the same subspace.

First we can compute the projection matrices for each frequency sample similarly to what was done in (4.3) and then column stack the matrices to obtain a common projection matrix. For  $n$  frequency samples we obtain the corresponding projection matrices  $P_{q_i}$  ( $i = 1, 2, \dots, n$ ) with the expansion points chosen as equal to the frequency samples, then the common projection matrix is defined as in (4.5). Once the reduced matrices are computed, they are interpolated to build the response of the system on a dense grid. Here we have used linear interpolation using the matlab command `interp1`.

The common projection matrix is not truncated based on its singular values during the iterative procedure of the adaptive sampling algorithm. It is truncated once the required samples have been adaptively chosen using the proposed sampling technique proposed, which allows compacting the size of the ROM.

#### 4.3.2 Hybrid Adaptive Sampling Algorithm

To obtain the frequency dependent state-space matrices we can use full-wave EM techniques. At times they are very expensive, that one might limit the number of samples in order to get results in a moderate amount of time. If the samples are reduced then there is a serious chance of undersampling of the frequency response, which can cause the loss of certain important features such as coupling effect or resonances. Even if most of the desired frequency range is oversampled, some im-

portant effects can still be missed due to local undersampling [18]. The proposed algorithm adaptively samples the frequency range of interest, on the cost of certain threshold values set for the HAS algorithm. It is important to choose adaptively the expansion points in order to minimize the cost of evaluation of the ROM.

#### 4.3.2.1 Reflective exploration (RE)

Similarly to what was done in Section 4.2.3 the exploration algorithm starts with a set of initial samples  $S_f$  that are spaced uniformly over the frequency of interest. The state-space matrices for these samples of frequencies are reduced to an order  $q = mP_{in}$  ( $m$  is an integer and is 1 for the first iteration  $I = 1$  and  $P_{in}$  is the number of input ports), using a common projection matrix as in (4.5) for the first iteration. Starting with a reduced order for each sample equal to  $P_{in}$ , guarantees accuracy at the sample points by considering expansion point equal to the frequency sample. In order to obtain the model behavior over the frequency range of interest, linear interpolation is performed on a dense grid. Its important to note that the density of the grid considered for each iteration throughout the algorithm must remain constant. In the second iteration ( $I = 2$ ), the reduced order  $q$  is incremented by  $P_{in}$  and similarly the frequency response is found. Then the reflective function i.e., the RMS error  $Err_{est}$  (4.6) is computed.

This error (4.6) is used as a measure to validate the quality of the model. Usually, the threshold for the error is set depending on the desired accuracy of the model. But as the comparison is made with the models in the reduced form and not with the detailed model, the error (4.6) is an estimated error and not the actual one. Henceforth the estimated error threshold  $\delta_{est}$  set might give an accurate model and also might not. In order to overcome this problem, a BS over the samples obtained through RE is followed, and thereby the final accuracy is not much affected by the estimated error threshold  $\delta_{est}$ .

For each iteration the reduced order is incremented by the number of ports and  $Err_{est}^I$  is calculated, which forms the adaptive modeling loop. For the adaptive sampling loop, the difference between the  $Err_{est}^I$  and  $Err_{est}^{I-1}$  being less than a threshold value  $\delta_{comp}$  is used as a criterion to say that the ROMs are the same. The sampling loop is then extended to check if the response changes by the addition of a new sample. To select the new sample the error  $Err_{s_k}$  (4.17) is computed. The new sample is located at the frequency where the error  $Err_{s_k}$  is maximum when computed over a dense frequency grid. Note that in Section 4.2.3 (4.8) the error was computed in comparison with the original system, but in this case we assume that the original model is not computed.

The error at each frequency  $s_k$   $Err_{s_k}$  is calculated as the standard 2-norm

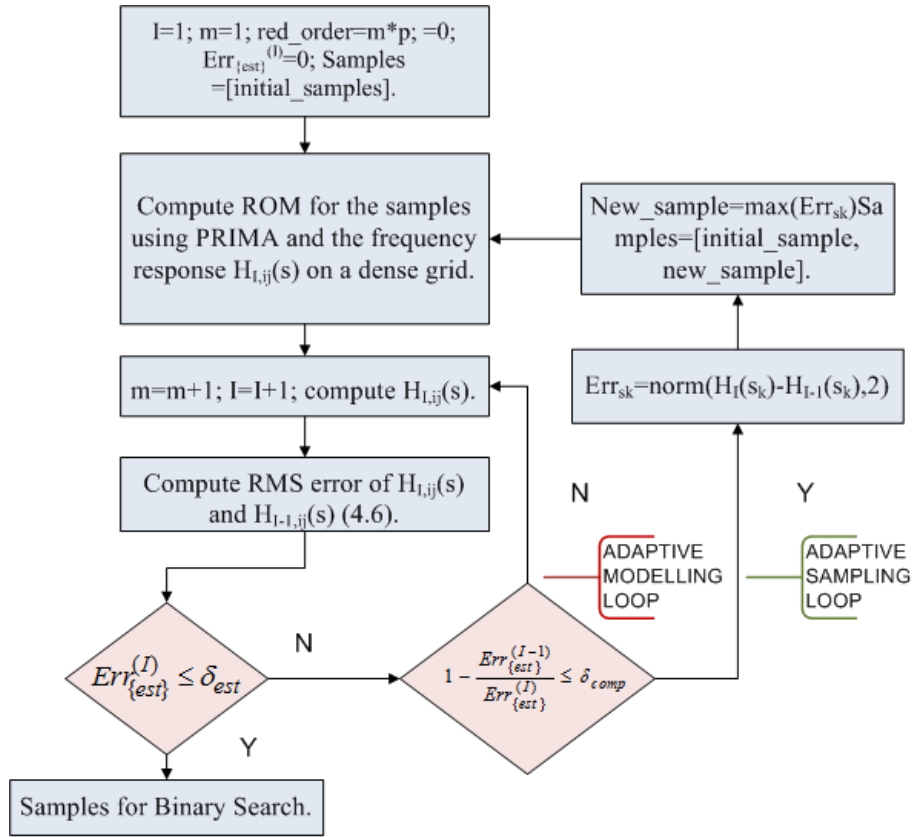


Figure 4.14: Flowchart for Reflective Exploration.

which is the difference between the frequency responses,

$$\begin{aligned} Err_{s_k} &= \|H_I(s_k) - H_{I-1}(s_k)\|; \\ k &= 1, \dots, K_s. \end{aligned} \quad (4.17)$$

The exploration is terminated when the reflective function  $Err_{est}$  (4.6) is equal to or less than the estimated error threshold  $\delta_{est}$  set. The flowchart for the RE technique is shown in Fig.4.14.

Note that the number of samples considered at the start of the RE iteration and the threshold values set for the RE algorithm can be set based on the user's preference.

#### 4.3.2.2 Binary search (BS)

A binary search is also known as half interval search or a dichotomy. With the samples obtained from RE and the common projection matrix (4.5), the ROM for each frequency sample is obtained through a congruence transformation at the selected sample points. Then a linear interpolation for the ROM at the midpoint of two samples is used. The response is then compared with the actual model at the midpoint using the EM simulator [15]. If the section error satisfies a threshold value  $\delta_{sect}$ , then the algorithm terminates. Otherwise, the midpoints were the threshold was not met are considered as new sample points. When the midpoint satisfies the error threshold, the corresponding interval is considered to be accurately modeled and is not accounted in the next iteration. The comparison point for each iteration is the midpoint of the intervals between the samples, except for the ones that were accurate in the previous iterations. The error at the midpoint is defined in a similar way as the estimation error (4.6), but it is defined at one point and therefore  $K_s = 1$  and the evaluation frequency is the corresponding frequency at the midpoint. The flowchart for the BS technique is shown in Fig.4.15.

#### 4.3.2.3 Model compacting (MC)

Once the state-space matrices ( $\mathbf{E}(s)$ ,  $\mathbf{A}(s)$ ,  $\mathbf{B}(s)$ ,  $\mathbf{C}(s)$ ,  $\mathbf{D}(s)$ ) for the samples chosen adaptively and the frequency response of the best model  $H_I(s)$  are obtained from the HAS, it might be possible to further compact the ROM with the information obtained from the singular values of the common projection matrix (4.5).

The ROM obtained by the truncation of the common projection matrix with respect to the singular values, is compared with the best model obtained from RE and BS. If the RMS error is less than a threshold  $\delta_{trunc}$ , then we shall truncate the singular values, else we keep the model with the reduced order obtained using the sampling algorithms. To truncate the singular values, an adaptive algorithm is proposed as shown in Fig. 4.2.

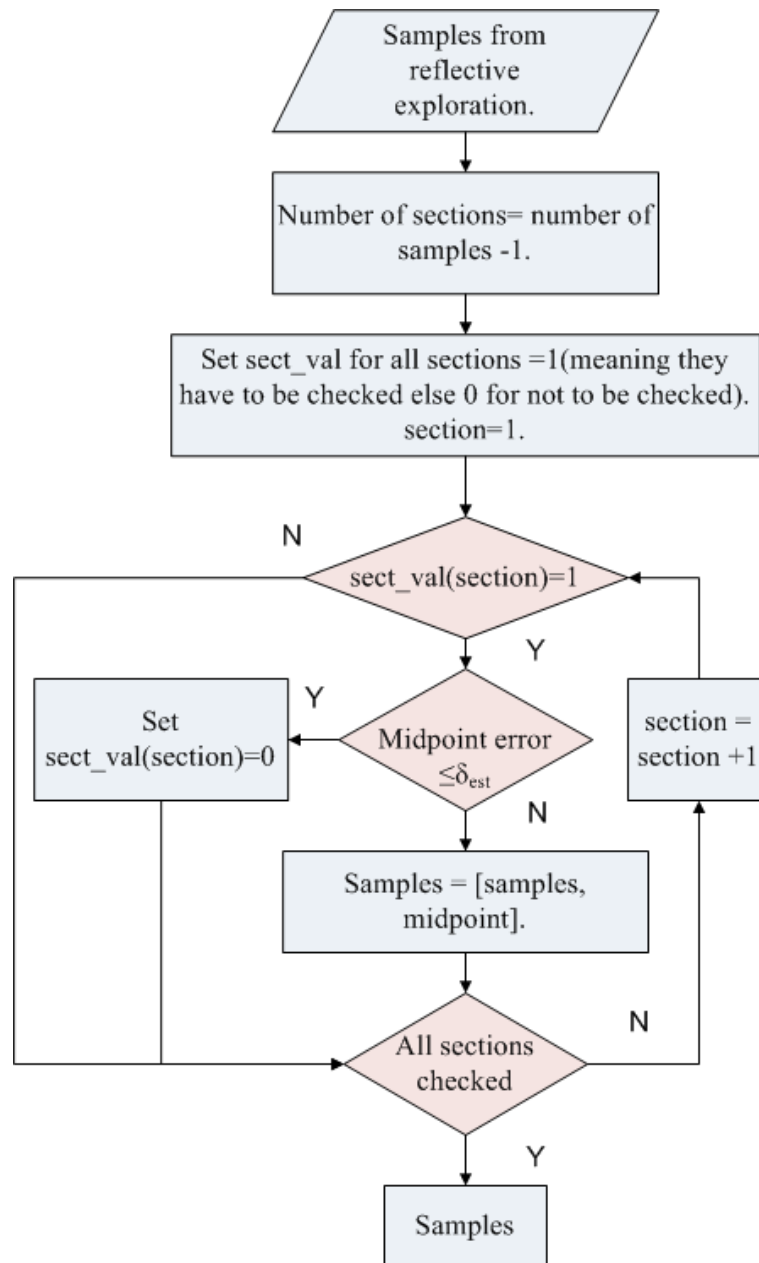


Figure 4.15: Flowchart for Binary Search.

The economy-size  $SVD$  is computed for the common projection matrix as in (4.9). Thus the common project matrix for the samples chosen adaptively is,

$$Q_{comm} = U(:, 1 : q_{comm}) \quad (4.18)$$

Thus, on an average it can be noted that per sample it requires a reduced order  $q_{samp}$  (4.12) to guarantee accuracy at that sample point.

The projection matrix  $Q_{comm}$  with congruence transformation (4.4) computes the ROMs of dimension  $q_{comm}$  for the sample points chosen adaptively. Then, the frequency dependent ROMs are interpolated to build the frequency response of the system for each frequency sample of interest.

### 4.3.3 Numerical Results for frequency dependent state-space matrices

Some pertinent numerical examples are used to demonstrate the proposed HAS algorithm. For the proposed HAS algorithm the following threshold values as mentioned in Table 4.4 have been considered for the numerical examples. The adaptive sampling starts with  $S_f$  equal to 3 samples for the exploration and for the accuracy evaluations the number of frequency samples considered on a dense grid is equal to 200.

Threshold	Values
$\delta_{est}$	$10^{-2}$
$\delta_{comp}$	$10^{-1}$
$\delta_{sect}$	$10^{-3}$
$\delta_{trunc}$	$10^{-4}$

Table 4.4: Threshold values set for the HAS algorithm.

#### 4.3.3.1 2TL: Two coupled transmission lines

In the first example, a 5 cm long coupled transmission line structure [28] is considered. The transmission line matrices of order 1402 are frequency dependent, thereby including the effects of skin effect and dielectric losses. The frequency dependent parameters are detailed in [28], where it is denoted as *Line 2*.

The frequency dependent state-space matrices can be derived as described in [27]. The frequency range considered is [1 KHz - 10 GHz].

*Reflective Exploration*- The sampling starts by considering  $S_f$  equal to three samples, that are spaced uniformly over  $[\omega_{min}, \omega_{max}]$ . The reduced order for the first

iteration is equal to 4. Then, as discussed in Section 4.3.2.1, the frequency responses are computed by the linear interpolation of the three sample state-space matrices of order 4. In the next step the frequency response is computed for the same samples with an increased order of 8, i.e; it is increased by the number of ports. Then we compute the difference in response between the two models using (4.6). The error obtained is 4.2, which is greater than  $\delta_{est}$ , the threshold set for the estimated error. Therefore, the algorithm continues to increase the order till the difference between successive estimated error is less than  $\delta_{comp}$ . Next the adaptive sampling loop starts to find the new sample, by computing the norm of the frequency responses of the two best models (4.8). The new sample point is considered at the frequency at which the error (4.8) is maximum. Then again the frequency response is computed with all the samples and also with increment of the reduced order by 4. Similarly in this manner the sampling process is iterated till the estimated error (4.6) is less than threshold value  $\delta_{est} = 10^{-3}$ .

Table 4.5 shows the number of samples used during each iteration of RE to achieve an estimated error less than  $\delta_{est}$ .

Sample	RMS Error (4.6)
3	4.2
4	0.12
5	1.24
6	1.57
7	$1.3 \times 10^{-4}$

Table 4.5: 2TL: Sampling and Modeling in Reflective Exploration with RMS error.

Figure 4.16, shows the frequency responses obtained during the RE for different iterations. A best model of dimension 112 is obtained with 7 samples within a CPU time of 40.57 s.

*Binary Search-* For the BS we start with the samples obtained from RE and the reduced order for each sample is considered as 16, which is calculated as an average from the total model order divided by the number of samples obtained from RE. The section error is computed for 6 sections, i.e., between the samples as mentioned in section 4.3.2.2. If the error is less than or equal to the threshold value  $\delta_{sect}$ , then the section is considered to be accurately modeled, else the midpoint is considered as a new sample as shown in table 4.7. The sampling is continued till all the sections are accurately modeled.

Figure 4.17, shows the frequency responses obtained during the BS, with a computation time of 131.28 s. It can be seen that with BS we were able to obtain a more accurate model which captures the model behavior that were missed by RE.



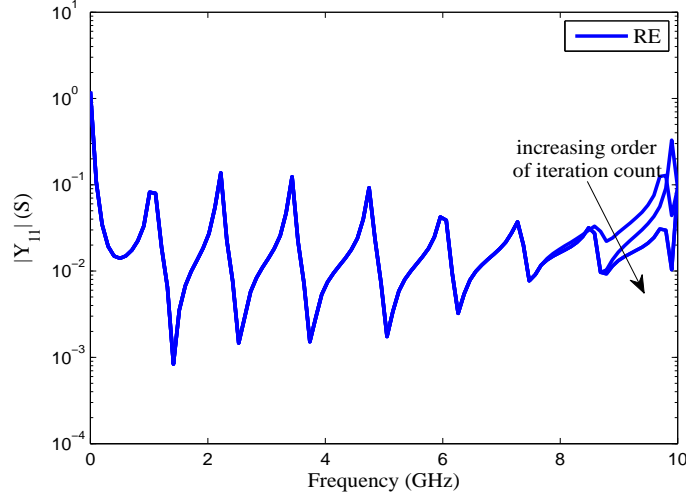


Figure 4.16: 2TL: Magnitude of  $Y_{11}$  for the different iteration steps of RE.

Section	Section Error	midpoint considered as sample (Section error $> \delta_{sect}$ )
1	0.056	yes
2	0.007	no
3	0.002	no
4	0.056	yes
5	0.981	yes
6	0.179	yes

Table 4.6: 2TL: Sampling using Binary Search.

The order of the model obtained is 400, with 16 samples. Note that the computational time for BS will be in general more expensive than the RE as in BS the new frequency samples are obtained by comparing the ROM at the midpoint of a section, in each iteration with the original model at that frequency obtained from the solver.

*Model compacting-* Finally the model is compacted based on the truncation of the singular values of the common projection matrix as shown in Figure 4.18. Using the truncation algorithm described in Figure 4.2, a ROM of dimension 104 is obtained in 4.1 s.

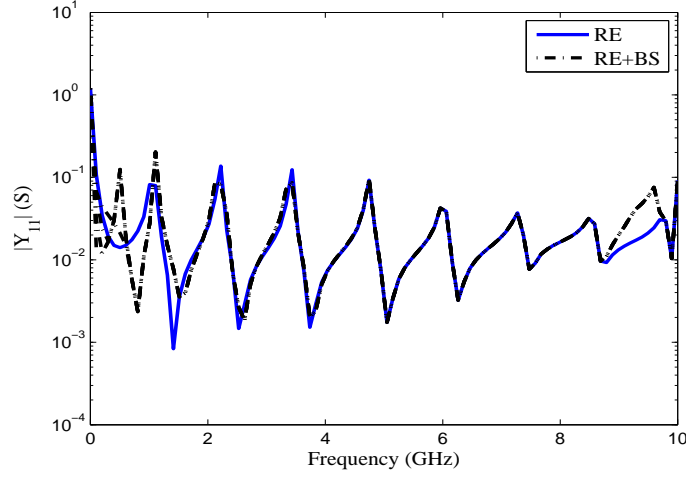


Figure 4.17: 2TL: Magnitude of  $Y_{11}$  obtained with BS.

Threshold	RMS Error (Best Model and truncated model)	Dimension of ROM
$10^{-2}$	0.55	62
$10^{-4}$	0.016	70
$10^{-6}$	0.007	81
$10^{-8}$	0.0003	104

Table 4.7: 2TL: Adaptive truncation for model compacting.

Thus from the reduced model order obtained for the 16 samples chosen adaptively, we can infer that for a reduced order of 7 per samples ( $\approx 104/16$ ), an accurate frequency response is generated. The reduced state-space matrices are interpolated linearly to obtain the frequency response. The elements in the state-space matrices varies as shown in Fig. 4.19.

The frequency response obtained after RE, BS and model compacting in comparison with the original model is plotted in Fig. 4.20.

Only in order to validate the algorithm, the original model was simulated over a dense frequency grid of 200 samples, for which a RMS error of  $2.1e-3$  was obtained for the ROM. The computation time needed to compute a frequency sample by the original solver is 6.98 s and that with the interpolation of the frequency dependent reduced state-space matrices is 0.019 s, thereby achieving a speed up of

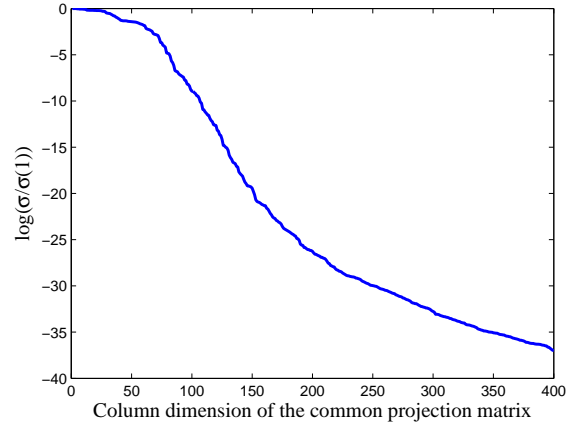


Figure 4.18: 2TL: Singular value of the common projection matrix.

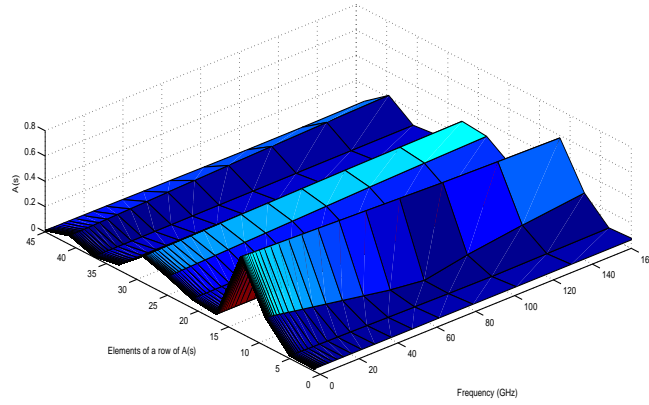


Figure 4.19: 2TL: Variation of matrix element with frequency.

367 times. Thus, the HAS technique was able to automate the generation of accurate reduced frequency dependent state-space matrices with adaptive selection of the frequency samples.

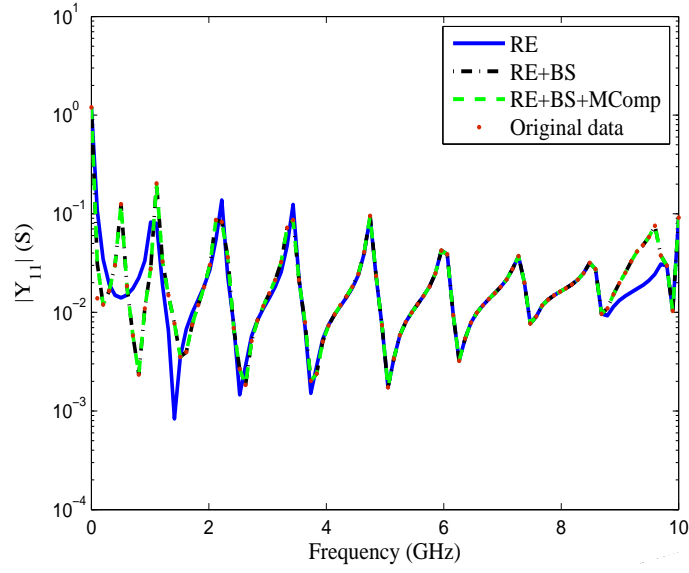


Figure 4.20: 2TL: Magnitude of  $Y_{11}$  obtained using the HAS algorithm.

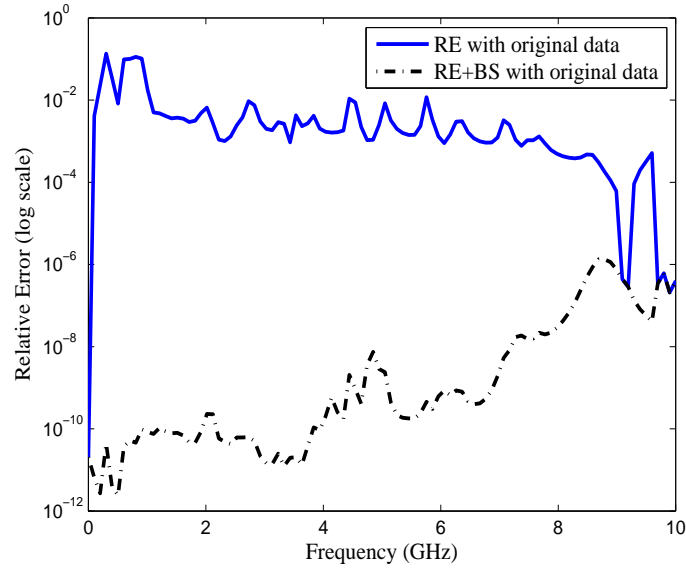


Figure 4.21: 2TL: Relative error of the original model with the reduced order models obtained from RE and BS.

#### 4.3.3.2 IEM: Inverted Embedded microstrip line

The cross-section of the IEM line having a finite length of 1mm is shown in Fig. 4.22. The frequency-dependent behavior is determined using a very accurate, but slow, 2-D electromagnetic (EM) solver [29, 30]. The order of the original frequency dependent state-space matrix is 1202.

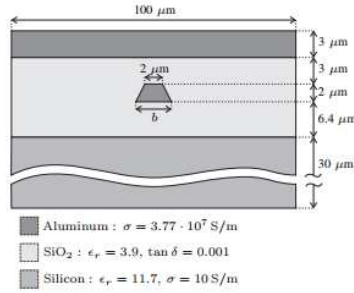


Figure 4.22: IEM: Cross section of IEM line.

*Reflective Exploration-* As discussed in the former example, the sampling starts with 3 samples for the first iteration. Table 4.8 shows the number of samples used during each iteration of RE to achieve an estimated error less than  $\delta_{est}$ .

*Binary Search-* For the BS, similar to the previous example we start with the sam-

Sample	RMS Error (4.6)
3	1.32
4	0.022
5	0.0064

Table 4.8: IEM: Sampling and Modeling in Reflective Exploration with RMS error.

ples obtained from RE. The section error is computed for 4 sections, i.e., between the samples as mentioned in section 4.3.2.2. If the error is less than or equal to the threshold value  $\delta_{sect}$ , then the section is considered to be accurately modeled, else the midpoint is considered as a new sample. The sampling is continued till all the sections are accurately modeled. Thus a model of order 416 with 26 samples is obtained. Figure 4.25 gives the relative error plot of the reduced order models obtained from RE and RE with BS in comparison with the original model.

*Model compacting-* Finally the model is compacted as described in Section 4.3.2.3. Thus, the proposed algorithm was able to generate ROM of dimension 82

with 26 frequency samples. Table 4.9 gives the number of samples generated with the size of the ROM and computation time taken for each section of the proposed HAS algorithm.

Approach	Number of samples	Dimension of ROM	CPU time (s)
Reflective Exploration	5	80	33.80
Binary Search	26	416	245.7
Model Compacting	26	82	1.51

Table 4.9: IEM: Samples, Size of ROM and Computation time for each step of the HAS algorithm.

The reduced state-space matrices are interpolated linearly to obtain the frequency response. The elements in the state-space matrices varies as shown in Fig. 4.23. The frequency response obtained after RE, BS and MC in comparison with the original model is plotted in Fig. 4.24.

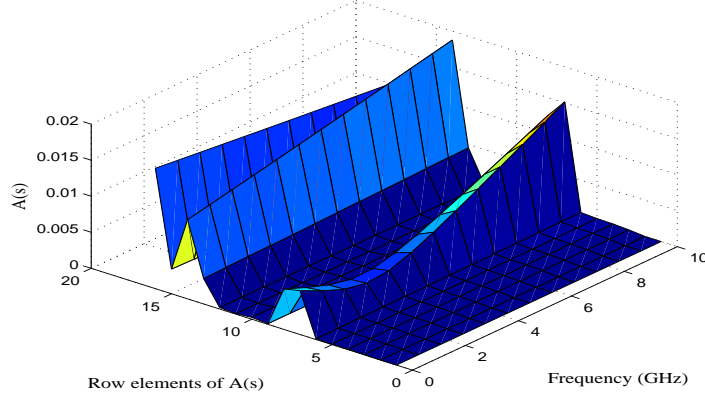


Figure 4.23: IEM: Variation of matrix element with frequency.

Fig. 4.26 and Fig. 4.27 plots the magnitude and phase of  $Y_{13}$  of the ROM obtained using the proposed HAS algorithm in comparison with the original model.

The computation time needed to compute a frequency sample by the original solver is 13.943s and that with the interpolation of the frequency dependent reduced state-space matrices is 0.025s, thereby achieving a speed up of 558 times. Thus, the HAS technique was able to automate the generation of accurate reduced

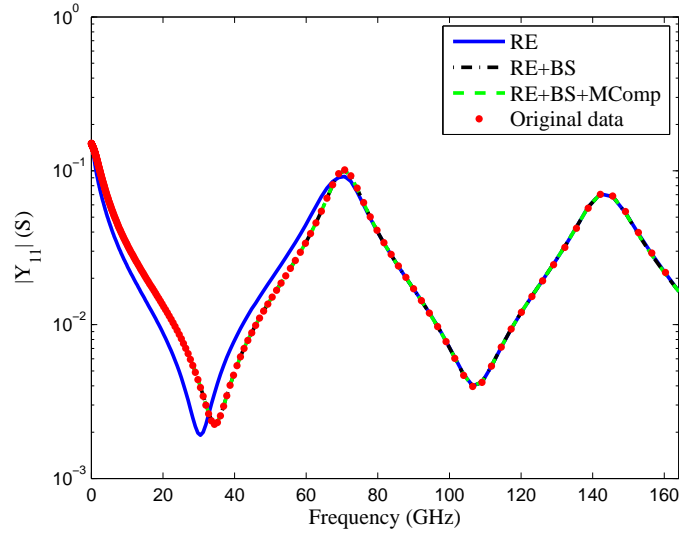


Figure 4.24: IEM: Magnitude of  $Y_{11}$  obtained using the HAS algorithm.

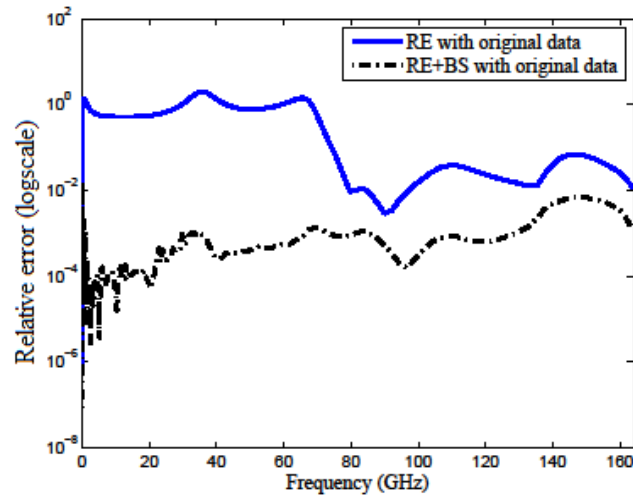


Figure 4.25: IEM: Relative error of the original model with the reduced order models obtained from RE and BS.

frequency dependent state-space matrices with adaptive selection of the frequency samples.

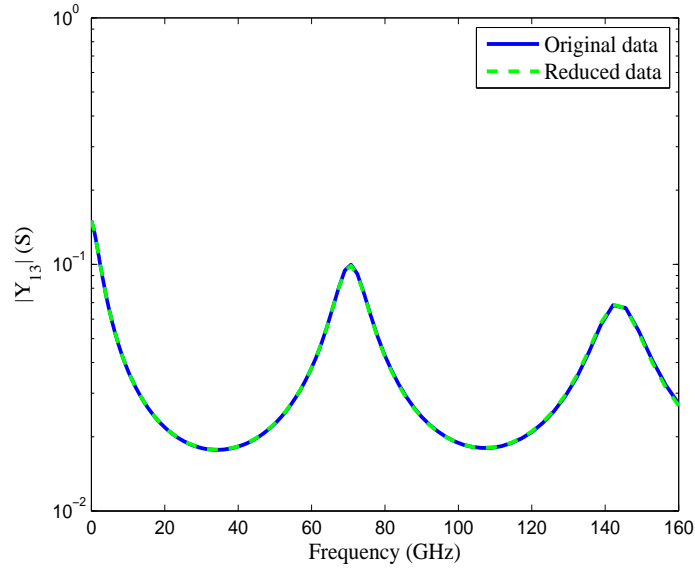


Figure 4.26: IEM: Magnitude of  $Y_{13}$  obtained using the HAS algorithm.

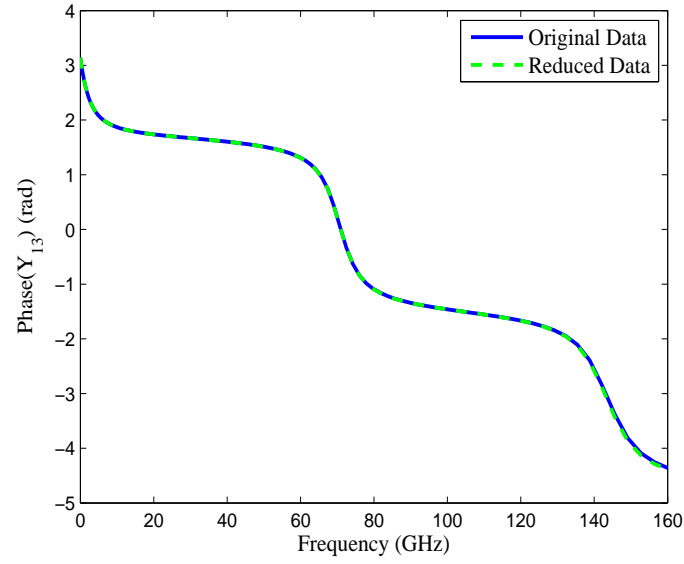


Figure 4.27: IEM: Phase of  $Y_{13}$  obtained using the HAS algorithm.



## 4.4 Conclusion

In this chapter, a novel hybrid adaptive sampling algorithm to automate the generation of reduced order models for systems with frequency dependent and frequency independent state-space models has been proposed. The proposed algorithm combines (i) the active selection of samples and (ii) the reduced order for each sample. The samples are adaptively chosen using reflective exploration that is further refined using a binary search. Then in order to obtain a compact model the projection matrices obtained from the samples are truncated with respect to their singular values and then the frequency dependent ROMs are interpolated to obtain the frequency response of the system. Numerical results illustrates the efficiency and accuracy of the proposed technique.

For the estimation of the reduced order per sample the technique initially assumes that the order is equal to the number of ports, this might not be advisably for systems with large number of ports. In such cases, the MOR technique for systems with large number of ports has to be considered [31].

For the systems with frequency dependent state-space matrices, after obtaining the reduced order state-space matrices per sample point, it is then interpolated to obtain the frequency response, this is with an assumption that the initial models are unique or in other words from a common subspace. But if the state-space matrices are not unique then on interpolation a smooth model may not be obtained. In such cases an unique realization is required which is proposed in Chapter 5.

## Acknowledgment

This work was supported by the Interuniversity Attraction Poles Programme BEST-COM initiated by the Belgian Science Policy Office and the Research Foundation Flanders (FWO).

## References

- [1] U. Beyer and F. Śmieja. *Data exploration with reflective adaptive models*. Computational Statistics & Data Analysis, 22(2):193 – 211, 1996.
- [2] R. F. Harrington and J. L. Harrington. *Field Computation by Moment Methods*. Oxford University Press, 1st edition, 1996.
- [3] A. E. Ruehli and P. A. Brennan. *Efficient Capacitance Calculations for Three-Dimensional Multiconductor Systems*. IEEE Transactions on Microwave Theory and Techniques, 21(2):76–82, 1973.
- [4] L. Pillage and R. Rohrer. *Asymptotic waveform evaluation for timing analysis*. IEEE Transactions on Computer-Aided Design of Integrated Circuits and Systems, 9(4):352–366, 1990.
- [5] K. Gallivan, E. Grimme, and P. V. Dooren. *Asymptotic waveform evaluation via a Lanczos method*. Appl. Math. Lett, 7:75–80, 1994.
- [6] R. W. Freund and P. Feldmann. *Small-Signal Circuit Analysis and Sensitivity Computations with the PVL Algorithm*. IEEE Trans. Circuits and Systems—II: Analog and Digital Signal Processing, pages 577–585, 1996.
- [7] E. Grimme and K. Gallivan. *A Rational Lanczos Algorithm for Model Reduction II: Interpolation Point Selection*. Numerical Algorithms, 12:33–63, 1998.
- [8] A. Odabasioglu, M. Celik, and L. Pileggi. *PRIMA: passive reduced-order interconnect macromodeling algorithm*. IEEE Transactions on Computer-Aided Design of Integrated Circuits and Systems, 17(8):645–654, 1998.
- [9] I. M. Elfadel and D. D. Ling. *A Block Rational Arnoldi Algorithm for Multipoint Passive Model-order Reduction of Multiport RLC Networks*. Proceedings of the 1997 IEEE/ACM International Conference on Computer-aided Design, pages 66–71, 1997.
- [10] J.-R. Li, F. Wang, and J. White. *An efficient Lyapunov equation-based approach for generating reduced-order models of interconnect*. Proceedings 36th Design Automation Conference, pages 1–6, 1999.
- [11] Q. Yu, J. Wang, and E. Kuh. *Passive multipoint moment matching model order reduction algorithm on multiport distributed interconnect networks*. IEEE Transactions on Circuits and Systems I: Fundamental Theory and Applications, 46(1):140–160, 1999.

- [12] J. Phillips. *Variational interconnect analysis via PMTBR*. IEEE/ACM International Conference on Computer Aided Design ICCAD, pages 872–879, 2004.
- [13] J. Phillips, E. Chiprout, and D. Ling. *Efficient full-wave electromagnetic analysis via model-order reduction of fast integral transforms*. 33rd Design Automation Conference Proceedings, pages 377–382, 1996.
- [14] T. Klemas, L. Daniel, and J. White. *Segregation by primary phase factors: a full-wave algorithm for model order reduction*. Proceedings 42nd Design Automation Conference, 2005, pages 943–946, June 2005.
- [15] F. Ferranti, M. Nakhla, G. Antonini, T. Dhaene, L. Knockaert, and A. Ruehli. *Multipoint Full-Wave Model Order Reduction for Delayed PEEC Models With Large Delays*. IEEE Transactions on Electromagnetic Compatibility, 53(4):959–967, 2011.
- [16] G. Antonini, D. Deschrijver, and T. Dhaene. *Broadband Rational Macromodeling Based on the Adaptive Frequency Sampling Algorithm and the Partial Element Equivalent Circuit Method*. IEEE Transactions on Electromagnetic Compatibility, 50(1):128–137, 2008.
- [17] J. Brittingham, E. Miller, and J. Willows. *Pole extraction from real-frequency information*. Proceedings of the IEEE, 68(2):263–273, 1980.
- [18] J. D. Geest, T. Dhaene, N. Fach, and D. D. Zutter. *Adaptive CAD-Model Building Algorithm for General Planar Microwave Structures*. IEEE Transactions on Microwave Theory and Techniques, 47(9):1801–1809, 1999.
- [19] E. Samuel, F. Ferranti, L. Knockaert, and T. Dhaene. *Passivity-Preserving Parameterized Model Order Reduction Using Singular Values and Matrix Interpolation*. IEEE Transactions on Components, Packaging and Manufacturing Technology, 3(6):1028–1037, 2013.
- [20] B. Anderson and S. Vongpanitlerd. *Network Analysis and Synthesis*. Prentice-Hall, Englewood Cliffs, NJ., 1973.
- [21] L. Knockaert, T. Dhaene, F. Ferranti, and D. D. Zutter. *Model order reduction with preservation of passivity, non-expansivity and Markov moments*. Systems & Control Letters, 60(1):53–61, Jan. 2011.
- [22] S. Boyd, L. El Ghaoui, E. Feron, and V. Balakrishnan. *Linear Matrix Inequalities in System and Control Theory*. Philadelphia, PA:SIAM 1994.
- [23] P. Gahinet and P. Apkarian. *An LMI-based Parametrization of all  $H_\infty$  Controllers with Applications*. Proceedings of the 32nd Conference on Decision and Control, pages 656–661, Dec. 1993.

- [24] P. Gahinet, A. Nemirovski, A. Laub, and M. Chilali. *LMI Control Toolbox User's Guide*. The MathWorks, Inc., Version 1, 1995.
- [25] G. Balas, R. Chiang, A. Packard, and M. Safonov. *Robust Control Toolbox User's Guide*. The MathWorks, Inc., Version 3, 2005.
- [26] M. Khalaj-Amirhosseini. *Progress In Electromagnetics Research*. 60:107–117, 2006.
- [27] L. Knockaert and D. De Zutter. *Laguerre-SVD reduced-order modeling*. IEEE Transactions on Microwave Theory and Techniques, 48(9):1469 – 1475, Sept. 2000.
- [28] A. Ruehli, A. Cangellaris, and H.-M. Huang. *Three test problems for the comparison of lossy transmission line algorithms*. pages 347–350, Oct 2002.
- [29] T. Demeester and D. De Zutter. *Quasi-TM Transmission Line Parameters of Coupled Lossy Lines Based on the Dirichlet to Neumann Boundary Operator*. IEEE Transactions on Microwave Theory and Techniques, 56(7):1649–1660, July 2008.
- [30] T. Demeester, D. Vande Ginste, and D. De Zutter. *Accurate study of the electromagnetic and circuit behavior of finite conducting wedges and interconnects with arbitrary cross-sections*. IEEE 19th Conference on Electrical Performance of Electronic Packaging and Systems (EPEPS), pages 133–136, Oct 2010.
- [31] P. Feldmann and F. Liu. *Sparse and efficient reduced order modeling of linear subcircuits with large number of terminals*. In IEEE/ACM International Conference on Computer Aided Design, pages 88–92, Nov 2004.

# 5

## Guaranteed Passive Parameterized Macromodeling by Using Sylvester State-Space Realizations

Based on the publication:

**Elizabeth Rita Samuel, Luc Knockaert, Francesco Ferranti, Tom Dhaene.**  
*Guaranteed Passive Parameterized Macromodeling by Using Sylvester  
State-Space Realizations. Published in IEEE Transactions on Microwave  
Theory and Techniques, 61(4):1444–1454, April 2013.*

\*\*\*

*In the previous chapter, the interpolation of the reduced frequency dependent state-space matrices is performed based on the assumption that the state-space matrices are in the same subspace or in other words that they are unique, such that on interpolating a smooth model is obtained. Even for a PMOR based on state-space interpolation, the realization of the state-space matrices is important. It allows to assume smoothness of variation for the state-space matrices with respect to the design parameters. Thus, it is seen that the realization of the state-space matrices is important to obtain an accurate parameterized model. Therefore, in this chapter, a novel state-space realization is proposed using the Sylvester technique. A judicious choice of the state-space realization is required to exploit the assumed smoothness of the state-space matrices with respect to the design parameters. The*

*Sylvester technique is used in combination with suitable interpolation schemes to on a set of state-space matrices. The poles and residues are hereby interpolated indirectly, in order to build accurate parameterized macromodels. The key points of the novel state-space realizations are the choice of a proper pivot matrix and a well-conditioned solution of a Sylvester equation. Stability and passivity are guaranteed by construction for the interpolation over the design space of interest. Pertinent numerical examples illustrate the proposed Sylvester realization for parameterized macromodeling.*

## 5.1 Introduction

As briefed in Section 2.3, parameterized macromodels are multivariate models that describe the complex behavior of EM systems, typically characterized by frequency (or time) and several geometrical and physical design parameters, such as layout or substrate features. Recently, parameterized macromodeling techniques that are able to guarantee overall stability and passivity have been proposed in [1–4]. The techniques described in [1] and [2] are based on the interpolation of a set of univariate macromodels, called *root macromodels*. This interpolation process of input-output systems leads to parameterization of the residues, but unfortunately not of the poles. Passive interpolation of the state-space matrices of a set of *root macromodels* is proposed in [3] and [4], providing an increased modeling capability with respect to [1] and [2], due to the parameterization of both poles and residues. Unfortunately, these methods are sensitive to issues related to the interpolation of state-space matrices [5], such as the lack of smoothness of variation in between the state-space matrices as a function of the parameters.

In this chapter, we propose a novel state-space realization that is suitable to build accurate parameterized macromodels. The direct parameterization of poles and residues is avoided, due to their potentially non-smooth behavior with respect to the design parameters. The Vector Fitting (VF) technique is initially used to build a set of *root macromodel* for different combinations of design variables. Stability for each *root macromodel* is enforced by pole flipping [6], while passivity is checked and enforced by means of standard techniques (e.g., [6–9]). The transformation of a pole-residue form obtained by means of VF to a Sylvester realization is computed for each *root macromodel*. The key advantages of the Sylvester realization are the choice of a pivot or reference matrix and the obtention of a well-conditioned solution to the Sylvester equation. Since the same pivot matrix is used for all the state-space realization of all the *root macromodels*, smooth variations of the state-space matrices with respect to the design parameters can be expected. The state-space matrices obtained from the Sylvester realization are used to obtain matrix solutions of the linear matrix inequalities (LMIs) pertaining to the positive-real or bounded-real lemma [10], and this information is then used

to perform a passivity preserving interpolation of the state-space matrices. Computationally, the solution of LMIs or algebraic Riccati equations (AREs) generates a descriptor state-space form that preserves positive-realness or bounded-realness of the model. Finally, suitable interpolation schemes are used to build accurate parameterized macromodels which preserve stability and passivity.

The proposed Sylvester realization for macromodeling based on interpolation of state-space matrices is illustrated using suitable numerical examples.

## 5.2 Parameterized Macromodeling

Starting from a set of data samples  $\{(s, \vec{p})_k, \mathbf{H}(s, \vec{p})_k\}$ , a set of frequency-dependent rational models is built for an initial selection of design space points by means of system identification techniques [11], in our case the VF technique [6]. The result of this initial procedure is a set of rational univariate macromodels, called *root macromodels*. Each *root macromodel* is related to a design space point  $\vec{p}_k = (p_{k_1}^{(1)}, \dots, p_{k_M}^{(M)})$ . Two data grids are used in the modeling process: an estimation grid and a validation grid. The estimation grid is utilized to build the *root macromodels* that, combined with suitable interpolation schemes, are able to provide stable and passive parameterized macromodels. The validation grid is utilized to assess the interpolation capability of the parameterized macromodel and its capability of describing the system under study in points of the design space previously unused for the construction of the *root macromodels*.

Suppose we have a set of *root macromodels*  $\mathcal{S}_{\vec{p}_k}$ ,  $k = 1, \dots, N$  with a minimal realization

$$\mathcal{S}_{\vec{p}_k} \equiv \begin{bmatrix} \mathbf{A}_{\vec{p}_k} & \mathbf{B}_{\vec{p}_k} \\ \mathbf{C}_{\vec{p}_k} & \mathbf{D}_{\vec{p}_k} \end{bmatrix}, \quad (5.1)$$

the state-space equations become

$$\dot{x} = \mathbf{A}_{\vec{p}_k} x + \mathbf{B}_{\vec{p}_k} u \quad (5.2)$$

$$y = \mathbf{C}_{\vec{p}_k} x + \mathbf{D}_{\vec{p}_k} u \quad (5.3)$$

while the transfer functions are given by

$$\mathbf{H}_{\vec{p}_k}(s) = \mathbf{C}_{\vec{p}_k} (s\mathbf{I} - \mathbf{A}_{\vec{p}_k})^{-1} \mathbf{B}_{\vec{p}_k} + \mathbf{D}_{\vec{p}_k}. \quad (5.4)$$

We assume in this chapter that all realizations  $\mathcal{S}_{\vec{p}_k}$  have the same McMillan degree  $n$  [12] and a number of ports  $m \leq n$ . We further suppose that all matrices  $\mathbf{A}_{\vec{p}_k}$  are Hurwitz stable i.e; every eigenvalue of  $\mathbf{A}_{\vec{p}_k}$  has a strictly negative real part [13].

We propose a generic parameterized realization of the form

$$\mathcal{S}(\vec{p}) \equiv \begin{bmatrix} \mathbf{A}(\vec{p}) & \mathbf{B}(\vec{p}) \\ \mathbf{C}(\vec{p}) & \mathbf{D}(\vec{p}) \end{bmatrix} \quad (5.5)$$

with  $\vec{p} = (\vec{p}^{(1)}, \dots, \vec{p}^{(M)})$ . The models  $\mathcal{S}_{\vec{p}_k}$  can be considered as snapshots of  $\mathcal{S}(\vec{p})$ .  $\mathcal{S}_{\vec{p}_k}$  needs to be able to accurately model the system behavior as a function of the complex frequency  $s$  and the vectorial parameter  $\vec{p}$  while guaranteeing stability and passivity over the design space of interest.

### 5.3 State-Space Realization For Parameterized Macro-modeling

To obtain accurate parameterized macromodels by interpolation of the state-space matrices, the choice of the state-space realization is fundamental.

In this section, we will discuss the well-known Gilbert realization, the balanced realization, the barycentric realization, and then the proposed novel Sylvester realization, preceded by an important subsection on passive parameterized interpolation.

#### 5.3.1 Gilbert Realization

The minimal state-space realization problem for linear time invariant (LTI) systems was first formulated by Gilbert [14], who gave an algorithm for transforming a transfer function into a system of differential equations. The approach of Gilbert is based on partial-fraction expansions.

$$\mathbf{H}(s) = R_{0,\vec{p}_k} + \sum_{n=1}^N \frac{R_{n,\vec{p}_k}}{s - z_{n,\vec{p}_k}} \quad (5.6)$$

where  $R_{n,\vec{p}_k}$  and  $z_{n,\vec{p}_k}$  are respectively the model residues and poles, with  $R_{0,\vec{p}_k}$  being the direct coupling constant. The poles and the residues are stamped directly in the  $A(\vec{p})$  and  $C(\vec{p})$  matrices using the Gilbert realization [14]. It is well-known that model poles and residues are very sensitive to even small variations of the design parameters, resulting in quite irregular variations of each pole in the design space, e.g. bifurcation effects [15]. Since poles and residues may present a highly non-smooth behavior with respect to the design parameters, achieving a reasonable accuracy in parameterized macromodels built by interpolation of state-space matrices becomes difficult, due to the fact that pole and residue trajectories as a function of  $\vec{p}$  are not well defined.

#### 5.3.2 Balanced Realization

A minimal and stable realization is called balanced [16, 17], if the controllability and observability Gramians [16] are equal and diagonal. Every minimal system can be brought into balanced form. The balanced realization can be calculated



using the Matlab function `balreal`. This routine uses the eigendecomposition of the product of the observability and controllability Gramians to construct the balancing transformation matrix [12].

The most interesting property of a balanced realization is associated with the uniqueness properties of the balancing transformation [18]. As the eigenvalues (real and nonnegative) of the product of the controllability and observability Gramians, are distinct, then the balancing transformation matrix is unique. If, on the other hand, two or more eigenvalues are repeated, then their corresponding eigenvectors can be rotated arbitrarily in the corresponding eigenspace. Thus as stated in [5, 18, 19], uniqueness is guaranteed up to a sign and it may affect the smoothness of the state-space matrices as functions of the design parameters.

### 5.3.3 Barycentric Realization

In what follows, the barycentric realization [15, 20] is described. The transfer function of the macromodel related to a generic point  $\vec{p} = (p_{k_1}^{(1)}, \dots, p_{k_M}^{(M)})$  in the design space is converted from the rational pole residue form

$$\mathbf{H}(s) = R_{0,\vec{p}_k} + \sum_{n=1}^N \frac{R_{n,\vec{p}_k}}{s - z_{n,\vec{p}_k}} \quad (5.7)$$

obtained by means of VF, into the barycentric realization [15, 21]

$$\mathbf{H}(s) = \frac{F_{0,\vec{p}_k} + \sum_{n=1}^N F_{n,\vec{p}_k} \phi_n(s)}{f_{0,\vec{p}_k} + \sum_{n=1}^N f_{n,\vec{p}_k} \phi_n(s)} \quad (5.8)$$

with basis functions defined as follows

$$\phi_n(s) = \frac{1}{s - a_n}, \quad n = 1, \dots, N \quad (5.9)$$

and where the barycentric basis poles  $\{a_n\}_{n=1}^N$  are fixed and do not depend on  $\vec{p}_k$ . The barycentric realization (5.8) can be split into a numerator and a denominator, i.e;

$$\mathbf{H}(s) = \frac{N_{\vec{p}_k}(s)}{\Delta_{\vec{p}_k}(s)} \quad (5.10)$$

where

$$N_{\vec{p}_k}(s) = F_{0,\vec{p}_k} + \sum_{n=1}^N F_{n,\vec{p}_k} \phi_n(s) \quad (5.11)$$

$$\Delta_{\vec{p}_k}(s) = f_{0,\vec{p}_k} + \sum_{n=1}^N f_{n,\vec{p}_k} \phi_n(s) \quad (5.12)$$

This factorization can be seen as a special case of the so called right coprime factorization [22]. A state-space realization for each *root macromodel* is obtained

by means of (5.11)-(5.12). First, we construct two separate state-space realizations for the numerator and denominator. We have

$$N_{\vec{p}_k}(s) = \begin{bmatrix} \tilde{\mathbf{A}}_{\vec{p}_k}^{num} & \tilde{\mathbf{B}}_{\vec{p}_k}^{num} \\ \tilde{\mathbf{C}}_{\vec{p}_k}^{num} & \tilde{\mathbf{D}}_{\vec{p}_k}^{num} \end{bmatrix} \quad (5.13)$$

$$\Delta_{\vec{p}_k}(s) = \begin{bmatrix} \tilde{\mathbf{A}}_{\vec{p}_k}^{den} & \tilde{\mathbf{B}}_{\vec{p}_k}^{den} \\ \tilde{\mathbf{C}}_{\vec{p}_k}^{den} & \tilde{\mathbf{D}}_{\vec{p}_k}^{den} \end{bmatrix} \quad (5.14)$$

where

- $\mathbf{A}_{\vec{p}_k}^{num} = \mathbf{A}_{\vec{p}_k}^{den} = \text{blkdiag}\{a_n I_P\}$ ,  $n = 1, \dots, N$ , where  $I_P$  is the identity matrix of order  $P$
- $\mathbf{B}_{\vec{p}_k}^{num} = \mathbf{B}_{\vec{p}_k}^{den} = [I_P, \dots, I_P]^T$  is a block-column matrix obtained by stacking  $N$  identity matrices  $I_P$
- $\mathbf{C}_{\vec{p}_k}^{num} = [F_{1,\vec{p}_k}, \dots, F_{N,\vec{p}_k}]$
- $\mathbf{C}_{\vec{p}_k}^{den} = [f_{1,\vec{p}_k} I_P, \dots, f_{N,\vec{p}_k} I_P]$
- $\mathbf{D}_{\vec{p}_k}^{num} = F_{0,\vec{p}_k}$
- $\mathbf{D}_{\vec{p}_k}^{den} = f_{0,\vec{p}_k} I_P$

Remark that, whenever some of the basis poles in the set of  $\{a_n\}_{n=1}^N$  are complex, the above state-space matrices are complex. However, standard state-space coordinate transformations can be applied such that the resulting realization is real. The matrix  $\mathbf{A}_{\vec{p}_k}^{num} = \mathbf{A}_{\vec{p}_k}^{den}$  can be seen as a pivot matrix for the barycentric realization. Although the denominator function (5.12) is scalar, its realization has been chosen to have  $P$  ports, in order to be compatible in size with the realization of (5.11). We have

$$\mathbf{H}(s) = N_{\vec{p}_k}(s) \Delta_{\vec{p}_k}(s)^{-1} I_P \quad (5.15)$$

Then after some standard manipulations [15], we can write the final state-space realization of (5.10) as

$$\mathbf{H}(s) = \begin{bmatrix} \tilde{\mathbf{A}}_{\vec{p}_k} & \tilde{\mathbf{B}}_{\vec{p}_k} \\ \tilde{\mathbf{C}}_{\vec{p}_k} & \tilde{\mathbf{D}}_{\vec{p}_k} \end{bmatrix} \quad (5.16)$$

with

$$\tilde{\mathbf{A}}_{\vec{p}_k} = \mathbf{A}_{\vec{p}_k}^{den} - \mathbf{B}_{\vec{p}_k}^{den} (\mathbf{D}_{\vec{p}_k}^{den})^{-1} \mathbf{C}_{\vec{p}_k}^{den} \quad (5.17a)$$

$$\tilde{\mathbf{B}}_{\vec{p}_k} = \mathbf{B}_{\vec{p}_k}^{den} (\mathbf{D}_{\vec{p}_k}^{den})^{-1} \quad (5.17b)$$

$$\tilde{\mathbf{C}}_{\vec{p}_k} = \mathbf{C}_{\vec{p}_k}^{num} - \mathbf{D}_{\vec{p}_k}^{num} (\mathbf{D}_{\vec{p}_k}^{den})^{-1} \mathbf{C}_{\vec{p}_k}^{den} \quad (5.17c)$$

$$\tilde{\mathbf{D}}_{\vec{p}_k} = \mathbf{D}_{\vec{p}_k}^{num} (\mathbf{D}_{\vec{p}_k}^{den})^{-1} \quad (5.17d)$$

The barycentric realization (5.17) for a *root macromodel* can be computed using different methods. The robustness of this conversion is an important aspect. The computation of the barycentric realization (5.17) requires the identification of the matrices  $\mathbf{C}_{\vec{p}_k}^{num}$  and  $\mathbf{C}_{\vec{p}_k}^{den}$ , which can be found using any of the approaches described below.

1. *Pole placement approach:*

An interesting and robust approach to compute the barycentric realization uses the pole placement technique [23]. The calculation of the matrix

$$\tilde{\mathbf{A}}_{\vec{p}_k} = \mathbf{A}_{\vec{p}_k}^{den} - \mathbf{B}_{\vec{p}_k}^{den} (\mathbf{D}_{\vec{p}_k}^{den})^{-1} \mathbf{C}_{\vec{p}_k}^{den} \quad (5.18)$$

requires the identification of  $\mathbf{C}_{\vec{p}_k}^{den}$  which can be computed using the technique proposed in [23]. Another interesting approach based on the solution of a Sylvester equation can be found in [24]. Some assumptions concerning observability and controllability must be satisfied for these approaches and for the uniqueness of the solution [23, 24]. The matrix  $\mathbf{C}_{\vec{p}_k}^{den}$  is used to place the eigenvalues of the  $\tilde{\mathbf{A}}_{\vec{p}_k}$  matrix, and therefore the poles of the *root macromodels* in such a way that they are equal to  $z_{n,\vec{p}_k}$ . Once  $\mathbf{C}_{\vec{p}_k}^{den}$  is obtained, the next step is to compute the  $\mathbf{C}_{\vec{p}_k}^{num}$  matrix. Each block  $F_{n,\vec{p}_k}$ ,  $n = 1, \dots, N$  can be easily computed by means of [15]

$$F_{n,\vec{p}_k} = f_{n,\vec{p}_k} \mathbf{H}(a_n). \quad (5.19)$$

2. *Linear system approach:*

The matrix  $\mathbf{C}_{\vec{p}_k}^{den}$  is computed solving a linear system in [15]. This approach uses the solution of a linear system that contains the products of poles and becomes ill-conditioned if the order of the system is high and the bandwidth of interest is large. Once  $\mathbf{C}_{\vec{p}_k}^{den}$  is obtained, the computation of  $\mathbf{C}_{\vec{p}_k}^{num}$  is done as in the pole placement approach described above.

### 5.3.3.1 Passive Parameterized Interpolation

When the macromodel is utilized in a circuit simulator for transient analysis, stability and passivity are the fundamental properties to be guaranteed. It is known that while a passive system is also stable, the reverse is not necessarily true. A passive system denotes a system that is incapable of generating energy, and hence one that can only absorb energy from the sources used to excite it [25]. Passivity is an important property to satisfy because stable, but not passive macromodels can produce unstable systems when connected to other stable, even passive, loads.

The interpolation of state-space matrices does not in general result in the preservation of stability and passivity over the design space even if the root macromodels

(5.1) are stable and passive. First, we need to define what we mean by passive interpolation. Since each *root macromodel*  $\mathcal{S}_{\vec{p}_k}$  is passive, the bounded real lemma or positive real lemma [25] states that this is the case if there exists a positive definite symmetric matrix  $P_{p_k}$  such that the (LMI) [20, 26, 27]

$$\mathcal{L}_{\vec{p}_k} = \begin{bmatrix} \mathbf{A}'_{\vec{p}_k} P_{p_k} + \mathbf{P}_{p_k} \mathbf{A}_{\vec{p}_k} & \mathbf{P}_{\vec{p}_k} \mathbf{B}_{\vec{p}_k} & \mathbf{C}'_{\vec{p}_k} \\ (\mathbf{P}_{p_k} \mathbf{B}_{\vec{p}_k})' & -I & \mathbf{D}'_{\vec{p}_k} \\ \mathbf{C}_{\vec{p}_k} & \mathbf{D}_{\vec{p}_k} & -I \end{bmatrix} \leq 0 \quad (5.20)$$

for S-parameters [28] or

$$\mathcal{L}_{\vec{p}_k} = \begin{bmatrix} \mathbf{A}'_{\vec{p}_k} \mathbf{P}_{\vec{p}_k} + \mathbf{P}_{\vec{p}_k} \mathbf{A}_{\vec{p}_k} & \mathbf{P}_{\vec{p}_k} \mathbf{B}_{\vec{p}_k} - \mathbf{C}'_{\vec{p}_k} \\ (\mathbf{P}_{\vec{p}_k} \mathbf{B}_{\vec{p}_k} - \mathbf{C}'_{\vec{p}_k})' & -\mathbf{D}_{\vec{p}_k} - \mathbf{D}'_{\vec{p}_k} \end{bmatrix} \leq 0 \quad (5.21)$$

for Y-parameters is satisfied.

Solving the LMI can be replaced by equivalently solving an ARE, which is known to be a more efficient approach [29, 30] as the number of operations required to solve a Riccati equation is  $O(n^3)$ , while the cost of solving an equivalent LMI is  $O(n^6)$ . Thus for high orders it is advisable to solve using ARE as it is computationally much cheaper in comparison to the LMI.

For the S-parameters and Y-parameters, the AREs can respectively be written as

$$\begin{aligned} & \mathbf{A}'_{\vec{p}_k} \mathbf{P}_{\vec{p}_k} + \mathbf{P}_{\vec{p}_k} \mathbf{A}_{\vec{p}_k} + \mathbf{C}'_{\vec{p}_k} \mathbf{C}_{\vec{p}_k} + \\ & (\mathbf{P}_{\vec{p}_k} \mathbf{B}_{\vec{p}_k} + \mathbf{C}'_{\vec{p}_k} \mathbf{D}_{\vec{p}_k}) \mathbf{W}_s (\mathbf{P}_{\vec{p}_k} \mathbf{B}_{\vec{p}_k} + \mathbf{C}'_{\vec{p}_k} \mathbf{D}_{\vec{p}_k})' = 0 \end{aligned} \quad (5.22)$$

and

$$\mathbf{A}'_{\vec{p}_k} \mathbf{P}_{\vec{p}_k} + \mathbf{P}_{\vec{p}_k} \mathbf{A}_{\vec{p}_k} + (\mathbf{P}_{\vec{p}_k} \mathbf{B}_{\vec{p}_k} - \mathbf{C}'_{\vec{p}_k}) \mathbf{W}_a (\mathbf{P}_{\vec{p}_k} \mathbf{B}_{\vec{p}_k} - \mathbf{C}'_{\vec{p}_k})' = 0 \quad (5.23)$$

if  $\mathbf{W}_s = (\mathbf{I}_m - \mathbf{D}'_{\vec{p}_k} \mathbf{D}_{\vec{p}_k})^{-1}$  and  $\mathbf{W}_a = (\mathbf{D}_{\vec{p}_k} + \mathbf{D}'_{\vec{p}_k})^{-1}$  exist, i.e;  $(\mathbf{I}_m - \mathbf{D}'_{\vec{p}_k} \mathbf{D}_{\vec{p}_k}) > 0$  and  $\mathbf{D}_{\vec{p}_k} + \mathbf{D}'_{\vec{p}_k} > 0$ .

Once the matrix  $\mathbf{P}_{\vec{p}_k}$  is obtained for each *root macromodel*, it is possible to convert the transfer function from the form (5.4) to the descriptor state-space form

$$\mathbf{H}_{\vec{p}_k}(s) = \mathbf{C}_{\vec{p}_k} (s \mathbf{P}_{\vec{p}_k} - \mathbf{P}_{\vec{p}_k} \mathbf{A}_{\vec{p}_k})^{-1} \mathbf{P}_{\vec{p}_k} \mathbf{B}_{\vec{p}_k} + \mathbf{D}_{\vec{p}_k}. \quad (5.24)$$

which will be useful for obtaining the passive parameterized interpolation.

Next, consider a positive interpolation kernel [31]  $\mu_{p_k}(\vec{p})$  satisfying [32]

$$\begin{aligned} \mu_{p_k}(\vec{p}) &\geq 0, \quad \mu_{p_k}(\vec{p}_l) = \delta_{p_k, l} \\ \sum_{p_k} \mu_{p_k}(\vec{p}) &= 1 \end{aligned} \quad (5.25)$$

We assume that the interpolation kernel only depends on the design space grid points and not on the values of the functions to be interpolated. The kernel computation does not require the solution of a linear system to impose the interpolation constraints. In what follows, each interpolation kernel  $\mu_{p_k}(\vec{p})$ , is selected as in the piecewise linear interpolation.

It is straightforward to prove that, if each state-space matrix is interpolated by a positive interpolation scheme with an interpolation kernel that depends locally on the data points, this is equivalent with the interpolation of the LMI (5.20) with the same interpolation scheme i.e;

$$\mathcal{L}(\vec{p}) = \sum_{p_k=1}^N \mu_{p_k}(\vec{p}) \mathcal{L}_{p_k} \quad (5.26)$$

Hence if we parameterize all entries of the  $\mathbf{P}_{\vec{p}_k}, \mathbf{A}_{\vec{p}_k}, \mathbf{B}_{\vec{p}_k}, \mathbf{C}_{\vec{p}_k}, \mathbf{D}_{\vec{p}_k}, \mathbf{P}_{\vec{p}_k}$  matrices as

$$\mathbf{P}(\vec{p})\mathbf{A}(\vec{p}) = (\mathbf{PA})(\vec{p}) = \sum_{k=1}^N \mu_{p_k}(\vec{p}) \mathbf{P}_{\vec{p}_k} \mathbf{A}_{\vec{p}_k} \quad (5.27a)$$

$$\mathbf{P}(\vec{p})\mathbf{B}(\vec{p}) = (\mathbf{PB})(\vec{p}) = \sum_{k=1}^N \mu_{p_k}(\vec{p}) \mathbf{P}_{\vec{p}_k} \mathbf{B}_{\vec{p}_k} \quad (5.27b)$$

$$\mathbf{C}(\vec{p}) = \sum_{k=1}^N \mu_{p_k}(\vec{p}) \mathbf{C}_{\vec{p}_k} \quad (5.27c)$$

$$\mathbf{D}(\vec{p}) = \sum_{k=1}^N \mu_{p_k}(\vec{p}) \mathbf{D}_{\vec{p}_k} \quad (5.27d)$$

$$\mathbf{P}(\vec{p}) = \sum_{k=1}^N \mu_{p_k}(\vec{p}) \mathbf{P}_{\vec{p}_k} \quad (5.27e)$$

it is seen by inspection that the parameterization  $(\mathbf{PA})(\vec{p}), (\mathbf{PB})(\vec{p}), \mathbf{C}(\vec{p}), \mathbf{D}(\vec{p}), \mathbf{P}(\vec{p})$  thus obtained is passive. Since any non-negative linear combination of positive (negative) semi-definite real matrices is a positive (negative) semi-definite real matrix, stability and passivity are preserved over the entire design space. Similar results can be obtained for admittance and impedance representations [3].

The problem with the passive parameterized interpolation procedure for the Gilbert and balanced realizations are twofold. First, there are 5 interpolation equations (5.27) to be satisfied. Secondly the interpolation technique yields by construction the discrete macro-model  $\mathcal{S}_{\vec{p}_k}$  for  $\vec{p} = \vec{p}_k$  it is not at all sure that the interpolated matrices  $\mathbf{A}(\vec{p}), \mathbf{B}(\vec{p}), \mathbf{C}(\vec{p}), \mathbf{D}(\vec{p})$  (or related descriptor form) will behave smoothly in between the nodes  $\vec{p}_k$ . The reason for this is that minimal realizations are all equivalent modulo a similarity transformation. This means that two

realizations related by

$$\begin{bmatrix} \tilde{\mathbf{A}}_{\vec{p}_k} & \tilde{\mathbf{B}}_{\vec{p}_k} \\ \tilde{\mathbf{C}}_{\vec{p}_k} & \tilde{\mathbf{D}}_{\vec{p}_k} \end{bmatrix} = \begin{bmatrix} \mathbf{X}^{-1} \mathbf{A}_{\vec{p}_k} \mathbf{X} & \mathbf{X}^{-1} \mathbf{B}_{\vec{p}_k} \\ \mathbf{C}_{\vec{p}_k} \mathbf{X} & \mathbf{D}_{\vec{p}_k} \end{bmatrix} \quad (5.28)$$

where  $\mathbf{X}$  is any nonsingular matrix, yield the same transfer function

$$\mathbf{H}_{\vec{p}_k}(s) = \mathbf{C}_{\vec{p}_k} (s\mathbf{I} - \mathbf{A}_{\vec{p}_k})^{-1} \mathbf{B}_{\vec{p}_k} + \mathbf{D}_{\vec{p}_k} = \tilde{\mathbf{C}}_{\vec{p}_k} (s\mathbf{I} - \tilde{\mathbf{A}}_{\vec{p}_k})^{-1} \tilde{\mathbf{B}}_{\vec{p}_k} + \tilde{\mathbf{D}}_{\vec{p}_k} \quad (5.29)$$

It is important to note that the interpolation of state-space matrices allows for a higher modeling capability than the interpolation of transfer functions [1, 2], but unfortunately these methods are sensitive to the possible lack of smoothness of the variation of state-space matrices as a function of the parameters.

In the next subsections, we describe the proposed Sylvester realization to get around this problem.

### 5.3.4 Sylvester Realization

For the Sylvester realization we propose the following state-space feedback realization with feedback matrix  $\mathbf{F}$  and pivot matrix  $\tilde{\mathbf{A}}$ .

$$\dot{x} = \tilde{\mathbf{A}}x + \tilde{\mathbf{B}}_{\vec{p}_k} v \quad (5.30a)$$

$$y = \tilde{\mathbf{C}}_{\vec{p}_k} x + \tilde{\mathbf{D}}_{\vec{p}_k} v \quad (5.30b)$$

$$v = -\mathbf{F}x + u \quad (5.30c)$$

where  $\tilde{\mathbf{A}}$  is a fixed  $n \times n$  pivot matrix and  $\mathbf{F}$  is a fixed  $m \times n$  state-space feedback matrix. This realization can be written as

$$\mathcal{R}_{\vec{p}_k} \equiv \begin{bmatrix} \tilde{\mathbf{A}} - \tilde{\mathbf{B}}_{\vec{p}_k} \mathbf{F} & \tilde{\mathbf{B}}_{\vec{p}_k} \\ \tilde{\mathbf{C}}_{\vec{p}_k} - \tilde{\mathbf{D}}_{\vec{p}_k} \mathbf{F} & \tilde{\mathbf{D}}_{\vec{p}_k} \end{bmatrix} = \begin{bmatrix} \tilde{\mathbf{A}} - \tilde{\mathbf{B}}_{\vec{p}_k} \mathbf{F} & \tilde{\mathbf{B}}_{\vec{p}_k} \\ \tilde{\mathbf{C}}_{\vec{p}_k} & \tilde{\mathbf{D}}_{\vec{p}_k} \end{bmatrix} \quad (5.31)$$

For  $\mathcal{R}_{\vec{p}_k}$  and  $\mathcal{S}_{\vec{p}_k}$  to be equivalent requires the existence of nonsingular matrices  $\mathbf{X}_k$  such that

$$\tilde{\mathbf{A}} - \tilde{\mathbf{B}}_{\vec{p}_k} \mathbf{F} = \mathbf{X}_k^{-1} \mathbf{A}_{\vec{p}_k} \mathbf{X}_k \quad (5.32a)$$

$$\tilde{\mathbf{B}}_{\vec{p}_k} = \mathbf{X}_k^{-1} \mathbf{B}_{\vec{p}_k} \quad (5.32b)$$

$$\tilde{\mathbf{C}}_{\vec{p}_k} = \mathbf{C}_{\vec{p}_k} \mathbf{X}_k \quad (5.32c)$$

is needed.

By eliminating (5.32b) from (5.32a) we obtain the Sylvester equation

$$\mathbf{A}_{\vec{p}_k} \mathbf{X}_k - \mathbf{X}_k \tilde{\mathbf{A}} + \mathbf{B}_{\vec{p}_k} \mathbf{F} = 0 \quad (5.33)$$

for the unknown matrix  $\mathbf{X}_k$ . We need the following to hold:

*Theorem 1:* The Sylvester equation (5.33) has a unique nonsingular solution  $\mathbf{X}_k$  provided the pair  $(\mathbf{A}_{\vec{p}_k}, \mathbf{B}_{\vec{p}_k})$  is controllable, the pair  $(\tilde{\mathbf{A}}, \mathbf{F})$  is observable, and the intersection of the eigenspectra of  $\mathbf{A}_{\vec{p}_k}$  and  $\tilde{\mathbf{A}}$  is empty.

*Proof.* See [24, 33]. □

Note that Sylvester equations are routinely solved by the Matlab function `lyap` and that the solution comes with a computational cost of  $O(n^3)$ .

*Remark 1:* The Sylvester realization for a given pivot matrix  $\tilde{\mathbf{A}}$  and feedback matrix  $\mathbf{F}$ , is unique by construction. For the choice of  $\tilde{\mathbf{A}}$  we can take a block-diagonal or block-Jordan matrix [24], which never shares eigenvalues with any of the  $\mathbf{A}_{\vec{p}_k}$  matrices. This can be accomplished by choosing the eigenvalues of  $\tilde{\mathbf{A}}$  close to the imaginary axis (see also the numerical simulations), similarly to  $\mathbf{A}_{\vec{p}_k}^{num}$  and  $\mathbf{A}_{\vec{p}_k}^{den}$  in (5.11) and (5.12). The choice of  $\mathbf{F}$  is subject to the requirement that the pair  $(\tilde{\mathbf{A}}, \mathbf{F})$  has to be observable. In this chapter we have considered  $\mathbf{F}$  as  $\mathbf{B}_{\vec{p}_k}^{num} = \mathbf{B}_{\vec{p}_k}^{den}$  as described in Section 5.3.3 with proper transformation.

More generally speaking,  $\mathbf{F}$  can be chosen quite freely, or its choice can be embedded in the overall Sylvester algorithm [34]. It is important to choose the  $\tilde{\mathbf{A}}$  and  $\mathbf{F}$  matrices properly to have a well-conditioned Sylvester equation solution.

The Sylvester realization state-space matrices generate their own LMIs similarly to (5.20) for S-parameters and as in (5.21) for Y-parameters, i.e;

$$\begin{bmatrix} (\tilde{\mathbf{A}} - \tilde{\mathbf{B}}_{\vec{p}_k} \mathbf{F})' \tilde{\mathbf{P}}_{\vec{p}_k} + \tilde{\mathbf{P}}_{\vec{p}_k} (\tilde{\mathbf{A}} - \tilde{\mathbf{B}}_{\vec{p}_k} \mathbf{F}) & \tilde{\mathbf{P}}_{\vec{p}_k} \tilde{\mathbf{B}}_{\vec{p}_k} & \tilde{\mathbf{C}}'_{\vec{p}_k} \\ (\tilde{\mathbf{P}}_{\vec{p}_k} \tilde{\mathbf{B}}_{\vec{p}_k})' & -\mathbf{I} & \tilde{\mathbf{D}}'_{\vec{p}_k} \\ \tilde{\mathbf{C}}_{\vec{p}_k} & \tilde{\mathbf{D}}_{\vec{p}_k} & -\mathbf{I} \end{bmatrix} \leq 0 \quad (5.34)$$

for S-parameters and

$$\begin{bmatrix} (\tilde{\mathbf{A}} - \tilde{\mathbf{B}}_{\vec{p}_k} \mathbf{F})^T \tilde{\mathbf{P}}_{\vec{p}_k} + \tilde{\mathbf{P}}_{\vec{p}_k} (\tilde{\mathbf{A}} - \tilde{\mathbf{B}}_{\vec{p}_k} \mathbf{F}) & \tilde{\mathbf{P}}_{\vec{p}_k} \tilde{\mathbf{B}}_{\vec{p}_k} - \tilde{\mathbf{C}}'_{\vec{p}_k} \\ (\tilde{\mathbf{P}}_{\vec{p}_k} \tilde{\mathbf{B}}_{\vec{p}_k} - \tilde{\mathbf{C}}'_{\vec{p}_k})' & -\tilde{\mathbf{D}}_{\vec{p}_k} - \tilde{\mathbf{D}}'_{\vec{p}_k} \end{bmatrix} \leq 0$$

for Y-parameters. The ARE can also be similarly recast.

It is then parameterized as in the four last equations of (5.27), i.e.,

$$\tilde{P}(\vec{p})\tilde{\mathbf{B}}(\vec{p}) = (\tilde{\mathbf{P}}\tilde{\mathbf{B}})(\vec{p}) = \sum_{k=1}^N \mu_k(\vec{p})\tilde{\mathbf{P}}_{\vec{p}_k}\tilde{\mathbf{B}}_{\vec{p}_k} \quad (5.35a)$$

$$\tilde{\mathbf{C}}(\vec{p}) = \sum_{k=1}^N \mu_k(\vec{p})\tilde{\mathbf{C}}_{\vec{p}_k} \quad (5.35b)$$

$$\tilde{\mathbf{D}}(\vec{p}) = \sum_{k=1}^N \mu_k(\vec{p})\tilde{\mathbf{D}}_{\vec{p}_k} \quad (5.35c)$$

$$\tilde{\mathbf{P}}(\vec{p}) = \sum_{k=1}^N \mu_k(\vec{p})\tilde{\mathbf{P}}_{\vec{p}_k} \quad (5.35d)$$

The first equation of (5.27) has no counterpart in equations (5.35) since it is easy to show that

$$(\tilde{P}[\tilde{A} - \tilde{B}F])(\vec{p}) = \sum_{k=1}^N \mu_{p_k}(\vec{p})\tilde{P}_{\vec{p}_k}[A - B(\vec{p}_k)F] \quad (5.36)$$

always holds.

Finally, the parameterized Sylvester realization in descriptor format is then simply generated by the interpolated matrices  $(\tilde{\mathbf{P}}\tilde{\mathbf{A}})(\vec{p})$ ,  $(\tilde{\mathbf{P}}\tilde{\mathbf{B}})(\vec{p})$ ,  $\tilde{\mathbf{C}}(\vec{p})$ ,  $\tilde{\mathbf{D}}(\vec{p})$ ,  $\tilde{\mathbf{P}}(\vec{p})$  and the parameterized transfer function is

$$\mathbf{H}_{\vec{p}}(s) = \tilde{\mathbf{C}}_{\vec{p}}(s\tilde{\mathbf{P}}(\vec{p}) - \tilde{\mathbf{P}}(\vec{p})\tilde{\mathbf{A}}(\vec{p}))^{-1}\tilde{\mathbf{P}}\tilde{\mathbf{B}}(\vec{p}) + \tilde{\mathbf{D}}(\vec{p}) \quad (5.37)$$

*Remark 2:* Note that, even if passivity is not required, the Sylvester realizations  $\mathcal{R}_{\vec{p}_k}$  can be very useful for parameterization. Suppose the interpolation kernel  $\mathcal{K}(\vec{p}_k, \vec{p}) = \mu_{p_k}(\vec{p})$  is not necessarily positive, but satisfies partition of unity i.e.,

$$\sum_{p_k} \mu_{p_k}(\vec{p}) = 1, \quad \mu_{p_k}(\vec{p}_l) = \delta_{p_k, l} \quad (5.38)$$

Then it is clear that the interpolation procedure

$$\tilde{\mathbf{B}}(\vec{p}) = \sum_{p_k=1}^N \mu_{p_k}(\vec{p})\tilde{\mathbf{B}}_{\vec{p}_k} \quad (5.39a)$$

$$\tilde{\mathbf{C}}(\vec{p}) = \sum_{p_k=1}^N \mu_{p_k}(\vec{p})\tilde{\mathbf{C}}_{\vec{p}_k} \quad (5.39b)$$

$$\tilde{\mathbf{D}}(\vec{p}) = \sum_{p_k=1}^N \mu_{p_k}(\vec{p})\tilde{\mathbf{D}}_{\vec{p}_k} \quad (5.39c)$$

is a very simple way to generate a parameterized macromodel.



## 5.4 Numerical Examples

In the following examples, we show the importance of the state-space realization. We validate the novel Sylvester realization approach by a comparison with the standard Gilbert, the balanced and the barycentric realization. The pole placement approach described in Section 5.3.3 [24] is used for the barycentric realization as it gives a more robust solution in comparison to the linear system approach [15].

### 5.4.1 CM: Two Coupled Microstrip with Variable Spacing

Two coupled microstrip lines (length  $L=2\text{cm}$ ) are considered in this example. The cross-section is shown in Fig.5.1. The conductors have a width  $W$  of  $500\text{ }\mu\text{m}$  and

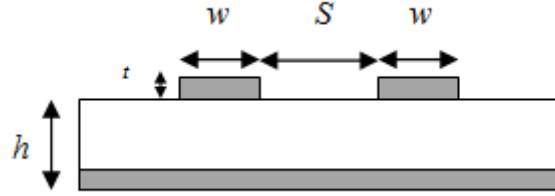


Figure 5.1: CM: Two coupled microstrips.

the height  $h$  of the dielectric ( $\epsilon_r = 9.6$ ) is  $800\text{ }\mu\text{m}$ . A bivariate macromodel is built as a function of the spacing  $S$  between the microstrips and the frequency,  $freq$ . Their corresponding ranges are shown in Table 5.1.

Parameter	Min	Max
Frequency ( $freq$ )	20 MHz	4 GHz
Spacing ( $S$ )	1 mm	3 mm

Table 5.1: CM: Parameters of the coupled microstrip

The scattering parameters were obtained by means of a full-wave solver based on the Partial Element Equivalent Circuit method [20] over a grid of  $200 \times 15$  samples, for frequency and spacing respectively. We have built *root macromodels* for 8 values of the spacing by means of VF, each with an order equal to 8.

As described in Section 5.3.4, a pivot matrix and a feedback matrix must be chosen such that a well-conditioned solution is obtained for the Sylvester equation (5.33). We use a pivot matrix based on the set of poles  $\{a_n\}_{n=1}^N$ , chosen as follows

```
N ; % Order of approximation
%Complex conjugate pairs, linearly spaced:
```

```

 $\beta = \text{linspace}(\omega(1), \omega(\text{end}), N/2); \% \omega = 2\pi \text{freq}$ 
poles=[];
for n=1:length( $\beta$ )
 $\alpha = -\beta(n) * 1e-2;$ 
poles=[poles ( $\alpha - i * \beta(n)$ ) ( $\alpha + i * \beta(n)$ ) ];
end

```

i.e; the pole pairs are chosen as

$$a_n = -\alpha + j\beta, \quad a_{n+1} = -\alpha - j\beta$$

where,  $\alpha = \beta/100$ .

Also, since the eigenvalues of the pivot matrix and those of the *root macromodels* obtained from Gilbert realization must not be the same, we choose the poles very close to the imaginary axis as shown in Fig.5.2. The feedback ma-

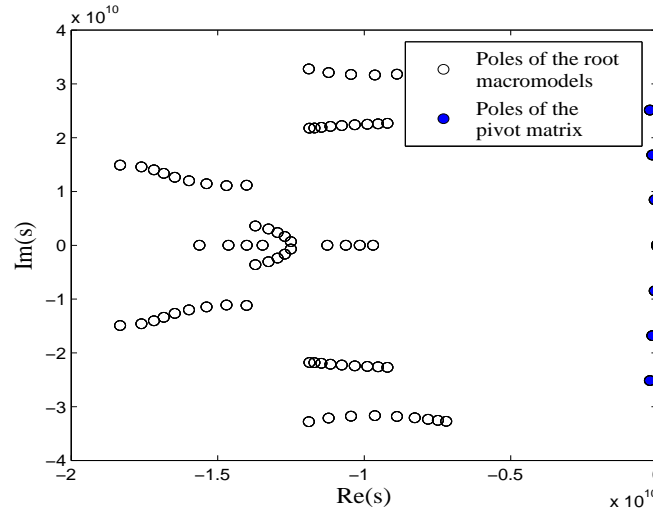


Figure 5.2: CM: Eigenvalues of the pivot matrix and the root macromodels obtained from Gilbert realization.

trix is chosen as described in Section 5.3.4. A similarity transformation is then performed using the Sylvester solution to obtain the state-space matrices of the Sylvester realization.

Then the four realizations are converted to a passive descriptor state-space form using LMI (5.34) as described in Section 5.3 with the help of CVX [35]. A bivariate macromodel is then obtained by linear interpolation of the corresponding

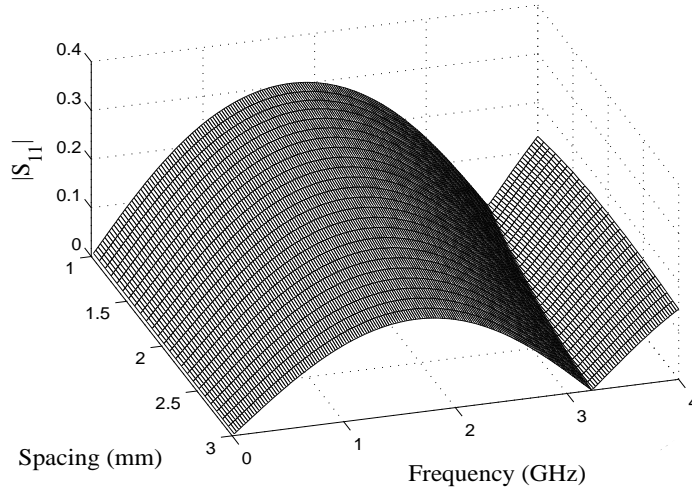


Figure 5.3: CM: Magnitude of the bivariate macromodel  $S_{11}(s, S)$  (Sylvester realization).

state-space matrices. The parameterized macromodel obtained by the Sylvester realization is shown in Fig.5.3 . Fig.5.4 compares  $S_{11}(s, S)$  and its macromodel using the proposed realization for the spacing values  $S = \{1.08, 2.08, 2.91\}$  mm that have not been used for the generation of the *root macromodels*.

The error plot in Fig.5.5 shows the absolute error at the validation points for the different realizations. It can be seen that the proposed Sylvester realization method gives a more accurate parametric macromodel with an absolute maximum error of  $-55.77$  dB in comparison with the other realization techniques. The error plot of barycentric realization and the proposed technique is almost similar, but the proposed technique is computationally cheaper in comparison with barycentric realization.

Technique	Maximum Error (dB)	CPU time (sec)
Gilbert	-0.505	-
Balanced	3.134	0.115
Barycentric	-55.032	0.281
Sylvester	-55.766	0.095

Table 5.2: CM: Comparison of the different techniques

Table 5.2 compares the accuracy and CPU time needed for the four realizations. As the initial set of data samples are built using the VF technique, the *root macromodels* are in the standard Gilbert form. Thus 5.2 gives the CPU time for

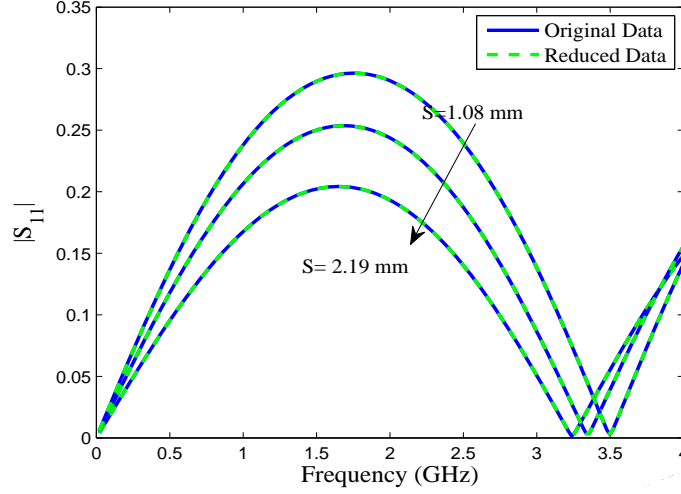


Figure 5.4: CM: Magnitude of the bivariate macromodel of  $S_{11}(s, S)$  ( $S = \{1.08, 2.08, 2.91\}$  mm using the Sylvester realization.

the transformation from the Gilbert state-space form to the respective state-space realization forms. It can be noted, that the proposed Sylvester realization is accurate and has the least computation. The distribution of the poles is shown in Fig.5.6 ; a bifurcation effect on a couple of poles is visible with two real poles moving towards each other and becoming a complex conjugate pole-pair, causing the slope of the corresponding trajectory to become discontinuous. This example shows that direct parameterization of the poles should be avoided due to potentially non-smooth behavior with respect to the design parameters. The effect of the bifurcation for the Gilbert realization can be seen in Fig.5.7. In order to verify the properties of the parameterized macromodel using Sylvester realization, we check the poles of the parameterized macromodel over a dense sample (i.e; 200 samples) of the spacing  $S$  and is seen in Fig.5.8 that the real part of the poles are negative and thus the system is stable.

The  $H_\infty$  norm [36] of the system for the same dense samples of the spacing  $S$  is plotted in Fig.5.9 and is found to be always less than 1 which shows that the system is passive. Thus the proposed Sylvester realization is able to provide a more accurate parameterized macromodel than the Gilbert realization and balanced realization, and a computationally cheaper model in comparison with barycentric realization. Also by using an LMI along with the Sylvester realization a stable and passive parameterized macromodel is obtained.

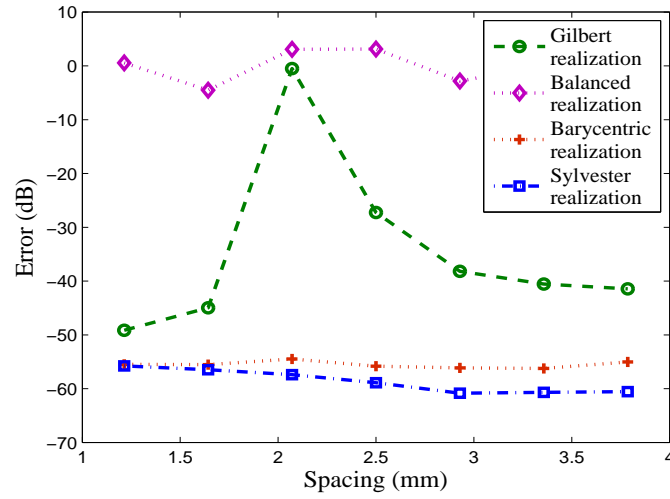


Figure 5.5: CM: Error comparison for the different realizations.

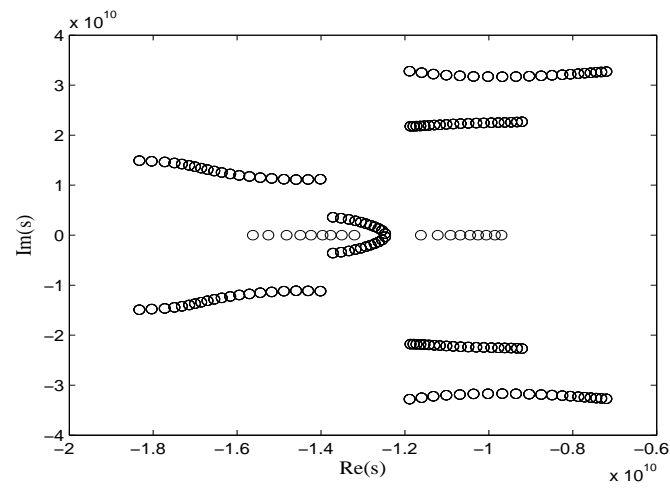


Figure 5.6: CM: Model poles as a function of spacing for the root macromodels.

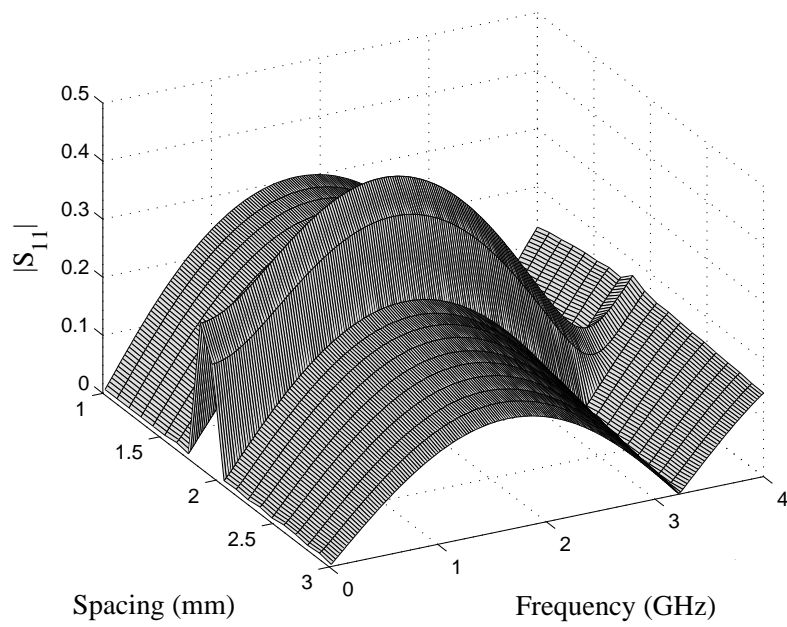


Figure 5.7: CM: Magnitude of the bivariate macromodel  $S_{11}(s, S)$  using the Gilbert realization.

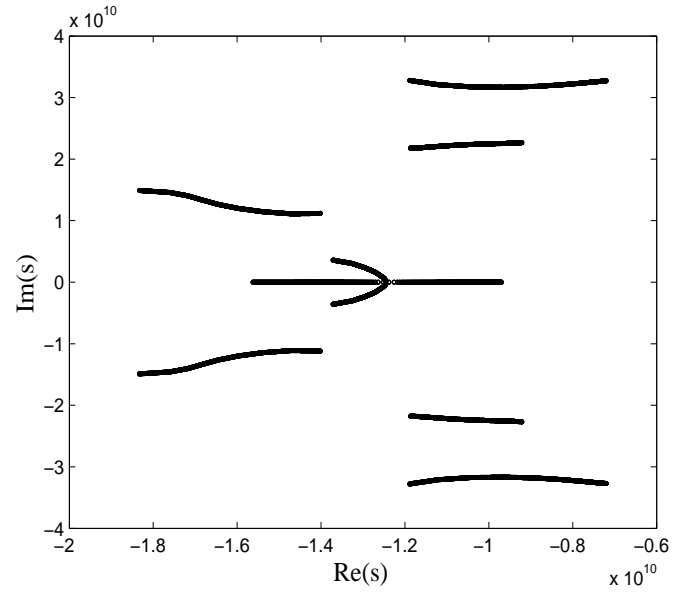


Figure 5.8: CM: Poles of the bivariate macromodel  $S(s, S)$  using the Sylvester realization.

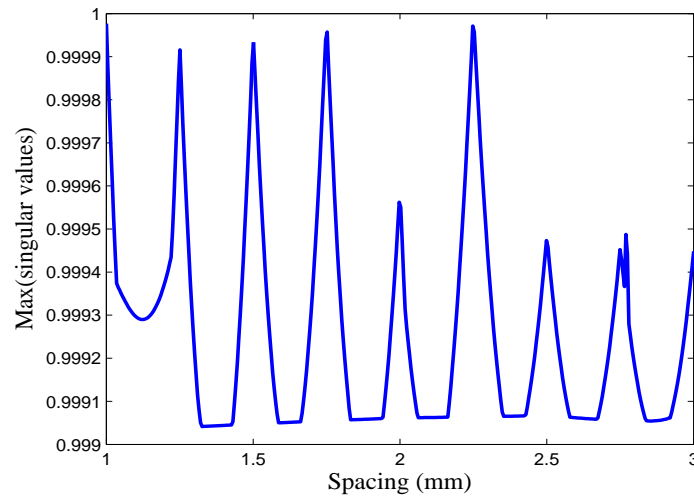


Figure 5.9: CM:  $H_\infty$  norm for the bivariate macromodel  $S(s, S)$  using the Sylvester realization.

### 5.4.2 NF: Folded Stub Notch Filter with Variable Length and Variable Spacing

A folded stub microwave notch filter on a substrate with relative permittivity  $\epsilon_r = 9.6$  and a thickness of  $0.635 \text{ mm}$  is modeled in this example. The layout of this filter is shown in Fig.5.10.

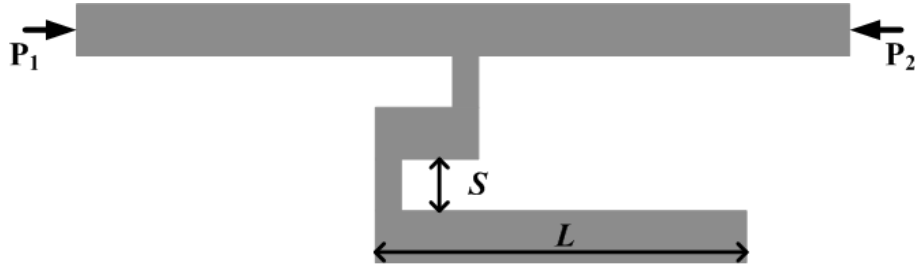


Figure 5.10: NF: Layout of the folded stub notch filter.

The spacing  $S$  and the length  $L$  of the stub are chosen as design variables in addition to frequency. Their corresponding ranges are shown in Table 5.3. The

Parameter	Min	Max
Frequency ( $freq$ )	2 GHz	4 GHz
Length ( $L$ )	5 mm	10 mm
Spacing ( $S$ )	0.5 mm	0.7 mm

Table 5.3: NF: Parameters of the folded stub filter

scattering parameters were computed with advanced design system (ADS) momentum over a grid of  $11 \times 11$  samples, for length and spacing respectively. We have built root *macromodels* for  $6 \times 6$  values of the length and spacing respectively by means of VF, each with an order 6. As in the previous example, a pivot matrix and feedback matrix are found, and the eigenvalues of the pivot matrix and of the root *macromodels* are different as shown in Fig.5.11. Then a similarity transformation is done using the Sylvester solution to obtain the state-space matrices of the Sylvester realization. In order to convert the state-space matrices to a passive descriptor state-space form, we solve the LMI (5.34) using CVX [35] for the three realizations. Thus, an accurate trivariate macromodel is obtained by the multilinear interpolation of the corresponding state-space matrices. Fig.5.12 shows the parameterized macromodel obtained using the Sylvester realization .

Fig.5.13 compares  $S_{12}(s, L, S)$  and its macromodel for the length values  $L = \{5.5, 6.5, 7.5, 8.5\}$  mm that have not been used for the generation of the root *macromodels* using the Sylvester realization.



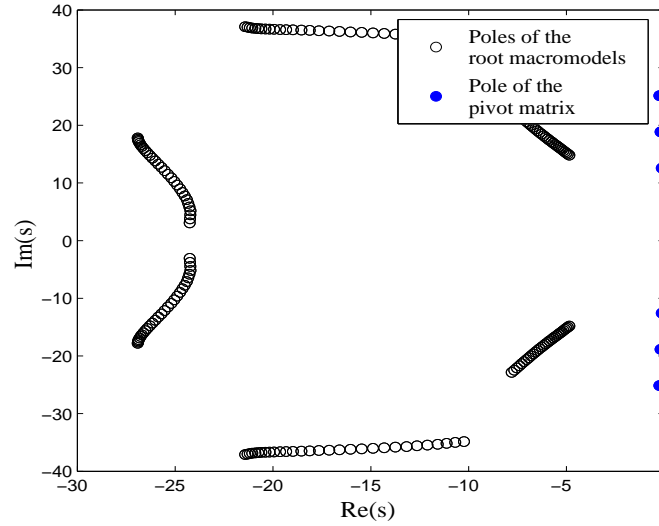


Figure 5.11: NF: Eigenvalues of the pivot matrix and the root macromodels obtained from Gilbert realization.

As in the case of the two coupled microstrips, in this example also we can see from the error plot in Fig.5.14 that the proposed realization method gives an accurate parameterized macromodel with an absolute maximum error of  $-43.62$  dB. While the barycentric realization provides a slightly better accuracy than the

Technique	Maximum Error (dB)	CPU time (sec)
Gilbert	-21.201	-
Balanced	9.718	0.891
Barycentric	-45.552	0.963
Sylvester	-43.617	0.378

Table 5.4: NF: Comparison of the different techniques

Sylvester-based realization, but it results to be computationally more expensive as shown in Table 5.4.

Fig.5.15 shows the parameterized macromodel using balanced realization, and we note that the behavior is very erratic in comparison with Fig.5.12. This is due to the abrupt changes in the elements of the state-space matrices obtained through the balanced realization.

The behavior of one of the elements in the matrix  $A_{p_k}$  is shown in Fig. 5.16. The figure compares the behavior of the corresponding element in Sylvester real-

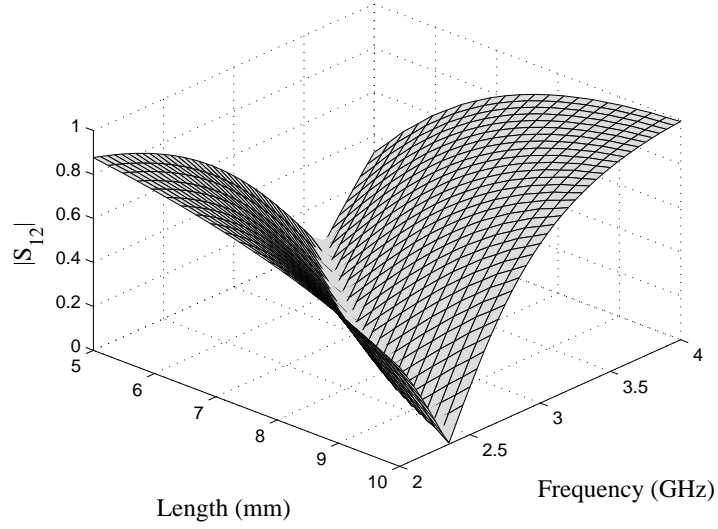


Figure 5.12: NF: Magnitude of the trivariate macromodel  $S_{12}(s, L, S)$  for  $S = 0.5\text{mm}$  using Sylvester realization.

ization and can be seen to have a smooth variation.

In order to verify the stability and passivity of the parameterized macromodel using the Sylvester realization, we check its poles over a dense sampling (i.e. of  $200 \times 200$  samples of the spacing  $S$  and length  $L$ ). In Fig.5.17 we can see that the real part of the poles is always negative and therefore the system is stable.

For passivity similar to the previous example, the  $H_\infty$  of the system is plotted in Fig.5.18 and it is found to be less than 1 for all cases.

Thus the proposed Sylvester realization is able to provide a more accurate parameterized macromodel in comparison to Gilbert realization and balanced realization, and a computationally cheaper parameterized macromodel in comparison with barycentric realization. The stability and passivity of the system can be preserved by solving LMI and by using suitable interpolation schemes.

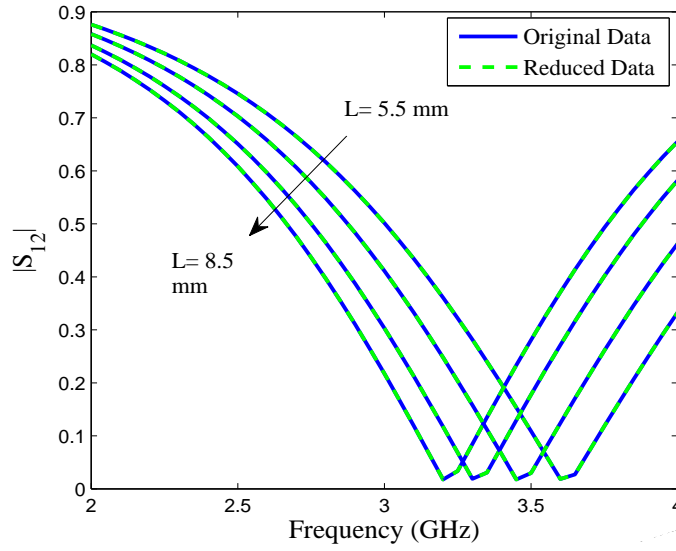


Figure 5.13: NF: Magnitude of the trivariate macromodel for  $S = 0.6$  mm of  $S_{12}(s, L, S)$  ( $L = \{5.5, 6.5, 7.5, 8.5\}$  mm) using Sylvester realization.

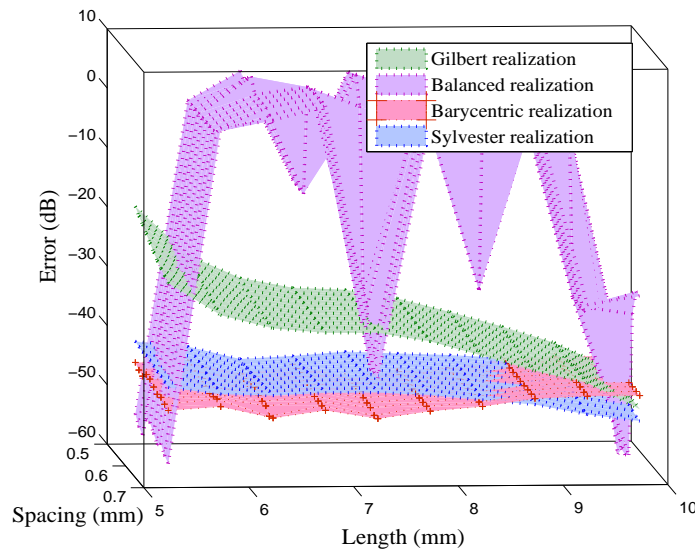


Figure 5.14: NF: Error comparison for the different state-space realizations.

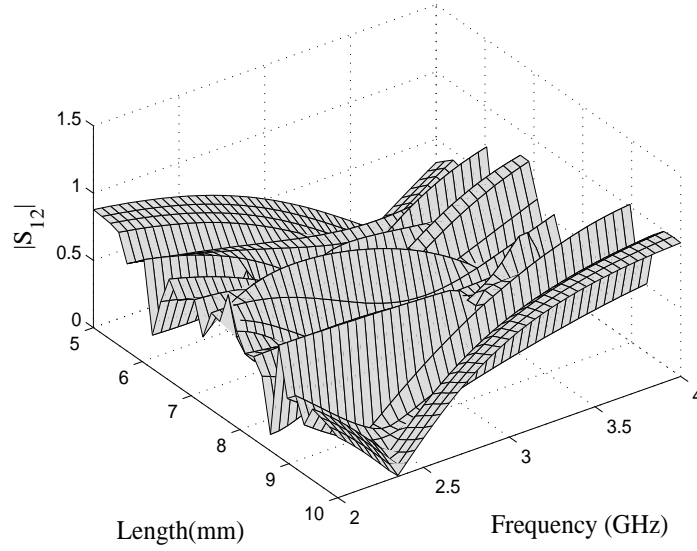


Figure 5.15: NF: Magnitude of the trivariate macromodel  $S_{12}(s, L, S)$  using balanced realization for each root macromodel).

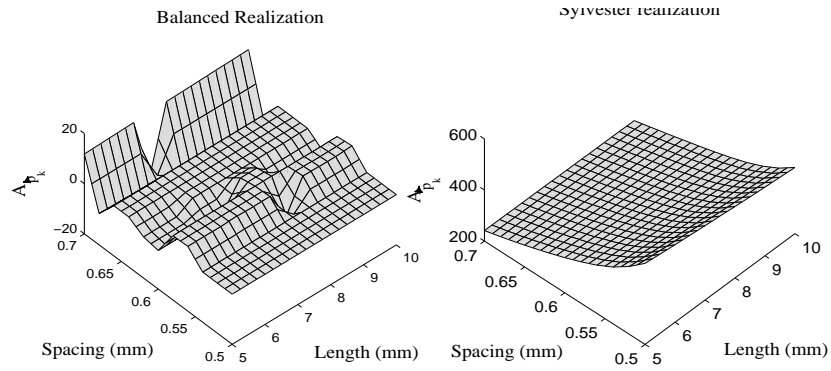


Figure 5.16: NF: An entry of the  $\tilde{A}_{\vec{p}}$ .

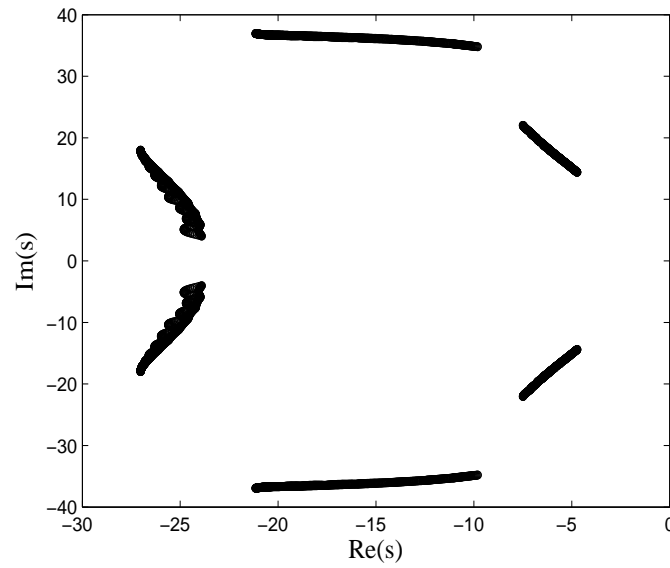


Figure 5.17: NF: Poles of the trivariate macromodel  $S(s, L, S)$  using Sylvester realization.

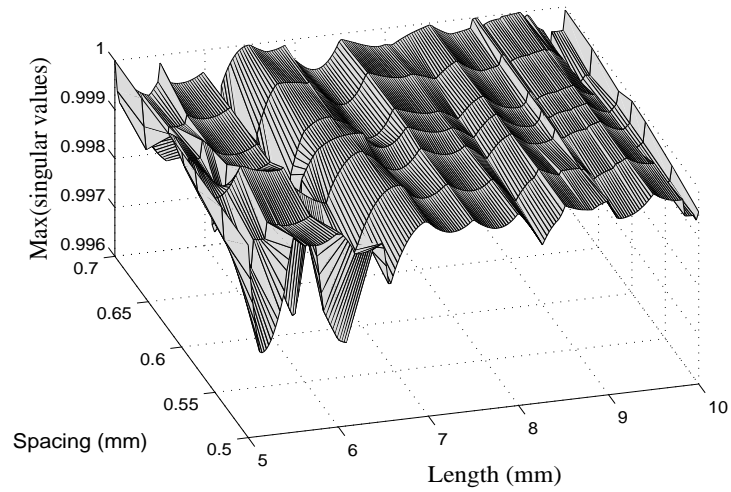


Figure 5.18: NF:  $H_\infty$  norm of the trivariate macromodel  $S(s, L, S)$  (Sylvester realization).

## 5.5 Conclusion

This chapter proposes a novel state-space realization for parameterized macro-modeling based on interpolation of state-space matrices. A judicious choice of the state-space realization is required to account for the generally assumed smoothness of the state-space matrices with respect to the parameters. Suitable interpolation schemes along with Sylvester realization are used to interpolate a set of *root* state-space matrices in order to build accurate parameterized macromodels. The essential aspects of this novel realization are to find a proper pivot matrix and to obtain a well-conditioned solution for a Sylvester equation. The numerical examples and related comparison results show that the proposed Sylvester realization provides very accurate parameterized macromodel with a low computation cost. The stability and passivity of the system can be preserved with the help of LMI and by the use of proper interpolation schemes.

Note that the Sylvester technique has a computational complexity of  $O(n^3)$  and thus becomes expensive for state-space systems with large size. Thus in Chapter 6, parameterized model order reduction using state-space interpolation is proposed.

## Acknowledgment

This work was supported by the Interuniversity Attraction Poles Programme BEST-COM initiated by the Belgian Science Policy Office and the Research Foundation Flanders (FWO).

## References

- [1] F. Ferranti, L. Knockaert, and T. Dhaene. *Guaranteed Passive Parameterized Admittance-Based Macromodeling*. IEEE Transactions on Advanced Packaging, 33(3):623–629, Aug. 2010.
- [2] F. Ferranti, L. Knockaert, and T. Dhaene. *Parameterized S-Parameter Based Macromodeling With Guaranteed Passivity*. IEEE Microwave and Wireless Component Letters, 19(10):608–610, Oct. 2009.
- [3] F. Ferranti, L. Knockaert, T. Dhaene, and G. Antonini. *Passivity-Preserving Parametric Macromodeling for Highly Dynamic Tabulated Data Based on Lur'e Equations*. IEEE Transactions on Microwave Theory and Techniques, 58(12):3688–3696, Dec. 2010.
- [4] P. Triverio, M. Nakhla, and S. Grivet-Talocia. *Passive parametric modeling of interconnects and packaging components from sampled impedance, admittance or scattering data*. Electronic System-Integration Technology Conference, pages 1–6, Sept. 2010.
- [5] J. De Caigny, J. F. Camino, and J. Swevers. *Interpolating model identification for SISO linear parameter-varying systems*. Mechanical Systems and Signal Processing, 23(8):2395–2417, 2009.
- [6] B. Gustavsen and A. Semlyen. *Rational approximation of frequency domain responses by vector fitting*. IEEE Transaction on Power Delivery, 14:1052–1061, Jul. 1999.
- [7] T. Dhaene, D. Deschrijver, and N. Stevens. *Efficient algorithm for passivity enforcement of S-parameter based macromodels*. IEEE Transactions on Microwave Theory and Techniques., 57(2):415–420, Feb. 2009.
- [8] D. Saraswat, R. Achar, and M. Nakhla. *Global passivity enforcement algorithm for macromodels of interconnect subnetworks characterized by tabulated data*. IEEE Transactions on Very Large Scale Integration (VLSI) Systems., 13(7):819–832, July 2005.
- [9] S. Grivet-Talocia. *Passivity enforcement via perturbation of Hamiltonian matrices*. Circuits and Systems I: Regular Papers, IEEE Transactions on, 51(9):1755–1769, Sept. 2004.
- [10] L. Knockaert, T. Dhaene, F. Ferranti, and D. D. Zutter. *Model order reduction with preservation of passivity, non-expansivity and Markov moments*. Systems & Control Letters, 60(1):53–61, Jan. 2011.

- [11] R. Pintelon, P. Guillaume, and Y. Rolain. *Parametric Identification of Transfer Functions in the Frequency Domain- A Survey*. IEEE Transactions on Automatic Control, 39(11):2245–2260, Nov. 1994.
- [12] K. Glover. *All optimal Hankel-norm approximations of linear multivariable systems and their  $L^\infty$ -error bounds*. International Journal of Control, 39(6):1115–1193, 1984.
- [13] Rolf Jeltsch and Mohamed Mansour. *Stability Theory: Hurwitz Centenary Conference Centro Stefano Franscini, Ascona, 1995*. Birkhuser, 1996 edition (August 28, 1996).
- [14] E. G. Gilbert. *Controllability and observability in multi-variable control systems*. SIAM Journal on Control, 1(2):128–151, 1963.
- [15] P. Triverio, S. Grivet-Talocia, and M. Nakhla. *A Parameterized Macromodeling Strategy With Uniform Stability Test*. IEEE Transactions on Advanced Packaging, 32(1):205–215, Feb. 2009.
- [16] B. Moore. *Principal component analysis in linear systems: Controllability, observability, and model reduction*. IEEE Transactions Automatic Control, 26(1):17–31, Feb. 1981.
- [17] L. Pernebo and L. M. Silverman. *Model reduction via balanced state space representations*. IEEE Transactions Automatic Control, 27(2):382–387, 1982.
- [18] M. Lovera and G. Mercere. *Identification for gain-scheduling: a balanced subspace approach*. American Control Conference, 2007., pages 858–863, July 2007.
- [19] R. Peeters, M. Olivi, and B. Hanzon. *Balanced Realization of Lossless Systems: Schur Parameters, Canonical Forms and Applications*. 15th IFAC Symposium on System Identification, pages 273–283, 2009.
- [20] F. Ferranti, L. Knockaert, T. Dhaene, and G. Antonini. *Parametric macromodeling for S-parameter data based on internal nonexpansivity*. International Journal of Numerical Modelling: Electronic Networks, Devices and Fields, 26(1):15–27, 2013.
- [21] L. Knockaert, F. Ferranti, and T. Dhaene. *Vector Fitting vs. Levenberg-Marquardt : Some experiments*. IEEE Workshop on Signal Propagation on Interconnects, 2009. SPI '09., pages 1–4, May 2009.
- [22] S. Skogestad and I. Postlethwaite. *Multivariable Feedback Control Analysis and Design*. Wiley, 1996.



- [23] J. Kautsky, N. K. Nichols, and P. Van Dooren. *Robust pole assignment in linear state feedback*. International Journal of Control, 41(5):1129–1155, 1985.
- [24] A. Varga. *Robust Pole Assignment via Sylvester Equation Based State Feedback Parametrization*. Proceedings of the IEEE International Symposium on Computer-Aided Control System Design, pages 13–18, 2000.
- [25] B. Anderson and S. Vongpanitlerd. *Network Analysis and Synthesis*. Prentice-Hall, Englewood Cliffs, NJ., 1973.
- [26] S. Boyd, L. El Ghaoui, E. Feron, and V. Balakrishnan. *Linear Matrix Inequalities in System and Control Theory*. Philadelphia, PA:SIAM 1994.
- [27] P. Triverio, M. Nakhla, and S. Grivet-Talocia. *Passive parametric macro-modeling from sampled frequency data*. IEEE International Conference on Signal Propagation and Interconnects, pages 117 –120, May 2010. doi:10.1109/SPI.2010.5483554.
- [28] P. Gahinet and P. Apkarian. *An LMI-based Parametrization of all  $H_\infty$  Controllers with Applications*. Proceedings of the 32nd Conference on Decision and Control, pages 656–661, Dec. 1993.
- [29] P. Gahinet, A. Nemirovski, A. Laub, and M. Chilali. *LMI Control Toolbox User's Guide*. The MathWorks, Inc., Version 1, 1995.
- [30] G. Balas, R. Chiang, A. Packard, and M. Safonov. *Robust Control Toolbox User's Guide*. The MathWorks, Inc., Version 3, 2005.
- [31] F. Ferranti, L. Knockaert, and T. Dhaene. *Passivity-Preserving Parametric Macromodeling by Means of Scaled and Shifted State-Space Systems*. IEEE Transactions on Microwave Theory and Techniques, 59(10):2394 – 2403, Oct. 2011.
- [32] G. Allasia. *A class of interpolating positive linear operators: theoretical and computational aspects*. : Dordrecht, Singh SP (ed.), In Recent Developments in Approximation Theory, Wavelets and Applications, Kluwer, 1995.
- [33] E. de Souza and S. Bhattacharyya. *Controllability, observability and the solution of  $AX - XB = C$* . Linear Algebra and its Applications, 39:167 – 188, 1981.
- [34] J. Carvalho, K. Datta, and Y. Hong. *A new block algorithm for full-rank solution of the Sylvester-observer equation*. IEEE Transactions on Automatic Control, 48(12):2223 – 2228, Dec. 2003.

- [35] M. Grant and S. Boyd. *CVX: Matlab software for disciplined convex programming (web page and software)*. July 2008. Available from: <http://www.stanford.edu/~boyd/cvx/>.
- [36] R. A. Horn and C. R. Johnson. *Matrix Analysis*. Cambridge University Press, Cambridge, 1990.

# 6

## Passivity-Preserving Parameterized Model Order Reduction using Singular Values and Matrix Interpolation

Based on the publications:

**Elizabeth Rita Samuel, Francesco Ferranti, Luc Knockaert, Tom Dhaene,**  
*“Passivity-Preserving Parameterized Model Order Reduction Using Singular  
Values and Matrix Interpolation”*, published in *IEEE Transactions on  
Components Packaging and Manufacturing Technology*, 3(6):1028–1037,  
June 2013.

**Elizabeth Rita Samuel, Krishnan Chemmangat, Dirk Deschrijver, Luc  
Knockaert, Tom Dhaene,**  
*“Model order reduction of parameterized state-space systems with sequential  
sampling”*, published in *proceedings of the International Symposium on  
Electromagnetic Compatibility*, pages 342–347, Brugge, Belgium, 2013

\*\*\*

*As mentioned in Section 2.3, PMOR methods can reduce large systems of equations with respect to frequency or time and also other design parameters of the circuit and are therefore well suited to efficiently perform EM design activities. The*

*focus in Section 6.2 of this chapter is on state-space interpolation based PMOR and on the estimation of the reduced order for the PMOR in a design space. For this a fast technique using Gramians is utilized to estimate the reduced order and then common projection matrices are used to build parameterized reduced order models. The design space is divided into cells and a Krylov subspace is computed for each cell vertex model. The truncation of the singular values of the merged Krylov subspaces from the models located at the vertices of each cell yields a common projection matrix per design space cell. Finally, the reduced system matrices are interpolated using positive interpolation schemes to obtain a guaranteed passive parameterized reduced order model. Then in Section 6.3 the importance of sequential sampling in the modeling of PMOR is proposed and illustrated using pertinent examples.*

## 6.1 Introduction

A number of PMOR methods have been developed in recent years. The multiparameter moment-matching methods presented in [1, 2] use a subspace projection approach. However, the resulting ROMs usually suffer from oversize when the number of moments to match is high, either because high accuracy is required or because the number of parameters is large. The parameterized interconnect macromodeling obtained using a two-directional Arnoldi process (PIMTAP) algorithm presented in [3], preserves the passivity of the parameterized *RLC* networks. However, as all multiparameter moment-matching-based PMOR techniques, it is suitable only for a low-dimensional design space. The selection of the multidimensional expansion points and the number of multiparameter moments needs to be addressed in these methods. The technique presented in [4] combines traditional passivity-preserving MOR methods and interpolation schemes based on a class of positive interpolation operators. A PMOR method that is based on the EM matrix parameterization and projection subspaces is proposed in [5]. Overall passivity of PROMs is guaranteed over the design space of interest in [4, 5]. A matrix interpolation-based technique [6] computes a set of reduced system matrices in a common subspace and interpolates them to generate a PROM. This technique avoids the oversize problem of multiparameter moment matching algorithms, but the reduced system matrices that are needed for the interpolation must have the same reduced order and must be postprocessed for reprojection onto a common subspace. The passivity of PROM is not guaranteed with this approach.

In Section 6.2 a novel PMOR technique that remedies the shortcomings of the method in [6] is proposed by combining an a-priori reduced order estimation, common projection matrices (locally (cell by cell) or globally), design space decomposition and passivity-preserving parameterization schemes. A fast technique using Gramians is first utilized to estimate the reduced order. After that projection matri-

ces are used to build parameterized models. The design space is divided into cells and a Krylov subspace is computed for each cell and each cell vertex model. The truncation of the singular values of the merged Krylov subspaces computed from the models at the vertices of each cell generates a common projection matrix per cell for the *local* approach. For the *global* approach the whole design space is considered as one cell and a common projection matrix is computed globally. Next, the reduced system matrices are interpolated using positive interpolation schemes to obtain a passive PROM. The Krylov subspaces are obtained using Krylov-based MOR methods. In this chapter we use the Laguerre-SVD technique [7].

Most of the PMOR techniques are based on the interpolation of univariate *nodal* macromodels (also called *nodes*) which are a priori sampled over the parameter design space [8]. The rules of thumb used to sample the space are neither optimal nor automated. One of the main challenges is to find a reduced set of nodes that are well-chosen in the parameter design space in order to reduce the model evaluation cost [9–12]. Thus in Section 6.3, it is illustrated that sequential sampling techniques can facilitate this step and deliver promising results.

Sequential sampling techniques can be classified into three main categories, namely input-based methods [13], output-based methods [11, 14, 15] and model-based methods [9, 10]. In this chapter, an algorithm similar to [16] is used for selecting the optimal number of nodes with the aim of generating an accurate PROM. In contrast to the data driven approach presented in [16], additional nodes are selected by comparing the reduced model order of the nodes along the edges of the parameter design space.

The advantages of combining a sequential sampling technique [16] along with a PROM technique described in Section 6.2 are numerous: the approach can be applied to multidimensional problems [17, 18], it is portable to parallel computing platforms and it reduces the expensive model evaluation time. The sampling of the parameter design space is fully automated and doesn't need to be specified a priori, hereby avoiding undersampling/oversampling in a natural way. Note that undersampling generates poor model quality whereas oversampling often results in a waste of computational resources. Finally, it is noted that the local interpolation ensures that the models are stable and passive.

## 6.2 Passivity-Preserving Parameterized Model Order Reduction using Singular Values and Matrix Interpolation

### 6.2.1 Estimation of the reduced order based on Grammians

An a-priori reduced order estimation makes the construction of PROMs much more efficient. The reduced order can be estimated by studying the so-called Hankel singular values of the model which are based on the system Grammians. The system Grammians are positive-semidefinite matrices that express the controllability and observability properties of systems or models.

The reduced order is computed at the corner points of the design space. The design space is sampled as described in [5]. It contains all parameters except frequency. Two data grids are used in the modeling process: an estimation grid and a validation grid as is shown in Fig. 6.1. The parametrized ROMs are estimated

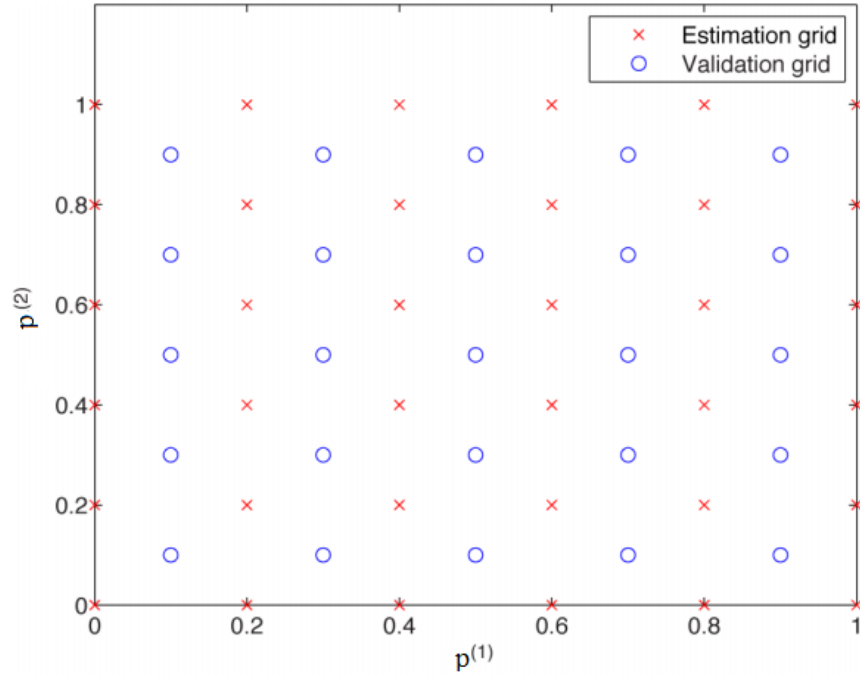


Figure 6.1: Example of an uniformly sampled estimation and validation design space grids.

either locally (cell by cell) or globally using the estimation grid and are validated over the validation grid. First, we estimate the reduced order as follows.

Consider a parameterized dynamical system with  $N$  design parameters  $\vec{p} = (p^{(1)}, \dots, p^{(N)})$  in a descriptor state-space form :

$$\begin{aligned} \mathbf{E}(\vec{p}) \frac{d\mathbf{x}(t, \vec{p})}{dt} &= \mathbf{A}(\vec{p})\mathbf{x}(t, \vec{p}) + \mathbf{B}\mathbf{u}(t) \\ \mathbf{y}(t, \vec{p}) &= \mathbf{C}\mathbf{x}(t, \vec{p}) + \mathbf{D}\mathbf{u}(t) \end{aligned} \quad (6.1)$$

The fast and efficient modified Smith technique [19, 20] enables to find the controllability Gramian ( $\mathbf{W}_c$ ) and the observability Gramian ( $\mathbf{W}_o$ ) of a large system. For the state-space model described in (6.19), the generalized Gramians are defined as the unique solutions of the linear equations

$$\mathbf{E}(\tilde{\mathbf{p}})\mathbf{W}_c\mathbf{A}(\tilde{\mathbf{p}})' + \mathbf{A}(\tilde{\mathbf{p}})\mathbf{W}_c\mathbf{E}(\tilde{\mathbf{p}})' + \mathbf{B}\mathbf{B}' = 0 \quad (6.2)$$

$$\mathbf{E}(\tilde{\mathbf{p}})'\mathbf{W}_o\mathbf{A}(\tilde{\mathbf{p}}) + \mathbf{A}(\tilde{\mathbf{p}})'\mathbf{W}_o\mathbf{E}(\tilde{\mathbf{p}}) + \mathbf{C}'\mathbf{C} = 0 \quad (6.3)$$

For every real scalar  $g < 0$ , the Stein equation [21] can be written for (6.2) as shown:

$$\tilde{\mathbf{A}}_g \mathbf{W}_c \tilde{\mathbf{A}}_g' - \mathbf{W}_c + \mathbf{B}_g \mathbf{B}_g' = 0 \quad (6.4)$$

where  $\tilde{\mathbf{A}}_g = (g\mathbf{E}(\vec{p}) + \mathbf{A}(\vec{p}))^{-1}(g\mathbf{E}(\vec{p}) - \mathbf{A}(\vec{p}))$ , and  $\mathbf{B}_g = \sqrt{(-2g)}(g\mathbf{E}(\vec{p}) + \mathbf{A}(\vec{p}))^{-1}\mathbf{B}$ . It follows that  $\mathbf{W}_c = \sum_{j=0}^{\infty} \tilde{\mathbf{A}}_g^j \mathbf{B}_g \mathbf{B}_g' (\tilde{\mathbf{A}}_g')^j$  [21–23]. In practice the spectral radius of  $\tilde{\mathbf{A}}_g$  should be minimized so that the power terms decay quickly and the infinite summation can be well approximated by finite terms.

$$\mathbf{W}_c \approx \sum_{j=0}^{k-1} \tilde{\mathbf{A}}_g^j \mathbf{B}_g \mathbf{B}_g' (\tilde{\mathbf{A}}_g')^j = \mathcal{K}_k(\tilde{\mathbf{A}}_g, \mathbf{B}_g) \mathcal{K}_k(\tilde{\mathbf{A}}_g, \mathbf{B}_g)' \quad (6.5)$$

where  $\mathcal{K}_k(\tilde{\mathbf{A}}_g, \mathbf{B}_g) = [\mathbf{B}_g \tilde{\mathbf{A}}_g \mathbf{B}_g \dots \mathbf{A}_g^{k-1} \mathbf{B}_g]$  is called the  $k$ th order Krylov matrix and serves as a Cholesky factor of  $\mathbf{W}_c$ . Similarly, taking  $\tilde{\mathbf{A}}_g = (g\mathbf{E}(\vec{p}) - \mathbf{A}(\vec{p}))(g\mathbf{C}(\vec{p}) - \mathbf{G}(\vec{p}))^{-1}$ , and  $\mathbf{C}_g = \sqrt{(-2g)}\mathbf{C}'(g\mathbf{E}(\vec{p}) + \mathbf{A}(\vec{p}))^{-1}$ , the observability Gramian  $\mathbf{W}_o$  can be computed.

The value of  $k$  in (6.5) can be found from the convergence criterion:

$$\frac{\|\mathbf{W}_c^{k-1} - \mathbf{W}_c^k\|_2}{\|\mathbf{W}_c^{k-1}\|_2} \leq \text{threshold} \quad (6.6)$$

The Smith method is similar to the alternating direction implicit (ADI) method [24–26]. The Smith method is chosen because of its ease of exposition and also because it requires only one large-scale matrix inversion (in finding  $\tilde{\mathbf{A}}_g$ ).

Next, the Hankel singular values  $\sigma_i$ , which quantifies the reachability and observability of a system, are defined as the square root of the eigenvalues of the product of the Gramians as shown:

$$\sqrt{\text{eig}(\mathbf{W}_c \mathbf{W}_o)} = \sigma_i \quad (6.7)$$

Here we define the reduced order  $q$ , based on the first  $q$  significant singular values, by setting a threshold for the ratio of the Hankel singular values and the largest singular value.

$$\frac{\sigma_i}{\sigma_{max}} \geq threshold_{\sigma}, i = 1, 2, \dots, q \quad (6.8)$$

There are no a priori rules for setting the threshold, it can be adjusted to achieve the desired level of accuracy and compactness for the PROM.

Two strategies are proposed for the order estimation. First the reduced order is estimated at the corner points of the design space. Two strategies can be followed:

1. worst-case reduced order: the highest estimated reduced order at the corner points is extended to the entire design space. This approach can guarantee an accurate reduction over the design space.
2. best-case reduced order: the lowest estimated reduced order is extended to the design space. The approach guarantees more compact models with respect to the worst-case, but the reduced order may need to be increased for some design space regions by a bottom-up approach to guarantee the desired accuracy level.

## 6.2.2 Common projection matrix computation

For each point in the estimation design space grid as described in Section 6.2.1, a Krylov-based MOR method is applied to the corresponding system and a set of projection matrices is obtained. In this chapter, the Laguerre-SVD method [7] is used for this aim.

All the projection matrices will have the same dimension in the worst-case reduced order scenario, while it may have different dimensions for the best-case reduced order scenario. We propose two approaches for the construction of common projection matrices, namely *local* and *global*.

In the *local* approach, each design space cell has  $M$  vertices and for each cell an union of the vertex projection matrices is performed by column stacking

$$\mathbf{P}_{union} = [P_1, P_2, \dots, P_M] \quad (6.9)$$

In the *global* approach, the whole design space is considered as one cell and the projection matrices are computed for all points on the estimation grid. All the projection matrices are merged by column stacking similarly as in (6.9). The dimension of  $\mathbf{P}_{union}$  is  $n \times w$  where  $n$  is the order of the system and  $w = (q_1 + q_2 + \dots + q_M)$  with  $q_i$  the reduced order of the  $i$ -th vertex of the cell. Then, the economy-size *svd* is computed for the union of the projection matrices

$$\mathbf{U}\Sigma\mathbf{V}' = svd(\mathbf{P}_{union}) \quad (6.10)$$



A common reduced order  $r$  for a cell is defined based on the first  $r$  significant singular values, by setting a threshold value for the ratio of the singular values with respect to the largest singular value. As in the case of the previous threshold value (6.8), there are no a priori rules for setting the threshold, it can be adjusted to achieve the desired level of accuracy and compactness for the PROM. A common projection matrix  $\mathbf{Q}_{comm}$  is obtained by the QR orthonormalization of  $\mathbf{P}_{comm}$ .

$$\begin{aligned}\mathbf{P}_{comm} &= \mathbf{U}_r \Sigma_r \mathbf{V}_r' \\ [\mathbf{Q}_{comm}, \mathbf{R}] &= qr(\mathbf{P}_{comm})\end{aligned}\quad (6.11)$$

where  $\mathbf{U}_r$ ,  $\Sigma_r$  and  $\mathbf{V}_r$  have a truncated dimension of  $n \times r$ ,  $r \times r$  and  $r \times r$  respectively. The congruence transformation using  $\mathbf{Q}_{comm}$ , the common projection matrix of dimension  $n \times r$ , on the original models of the design space gives the reduced system matrices for the specific cell. Using the *global* approach, means that one  $\mathbf{Q}_{comm}$  is used over the entire design space.

Regarding the state-space equations of the system under study we assume that a topologically fixed discretization mesh is used and is independent of the specific design parameter values [5]. It preserves the size of the system matrices as well as the numbering of the mesh nodes and mesh edges. The mesh is only locally stretched or shrunk when shape parameters are modified. The matrices  $\mathbf{B}$ ,  $\mathbf{C}$  are uniquely determined by the circuit topology and therefore remains constant, while the matrices  $\mathbf{E}$  and  $\mathbf{A}$  are defined as functions of the design parameters. Starting from a set of models in the estimation design space (generated with respect to a common space) using common projection matrices, it is straightforward to prove that all the reduced system matrices in the estimation grid are in the same subspace (locally or globally) and hence can be interpolated.

A flowchart that describes the different steps of the proposed technique is shown in Fig.6.2.

From the flowchart one can see that the technique can use a combination of best-case or worst-case reduced order strategy with a *local* or a *global* approach. Depending on the scenario selected, the computation complexity as well as the accuracy and compactness of the PROM change. For the *local* approach a PROM is built cell by cell in the design space. In this chapter, a hypercube [4] is considered as elementary design space cell for the *local* approach and it has  $2^N$  vertices. The amount of vertices increases exponentially with the number of dimensions, but this number still remains smaller than the number of estimation points in the whole design space that are used in the *global* approach. From Table 6.1 we can obtain the dimension of the merged projection matrix (6.9), for the different approaches before computing the compact common projection matrix. The following notations are used in the table:

-  $q_{min}$  the minimum of the reduced order estimated at the corner points of the design space.

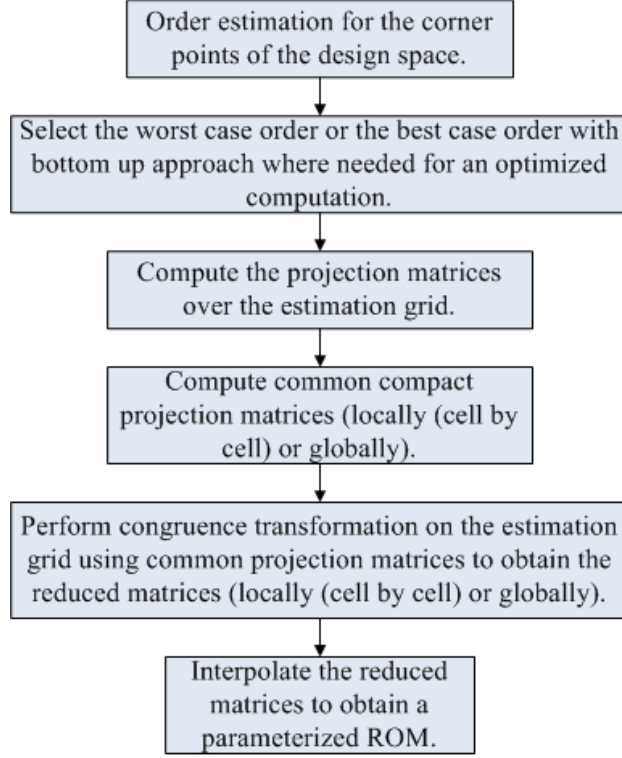


Figure 6.2: Flowchart of the proposed technique.

Approach	Best-Case	Worst-Case
<i>Local</i>	$2^N(q_{min}) + \sum_{i=1}^{2^N} q_{bu_i}$	$2^N(q_{max})$
<i>Global</i>	$M(q_{min}) + \sum_{i=1}^M q_{bu_i}$	$M(q_{max})$

Table 6.1: Column size ( $w$ ) of the Projection matrix ( $\mathbf{P}_{union}$ )

- $q_{max}$  the maximum of the reduced order estimated at the corner points of the design space.
- $N$  the number of design parameters.
- $M$  the total number of estimation points and  $M \geq 2^N$ .
- $q_{bu_i}$  the order by which the best-case order is increased at the  $i - th$  design space point using a bottom-up approach.

Concerning the complexity of the proposed technique, it can be noted that the

most expensive step is related to the Smith's technique for the order estimation at the corner points of the design space, where the inverse of  $\tilde{\mathbf{A}}_g$  (6.4) is required and its complexity is  $O(n^3)$  with  $n$  equal to the actual order of the system. Then the projection matrix can be computed at each estimation point using any model order reduction technique that influences the complexity of this step. After computing the merged projection matrix (6.9), the *SVD* has to be performed to obtain the common projection matrix, which has a complexity of  $O(4n^2w)$  where  $w$  is the column size of the merged projection matrix. Therefore, depending on the approach chosen, as stated in Table 6.1, the complexity of *SVD* varies. When the *local* approach is chosen, the model will be quite compact as only  $2^N$  points are considered for each design space cell. It is important to note that each cell will have its own compact common projection matrix. While in the case of the *global* approach, the projection matrix is computed using the projection matrices of all estimation points. Therefore, it will be less compact than the *local* approach. On the other hand, it is computed once for the entire design space and then only one *SVD* computation must be performed. When the number of design parameters increases, it leads to increase the size of the merged projection matrix and the computational complexity of the related *SVD* operation (6.10). In high dimensional design spaces, the *local* approach is more feasible since it works cell by cell. After obtaining the common projection matrix, congruence transformation has to be performed and its complexity is equivalent to matrix multiplication. Then, the complexity of the last step depends on the selected interpolation scheme.

### 6.2.3 Multivariate Interpolation

Once the reduced matrices are computed, they are interpolated to build a PROM. Multivariate interpolation can be realized by means of tensor product [27] or tessellation methods [28]. Any interpolation scheme in the class of positive interpolation operators [4] can be used, e.g., multilinear and simplicial methods [29], to preserve overall passivity as described in the sequel.

For example considering multilinear interpolation, each interpolated matrix  $\mathbf{T}(p^{(1)}, \dots, p^{(N)})$  is

$$\mathbf{T}(p^{(1)}, \dots, p^{(N)}) = \sum_{k_1=1}^{K_1} \cdots \sum_{k_N=1}^{K_N} \mathbf{T}_{(p_{k_1}^{(1)}, \dots, p_{k_N}^{(N)})} l_{k_1}(p^{(1)}) \cdots l_{k_N}(p^{(N)}) \quad (6.12)$$

where  $K_1$  is the number of estimation points and the interpolation kernel  $l_{k_i}(p^{(i)})$  satisfies the following constraints

$$\begin{aligned} 0 &\leq l_{k_i}(p^{(i)}) \leq 1, \\ l_{k_i}(p^{(i)}) &= \delta_{k_i, i} \\ \sum_{k=1}^{K_1} l_{k_i}(p^{(i)}) &= 1 \end{aligned} \quad (6.13)$$

It should be noted that the interpolation kernel functions of these methods only depend on the design space grid points and their computation does not require the prior solution of a linear system to impose an interpolatory constraint. Positive interpolation schemes have already been used in [4], where a parameterized macromodel is built by interpolating a set of ROMs treated as input-output systems, while preserving overall stability and passivity. Therefore, interpolating systems, matrices or scalars does not make any difference for these *local* interpolation kernel functions.

When performing transient analysis, stability and passivity must be guaranteed. It is known that, while a passive or positive-real system is also stable, the reverse is not necessarily true [30], which is crucial when the macromodel is to be utilized in a time domain simulator. Passive systems cannot generate more energy than they absorb through their ports. When the system is terminated on any arbitrary passive load, none of them will cause the system to become unstable [31, 32].

#### 6.2.4 Systems with a special state-space form

In the PRIMA and Laguerre-SVD methods, the original systems are assumed to be in the descriptor state-space form (6.19). If the following conditions are satisfied:

$$\begin{aligned} \mathbf{E} &= \mathbf{E}' \geq 0 \\ \mathbf{A} + \mathbf{A}' &\leq 0 \\ \mathbf{B} &= \mathbf{C}' \end{aligned} \quad (6.14)$$

the passivity of the system with transfer function  $\mathbf{Y}(s) = \mathbf{L}'(s\mathbf{C} + \mathbf{G})^{-1}\mathbf{B}$  is guaranteed [33]. For this specific format, PRIMA and Laguerre-SVD methods guarantee the passivity of the reduced model built by congruence transformation using the projection matrix  $\mathbf{Q}_{comm}$

$$\begin{aligned} \mathbf{E}_r(\vec{p}) &= \mathbf{Q}_{comm}' \mathbf{E}(\vec{p}) \mathbf{Q}_{comm} \geq 0 \\ \mathbf{A}_r(\vec{p}) &= \mathbf{Q}_{comm}' \mathbf{A}(\vec{p}) \mathbf{Q}_{comm} \leq 0 \\ \mathbf{B}_r(\vec{p}) &= \mathbf{Q}_{comm}' \mathbf{B}(\vec{p}) \\ \mathbf{C}_r(\vec{p}) &= \mathbf{C}(\vec{p}) \mathbf{Q}_{comm} \end{aligned} \quad (6.15)$$

Since any nonnegative linear combination of positive semi-definite matrices is a positive semi-definite matrix, stability and passivity are preserved over the entire design space if positive interpolation operators are used to interpolate the reduced matrices.

#### 6.2.4.1 System with a general state-space form

Consider the following state-space form

$$\begin{aligned}\frac{d\mathbf{x}(t, \vec{p})}{dt} &= \mathbf{A}(\vec{p})\mathbf{x}(t, \vec{p}) + \mathbf{B}\mathbf{u}(t) \\ \mathbf{y}(t, \vec{p}) &= \mathbf{C}\mathbf{x}(t, \vec{p}) + \mathbf{D}\mathbf{u}(t)\end{aligned}\quad (6.16)$$

To build passive parameterized reduced order models, some additional steps with respect to the previous case are required. A MOR technique that preserves passivity of systems in the form (6.16) by using the solution of linear matrix inequalities (LMI) to generate a descriptor state-space format has been proposed in [34]. The original systems after LMI matrix computations are in a descriptor form satisfying properties (6.14), and therefore the passivity-preserving interpolation previously described can be used to build a passive PROM. This method is less expensive than the passivity-preserving technique described in [35], since only a single LMI equation has to be solved.

#### 6.2.5 Numerical Results

Some pertinent numerical examples are used to demonstrate the accuracy and efficiency of the proposed PMOR technique.

Let us define the weighted RMS error as

$$Err(\mathbf{Y}_1(s), \mathbf{Y}_2(s)) = \sqrt{\frac{\sum_{k=1}^{K_s} \sum_{i=1}^{P_{in}} \sum_{j=1}^{P_{out}} \frac{|Y_{1,(ij)}(s_k) - Y_{2,(ij)}(s_k)|^2}{W_{(ij)}(s_k)}}{P_{in} P_{out} K_s}} \quad (6.17)$$

$$W_{(ij)}(s_k) = |Y_{2,(ij)}(s_k)|^2$$

In (6.17)  $K_s$ ,  $P_{in}$  and  $P_{out}$  are the number of frequency samples, input and output ports of the system, respectively.

The worst case RMS error over the validation grid is chosen to assess the accuracy and the quality of PROMs

$$\begin{aligned}\mathbf{g}_{max} &= \operatorname{argmax} Err(\mathbf{g}), \quad \mathbf{g} \in \text{validation grid} \\ Err(\mathbf{g})_{max} &= Err(\mathbf{g}_{max})\end{aligned}\quad (6.18)$$

and it is used in the numerical examples. The proposed technique was implemented in MATLAB R2009A [36] and all experiments were carried out on Windows platform equipped with Intel(R) Xeon(R) CPU E5504@2.0 GHz and 6GB RAM.

##### 6.2.5.1 EM: EM model

An EM model satisfying (6.14), of an interconnection structure composed of six conductors having  $\epsilon_r = 9.6$ , with a length  $L = 2 \text{ cm}$ , a width  $w = 1 \text{ mm}$  and a

Parameter	Min	Max
Frequency ( $freq$ )	1 kHz	15 GHz
Horizontal spacing ( $S_x$ )	1 mm	2 mm
Vertical spacing ( $S_y$ )	2 mm	3 mm

Table 6.2: EM: Parameters of the model

thickness  $t = 0.2 \text{ mm}$  has been modeled in this example. Fig.6.3 shows its cross section.  $S_x$  and  $S_y$  represents the horizontal and vertical spacings between the conductors and are the two parameters that vary in addition to frequency. Their corresponding ranges are shown in Table 6.6. The order of the original models is 702. The design space is sampled uniformly over an estimation grid of  $4 \times 4$

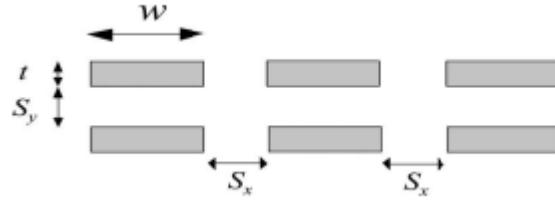


Figure 6.3: EM: Cross section of multiconductor system.

$(S_x, S_y)$  samples and a validation grid of  $3 \times 3$   $(S_x, S_y)$  samples. The validation design space points are located in the center of each cell of the rectangular estimation grid as shown in Fig.6.1. The reduced order is estimated at the corners of the design space by the truncation of the Hankel singular values with a threshold.

This threshold can be set based on the level of accuracy needed for the PMOR. For example we have set a threshold of 0.01 for (6.8), such that the weighted RMS error (6.17) at the corner points of the design space is not larger than 0.05. Depending on the accuracy and compactness required, one can increase or decrease the threshold. Then, the projection matrices are computed at the estimation points using Laguerre-SVD.

For *local* projection, the projection matrix is constructed cell by cell. For example, consider the cell with  $S_y$  varying from 2 mm to 2.3 mm and  $S_x$  varying from 1 mm to 1.3 mm, the *local* projection matrix is found by truncating the singular values of the union of the projection matrices computed at the vertices of the cell. If the common projection matrix is generated by the mere union of the projection matrices computed at the vertices of the cell, then the reduced order

is 178, but with the truncation of the merged projection matrices by a threshold of 0.01 as described in Section 6.2.2, the reduced order is 66 as shown in Fig.6.4. Thus a more useful projection matrix is obtained locally for the specified cell using the novel PMOR technique. The parameterized model is obtained by multilinear

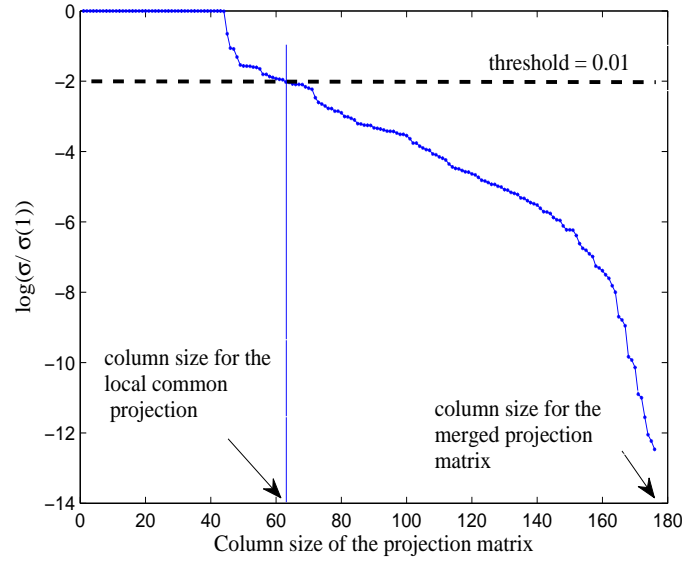


Figure 6.4: EM: Singular values of the projection matrix (best-case local approach).

interpolation of the reduced system matrices. Fig.6.5 shows the crosstalk term  $\mathbf{Y}_{16}(s, S_x, S_y)$  for  $S_x = 1.2 \text{ mm}$ . Fig.6.6 plots the magnitude of  $\mathbf{Y}_{16}(s, S_x, S_y)$  at the validation points of this design space cell. The worst-case RMS error (6.18) for the *local* approach is 0.0416 as shown in Fig.6.7.

The PROM can be built globally by computing a *global* common projection matrix for the entire design space. The whole design space is considered as one cell and then the projection matrices are found at the estimation points. The projection matrices are then merged and its singular values are truncated by a threshold of 0.01. It can be seen that the merged projection matrix, that is 708 has been reduced to 92 for the *global* common projection as shown in Fig.6.8. Thus we are able to obtain reduced order models at the estimation points globally.

The Table 6.3 below summarizes, the dimension of the merged and common projection matrix along with the CPU time for computing the reduced order and the common projection matrix using the different approaches. In this example, Table 6.3 shows that for a compact model the best-case scenario can be selected and that for a faster performance the worst-case scenario can be selected. It should

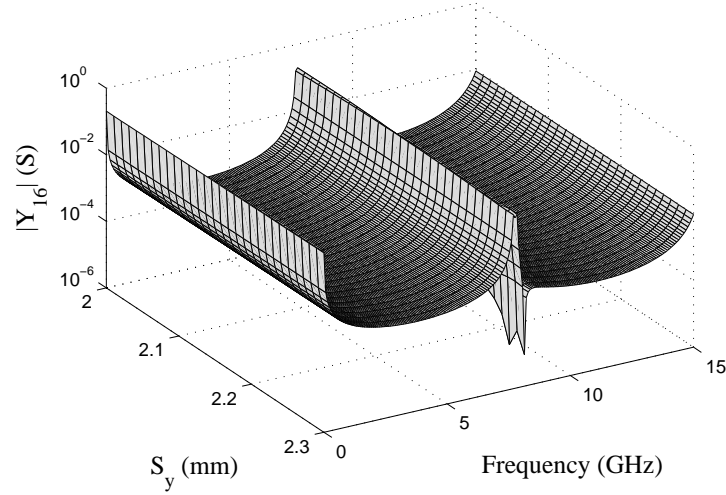


Figure 6.5: EM: Magnitude of  $\mathbf{Y}_{16}(s, S_x, S_y)$  for  $S_x = 1.2$  mm.

Approach	Column size of $\mathbf{P}_{\text{union}}$	Column size of $\mathbf{P}_{\text{comm}}$	Computation time (sec)
Best-case <i>local</i>	178	66	41.58
Best-case <i>global</i>	708	92	82.71
Worst-case <i>local</i>	184	71	38.13
Worst-case <i>global</i>	736	128	57.64

Table 6.3: EM: Column size of the projection matrix with computation time

also be noted that the results of the *local* approach are related to the cell with  $S_y$  varying from 2 mm to 2.3 mm and  $S_x$  varying from 1 mm to 1.3 mm. We recall that each design space cell has its own common projection matrix using the *local* approach. While for the *global* approach the common projection matrix can be used for the whole design space. The parameterized model is obtained by multilinear interpolation of the reduced system matrices. Fig. 6.9 compares the actual data and PROM obtained by interpolation for the spacing  $S_y = \{2.2, 2.5, 2.9\}$  mm and  $S_x = 1.3$  mm. These specific spacing values have not been used for the estimation grid. The worst case RMS error (6.18) for the *global* approach is 0.0512. It is clear that, the PROM captures the behavior of the system very accurately with passivity guaranteed by construction.



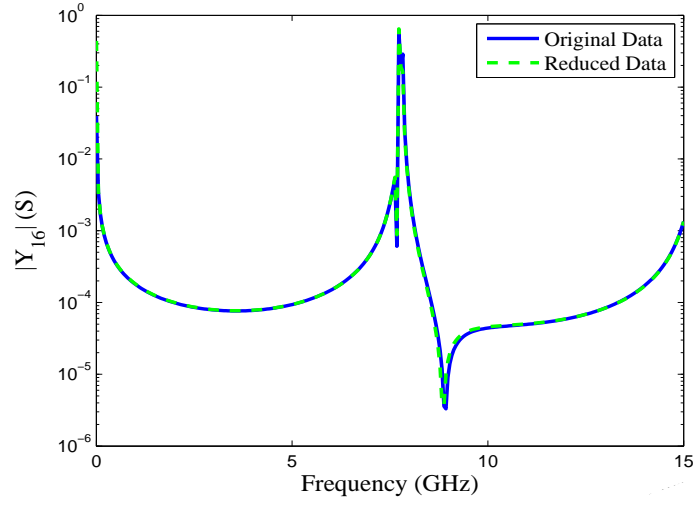


Figure 6.6: EM: Magnitude of  $\mathbf{Y}_{16}(s, S_x, S_y)$  for  $S_x = 1.2$  mm and  $S_y = 2.1$  mm using a best-case local projection.

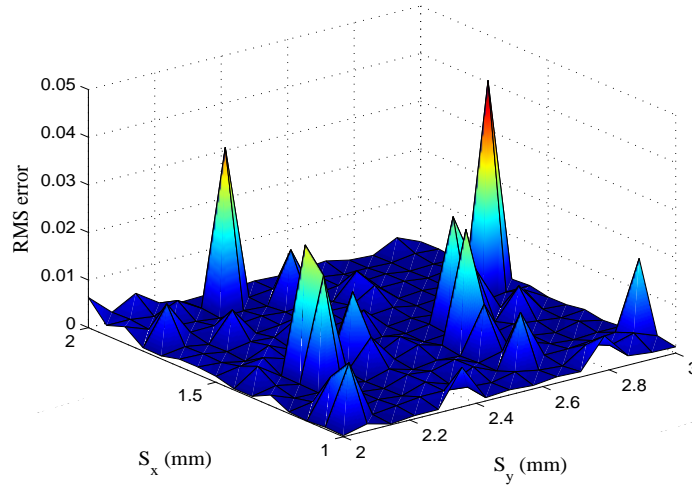


Figure 6.7: EM: RMS error using the local approach for the design space.

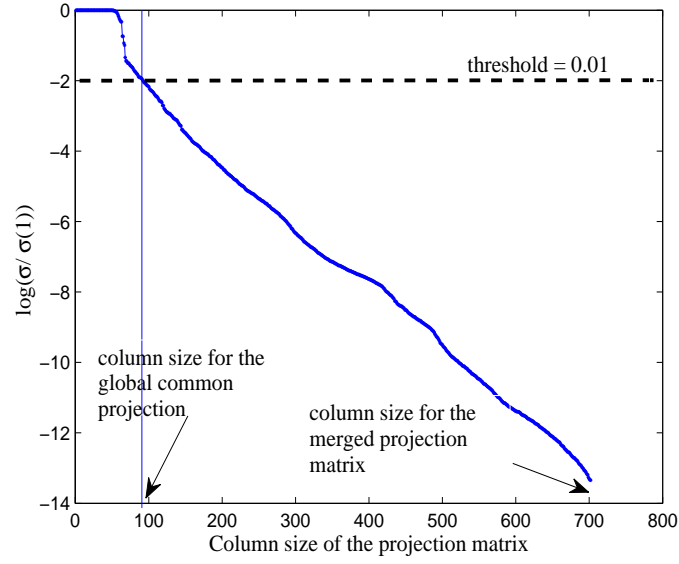


Figure 6.8: EM: Singular values of the projection matrix (best-case global approach).

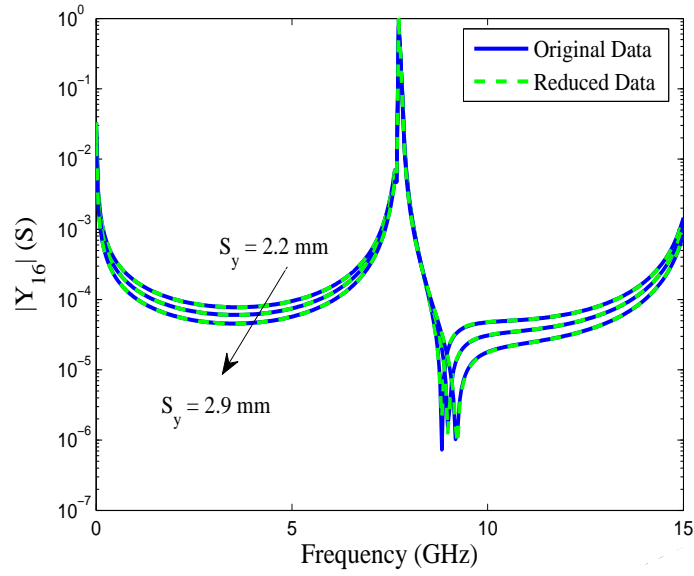


Figure 6.9: EM: Magnitude of  $\mathbf{Y}_{16}(s, S_x, S_y)$  for  $S_x = 1.3$  mm and  $S_y = \{2.2, 2.5, 2.9\}$  mm using a best-case global common projection matrix.

### 6.2.5.2 3MTL: Three coupled microstrip lines

Parameter	Min	Max
Frequency ( $freq$ )	1 kHz	4 GHz
Spacing ( $S$ )	200 $\mu\text{m}$	400 $\mu\text{m}$
Length ( $L$ )	2 cm	6 cm

Table 6.4: 3MTL: Parameters of the model

Three coupled microstrip lines are modeled [7] starting from known per-unit-length parameters. Fig.6.10 shows the cross section of the setup. The conductors

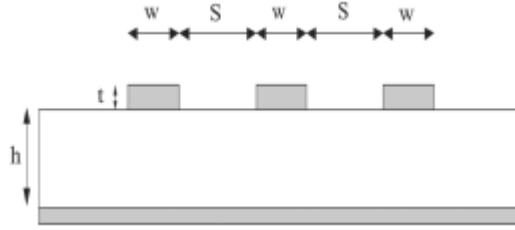


Figure 6.10: 3MTL: Cross section of three coupled microstrip line.

have width  $w = 100 \mu\text{m}$  and thickness  $t = 50 \mu\text{m}$ . The spacing  $S$  between the conductors and the length  $L$  of the lines are considered to be variable parameters in addition to frequency. Their corresponding ranges are shown in Table 6.4. The  $\mathbf{C}$ ,  $\mathbf{G}$ ,  $\mathbf{B}$ ,  $\mathbf{L}$  matrices are obtained for 5 values of  $S$  and 5 values of  $L$ . The original models are represented as in (6.19) and have an order of 10203. A  $3 \times 3$  ( $S, L$ ) estimation grid and a validation grid of  $2 \times 2$  ( $S, L$ ) samples is considered. The reduced order at the corner points of the design space is estimated by truncating the Hankel singular values, similarly to the previous example a threshold level of 0.01 is chosen.

For the *global* approach the projection matrices are computed at all the estimation points in the design space to obtain a common *global* projection matrix. Similar to the previous example, it can be seen that the size 298 for the merged projection matrix can be reduced to 81 by truncating the singular values as shown in Fig.6.11. The PROM is obtained using multilinear interpolation. Fig.6.12 plots the magnitude of  $\mathbf{Y}_{11}(s, S, L)$  for  $S = 200 \mu\text{m}$ . Fig.6.13 plots the magnitude of  $\mathbf{Y}_{11}(s, S, L)$  for a  $S = 200 \mu\text{m}$  and  $L = \{3, 5\} \text{ cm}$ . The worst case RMS error (6.18) for the *global* approach is 0.057.

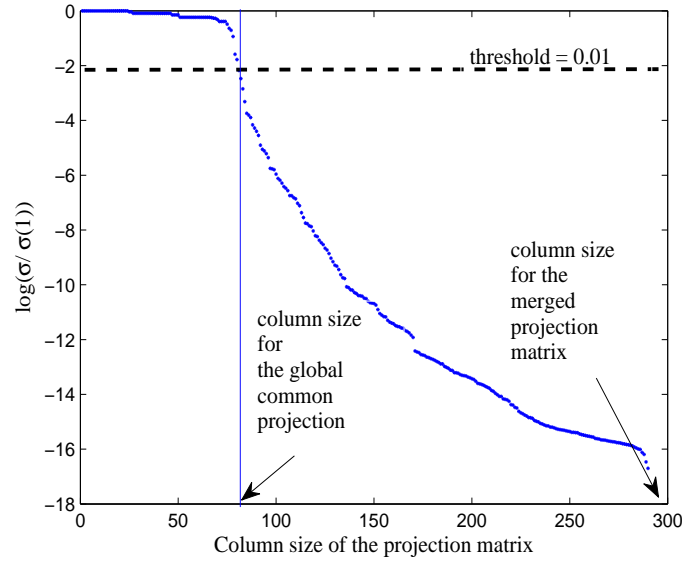


Figure 6.11: 3MTL: Singular values of the projection matrix (best-case global approach).

As explained before, for *local* projection the projection matrix is found cell by cell. For example, the cell with  $S$  varying from  $200 \mu m$  to  $297.44 \mu m$  and  $L$  varying from  $2 cm$  to  $4 cm$ , the *local* projection matrix is found by truncating the singular values of the union of the projection matrices computed at the vertices of the cell. When the common projection matrix is the union of the projection matrices computed at the vertices of the cell, then the reduced order will be 162, but with the truncation of the merged projection matrix by a threshold of 0.01 as described in Section 6.2.2, the reduced order is 57 as shown in Fig.6.14. Thus a more useful projection matrix is obtained locally for each specified cell using the novel technique.

Similarly to the previous example, Table 6.5 below summarizes the dimension of the merged and common projection matrix along with the CPU time for computing the reduced order and the common projection matrix using the different approaches. In this example, the results of the *local* approach shown in Table 6.5 are related to the cell with  $S$  varying from  $200 \mu m$  to  $297.44 \mu m$  and  $L$  varying from  $2 cm$  to  $4 cm$ .

Fig.6.15 shows the magnitude of  $\mathbf{Y}_{11}(s, S, L)$  for  $S = 246.15 \mu m$  and  $L = 3 cm$ . The PROM with *local* approach has worst-case RMS error (6.18) equal to 0.0415.

As in the previous example, the PROM is able to accurately describe the pa-

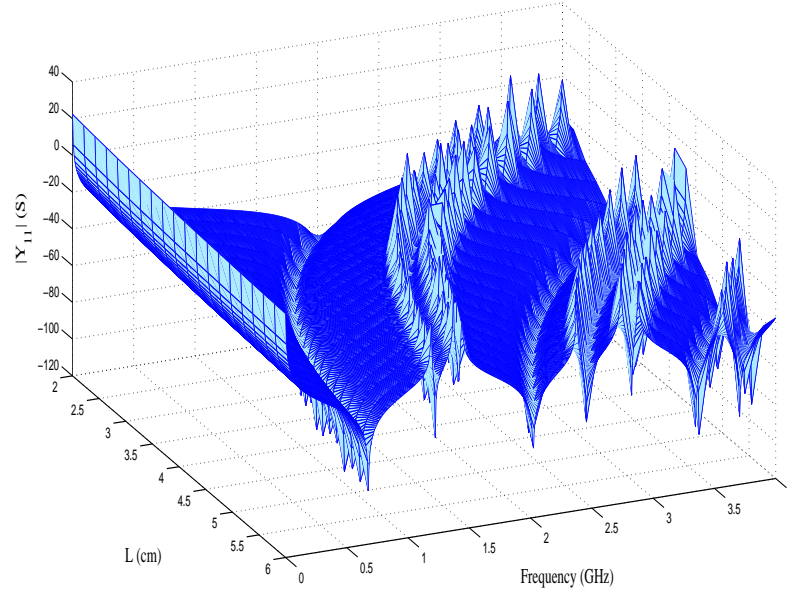


Figure 6.12: 3MTL: Magnitude of  $\mathbf{Y}_{11}(s, S, L)$  for  $S = 200 \mu\text{m}$ .

parameterized behavior of the system with a common projection matrix locally and globally. The passivity of the system is guaranteed by construction.

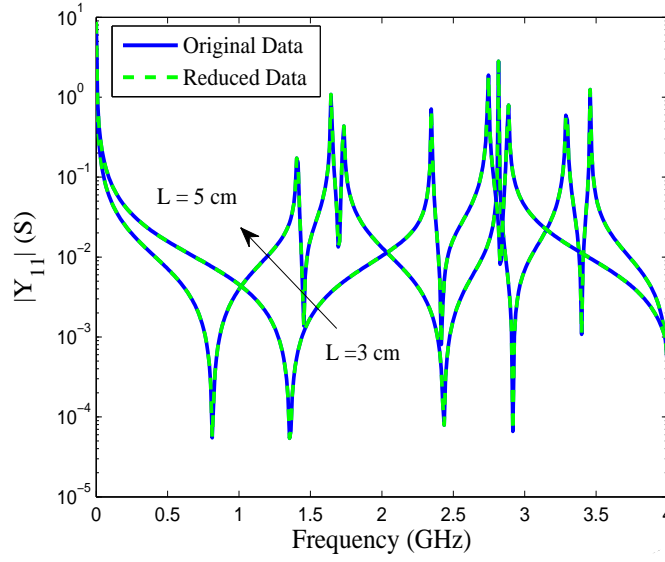


Figure 6.13: 3MTL: Magnitude of  $\mathbf{Y}_{11}(s, S, L)$  for  $S = 200 \mu\text{m}$  and  $L = \{3, 5\} \text{ cm}$  using a best-case global common projection matrix.

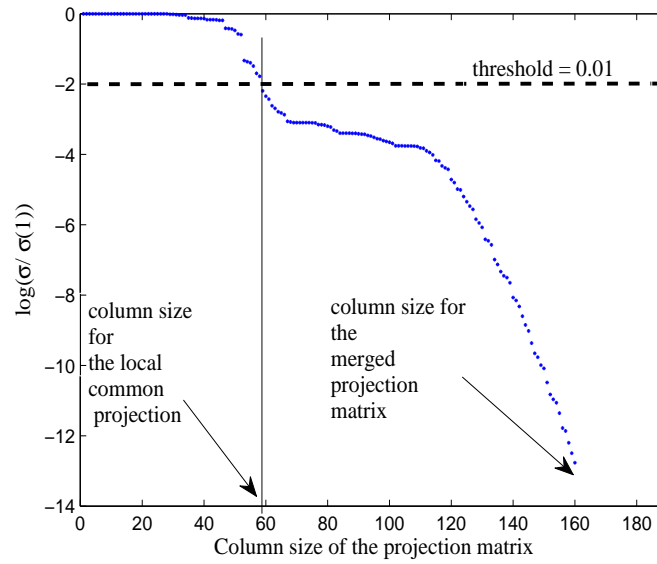
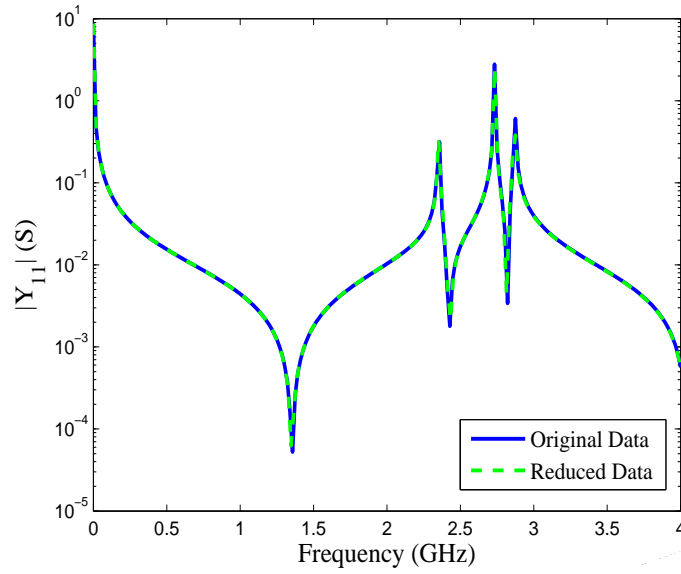


Figure 6.14: 3MTL: Singular values of the projection matrix (best-case local approach).

Approach	Column size of $\mathbf{P}_{\text{union}}$	Column size of $\mathbf{P}_{\text{comm}}$	Computation time (sec)
Best-case <i>local</i>	162	57	1502.36
Best-case <i>global</i>	298	81	3104.11
Worst-case <i>local</i>	168	62	1456.42
Worst-case <i>global</i>	378	103	3002.75

Table 6.5: 3MTL: Column of projection matrix with computation time

Figure 6.15: 3MTL: Magnitude of  $\mathbf{Y}_{11}(s, S, L)$  for  $S = 246.15 \mu\text{m}$  and  $L = 3 \text{ cm}$  using a best-case local projection.

## 6.3 Model Order Reduction of Parameterized State-Space Systems with Sequential Sampling

### 6.3.1 PMOR with Sequential Sampling

Consider a parameterized dynamical system with design parameters  $\vec{p} = (p^{(1)}, \dots, p^{(N)})$  in descriptor state-space form

$$\begin{aligned} \mathbf{E}(\vec{p}) \frac{d\mathbf{x}(t, \vec{p})}{dt} &= \mathbf{A}(\vec{p})\mathbf{x}(t, \vec{p}) + \mathbf{B}\mathbf{u}(t) \\ \mathbf{y}(t, \vec{p}) &= \mathbf{C}(\vec{p})\mathbf{x}(t, \vec{p}) + \mathbf{D}\mathbf{u}(t) \end{aligned} \quad (6.19)$$

In the sequel the parameter design space, will be denoted as  $\mathcal{P}(\vec{p})$ . The goal is to build an interpolated PMOR that approximates the large system (6.19) up to a predefined accuracy level. As a first step, a sequential sampling algorithm is used to identify a set of nodes on a multi-rectangular grid in the parameter design space  $\mathcal{P}(\vec{p})$ , henceforth called the *parameter subspace*. These nodes are located at the corner points of each grid cell and correspond to a ROM that characterizes the frequency domain behavior at a fixed point in the parameter design space. Secondly, a parameterization step is introduced to obtain a PROM that can be evaluated at every test point in the parameter design space. This parameterization is performed by picking the corner points of the corresponding cell and applying local interpolation on the state-space matrices.

Regarding the state-space equations of the system under study we assume that a fixed discretization mesh is used which is independent of the specific design parameter values [5]. The size of the system matrices as well as the numbering of the mesh nodes and mesh edges are preserved. The mesh is only locally stretched or shrunk when shape parameters are modified. The matrices  $\mathbf{B}$ ,  $\mathbf{C}$  are uniquely determined by the circuit topology and therefore remains constant, while the matrices  $\mathbf{E}$  and  $\mathbf{A}$  are functions of the design parameters. Starting from a set of models in the design space using common projection matrices, it is straightforward to prove that all the reduced system matrices in the estimation grid are in the same parameter subspace and hence can be interpolated.

#### 6.3.1.1 Sequential Sampling

The division of the parameter design space into multi-rectangular cells is implemented using a sequential sampling algorithm. Based on differences in the reduced order of each ROM, it is possible to identify the edge of the cell that corresponds to the most dynamic parameter. By selecting additional nodes at the midpoint of that edge, the parameter design space is recursively divided into 2 halves (i.e. 2 smaller subspaces). If the deviation between the original system and the PROM is too large, then the procedure is repeated. Note that this is a key difference with the



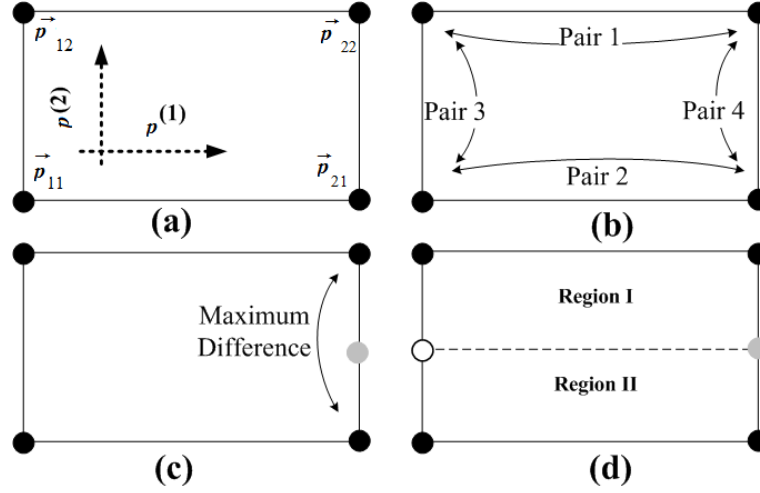


Figure 6.16: Division of the design space.

approach in [16], where the segmentation of the parameter design space is based uniquely on the difference in system responses and the division is performed at the geometric center.

As an example, consider a bivariate case with parameter vector  $\vec{p} = (p^{(1)}, p^{(2)})$  as shown in Fig. 6.16-a, where the four initial nodes are marked by  $\vec{p}_{ij} = (p_i^{(1)}, p_j^{(2)})$ ;  $i, j = 1, 2$ . Consider any corner point in the parameter subspace and estimate the reduced order at the corner point and its immediate neighbors in other words, the reduced order has to be estimated for  $N + 1$  points in the parameter subspace, as shown in Fig. 6.16-b where  $\vec{p}_{11}$  is considered and its immediate neighboring points are  $[\vec{p}_{12}, \vec{p}_{21}]$ . Next the difference between the reduced orders over each edge is computed, and the PROM is evaluated at the midpoint of the most dynamic edge. At this test node, the difference between the interpolated response of the PROM and the original model is calculated. If the deviation is too large, then the parameter subspace is further divided into two *child subspaces* along that edge and that procedure is repeated recursively, as shown in Fig. 6.16-c and Fig. 6.16-d. If the differences across the edges are the same then we can randomly select an edge. Otherwise, if the deviation is sufficiently small and all subspaces are covered, then the algorithm terminates. A flowchart is shown in Fig. 6.17.

### 6.3.2 5CM: Five Coupled Microstrip Lines

As an example, five coupled microstrips are considered ( $\epsilon_r = 9.6$ ), where the spacing  $S$  between the lines and the length  $L$  of the lines are chosen as design parameters in addition to frequency (see Fig. 6.18). Table 6.6 shows the ranges of

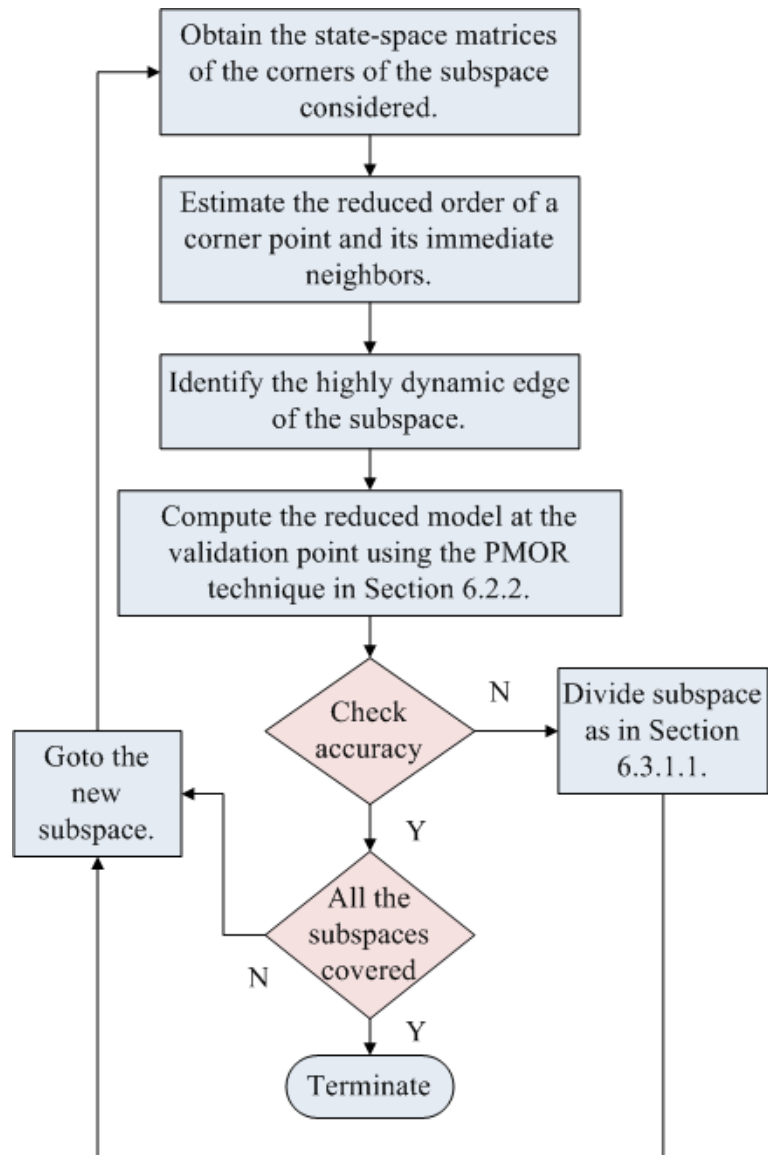


Figure 6.17: Flowchart of sequential sampling algorithm.

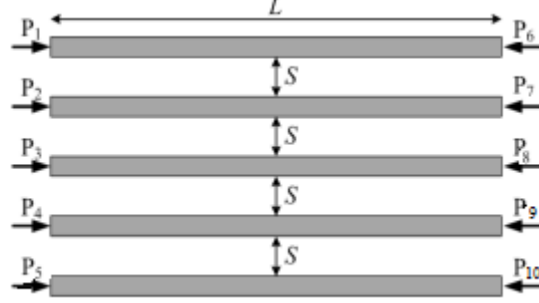


Figure 6.18: 5CM: Layout of five coupled microstrip.

Parameter	Min	Max
Frequency ( $freq$ )	0 GHz	5 GHz
Length ( $L$ )	5 mm	15 mm
Spacing ( $S$ )	0.04 mm	0.1 mm

Table 6.6: Parameters of coupled microstrips

the parameters and the number of frequency samples  $N_s$  is 120.

The order of the initial system is 1200. Here, the mean absolute error (MAE) is used as a measure to assess the accuracy of the ROM and  $-60$  dB is used as a target value. If  $P_{in}$  denotes the number of input ports and  $P_{out}$  denotes the number of output ports, then the MAE between the original frequency response  $H_{i,j}$  and the ROM  $R_{i,j}$  is calculated as follows

$$E^{\text{MAE}}(\vec{g}) = \frac{\sum_{i=1}^{P_{in}} \sum_{j=1}^{P_{out}} \sum_{k=1}^{N_s} |R_{i,j}(s_k, \vec{g}) - H_{i,j}(s_k, \vec{g})|}{P_{in} P_{out} N_s}. \quad (6.20)$$

As described in Section 6.2.1, a reduced order of 38 is estimated at the corner point of the parameter design space for  $L = 5$  mm and  $S = 0.04$  mm by truncating the Hankel singular values as shown in Fig.6.19. Similarly, the reduced order is estimated for the immediate neighbors of the considered parameter design space and is found to be 44 for  $L = 5$  mm and  $S = 0.1$  mm and 56 for  $L = 15$  mm and  $S = 0.04$ .

Additional nodes in the design space are selected by the sequential sampling algorithm (see Section 6.3.1.1) and the PROM is generated using multilinear interpolation (see Section 6.2.3). Fig.6.20 shows the final result, with as outcome 172 nodes spread in an adaptive non-uniform way. Based on the distribution of the nodes, it can be inferred that S-parameters corresponding to designs with small spacing  $S$  and large length  $L$  are changing more rapidly. As an illustration, Fig. 6.21 visualizes the magnitude  $S_{18}(L, S)$  for varying  $L$  and  $S = 0.045$  mm. Sim-

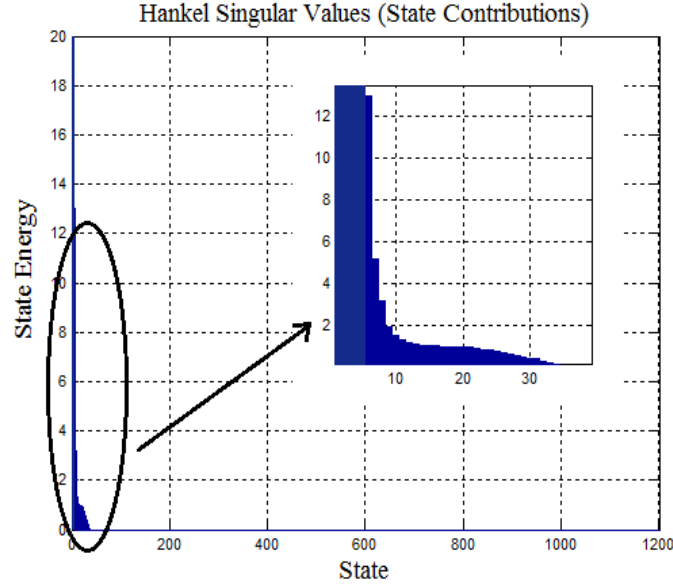


Figure 6.19: Hankel singular values of a node.

$L$ (mm)	$S$ (mm)	Uniform (dB)	Sequential (dB)
8.1	0.090	-66.04	-68.06
11.7	0.070	-56.51	-65.12
14.3	0.045	-43.91	-62.87

Table 6.7: 5CM: Comparison of Mean Absolute Error

ilarly, in Fig. 6.22 the magnitude of  $S_{1\ 10}$  is shown for varying  $S$  with  $L = 12.8$  mm. In both cases, we see that designs with a more resonant-like frequency response are effectively more densely sampled.

To validate goodness of fit of the node distribution, the result is compared to a PROM that is build using the same (slightly larger) number of nodes simulated over a classical uniform sampling (e.g., a uniform  $14 \times 14$  grid). The response of the PROMs is evaluated and compared for three validation points, marked by asterisks in Fig. 6.20.

Table 6.7 shows a comparison of the MAE over all frequencies at each validation point. It is clear that the accuracy in the sequential non-uniform case is significantly better than in the uniform case. As a final illustration it can be seen from Fig. 6.23 that the response of the reduced order model over the sequentially sampled parameter space has a better accuracy than in the uniformly sampled parameter design space case when compared to the original system.

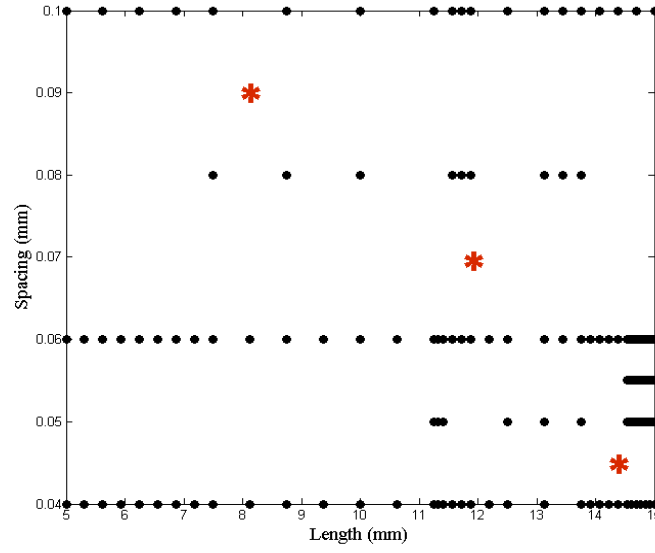


Figure 6.20: Sequentially sampled design space (validation points marked as \*)

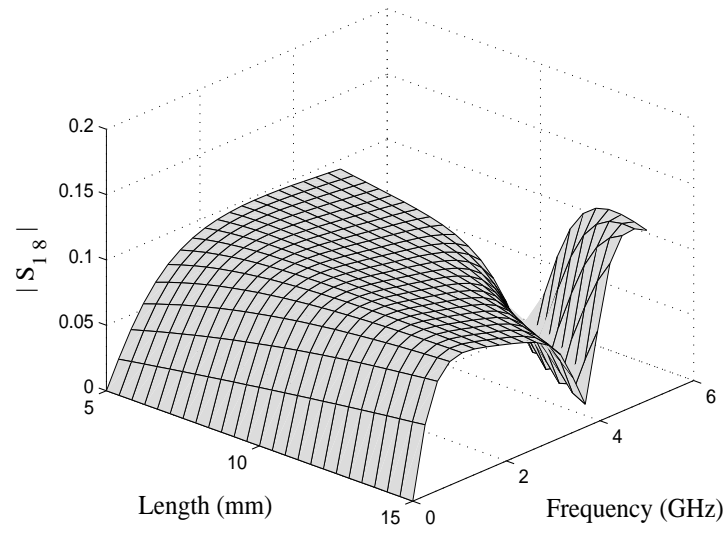


Figure 6.21: 5CM: Magnitude bivariate PMOR  $S_{18}(L, S)$  for  $S = 0.045$  mm.

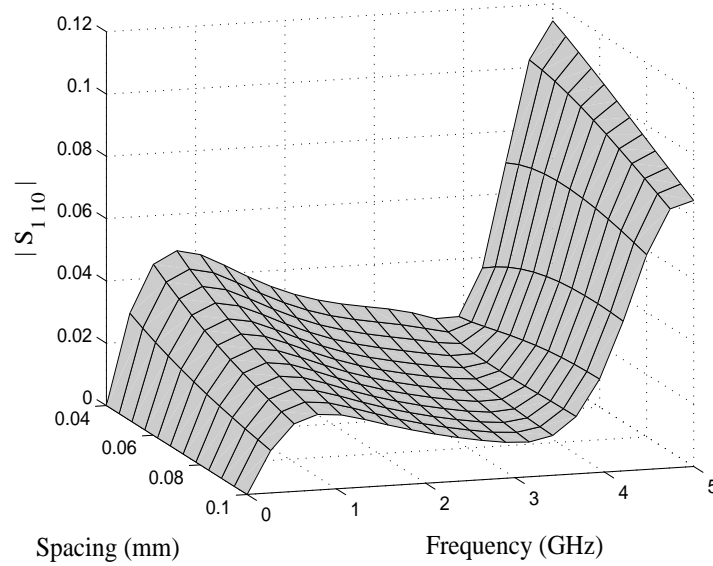


Figure 6.22: 5CM: Magnitude bivariate PROM  $S_{110}(L, S)$  for  $L = 12.8$  mm.

## 6.4 Conclusion

A novel PMOR method based on singular values and matrix interpolation has been proposed in this chapter. A fast technique using Gramians is first utilized to estimate the reduced order and then projection matrices are used to build parameterized reduced order models. The design space is divided into cells and a Krylov subspace is computed for each cell vertex model. The truncation of the singular values of the merged Krylov subspaces computed from the models at the vertices of each cell generates a common projection matrix per design space cell. The stability and passivity of the parameterized reduced order models are preserved using classical MOR methods and positive interpolation schemes. Also the importance of sequential sampling for building parameterized reduced order model has been demonstrated in this chapter. The model is obtained by combining a sequential sampling algorithm (that recursively divides the subspace by picking samples along the most dynamical edge) with a local matrix interpolation method. It is shown that an accurate PROM is obtained, while avoiding potential under-sampling or oversampling of the parameter space. The approach is illustrated with numerical results.

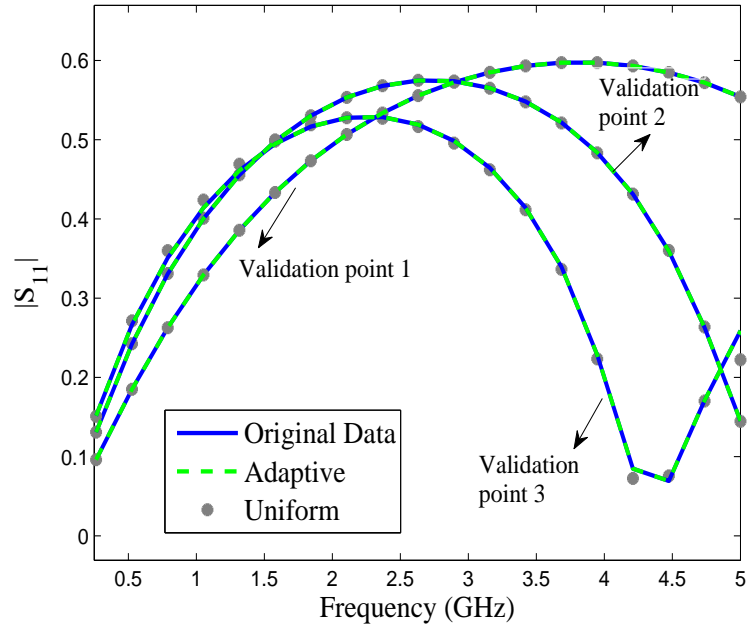


Figure 6.23: 5CM: Magnitude of  $S_{11}$  at validation points (uniform and sequential sampling).

## Acknowledgment

This work was supported by the Interuniversity Attraction Poles Programme BEST-COM initiated by the Belgian Science Policy Office and the Research Foundation Flanders (FWO).

## References

- [1] P. K. Gunupudi, R. Khazaka, M. Nakhla, T. Smy, and D. Celo. *Passive parameterized time-domain macromodels for high-speed transmission-line networks*. IEEE Transactions on Microwave Theory and Techniques, 51(12):2347 – 2354, Dec. 2003.
- [2] L. Daniel, O. C. Siong, L. Chay, K. H. Lee, and J. White. *A multiparameter moment-matching model-reduction approach for generating geometrically parameterized interconnect performance models*. IEEE Transactions on Computer-Aided Design of Integrated Circuits and Systems, 23(5):678 – 693, May 2004.
- [3] Y.-T. Li, Z. Bai, Y. Su, and X. Zeng. *Model Order Reduction of Parameterized Interconnect Networks via a Two-Directional Arnoldi Process*. IEEE Transactions on Computer-Aided Design of Integrated Circuits and Systems, 27(9):1571 – 1582, Sept. 2008.
- [4] F. Ferranti, G. Antonini, T. Dhaene, and L. Knockaert. *Guaranteed Passive Parameterized Model Order Reduction of the Partial Element Equivalent Circuit (PEEC) Method*. IEEE Transactions on Electromagnetic Compatibility, 52(4):974–984, Nov. 2010.
- [5] F. Ferranti, G. Antonini, T. Dhaene, L. Knockaert, and A. Ruehli. *Physics-Based Passivity-Preserving Parameterized Model Order Reduction for PEEC Circuit Analysis*. IEEE Transactions on Components, Packaging and Manufacturing Technology, 1(3):399 – 409, Mar. 2011.
- [6] H. Panzer, J. Mohring, R. Eid, and B. Lohmann. *Parametric Model Order Reduction by Matrix Interpolation*. Automatisierungstechnik, pages 475–484, Aug. 2010.
- [7] L. Knockaert and D. De Zutter. *Laguerre-SVD reduced-order modeling*. IEEE Transactions on Microwave Theory and Techniques, 48(9):1469 – 1475, Sept. 2000.
- [8] D. Deschrijver and T. Dhaene. *Stability and Passivity Enforcement of Parametric Macromodels in Time and Frequency Domain*. IEEE Transactions on Microwave Theory and Techniques, 56(11):2435 – 2441, Nov. 2008.
- [9] S. Peik, R. Mansour, and Y. Chow. *Multidimensional Cauchy method and adaptive sampling for an accurate microwave circuit modeling*. IEEE Transactions on Microwave Theory and Techniques, 46(12):2364 – 2371, Dec. 1998.



- [10] R. Lehmensiek and P. Meyer. *Creating accurate multivariate rational interpolation models of microwave circuits by using efficient adaptive sampling to minimize the number of computational electromagnetic analyses*. IEEE Transactions on Microwave Theory and Techniques, 49(8):1419–1430, Aug. 2001.
- [11] D. Deschrijver, K. Crombecq, H. Nguyen, and T. Dhaene. *Adaptive Sampling Algorithm for Macromodeling of Parameterized S-Parameter Responses*. IEEE Transactions on Microwave Theory and Techniques, 59(1):39–45, Jan. 2011.
- [12] D. Deschrijver, F. Vanhee, D. Pissort, and T. Dhaene. *Automated Near-Field Scanning Algorithm for the EMC Analysis of Electronic Devices*. IEEE Transactions on Electromagnetic Compatibility, 54(3):502–510, June 2012.
- [13] K. Crombecq, E. Laermans, and T. Dhaene. *Efficient space-filling and non-collapsing sequential design strategies for simulation-based modeling*. European Journal of Operational Research, 214(3):683–696, Nov. 2011.
- [14] K. Crombecq, D. Gorissen, D. Deschrijver, and T. Dhaene. *A Novel Hybrid Sequential Design Strategy for Global Surrogate Modeling of Computer Experiments*. SIAM Journal on Scientific Computing, 33(4):1948–1974, Aug. 2011.
- [15] S. Aerts, D. Deschrijver, W. Joseph, L. Verloock, F. Goeminne, L. Martens, and T. Dhaene. *Exposure assessment of mobile phone base station radiation in an outdoor environment using sequential surrogate modeling*. Bioelectromagnetics, 34(4):300–311, 2013.
- [16] K. Chemmangat, F. Ferranti, T. Dhaene, and L. Knockaert. *Tree-based sequential sampling algorithm for scalable macromodeling of high-speed systems*. 2012 IEEE 16th Workshop on Signal and Power Integrity, pages 49–52, May 2012.
- [17] D. Lewis. *Device model approximation using 2N trees*. IEEE Transactions on Computer-Aided Design of Integrated Circuits and Systems, 9(1):30–38, Jan. 1990.
- [18] G. P. Fang, D. C. Yeh, D. Zweidinger, L. A. Arledge, and V. Gupta. *Fast, accurate MOS table model for circuit simulation using an unstructured grid and preserving monotonicity*. In Proceedings of the 2005 Asia and South Pacific Design Automation Conference, ASP-DAC '05, pages 1102–1106, New York, NY, USA, 2005. ACM.

- [19] S. Gugercin, C. D. Sorensen, and C. A. Antoulas. *A modified Low-Rank Smith Method for Large Scale Lyapunov Equations*. Numerical Algorithms, 32(1):27–55, May 2001.
- [20] N. Wong, V. Balakrishnan, C. K. Koh, and T. S. Ng. *Two Algorithms for Fast and Accurate Passivity-Preserving Model Order Reduction*. IEEE Transactions on Computer-Aided Design of Integrated Circuits and Systems, 25(10):2062–2075, Oct. 2006.
- [21] S. Gugercin and J.-R. Li. *Smith-type methods for balanced truncation of large systems*. Proceedings of a Workshop held in Oberwolfach, Germany, Oct. 2003.
- [22] Q. Su. *Algorithms for model reduction of large scale RLC systems*. PhD thesis, West Lafayette, IN, USA, 2002.
- [23] Q. Su, V. Balakrishnan, and C.-K. Koh. *Efficient Approximate Balanced Truncation of General Large-Scale RLC Systems via Krylov Methods*. Proceedings of the 2002 Asia and South Pacific Design Automation Conference, pages 311–316, 2002.
- [24] K. Glover. *All optimal Hankel-norm approximations of linear multivariable systems and their  $L^\infty$ -error bounds*. International Journal of Control, 39(6):1115–1193, 1984.
- [25] J. Li. *Model reduction of large systems via low rank system Gramians*. PhD thesis, Cambridge, MA, 2000.
- [26] J.-R. Li and J. White. *Low-Rank Solution of Lyapunov Equations*. SIAM, 24(1):260–280, 2002.
- [27] E. W. Cheney. *Multivariate approximation theory : Selected topics*. CBMS NSF Regional Conference Series in Applied Mathematics, 51, Philadelphia, PA : SIAM, Dec. 1986.
- [28] D. F. Watson. *Computing the  $n$ -dimensional Delaunay tessellation with application to Voronoi polytopes*. The Computer Journal, 24(2):167–172, Feb. 1981.
- [29] A. Weiser and S. E. Zarantonello. *A Note on Piecewise Linear and Multilinear Table Interpolation in Many Dimensions*. Mathematics of Computation, 50(181):189–196, Jan. 1988.
- [30] R. Rohrer and H. Nosrati. *Passivity considerations in stability studies of numerical integration algorithms*. International Journal of Control, 28(9):857–866, Sept. 1981.

- [31] L. Weinberg. *Network Analysis and Synthesis*. McGraw-Hill Book Company, New York, 1962.
- [32] E. A. Guillemin. *Synthesis of Passive Networks*. Wiley, New York, 1957.
- [33] R. W. Freund. *Krylov-subspace methods for reduced-order modeling in circuit simulation*. J. Comput. Appl. Math., 123:395–421, Nov. 2000.
- [34] L. Knockaert, T. Dhaene, F. Ferranti, and D. D. Zutter. *Model order reduction with preservation of passivity, non-expansivity and Markov moments*. Systems & Control Letters, 60(1):53–61, Jan. 2011.
- [35] J. Phillips, L. Daniel, and L. Silveira. *Guaranteed passive balancing transformations for model order reduction*. IEEE Transactions on Computer-Aided Design of Integrated Circuits and Systems, 22(8):1027 – 1041, Aug. 2003.
- [36] *MATLAB Users Guide*. The MathWorks, Inc., Natick, 2009.



# 7

## Matrix Interpolation based Parametric Model Order Reduction for Multiconductor Transmission Lines with Delays

Based on the publication:

**Elizabeth Rita Samuel, Luc Knockaert, Tom Dhaene,**  
**“Matrix Interpolation based Parametric Model Order Reduction for**  
**Multiconductor Transmission Lines with Delays”, accepted in IEEE**  
**Transactions on Circuits and SystemsII: Express briefs, 2014.**

\*\*\*

*In this chapter the parameterized model order reduction (PMOR) technique based on the matrix interpolation as described in the previous chapter is extended to multiconductor transmission lines with delays having design parameter variations. As mentioned in the previous chapters, matrix interpolation overcomes the oversize problem caused by input-output system level interpolation based parameterized macromodels. The reduced state-space matrices are obtained using a higher-order Krylov subspace based MOR technique which is more efficient in comparison to the Gramian based parameterized modeling where the projection matrix is computed using a Cholesky factorization. The design space is divided*

*into cells and then the Krylov subspaces computed for each cell is merged and then truncated using an adaptive truncation algorithm with respect to their singular values to obtain a compact common projection matrix. The resulting reduced order state-space matrices and the delays are interpolated using positive interpolation schemes making it computationally cheap and accurate for repeated system evaluations under different design parameter settings. The proposed technique is successfully applied to RLC and multiconductor transmission line circuits with delays.*

## 7.1 Introduction

Circuit analysis using electromagnetic (EM) simulation methods [1] can generate very large systems of equations. Time delays must be included during the process of modeling, when the geometric dimensions of the lines become electrically large and the frequency content of signal waveform increases [2, 3]. In such cases, comprehensive model order reduction (MOR) techniques are crucial to reduce the complexity of large scale models and the computational cost of the simulations, while retaining the important physical features of the original system.

Time-delay systems (TDSs) in the Laplace domain contain transfer functions with elements of the form  $e^{-s\tau}$ , where  $\tau$  corresponds to the time delay present in the circuit. Several techniques of MOR for TDSs have been presented during recent years as briefed in Chapter 3, and any of the approaches based on Krylov-subspace algorithms [3–7] can be used as non-PMOR technique.

The system response of TDSs can be affected by design parameters, other than frequency or time, such as geometric features. Therefore, it is important to predict the response of the circuit as a function of general design parameters, such as geometric and physical features. PMOR methods are well suited to efficiently perform design activities.

A number of PMOR methods have been developed in recent years for TDSs based on input-output interpolation [8–10]. In [8], the approach is based on a multi-order Arnoldi algorithm which is used to implicitly calculate the moments with respect to frequency and the design parameters, as well as the cross-moments. Also in [9] an input-output based interpolation technique is presented with scaling and frequency shifting, which enhances the modeling capabilities. These PMOR methods use input-output system level interpolation which are proved to be robust and accurate, but the order of the parameterized macromodels may suffer from oversize due to the nature of the input-output system level interpolation. A Gramian-based PMOR for TDS is presented in [10] where an affine model is used to represent the parameterized behavior, but the technique is computationally expensive as Cholesky factorization is required for the computation of the projection matrix.

This chapter, proposes a matrix interpolated PMOR method for multiconductor transmission lines (MTLs) with delays. The proposed technique approximates the delays using an expansion series and uses higher-order Krylov subspace based MOR as described in Chapter 3. Then the reduced state-space systems are interpolated as in [11]. An adaptive truncation for the singular values of the common projection matrix is presented in this chapter in comparison to the truncation described in Section 6.2.2. As the approach is based on matrix interpolation it overcomes the oversize problem in input-output system level interpolation and the technique uses higher-order Krylov MOR to compute the reduced order models (ROMs) for TDS [6, 7]. This is more efficient in comparison to the augmented MOR technique proposed for PMOR TDS in [9], as the augmentation generates an equivalent first-order system which is larger than the size of the original model, and the Gramian based MOR for PMOR of TDS [10], as the computation of Gramians are expensive due to Cholesky factorization. The proposed approach computes a set of reduced system matrices in a common subspace using higher-order Krylov MOR and interpolates these ROM and the delays in order to generate PMOR for TDSs. The design space is first divided into cells and for each vertex model of the cell a Krylov subspace is computed. The Krylov subspaces are then merged and compacted by truncating with respect to their singular values to generate a common projection matrix. Next, the reduced system matrices of the delayed system are interpolated using positive interpolation for PMOR. The delays of the MTLs are also interpolated in a similar manner to obtain the parameterized model, as the delays are proportional to the length of the transmission lines (TLs), when modeled using the Method of Characteristics (MoC) [3].

## 7.2 Overview of Model Order Reduction for TDSs

A TDS of degree  $n$  with  $p$  ports having  $k$  delays  $\tau_j$ , present in both the state and descriptor matrices, can be represented in general delayed state space form as:

$$\begin{aligned} \sum_{j=0}^k \mathbf{E}_j \dot{x}(t - \tau_j) &= \sum_{j=0}^k \mathbf{A}_j x(t - \tau_j) + \mathbf{B}u(t) \\ y(t) &= \mathbf{C}x(t). \end{aligned} \quad (7.1)$$

Here,  $x(t) \in \mathcal{R}^n$  is the state vector;  $u(t) \in \mathcal{R}^p$  is the control input with  $u(t) = 0$  for  $t < 0$ ;  $y(t) \in \mathcal{R}^p$  is the output.  $\mathbf{A}_j, \mathbf{E}_j, \mathbf{B}, \mathbf{C}$  are constant sparse matrices with appropriate dimensions. The time delay  $\tau_0 = 0$  and  $\tau_j > 0, j = 1, 2, \dots, k$ . From (7.1) we obtain the transfer function as:

$$\mathbf{H}(s) = \mathbf{C} \left( s \sum_{j=0}^k \mathbf{E}_j e^{-s\tau_j} - \sum_{j=0}^k \mathbf{A}_j e^{-s\tau_j} \right)^{-1} \mathbf{B}. \quad (7.2)$$

In order to calculate the moments, the exponential terms of (7.2) are approximated using a Taylor series [6] or Laguerre expansion [7] upto an order  $r$ . On substituting the delay expansion in (7.2), a  $r$ -th order transfer function is obtained of the form:

$$\mathbf{H}(s) = \mathbf{C} (\sigma_r s^r + \sigma_{r-1} s^{r-1} + \dots + \sigma_1 s + \sigma_0)^{-1} \mathbf{B}. \quad (7.3)$$

The  $r$ -th order Krylov subspace is defined as in [12]

$$\mathcal{K}_q(\mathbf{G}_1, \mathbf{G}_2, \dots, \mathbf{G}_r, \mathbf{L}) = \text{colspan} [P_0, P_1, \dots, P_{q-1}] \quad (7.4)$$

where  $\mathbf{L} = \sigma_0^{-1} \mathbf{B}$  and  $\mathbf{G}_i = \sigma_0^{-1} \sigma_i$  for  $i = 1, 2, \dots, r$ , and

$$\begin{aligned} P_0 &= \mathbf{L}; \quad P_i = 0 \quad \text{for } i < 0 \\ P_j &= \mathbf{G}_1 P_{j-1} + \dots + \mathbf{G}_r P_{j-r}, \quad j = 1, \dots, q-1 \end{aligned} \quad (7.5)$$

where  $q$  is the reduced order that is estimated for the model.

This subspace is a generalization of Krylov subspaces for higher-order systems and eliminates the standard approach to model order reduction of large-scale higher-order linear dynamical systems, which is to rewrite the system as an equivalent first-order system and then employ Krylov-subspace techniques for model order reduction of first-order systems. Note that, to match the moments of an  $r$ -th order model, the matrix  $\sigma_0$  should be invertible.

The column-orthogonal projection matrix  $\mathbf{Q}$  for congruence transformation is found by means of the economy-size singular value decomposition (SVD):

$$\mathbf{U} \Sigma \mathbf{V}' = \text{SVD}(\mathcal{K}_q(\mathbf{G}_1, \mathbf{G}_2, \dots, \mathbf{G}_r, \mathbf{L}), 0). \quad (7.6)$$

In other words  $\mathbf{Q}$  is equal to the left SVD factor of dimension  $n \times q$  associated with the  $(r+1)^{\text{th}}$  Krylov subspace.

The reduced order state-space matrices are then obtained by the following classical congruence transformations:

$$\begin{aligned} \mathbf{A}_{j_r} &= \mathbf{Q}' \mathbf{A}_j \mathbf{Q}, \quad \mathbf{E}_{j_r} = \mathbf{Q}' \mathbf{E}_j \mathbf{Q}, \\ \mathbf{B}_r &= \mathbf{Q}' \mathbf{B}, \quad \mathbf{C}_r = \mathbf{C} \mathbf{Q}. \end{aligned} \quad (7.7)$$

### 7.3 Parameterized Model Order Reduction

Considering the effect of  $N$  design parameters  $\vec{p} = (p^{(1)}, \dots, p^{(N)})$ , the descriptor state-space form (7.1) becomes:

$$\begin{aligned} \mathbf{E}(\vec{p}, \tau) \dot{\mathbf{x}}(t, \vec{p}) &= \mathbf{A}(\vec{p}, \tau) \mathbf{x}(t, \vec{p}) + \mathbf{B}(\vec{p}) \mathbf{u}(t) \\ \mathbf{y}(t, \vec{p}) &= \mathbf{C}(\vec{p}) \mathbf{x}(t, \vec{p}). \end{aligned} \quad (7.8)$$



Two design space grids are used in the modeling process, an estimation grid and a validation grid [9]. The estimation grid is used for the construction of the PMOR while the validation grid is used to study the accuracy of the parameterized model at the points that were not used during construction. Once the design space is sampled, the reduced order  $q$  has to be estimated for the samples on the estimation grid that is used for the modeling of the PMOR. For this, we adopt the double-strategy approach of [11]. The reduced order is first estimated at the corner points of the design space using a bottom-up approach or from the Hankel singular values (HSV), and afterwards any of these two strategies can be followed for the remaining samples in the estimation grid. This yields:

1. *worst-case reduced order*: the highest estimated reduced order at the corner points is extended over the entire design space. This approach can guarantee an accurate reduction over the design space.
2. *best-case reduced order*: the lowest estimated reduced order is extended over the design space. This approach can guarantee more compact models with respect to the worst-case, but the reduced order may be increased for some design space regions by a bottom-up approach to guarantee the desired accuracy.

From a practical view point for better computation and accuracy it is advisable to choose the *worst-case reduced order* strategy as the highest reduced order is used for the entire design space and the reduced order need not be computed for each sample point in the design space as in the case for *best-case reduced order*.

### 7.3.1 Common projection matrix computation

For each point in the estimation grid, a higher-order Krylov-based MOR method for TDSs is applied to obtain a set of projection matrices. All the projection matrices have the same dimension in the worst-case reduced order scenario, while they may have different dimensions for the best-case reduced order scenario. Each design space cell has  $M$  vertices and for every cell the projection matrices at the vertices are merged by column stacking.

$$\mathbf{Q}_{union} = [\mathbf{Q}_1, \mathbf{Q}_2, \dots, \mathbf{Q}_M]. \quad (7.9)$$

Next, the economy-size  $SVD$  is computed for the merged projection matrices

$$\mathbf{U}\Sigma\mathbf{V}' = SVD(\mathbf{Q}_{union}, 0). \quad (7.10)$$

A common reduced order for a cell is defined based on the first  $q_{comm}$  significant singular values of  $\mathbf{Q}_{union}$  [11]. Thus a common projection matrix  $\mathbf{Q}_{comm}$  is obtained

$$\mathbf{Q}_{comm} = \mathbf{U}(:, 1 : q_{comm}). \quad (7.11)$$

*Adaptive singular values truncation:* In Chapter 3 the value of the threshold is set on a trial and error base for a desired level of accuracy and compactness for the PMOR. On truncating the singular values an approximated representation  $\hat{Q}_{union}$  of (7.9) is obtained, and can be noted that the approximation error  $\Delta$  is dependent on the truncation i.e.,

$$\begin{aligned}\Delta &= \|Q_{union} - \hat{Q}_{union}\|_2, \\ \Delta &= \left\| \sum_{i=1}^n U_i \Sigma_i V'_i - \sum_{i=1}^{q_{comm}} U_i \Sigma_i V'_i \right\|_2, \\ \Delta &= \left\| \sum_{i=q_{comm}+1}^n U_i \Sigma_i V'_i \right\|_2.\end{aligned}\tag{7.12}$$

which can be written as,

$$\Delta = \sum_{i=q_{comm}+1}^n d\Sigma_i^2.\tag{7.13}$$

where,  $d\Sigma$  are the diagonal elements of  $\Sigma$ . The adaptive algorithm for truncating the singular values of the common projection matrix  $\mathbf{Q}_{union}$  is given in algorithm 7.1.

**Data:**  $d\Sigma = \text{diag}(\Sigma)$  from (7.10) and threshold

**Result:**  $q_{comm}$  for (7.11)

$ds = \text{length}(d\Sigma);$

$q_{comm} = ds;$

$\Delta = 0;$

**while**  $\Delta \leq \text{threshold}$  **do**

$\Delta = \Delta + d\Sigma(q_{comm})^2;$

$q_{comm} = q_{comm} - 1;$

**end**

*algorithm 7.1: Truncation of the singular values for  $Q_{union}$*

For this chapter a threshold equal to 0.01 was considered to produce accurate ROMs. Then, with  $\mathbf{Q}_{comm}$  the common projection matrix with dimension  $n \times q_{comm}$ , the congruence transformations (7.7) are performed to obtain the ROMs for the design space considered.

### 7.3.2 Multivariate Interpolation

After the computation of the reduced matrices, they are interpolated to build a PMOR. Any interpolation scheme in the class of positive interpolation operators

[9] can be used, e.g., multilinear and simplicial methods [13]. Here we consider multilinear interpolation, where each interpolated matrix  $\mathbf{T}(p^{(1)}, \dots, p^{(N)})$  is

$$\mathbf{T}(p^{(1)}, \dots, p^{(N)}) = \sum_{k_1=1}^{K_1} \cdots \sum_{k_N=1}^{K_N} \mathbf{T}_{(p_{k_1}^{(1)}, \dots, p_{k_N}^{(N)})} l_{k_1}(p^{(1)}) \cdots l_{k_N}(p^{(N)}). \quad (7.14)$$

and  $K_1$  is the number of estimation points and the interpolation kernel  $l_{k_i}(p^i)$  satisfies the following constraints

$$\begin{aligned} 0 &\leq l_{k_i}(p^{(i)}) \leq 1, \\ l_{k_i}(p^{(i)}) &= \delta_{k_i, i} \\ \sum_{i=1}^N l_{k_i}(p^{(i)}) &= 1. \end{aligned} \quad (7.15)$$

For MTLs consisting of lumped RLC components and lossless transmission line (TLs) components, the MoC [3] technique is used to model the lossless TLs. The delay for the  $k$ -th transmission line in MoC is the  $k$ -th eigenvalue of  $d\sqrt{(C_{pul}L_{pul})}$  ( $L_{pul}$  and  $C_{pul}$  are the per-unit-length (P.U.L.) parameter for the inductance and capacitance respectively and  $d$  denotes the length of the TLs). The  $L_{pul}$  and  $C_{pul}$  are symmetric and positive definite. Thus, as the delays are varying linearly with respect to  $d$  of the TLs, we can obtain a good parameterized reduced order delay model by interpolating all the delays using positive interpolating operators.

**Data:** Reduced order for  $M$  samples in the estimation grid.  
**Result:** Parameterized ROM  
 $Q_{union} = [ \quad ]$ ;  
**for**  $i \leftarrow 1$  **to**  $M$  **do**  
     $Q_i$ ;  
     $Q_{union} = [Q_{union} \quad Q_i]$ ;  
**end**  
 $\mathbf{U}\Sigma\mathbf{V}' = SVD(\mathbf{Q}_{union}, 0)$  (7.10);  
 $Q_{comm}$  using Algorithm 1 (Table 7.1);  
Perform congruence transformation to obtain the ROM of the TDSs ;  
Matrix interpolate the ROM and  $\tau$  to obtain the PMOR.  
Validate the PMOR with the validation grid.

algorithm 7.2: Parameterized Model Order Reduction Algorithm

It should be noted that the interpolation kernel functions of these methods only depend on the design space grid points and their computation does not require the prior solution of a linear system to impose an interpolatory constraint. The algorithmic steps of the proposed PMOR technique for TDSs is given in algorithm 7.2.

### 7.3.3 Complexity

Concerning the complexity of the proposed PMOR technique, the most expensive step is related to the computation of the higher-order Krylov subspaces for the estimation grid. It has a complexity of  $O(4n^2q)$  where  $q$  is the reduced order estimated for the model. But it can be seen that the proposed technique is much more efficient than the Gramian based PMOR for TDS [10] which has a complexity of  $O(n^3)$ . Then we have the computation of the singular values for the common projection matrix which uses an economy-size *SVD* to improve the computation. After obtaining the common projection matrix, congruence transformation is performed which has a complexity equivalent to that of matrix multiplication. Finally, the complexity of the last step depends on the selected interpolation scheme. Even though the most expensive step in the proposed PMOR technique is the MOR step the PMOR makes it more efficient for repeated design evaluations under different parameter settings in comparison to the conventional analysis techniques which requires the solution of partial differential equations [2]. The complexity of the proposed PMOR increases with the number of design parameters since the number of points on the estimation grid required for modeling increases and thereby increase the dimension of the column stacked projection matrix  $\mathbf{Q}_{union}$ , then the *SVD* would become expensive. In order to make the algorithm more efficient it is advised to perform adaptive sampling [14] of the design space and when the number of parameters is more than 5 then a dimension reduction technique [15] can be performed.

## 7.4 Numerical Examples

A distributed system as explained in [8] is used to illustrate the efficiency of the proposed technique as shown in Fig. 7.1. The RLC network is modeled using the

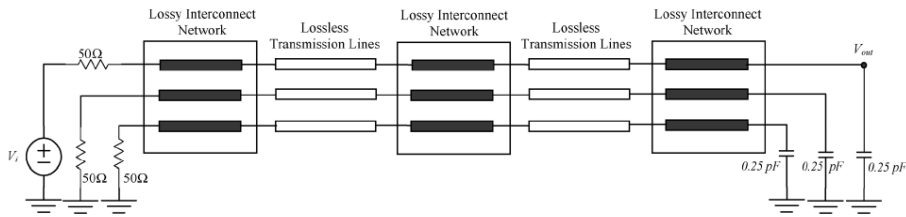


Figure 7.1: Schematic of RLC network including delay elements [8].

conventional lumped technique [2] and the lossless TLs which cause signal propagation delays, is modeled using MoC. The general form of the modified nodal analysis (MNA) matrices using the MoC and lumped elements is described in [3].

*Error criteria:* The weighted RMS error between the original frequency response  $H_{ij}$  and the reduced order model  $H_{r,(ij)}$  is defined as:

$$Err = \sqrt{\frac{\sum_{k=1}^{K_s} \sum_{i=1}^{P_{in}} \sum_{j=1}^{P_{out}} \frac{|H_{r,(ij)}(s_k) - H_{(ij)}(s_k)|^2}{W_{(ij)}(s_k)}}{P_{in} P_{out} K_s}} \quad (7.16)$$

Here  $K_s$ ,  $P_{in}$  and  $P_{out}$  are the number of frequency samples, input and output ports of the system, respectively. To illustrate the efficiency of the proposed PMOR technique, it is compared with the Gramian-based PMOR [10] which is also based on state-space interpolation.

#### 7.4.1 CASE I: Variation in Length of the lossless TLs

A TDS of order 2115 is constructed using a 3 port linear interconnected network connected with lossless 3 conductor TLs. In this case the total length  $d$  is varied for the range  $[1 \text{ cm} - 1.5 \text{ cm}]$  of the TLs for a frequency range of  $[1 \text{ kHz} - 4 \text{ GHz}]$ .

The state-space matrices is computed for 5 uniformly spaced values of  $d$ , for which the estimation points are  $d = \{1, 1.167, 1.33, 1.5\} \text{ cm}$  and the validation points are  $d = \{1.083, 1.25, 1.42\} \text{ cm}$ . We opt for the *best-case scenario* and the higher-order Krylov subspaces are computed for the estimation points as described in Section 7.3. Then a common projection matrix of dimension 360 is computed for the entire design space as described in Algorithm 1. The singular values of the merged Krylov subspaces is then truncated using Algorithm 2 to obtain a compact common projection matrix of size 148. Fig.7.2 and Fig.7.3 plots the magnitude and phase of input admittance parameter  $Y_{11}(s, d)$  respectively for  $d = \{1.083, 1.25, 1.42\} \text{ cm}$ . As mentioned in Section 7.3.3, the most expensive step in the PMOR technique is the MOR and as the number of estimation samples increases the computation becomes more expensive. But once an accurate PMOR is obtained, it becomes faster to predict the behavior of the system for different parameter ranges. The frequency response time for the original model is 277s and that for the ROM is 6.819s, obtaining about 39 times speed up.

#### 7.4.2 CASE II: Variation in Length of the TLs and P.U.L. parameters

For this case a TDS of order 9307 is constructed using a 4 port linear interconnected network connected with 40 lossless 4 conductor TLs. The total length  $d$  and the P.U.L. parameters of the TLs are varied. The dependencies of P.U.L. parameters of the distributed network on temperature  $T$  is modeled using a first-order relation. The parameters  $d$  varies from  $[1.5 \text{ cm} - 2 \text{ cm}]$  and  $T$  from  $[-20^\circ\text{C} - 60^\circ\text{C}]$  for a frequency range of  $[1 \text{ kHz} - 6 \text{ GHz}]$ . The state-space matrices with delays (as

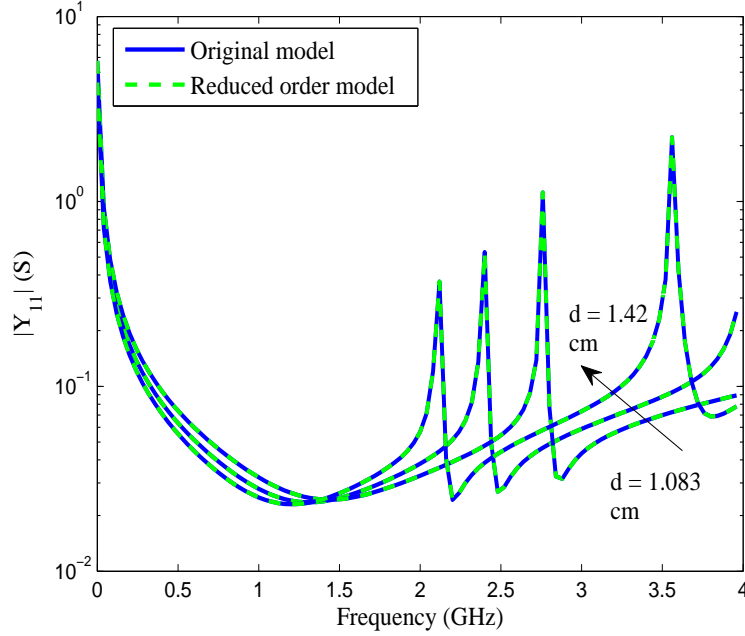


Figure 7.2: Magnitude of input admittance parameter  $Y_{11}(s, d)$  for  $d = \{1.083, 1.25, 1.42\}$  cm.

in (7.8)) are computed over an uniform grid of  $9 \times 9$  ( $d, T$ ). A  $5 \times 5$  ( $d, T$ ) estimation grid,  $d = \{1.5, 1.625, 1.75, 1.875, 2\}$  cm and  $T = \{-20, 0, 20, 40, 60\}^\circ\text{C}$  is considered and a validation grid of  $4 \times 4$  ( $d, T$ ),  $d = \{1.563, 1.687, 1.813, 1.937\}$  cm and  $T = \{-10, 10, 30, 50\}^\circ\text{C}$  is considered. For this case the *worst-case scenario* is used and the highest reduced order estimated is 252 for the models. The higher-order Krylov subspaces are computed over the estimation grid by means of the algorithm described in Section 7.3. Similar to the previous case by truncating the singular values of the merged projection matrix, a common projection matrix of size 324 is obtained. Fig.7.4 plots the PMOR for the magnitude of the transfer admittance parameter  $Y_{13}$  for  $T = 30^\circ\text{C}$ . The weighted RMS error (7.16) of the ROM with respect to the original model is 0.037. The frequency response time for the original model is 2967.1s and that for the ROM is 21.62s, obtaining 138 times speed up. As in the general analysis, the TLs can be modeled by many cascaded sections of RLC components. Nonetheless, the number of sections required depends on the electrical length of TLs. TLs sometimes require many sections to meet the reasonable accuracy. Thus, lumped RLC circuits extracted from layouts usually contain large circuit matrices that make the high CPU cost in

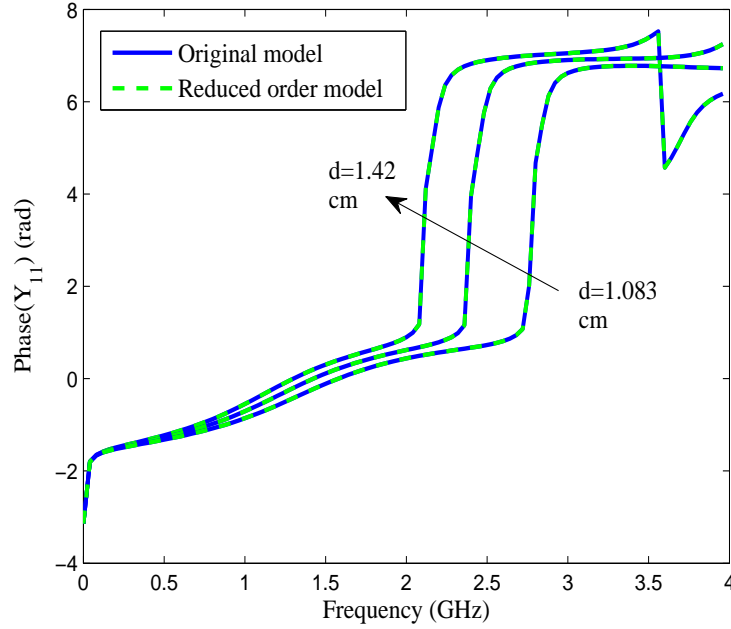


Figure 7.3: Phase of input admittance parameter  $Y_{11}(s, d)$  for  $d = \{1.083, 1.25, 1.42\}$  cm.

simulation [2]. The proposed PMOR technique thus helps to overcome this problem, as on obtention of an accurate PMOR, the repeated design evaluations under different parameter settings become more efficient.

### 7.4.3 Computational complexity

The computational efficiency of the proposed technique in comparison to the Gramian-based PMOR [10] is illustrated in Fig. 7.5. It plots the memory requirement and the CPU time of the most computational expensive steps of the respective PMOR for a 6 port TDSs with one parameter variation for systems of order =  $\{915, 2115, 5715, 9307\}$ . The computational cost for the Gramian-based PMOR [10] process is very high due to the Cholesky factorization and also due to the SVD computed on an order  $n \times n$ . While the computation complexity of the proposed technique is lesser for obtaining the Krylov subspace and also an economical SVD is performed on a matrix of size  $n \times qM$  (where,  $qM < n$ ) in order to obtain the PMOR.

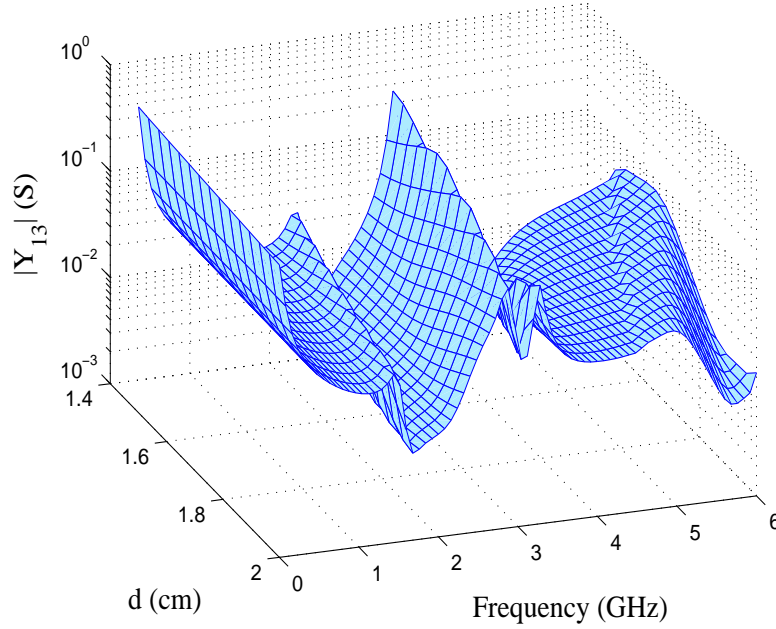


Figure 7.4: PMOR of transfer admittance parameter  $Y_{13}(s, d, T)$  for  $T = 30^\circ\text{C}$ .

## 7.5 Conclusion

A novel parameterized model order reduction technique for multiconductor transmission lines with delay based on matrix interpolation is presented in this chapter. Matrix interpolation preserves the same number of poles for parameterized model order reduction over the design space while for input-output interpolation the order of the parameterized macromodels, suffer from oversize due to the nature of the input-output system level interpolation. The reduced order models are obtained using a higher-order Krylov subspace decomposition. First, the design space is divided into cells and for each vertex model of the cell a Krylov subspace is computed and are then merged and adaptively truncated based on the singular values to obtain a common projection matrix. The resulting reduced order models and also the delays are interpolated using positive interpolation schemes such that the parameterized dependence is preserved. This parameterized model order reduction approach makes multiple system evaluations under different design parameter variations computationally cheap and still accurate. The numerical examples of the RLC and MTL circuits with delays illustrates the efficiency and accuracy of the proposed PMOR technique.



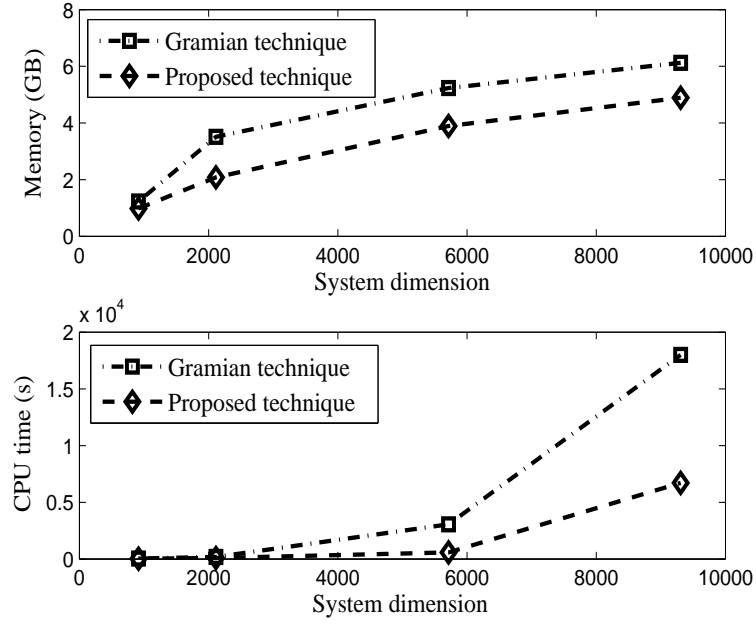


Figure 7.5: Comparison of the computational efficiency.

## Acknowledgment

This work was supported by the Interuniversity Attraction Poles Programme BEST-COM initiated by the Belgian Science Policy Office and the Research Foundation Flanders (FWO).

## References

- [1] A. Ruehli. *Equivalent Circuit Models for Three-Dimensional Multiconductor Systems*. IEEE Transactions on Microwave Theory and Techniques, 22(3):216 – 221, Mar. 1974.
- [2] C. Paul. *Analysis of Multiconductor Transmission Lines*. Wiley, New York, 1994.
- [3] W. Tseng, C. Chen, E. Gad, M. Nakhla, and R. Achar. *Passive Order Reduction for RLC Circuits With Delay Elements*. IEEE Transactions on Advanced Packaging, 30(4):830 –840, Nov. 2007.
- [4] J. Cullum, A. Ruehli, and T. Zhang. *A method for reduced-order modeling and simulation of large interconnect circuits and its application to PEEC models with retardation*. IEEE Transactions on Circuits and Systems II: Analog and Digital Signal Processing, 47(4):261 –273, Apr. 2000.
- [5] F. Ferranti, M. Nakhla, G. Antonini, T. Dhaene, L. Knockaert, and A. Ruehli. *Multipoint Full-Wave Model Order Reduction for Delayed PEEC Models With Large Delays*. IEEE Transactions on Electromagnetic Compatibility, 53(4):959 –967, Nov. 2011.
- [6] E. Rasekh and A. Dounavis. *Multiorder Arnoldi Approach for Model Order Reduction of PEEC Models With Retardation*. IEEE Transactions on Components, Packaging and Manufacturing Technology, 2(10):1629 –1636, Oct. 2012.
- [7] E. Samuel, L. Knockaert, and T. Dhaene. *Model Order Reduction of Time-Delay Systems Using a Laguerre Expansion Technique*. IEEE Transactions on Circuits and Systems I: Regular Papers, 61(6):1815–1823, June 2014.
- [8] M. Ahmadloo and A. Dounavis. *Parameterized Model Order Reduction of Electromagnetic Systems Using Multiorder Arnoldi*. IEEE Transactions on Advanced Packaging, 33(4):1012–1020, 2010.
- [9] F. Ferranti, M. Nakhla, G. Antonini, T. Dhaene, L. Knockaert, and A. Ruehli. *Interpolation-Based Parameterized Model Order Reduction of Delayed Systems*. IEEE Transactions on Microwave Theory and Techniques, 60(3):431–440, 2012.
- [10] X. Wang, Z. Zhang, Q. Wang, and N. Wong. *Gramian-based model order reduction of parameterized time-delay systems*. International Journal of Circuit Theory and Applications, 2012. doi:10.1002/cta.1884.

- [11] E. Samuel, F. Ferranti, L. Knockaert, and T. Dhaene. *Passivity-Preserving Parameterized Model Order Reduction Using Singular Values and Matrix Interpolation*. IEEE Transactions on Components, Packaging and Manufacturing Technology, 3(6):1028–1037, 2013.
- [12] B. Salimbahrami, R. Eid, and B. Lohmann. *Model reduction by second order Krylov subspaces: Extensions, stability and proportional damping*. 2006 IEEE International Symposium on Intelligent Control, pages 2997 –3002, Oct. 2006.
- [13] A. Weiser and S. E. Zarantonello. *A Note on Piecewise Linear and Multilinear Table Interpolation in Many Dimensions*. Mathematics of Computation, 50(181):189 – 196, Jan. 1988.
- [14] K. Chemmangat, T. Dhaene, and L. Knockaert. *Scalable macromodelling of microwave system responses using sequential sampling with path-simplexes*. Electronics Letters, 49(15):950–952, July 2013.
- [15] D. Deschrijver, A. Narbudowicz, E. Laermans, and T. Dhaene. *On the Application of Dimensional Analysis to Parametric Macromodeling*. IEEE Microwave and Wireless Components Letters, 20(4):190–192, April 2010.



# 8

## Conclusion

*“Everything should be as simple as possible, but not simpler.”*

–Albert Einstein (1879 - 1955)

### 8.1 Contribution

#### 8.1.1 Model order reduction

With roots dating back to many years in a wide variety of applications, reducing the order or dimension of models of large systems, is paramount to enabling the system simulations and verifications. Existing methods for LTI MOR can be broadly characterized into two types: those that are based on Krylov methods, and those based on balancing techniques as briefly discussed in Chapter 2. Krylov techniques were proved to be very appealing because of their simplicity and performance in terms of efficiency and accuracy. But still there are some shortcomings like strategy for error control and order selection, an automated expansion point selection for multipoint MOR. The alternative methods, those in the truncated balanced realization (TBR) family, perform reduction based on the concept of controllability and observability of the system states and are purported to produce nearly optimal models and have well defined error bounds. However, they are complex to implement and expensive to apply, which limits their applicability to small and medium sized problems. Hybrid techniques that combine some of the features of each type of methods have also been presented [1–3].

Contribution of this PhD thesis to MOR techniques:

1. MOR for TDSs using Laguerre expansion: The research contribution mainly focuses on Krylov based MOR techniques. In Chapter 3 the MOR technique is extended to systems with delays using higher-order Krylov. The delays are approximated using Laguerre expansion and the approach is able to approximate with lesser number of terms than in comparison with Taylor series. This helps to reduce the computational complexity of the MOR technique for systems with delay.
2. Adaptive frequency sampling: In Chapter 4, a new hybrid technique for adaptive frequency sampling for multipoint expansion MOR is presented. Reflective exploration is an effective technique when it is very expensive to obtain the model from EM simulators. For the exploration a reflective function is required to select a new expansion point. This helps to get an idea of the frequency behavior of the system. In the second step, the binary search is adopted. The binary search is a dichotomic divide and conquer search. At each step to validate the model obtained through reflective exploration. The ROM at the midpoint of two samples is computed by linear interpolation and compared with the actual model simulated at that point using an EM simulator. This is continued till all the sections are modeled with a user specified accuracy. In this technique the reduced order per frequency sample is also estimated in an iterative manner. Then as a last step SVD is performed on the obtained projection matrix to see if the projection matrix can further be compacted based on its singular values.

### 8.1.2 Parameterized modeling

The PhD thesis mainly contributes to research on state-space interpolation based PMOR.

1. Sylvester realization: In Chapter 5, a novel state-space realization for the system is proposed using a Sylvester technique. A judicious choice of the state-space realization is required in order to account for the assumed smoothness of the state-space matrices with respect to the design parameters. The Sylvester technique is used in combination with a suitable interpolation schemes to interpolate a set of state-space matrices. Hence the poles and the residues indirectly, in order to build accurate parameterized macro-models. The technique is compared with some of the existing techniques in the literature and is illustrated to be an efficient technique.
2. PMOR using SVD and matrix interpolation: In Chapter 6, a PMOR based on singular values and matrix interpolation is presented. Two strategies are

presented for the order estimation. Also depending on the scenario the technique can be interpreted in two ways the *local* and the *global*. The design space is first divided into cells and a Krylov subspace is computed for each cell. Next the merged Krylov subspace is truncated with respect to its singular values to obtain a common projection matrix for the design space. Finally, the reduced system matrices are interpolated using positive interpolation schemes to obtain a guaranteed passive PROM. The PMOR technique is applied to time-delay systems in Chapter 7 and an adaptive truncation of the singular values for the common projection matrix is presented.

3. PMOR with sequential sampling: In Chapter 6, it is also shown that an accurate PROM is obtained with sequential sampling, by avoiding potential undersampling or oversampling of the parameter space. The approach is illustrated with numerical results.

## 8.2 Future scope

A number of potential areas for further exploring MOR and PMOR based on the work presented are:

1. Systems with large number of ports: Most of the modern devices and power grids have a large number of ports and is an issue which is an ongoing research for Krylov based MOR. As current approaches rely on block iterations, where the size of the block equals the number of ports, each block iteration increases the size of the model by an amount equal to the number of ports. This leads to large models even for a moderate reduction order. Balanced truncation MOR is somewhat less sensitive to the number of input ports but systems with large number of ports are generally very large in size, which makes reduction based on balancing techniques impractical.

Some work that has been carried out for MOR with large number of ports are [4–6], and these techniques can be implemented for improving the MOR techniques proposed. It can be useful in Chapter 4 for the order estimation for hybrid adaptive sampling algorithm, where the initial estimate for the order is equal to the number of ports, which is not practical for systems with large ports.

2. Nonlinear Systems: Nonlinear MOR is very much desired for large scale CAD and simulations, but a general stable and widely usable technique is still an open challenge. Amongst the proposed techniques for nonlinear MOR, proper orthogonal decomposition (POD) technique is most preferred. It can be applied to very large systems and also a very efficient technique for

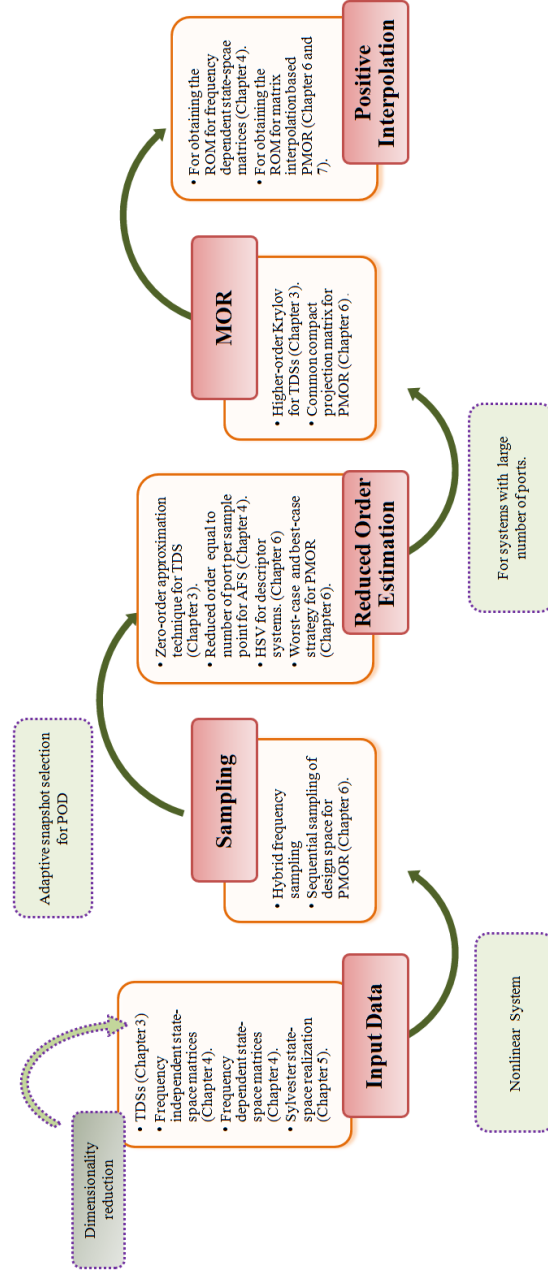


Figure 8.1: Contribution (orange solid line boxes) and future scope (purple dotted line boxes).



obtaining the reduced order model for nonlinear systems. Adaptive snapshot selection for POD technique is a challenge on which research is going on [7, 8].

### 3. Dimensionality reduction:

Parameterized modeling are now starting to be used as the basis for variability analysis models used in design. For high frequencies, at nano-scale feature sizes, process variability effects, as well as dependence on operating conditions become extremely important and has to be modeled [9]. Parameterized modeling techniques are very efficient but these techniques like other modeling methods are limited by the *curse of dimensionality*. The *curse of dimensionality* refers to various phenomena that arise when analyzing and organizing data in high-dimensional spaces.

Adaptive Sampling of high dimensional design space is also an open challenge. In [10, 11], some of the recent works related to adaptive sampling of the design space are proposed.

As a future scope some of the state-of-the-art dimensionality reduction techniques like supervised principle component analysis (SPCA), Kernel PCA [12] can be considered as a first step for parameterized modeling. High dimensional analysis will help determining the important parameters by prioritizing them based on their influences on the system response to be modeled.

The PhD thesis contributions and future scope is graphically represented in Fig. 8.1. The figure outlines the main steps in MOR techniques along with interpolation approach for obtaining a parameterized reduced order model. The orange solid line boxes represents the PhD thesis contribution and the purple dotted boxes represents the future scope.

## References

- [1] I. M. Jaimoukha and E. M. Kasenally. *Krylov Subspace Methods for Solving Large Lyapunov Equations*. SIAM Journal on Numerical Analysis, 31(1):pp. 227–251, 1994.
- [2] J.-R. Li, F. Wang, and J. K. White. *An Efficient Lyapunov Equation-based Approach for Generating Reduced-order Models of Interconnect*. In Proceedings of the 36th Annual ACM/IEEE Design Automation Conference, DAC '99, pages 1–6, 1999.
- [3] J. Phillips and L. Silveira. *Poor man's TBR: a simple model reduction scheme*. Proceedings of Design, Automation and Test in Europe Conference and Exhibition, 2:938–943, Feb 2004.
- [4] P. Feldmann and F. Liu. *Sparse and efficient reduced order modeling of linear subcircuits with large number of terminals*. In IEEE/ACM International Conference on Computer Aided Design, pages 88–92, Nov 2004.
- [5] J. Silva, J. Villena, P. Flores, and L. Silveira. *Outstanding Issues in Model Order Reduction*. In Scientific Computing in Electrical Engineering, volume 11 of *Mathematics in Industry*, pages 139–152. Springer Berlin Heidelberg, 2007.
- [6] R. Ionutiu, J. Rommes, and W. Schilders. *SparseRC: Sparsity Preserving Model Reduction for RC Circuits With Many Terminals*. IEEE Transactions on Computer-Aided Design of Integrated Circuits and Systems, 30(12):1828–1841, Dec 2011.
- [7] X. Chen, I. M. Navon, and F. Fang. *A dual-weighted trust-region adaptive POD 4D-VAR applied to a finite-element shallow-water equations model*. International Journal for Numerical Methods in Fluids, 65(5):520–541, 2011.
- [8] A. Paul-Dubois-Taine and D. Amsallem. *An adaptive and efficient greedy procedure for the optimal training of parametric reduced-order models*. International Journal for Numerical Methods in Engineering, 2014. doi:10.1002/nme.4759.
- [9] D. Spina, F. Ferranti, G. Antonini, T. Dhaene, and L. Knockaert. *Efficient Variability Analysis of Electromagnetic Systems Via Polynomial Chaos and Model Order Reduction*. IEEE Transactions on Components, Packaging and Manufacturing Technology, 4(6):1038–1051, June 2014.
- [10] C. Wang, Q. Duan, W. Gong, A. Ye, Z. Di, and C. Miao. *An evaluation of adaptive surrogate modeling based optimization with two benchmark problems*. Environmental Modelling & Software, 60(0):167 – 179, 2014.

- 
- [11] K. Chemmangat, T. Dhaene, and L. Knockaert. *Auto-generation of passive scalable macromodels for microwave components using scattered sequential sampling*. International Journal of Microwave and Wireless Technologies, FirstView:1–12, 10 2014.
  - [12] E. Barshan, A. Ghodsi, Z. Azimifar, and M. Z. Jahromi. *Supervised principal component analysis: Visualization, classification and regression on subspaces and submanifolds*. Pattern Recognition, 44(7):1357 – 1371, 2011.



